

**Golder Associates Pty Ltd**  
A.B.N. 64 006 107 857

124 Pacific Highway  
St Leonards, NSW 2065, Australia  
(PO Box 1302, Crows Nest, 1585)  
Telephone (02) 9478 3900  
Fax (02) 9478 3901  
<http://www.golder.com>



## REPORT ON

### **Broken Hill Operations Pty Ltd HYDROGEOLOGICAL ASSESSMENT FOR PROPOSED MINE EXPANSION, RASP MINE BROKEN HILL, NEW SOUTH WALES**

Submitted to :

Broken Hill Operations Pty Ltd  
130 Eyre Street  
BROKEN HILL NSW 2880

#### DISTRIBUTION:

1 Copy	-	Broken Hill Operations Pty Ltd
1 Copy	-	CBH
2 Copies	-	ERM
2 Copies	-	Golder Associates Pty Ltd

March 2008

087626006

**RECORD OF ISSUE**

<b>COMPANY</b>	<b>CLIENT CONTACT</b>	<b>VERSION</b>	<b>DATE ISSUED</b>	<b>METHOD OF DELIVERY</b>
Broken Hill Operations Pty Ltd	Brendan Barker	Rev0	07.03.08	Electronic
CBH	Gwen Wilson	Rev0	07.03.08	Electronic
ERM	Luke Stuart	Rev0	07.03.08	Electronic

## TABLE OF CONTENTS

SECTION	PAGE
1.0 INTRODUCTION.....	1
2.0 GEOLOGY .....	2
2.1 Regional Geological Settings .....	2
2.2 Structural elements.....	2
2.3 CML7 Geology.....	3
3.0 HYDROGEOLOGY .....	5
3.1 Regional Hydrogeology .....	5
3.1.1 Perched Aquifers in Shallow Quaternary Deposits .....	5
3.1.2 Colluvial Aquifers West of the Barrier Range.....	5
3.1.3 Bedrock Aquifers .....	6
3.1.4 Regional Conceptual Hydrogeological Model .....	6
3.2 Local Hydrogeology.....	7
3.2.1 Registered Wells.....	7
3.2.2 Groundwater Levels.....	7
3.2.3 Bedrock Hydraulic Properties and Average Yields .....	9
3.2.4 Estimation of Groundwater Inflow to Proposed Rasp Mine .....	9
3.2.5 Groundwater Quality .....	11
4.0 POTENTIAL SENSITIVE RECEPTORS.....	14
4.1 Groundwater Users .....	14
4.2 Surface Water Features .....	14
4.3 Groundwater Dependent Ecosystems.....	15
4.4 Town Water Supply .....	15
5.0 CONCLUSIONS.....	16
6.0 REFERENCES.....	18
7.0 LIMITATIONS.....	20
8.0 IMPORTANT INFORMATION.....	21

### LIST OF TABLES IN TEXT

Table 1: Summary of Groundwater Bore Data (from NZG, 2006) .....	8
Table 2: Summary of Groundwater Chemical Data (from Caritat et. al. 2005 and Caritat pers. comm. [EC and TDS]) .....	11

### LIST OF FIGURES IN TEXT

Figure A. Conceptual Hydrogeological Model of the Broken Hill domain (from Caritat et. al., 2002; not to scale).....	6
--	---

## **LIST OF FIGURES ATTACHED**

**Figure 1. Geology and Site Location**

**Figure 2. Geological Map of Broken Hill**

**Figure 3. Geology of the Broken Hill Line of Lode**

**Figure 4. Cross-section A-A'**

**Figure 5. Cross-section B-B' and C-C'**

**Figure 6. Cross-section D-D' and E-E'**

**Figure 7. Extended Cross-Section**

**Figure 8. Location of Boreholes - Regional**

**Figure 9. Electrical Conductivity ( $\mu\text{S}/\text{cm}$ )**

**Figure 10. Geology – Broken Hill**

**Figure 11. Surface Water Features**

## **LIST OF APPENDICES**

Appendix A ..... Background Figures for Groundwater Inflow Estimate

Appendix B..... Compendium of Reference Documents

Appendix C..... Important Information about your Environmental Site Assessment



## 1.0 INTRODUCTION

Golder Associates Pty Ltd (Golder) has prepared this *Hydrogeological Assessment* for the proposed Rasp Mine development at Broken Hill, New South Wales (NSW), to support the revised *Environmental Assessment* being prepared by Environmental Resource Management Australia Pty Ltd (ERM) on behalf of Broken Hill Operations Pty Ltd (BHOP).

The objective of this *Hydrogeological Assessment* is to characterise the groundwater resource in the vicinity of the proposed development, and to evaluate potential impacts to the resource resulting from the proposed development with regards to water supply, surface water bodies and maintenance of groundwater dependent ecosystems. The following tasks were completed in accordance with our scope of work:

- Place the location of intended mining, with particular attention to the geological structure (and potential transmissive zone) within the mining lease area;
- Provide data regarding groundwater quality associated with the Willyama Supergroup bedrock;
- Provide analysis regarding the expected extent of water level drawdown and hydraulic properties of the bedrock in the vicinity of the mining lease;
- Identify locations of potential sensitive receptors to groundwater depressurisation associated with mining, including extraction bores, surface water bodies and groundwater dependent ecosystems;
- Review the validity of the groundwater inflow volume reported in BHOPs water balance. It is our understanding that ERM are responsible for amendment of BHOPs water balance. Golder's analysis provides input into that process;
- Discuss the potential impact of water extraction on groundwater resources, drawing on the physical and chemical properties of water resource, and the locations of receptors; and
- Provide an assessment of the quality of referenced data cited in our report (as well as copies of the original referenced documents where possible).

This report addresses the above issues through a more robust development of the Conceptual Hydrogeological Model (CHM) as it specifically relates to the proposed mining operation expansion areas and potential sensitive receptors in the vicinity of the mine lease. Finally, the potential risks to the groundwater resource and identified receptors are evaluated on the basis of the refined CHM.

## **2.0 GEOLOGY**

### **2.1 Regional Geological Settings**

The Broken Hill mine is located in the south eastern part of the Curnamona Craton (Ruperto and Caritat, 2006). This large domain consists of a polydeformed sequence of inter-layered Early Proterozoic metasediments of about 7 to 11 km in thickness intruded by mafic and felsic igneous rocks (Willis et al., 1983).

The Willyama Supergroup has been divided into several major stratigraphic groups (Figure 1 and Figure 2; Stevens et al., 1988). The basal units of the Willyama Supergroup (Thackaringa Group and below) comprise of migmatitic gneiss and quartzofeldspathic rocks intercalated with psammopelites. Conformably overlying these rocks is the Broken Hill Group, comprised of pelitic to psammopelitic metasediments and minor calc-silicate rocks, amphibolites and basic gneisses. These rocks are principally derived from metamorphosed sedimentary rocks, although numerous quartz-feldspar-biotite gneisses have been interpreted partially as deformed volcanic rocks (e.g. Hores Gneiss). These are overlain by the Sundown and Paragon Groups which are a succession of psammite, pelite, calc-silicate rocks and graphitic phyllite and schist, interpreted to have been deposited during the post-extensional evolution of the basin (Willis et al., 1983). The Willyama group is unconformably overlain by a younger cover of the Adelaidean shallow marine sediments.

The Willyama Supergroup underwent multiple metamorphism and deformation events. The regional metamorphic grade broadly increases from the northwest towards the southeast of the block from greenschist to granulite facies, where the rocks have undergone extensive melting (Corbett and Phillips, 1981). The high grade metamorphism (under temperature 750–800°C and pressure 5–6 kbar) generated pegmatite and granite and was accompanied with at least two regional deformation phases producing schistosity defined by the high-grade minerals (sillimanite). A third deformation event occurred under retrograde conditions (550–600°C and 5–6 kbar). This deformation is characterised by a localized retrograde schistosity and initiation of retrograde shear zones (Laing et al., 1987).

### **2.2 Structural Elements**

The structural history of the Broken Hill region is characterised by multiple episodes of intense deformation, which has resulted in the current complex geological environment present in this region (Figure 1 and Figure 2). The Proterozoic bedrock has undergone a minimum of three major folding events, and all regional structures including synclines, anticlines and monoclines have a general north to north-east trend. Major folds in the Broken Hill area are first and second generation structures.

The Broken Hill Block is cross-cut by numerous retrograded shear-zones, which, because of their high mica content, are locally known as schist zones. Shear zones are sinuous or linear and commonly bifurcate and occur in three principal orientations: striking north-westerly, north-easterly and westerly. They are dominated by muscovite and chlorite schists, with the schistosity generally parallel or subparallel to the zone margins (Williams and Vernon, 2001).

Retrograde shear zones are typically steeply dipping (approximately vertical) planar or curvilinear. Many shear zones functioned as faults with an offset of units across the shear zone. Faults independent of shear zone are rare; an exception is the area north of Mt Robe, where faults are relatively abundant and produced significant displacement (Stevens et al., 1988).

The shear zones vary considerably in complexity, width and the sharpness of their boundaries. They occur as zones of few meters up to the several meters wide or they may be complex belts of several kilometres wide. All wide complex shear zones are characterized by retrograde metamorphism and abundance of granitoids – pegmatite, aplite, migmatite and granite developed within them. The most extensive of these wide belts is Apollyon Valley and Mt Franks shear zones. Narrower retrograde zones with similar character to Apollyon Valley occur along the west-trending Stephens Creek shear and Sundown area and along the Darling range (Figure 1; Marjoribanks et al., 1980).

### **2.3 CML7 Geology**

The Broken Hill ore body is made up of several distinctive lead lodes (2 and 3 Lens) and zinc lodes (1 Lens, A, B, C Lodes) stacked above each other over a strike length of approximately 8 km (Rothery, 2001). The stratigraphy of the mine area consists of three main suites which are equivalent to three groups in the formal stratigraphy of the Willyama Block, including Suite 3 (Thackaringa Group), Suite 4 (Broken Hill Group, which hosts the orebodies), and Suite 5 (Sundown Group).

These groups are further divided into lithostratigraphic units numbered as in case of Suite 4 from 4.1 to 4.8. The spatially highest Unit in the mine sequence is the Hanging Wall Gneiss (Rasp Ridge Gneiss Formation; Willis et al., 1983). Amphibolite (Unit 4.4) is present to the east from the hanging wall and occurs with minor breaks along the length of the line of lode and is followed by psammites and pelites (Unit 4.5). A pelitic sequence with banded iron-formation (Unit 4.6) lies in the immediate hanging wall of the lode horizon that hosts the ore bodies. The lode horizon consists of a mixed package of rocks (Unit 4.7) that includes quartz gahnite and garnet quartzite. In the footwall, a sequence of metasediments separates the lode horizon from the Footwall Potosi Gneiss and amphibolite. The footwall sequence has been assigned Suite and Unit numbers from 4.8 to 5 and back down through 4 to 3 (Haydon and McConachy, 1987). The last and spatially lowest is the Granite Gneiss (the Rasp Ridge Gneiss Formation).

The metasedimentary rocks around the Broken Hill ore body have then been folded into three major structures (Figure 3):

- Broken Hill Synform - an open, overturned and south-west plunging anticline;
- Hanging Wall Synform - south west plunging fold with axial plane dipping steeply north-west; and
- Broken Hill Antiform - inferred to exist between the Broken Hill Synform and the Hanging Wall Synform.

The Broken Hill ore body lies within the Broken Hill antiform (Laing et al., 1978). A major structure, the Globe–Vauxhall shear, lies 1 to 1.5 kilometres northwest of the ore body, and the ore body is cut by two smaller north trending D4 faults. Rothery (2001) re-evaluated the structural features of the Broken Hill Mine Area and concluded that the lack of correlation between rocks from the ore body hanging wall to the footwall does not support the existence of a Broken Hill Antiform.

Geological cross sections through and adjacent to the CML7 lease area are presented in Figure 4 to Figure 6 (cross section transects are labelled on Figure 3). The western mineralization, which is targeted for expansion to the resource, is stratigraphically related to, but is spatially separated from, the zinc and lead lodes in the main line of lode system. This mineralised zone is generally a tilted planar feature with an approximately NE strike and a steep westward dip (consistent with the local structure), located within a sequence of metasediments including amphibolite, pelite and gneiss. It is also associated with a large scale

fold within the mine lease, such that it is shallowest towards the middle of the mine lease (approximately 200 m below ground level [mbgl]) and becomes deeper toward the northern and southern site boundaries (approximately 600 mbgl at the southern site boundary). It is truncated at depth by the Globe Vauxhall Shear Zone to the west of the mine lease area (but does not directly intersect any major shear zones within the mine lease), and is repeated as the Centenary Mineralisation (Blampain and Plimer, 2006). An extended cross-section, oriented perpendicular to the strike of the primary structural elements, is presented in Figure 7, which demonstrates the repeated pattern of steeply dipping shear zones to the west of the mine lease area. The Globe Vauxhall and Main shear zones form distinct structural boundaries to the east and west of the lode horizon within the mine lease area; the implications of these structures with regards to the regional hydrogeological setting are described in detail in the following sections.

### **3.0 HYDROGEOLOGY**

This section summarises the available hydrogeological information with respect to the Rasp Mine project. A general discussion of the regional hydrogeology is provided followed by more specific local hydrogeological information based on available data.

#### **3.1 Regional Hydrogeology**

In the vicinity of Broken Hill, groundwater resources can be classified into three groups on the basis of aquifer type (Caritat et al., 2002; NZG, 2006):

- Perched groundwater present in the thin veneer of Quaternary sediments overlying the Proterozoic bedrock formations;
- Groundwater present in thick sequences of colluvial sediments that have accumulated on downthrown fault blocks along the western margin of the Barrier Ranges; and
- Groundwater present within structural features of the Proterozoic bedrock.

A conceptual hydrogeological model depicting the relationship between these aquifer types is presented in Figure A (page 6), and the various aquifer types are described in the following sections.

##### **3.1.1 Perched Aquifers in Shallow Quaternary Deposits**

The types of aquifers present are colluvial sediments, alluvial sediments, and sand dunes (NZG, 2006). However, only alluvial deposits along water courses are considered likely to contain significant volumes of groundwater.

An exploratory drilling program by Country Water and Energy has been undertaken in alluvial sediments in the vicinity of Stevens Creek to attempt to identify prospective locations for siting a water supply borefield. The program comprised drilling of approximately 20 boreholes, and was abandoned following the first stage of assessment as the majority of boreholes were dry. It was indicated that water supply borefields have therefore been sited within the thick colluvial sequences of the adjacent Mundi Mundi plains (Country Water and Energy, pers. comm., 2008).

##### **3.1.2 Colluvial Aquifers West of the Barrier Range**

The principal groundwater resources in the vicinity of Broken Hill are associated with thick sequences of Quaternary sediments, such as those present in the Mundi Mundi plains, overlying Proterozoic metamorphic bedrock (including the Willyama Supergroup). The thick sedimentary deposits were reported to have formed on downthrown fault blocks along the western margin of the Barrier Range, followed by accumulation of colluvial sediment (up to 200 m thick) transported from the adjacent ranges. These sediments generally consist of gravel, sand, and silt interbedded with clay, forming unconfined to semi-confined aquifer conditions at depth (Caritat et al., 2002).

Whilst these aquifers represent significant regional groundwater resources for rural water supply to the region, they are absent beneath the mine lease. The closest of these colluvial deposits is associated with the Mundi Mundi fault scarp approximately 30 to 40 km west of Broken Hill and therefore well outside the area of interest for this study.

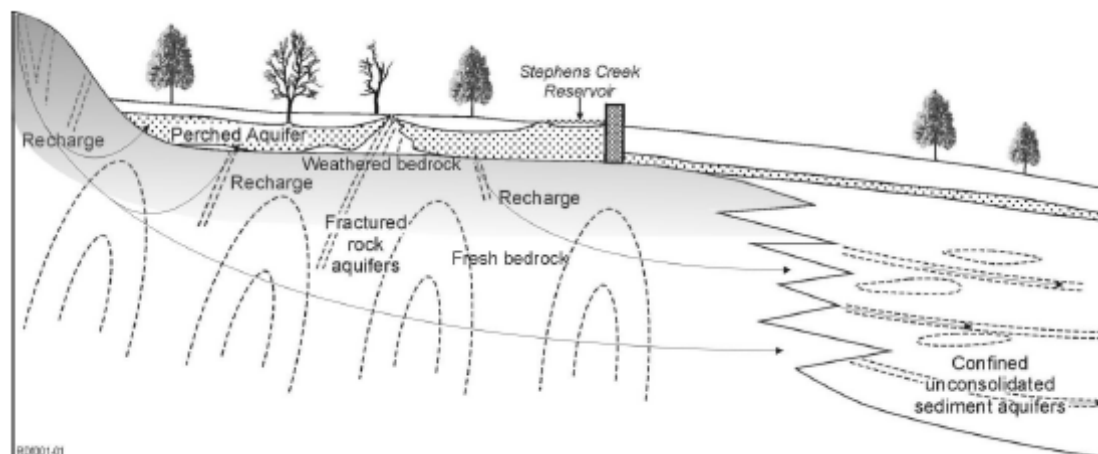
### 3.1.3 Bedrock Aquifers

The rock mass of the Willyama Supergroup metamorphics is reported to have a low primary porosity, and as such groundwater storage and flow is dominated by the structural geology of the formation including faults, lineaments and shear zones (Caritat et al., 2002; NZG, 2006). The primary structural features capable of storing and transmitting water are believed to be the shear zones and faults present across the study area. There is a predominant north-northeast trend to these structures in the vicinity of Broken Hill, which would comprise a significant anisotropic control on the groundwater flow regime in the area.

### 3.1.4 Regional Conceptual Hydrogeological Model

A simplified CHM depicting the relationships between the various aquifer types is presented in Figure A (adapted from Caritat et al., 2002). In general, the perched aquifer and thicker colluvial fault scarp aquifers are believed to be recharged primarily through infiltration of rainfall and vertical leakage from surface water bodies. There may be some interaction between bedrock and perched aquifers close to the foot slopes of the local mountain ranges. Groundwater in the structural bedrock features is likely to be recharged either through direct infiltration into outcropping structures, or through leakage from perched aquifers. In their 2002 study, Caritat et al. state *“There appears to be a poor connectivity between upland areas and the deep basin waters, suggesting the presence of a complex hydrologic system... the basin aquifers are relatively isolated from the upland aquifers and from the surface”*. From the available published data on groundwater quality it appears unlikely that there is significant interaction between groundwater present in bedrock structural features and perched groundwater in shallow Quaternary deposits (Caritat, 2002).

**Figure A. Conceptual Hydrogeological Model of the Broken Hill domain (from Caritat et al., 2002; not to scale)**



Based on the available hydrogeological data, this represents a robust CHM which may be revised in light of future investigation. There were limited data available on the aquifer thickness and groundwater elevation in the available databases (NR Atlas, 2008; BHGD, 2002). An alternative groundwater interpretation could be that the ‘perched’ water represents the water table. The bedrock, in bulk, behaves like a low permeability material, with local low transmissivity structural features. The bedrock is recharged from episodic or some winter rainfall via outcrops and by downward leakage from the water table. Because of the very low conductivity of the bedrock, the groundwater levels in the bedrock are much lower than those

of the shallow system. The shallow and deep system are understood to regionally behave in a hydraulically separated manner, based on the available information.

### **3.2 Local Hydrogeology**

This section describes the CHM relevant to the CML7 lease area and proposed western mineralisation mine workings. This section was developed on the basis of available geological and hydrogeological information.

Within the context of the CML7 mine lease, the primary water bearing features are expected to be the Globe Vauxhall and Main shear zones, which provide east and west lateral constraints to the target mining zone of the western mineralisation.

NBZ (2006) suggests that there have been anecdotal reports of a high yielding brecciated zone between the lode horizon and the hanging wall formation adjacent to the Potosi Gneiss. The source of this information, however, is uncertain. CBH indicated that they have not encountered this feature in over 50 exploration boreholes drilled along 1.2 km strike extent. This high yielding zone has also not been identified by recent comprehensive studies of the geological structure of the mine lease area (Rothery, 2001), and even if it was present there would be about 200m of competent bedrock separating it from the target mining zone.

#### **3.2.1 Registered Wells**

Development of groundwater resources associated with the fractured bedrock formations has historically been limited due to low yields and generally brackish water quality (further details on water quality are provided in subsequent sections). A search of bore information from the DWE database, as well as information supplied by researchers at Geosciences Australia, indicated that there are approximately 36 wells within 20 km of the mine lease (Figure 8 and Figure 9), and only two wells within close proximity of the lease area (Figure 10):

- GW600132, located approximately 1.5 km north-northwest of the lease area; and
- GW803404, located approximately 2 km north-northwest of the lease area.

These wells are installed to depths of 18 to 30 mbgl, respectively, with standing water levels at the time of installation of 9.0 and 22.0 mbgl, respectively. The screened intervals of these wells are likely to represent either Quaternary deposits or a weathered contact between bedrock and the overlying regolith.

#### **3.2.2 Groundwater Levels**

NZG (2006) assessed the potential for aquifer storage and recovery in the Broken Hill area and adapted a table from Jewell (2004) on groundwater levels based on NSW Department of Planning and Natural Resource (DIPNR<sup>1</sup>) information for 25 groundwater bores within a 15 km radius of Broken Hill. These data are reproduced in Table 1, together with the two closest wells situated within 2 km of the mine site.

---

<sup>1</sup> The department within DIPNR responsible for administration of water resources in NSW was transferred to the Department of Water and Energy (DWE) in 2007.

**Table 1: Summary of Groundwater Bore Data (from NZG, 2006)**

<b>Id</b>	<b>Bore Depth (m)</b>	<b>Bore logs</b>	<b>Depth to Top of Aquifer (m)</b>	<b>Supply (m<sup>3</sup>/day)</b>	<b>Standing Water Level (m bgl)</b>	<b>Quality</b>	<b>Other</b>
4297	-				-	-	
9812	22.3			112.32	7	-	Adjacent to fault
9653	131.1			0	-	-	
9782	21.3			6.912	18.3	Brackish	
9785	-		30.5	2.592	10.7	Good	
10089	15.5			13.824	9.1	Good	Adjacent to fault
10090	54.94			65.664	-	Good	
10091	27.4			Poor	18.3	Good	Adjacent to fault
10094	19.8			112.32	17.4	Good	
10095	30.5			112.32	21.3	Good	
10096	21.3			Good	17.7	Good	
10097	15.2			Fair	7.6	Good	
10098	15.2			Fair	6.1	Good	
10099	18.3		15.2	54.432	12.2	Good	
10136	27.4			4.4064	11.6	Very good	
10139	18.3		12.2	65.4912	12.2	Good	
10244	15.2			224.64	2.7	Good	
17685	42.7	0-42.7m grey shale		0	-		
18521	20.7	0-3.3m clay & gravel, 3.3-15.9m schist, 15-9-18.3m pegmatite, 18.3-20.7m schist	18.3	19.872	7.6	Stock	Fractured aquifer T=1.67m <sup>3</sup> /day/m (S=0.001)
20084	15.3	0-1.2m sand red clay, 1.2-7.9m yellow sandstone, 7.9-15.2m grey rock, 15.2-15.3m coarse gravel		25.92	10.1	-	
21680	24.4	0-4.3m clay, 4.3-24.4m rock	18.3	32.832	16.8	Stock	T=19.4 m <sup>3</sup> /day/m (S=0.001)
21882	67.1	0-1.8m soil, 1.8-61.0m granite, 61.0-67.1m coarse gravel	61	27.648	45.7	Stock	
61218	213.4				-	-	
500290	10			864	5	Domestic, stock	
600001	44.3			61.344	19	Domestic, stock	
600132	18				9	Domestic, stock	
803404	31				22	Domestic, stock	



### 3.2.3 Bedrock Hydraulic Properties and Average Yields

There is limited information regarding the hydraulic properties of the bedrock formation, as it has never been considered to be a significant resource worthy of detailed hydraulic assessment. It is noted that the high metamorphic grade of the bedrock implies limited to no porosity, therefore, it is expected that groundwater would only flow through structural features. NZG (2006) indicate that transmissivity values for the bedrock mass range between 20 and 80 m<sup>2</sup>/day, which are low for most purposes, considering the saturated thickness.

NZG (2006) reports that yields from wells that were tabulated by Jewell (2004) range between 0 and 864 m<sup>3</sup>/day, although the upper end of that range is defined by a shallow well located in the Mundi Mundi alluvial deposits. Of the wells tabulated by Jewell (2004) and presented in Table 1, the yield of wells >30 m depth, assumed to potentially intersect the weathered contact of underlying bedrock, range between 4.4 and 112 m<sup>3</sup>/d. It is noted, however, that these yields are derived from drilling records and therefore are likely to represent specific capacity estimates obtained following well installation rather than formal pumping tests.

NZG (2006) reports that a pumping test carried out at a Rising Sun shaft indicated that with a pumping rate of 520 L/s (44,928 m<sup>3</sup>/d) the drawdown was 20 m (the duration of that test was not reported). NZG also reported that a pumping test carried out at a White Leads shaft yielded less than 100 m<sup>3</sup>/d for three months, with a drawdown of 57 m. NZG (2006) states that exploration boreholes in the southern leases have yielded up to 500 m<sup>3</sup>/d.

A dewatering program has been ongoing within the mine lease for in excess of ten years (using Shaft No.7 towards the southern lease boundary) as a safety measure to reduce the potential for bursting of underground workings on the south adjacent mine lease. We understand that water levels are currently maintained at approximately 500 mbgl for this purpose, and BHOP have indicated that the steady state flowrate of 6 L/s (520 m<sup>3</sup>/d) at Perilya (BHOP, pers. comm., 2008) is required to maintain this water level depth.

### 3.2.4 Estimation of Groundwater Inflow to Proposed Rasp Mine

#### 3.2.4.1 Background

We understand that Broken Hill Operations Pty Ltd (BHOP) plans to extend underground workings in the Rasp Mine site (CML7) in the area of the old South Mine MMM operations. The underground workings are planned to be extended down over several years to around 800 m depth, particularly along the northwest side of the site area.

At present the Perilya mine pumps water from the Shaft No. 7 close to the south-west end of CML7 to reduce the groundwater inflow to its workings, which we understand extend to around 1100 m depth some distance southwest of CML7. We understand this pumping from No. 7 Shaft has operated over the last 10 years. Perilya reports that the pumped flow over the last year has been steady at about 6 L/s and that the water levels in the area of Shaft No 7 are maintained at approximately 500 mbgl. Planned deepening of the mine will require, dewatering to keep pace with mining in order to avoid problems with inflows from old workings.

#### 3.2.4.2 Groundwater Inflow Estimates

The diagram “South Mine MMM No. 7 Shaft Section, Projected Longitudinal Section”, presented in Appendix A, shows a relatively small portion of the old mine workings extend

below 1790' (546 m) depth down to 2400' (732 m) depth. Dewatering of these old workings over several years can be expected to add a small transient flow component to the groundwater inflow to be pumped.

The site area is approximately 342 ha (3.42 km in the southwest - northeast direction along the line of lode by 1.0 km in the southeast – northwest direction). Based on the aerial photograph of the site (Appendix A), it appears that about 75% of the site area consisting of old pits, would act as a catchment for rainfall. The average rainfall at Broken Hill is 253 mm/year and pan evaporation is 2800 mm/year.

The average rainfall ( $Q_r$ ) on this catchment area would be about:

$$Q_r = 0.253 \text{ (m/yr)} \times 3,420,000 \text{ (m}^2\text{)} \times 75/100 \times 1/365 \times 1/86.4 \text{ L/s}$$

$$Q_r = 21 \text{ L/s}$$

We estimate the potential rainfall contribution from this catchment to the flow pumped at Shaft No. 7 ( $Q_{rp}$ ) would be of the order of 15% of the total rainfall on this catchment area, ie.:

$$Q_{rp} = 3.1 \text{ L/s}$$

Of the 6 L/s reported pumped flow, this leaves a flow ( $Q_g$ ) of about 2.9 L/s coming as seepage from the ground around and below the old workings which are considered to be relatively permeable. This flow can be expected to come mainly from the northwest, northeast and southeast as Perilya is actively pumping from its deeper workings to the southwest of the site.

This flow may appear relatively small considering the depth of pumping and the large extent of old workings likely to be connected to the Shaft No. 7. The rock around the Broken Hill orebodies, however, is considered, generally, to be 'tight' (low hydraulic conductivity). The drawdown cone induced by the current pumping, therefore, is considered to be relatively steep to the northwest and southeast and relatively flat through the permeable old workings to the northeast.

The planned deepening and extending of the mine workings within the site area will deepen and extend the base of the drawdown cone but the gradient to the northeast will steepen as mining extends below the base of old workings.

Assuming Perilya continues dewatering southwest of the site, we estimate the increase in  $Q_g$  for the 250 m deepening to be of the order of 3% to 20%, resulting in  $Q_g$  in the range of 3.0 L/s to 3.5 L/s. The contribution from rainfall is not expected to change. Therefore the total steady state groundwater inflow with mining at 800 m depth is expected to be around 6 L/s to 6.5 L/s.

The actual inflow could be greater if high permeable zones within the rock mass are encountered during mining but this is considered unlikely.

### 3.2.4.3 Influence on Shallow Groundwater System

As discussed in the previous section, the deepening and extension of mining within the site area will cause steepening of the drawdown cone at depth. There will be very little if any change in the drawdown cone near the surface. Considering this and that wells GW600132 and GW803404 are installed within the Quaternary aquifer (see Section 3.2.1) the mine deepening is unlikely to have an additional impact on the groundwater levels in these and other shallow groundwater bores that may exist in the neighbourhood.

### 3.2.5 Groundwater Quality

Caritat et al. (2005) studied groundwater quality as part of a regional research project between February 2000 and February 2002. The objective of the study was to assess the interaction of groundwater with bedrock and mineralisation within the Curnamona Province (which includes Broken Hill) using sulphur, strontium, and lead isotopes, to understand whether groundwater chemistry could provide evidence of mineralisation. Of the several hundred samples collected, 46 were identified as being associated with the Barrier Ranges region, which includes Broken Hill (the sampling locations from this research in the vicinity of Broken Hill are indicated as red squares on Figure 8). The data from Caritat et. al. (2005) and Caritat (pers. comm.) is presented in Table 2.

**Table 2: Summary of Groundwater Chemical Data (from Caritat et. al. 2005 and Caritat pers. comm. [EC and TDS])**

ID	Name	Chloride (mg/L)	Sulfate (mg/L)	Lead (mg/L)	Zinc (mg/L)	EC ( $\mu$ S/cm)	TDS (mg/L)
BH100	Zig Zag Bore	1360	993	<0.001	0.0148	5970	<u>4718</u>
BH101	Alberta Well	1260	764	<0.001	0.0154	5020	<u>3569</u>
BH102	Old Corona Well	1800	829	0.0018	0.0115	6630	<u>4886</u>
BH103	Near Neds Tank	3510	<u>1810</u>	<0.001	<0.001	13060	<u>8407</u>
BH105	Warners Bore	515	253	<0.001	<0.001	2490	<u>1521</u>
BH106	Stevens Bore	1110	734	<0.001	<0.001	4870	<u>3417</u>
BH107	Brewery Bore	3520	<u>2570</u>	<0.001	0.0216	13230	<u>10053</u>
BH108	Poolamacca Well	4520	<u>2330</u>	0.0019	0.0687	15500	<u>11624</u>
BH109	Homestead Bore	1710	881	<0.001	0.022	6690	<u>4495</u>
BH115	Three Corners	936	740	0.0012	0.0082	4370	<u>3190</u>
BH116	Copper Mine Bore	1160	577	0.0022	0.0055	5090	<u>3899</u>
BH120	Nickatime Bore	1870	<u>2100</u>	<0.001	0.0557	8380	<u>6660</u>
BH121	Corner Bore	1600	<u>2100</u>	<0.001	0.0087	7610	<u>6086</u>
BH122	Gormans Bore	1320	<u>1610</u>	<0.001	0.1404	6160	<u>4905</u>
BH128	Old Corona Well Bore	394	201	<0.001	0.0048	2380	<u>1760</u>
BH130	Eight Mile Bore	2570	<u>1680</u>	<0.001	0.0215	10240	<u>7192</u>
BH131	Black Tank Bore	5880	<u>2750</u>	0.0032	0.0147	18680	<u>14231</u>
BH132	Silverton Commons Borehole 1	3590	<u>2110</u>	<0.001	0.0207	13870	<u>9889</u>
BH151	Mundi Mundi Ck Well	4210	<u>2400</u>	0.0011	<0.001	14990	<u>10986</u>
BH152	Sundown Borehole	1410	<u>1270</u>	0.0024	0.2581	6650	<u>4467</u>
BH153	Mt George Borehole	332	654	<0.001	0.0545	2640	<u>1721</u>

ID	Name	Chloride (mg/L)	Sulfate (mg/L)	Lead (mg/L)	Zinc (mg/L)	EC (µS/cm)	TDS (mg/L)
BH154	Mt George Well	<b>3860</b>	<u><b>2680</b></u>	<0.001	0.0045	15490	<u><b>10757</b></u>
BH155	Penrose Park #1	<b>12000</b>	<u><b>4150</b></u>	<0.001	0.0021	34900	<u><b>25390</b></u>
BH158	Limestone Well	<b>2010</b>	<u><b>1320</b></u>	0.0092	0.0993	8680	<u><b>5735</b></u>
BH159	House Bore	<b>884</b>	472	0.001	<0.001	4460	<b>2843</b>
SCK03	Farmcote Well	<b>4369</b>	<u><b>1698</b></u>	<b>0.029</b>	<b>12.5</b>	15670	<u><b>9925</b></u>
SCK04	Rangers Bore	<b>2404</b>	<b>999</b>	<b>0.072</b>	<b>8.3</b>	8970	<u><b>5785</b></u>
SCK05	Old Railway Bore	<b>1410</b>	<b>868</b>	<b>0.081</b>	<b>8.4</b>	6620	<u><b>4230</b></u>
SCK07	Springs Shear	<b>472</b>	202	0.027	<b>10.3</b>	2760	<b>1736</b>
SCK10	Ironblow Bore	<b>1066</b>	<b>747</b>	<u><b>0.13</b></u>	<b>10</b>	5320	<u><b>3428</b></u>
SCK11	Mulga Springs	<b>2462</b>	<b>769</b>	0.007	<b>13.6</b>	10270	<u><b>6381</b></u>
SCK12	Fords Well	<b>921</b>	304	0.006	<b>11</b>	4298	<b>2252</b>
SCK13	Stephens Creek Bore	<b>277</b>	100	<b>0.018</b>	<b>12.4</b>	1634	814
SCK14	Hidden Bore	<b>4784</b>	<u><b>2389</b></u>	<b>0.02</b>	<b>6.4</b>	19260	<u><b>11570</b></u>
SCK16	Parnell Bore	<b>4248</b>	<u><b>2647</b></u>	<u><b>0.12</b></u>	<b>7.2</b>	18310	<u><b>11099</b></u>
SCK17	Forking Bore	<b>2628</b>	<b>1829</b>	<b>0.033</b>	<b>8</b>	11110	<u><b>7338</b></u>
BH307	Elizabeth Bore	87	159	<0.001	0.0054	1697	<b>1364</b>
BH309	Jetpump bore	<b>2309</b>	<b>1171</b>	<0.001	0.043	9300	<u><b>5851</b></u>
BH310	LBH0005	<b>1051</b>	<b>573</b>	<0.001	0.0679	5190	<u><b>3303</b></u>
BH311	LA011	<b>5231</b>	<b>1677</b>	<0.001	0.0109	17890	<u><b>11251</b></u>
BH312	Oakdale Explo Bore	<b>851</b>	<b>614</b>	<0.001	0.0137	4760	<u><b>3088</b></u>
BH313	West Mountain Exploration Bore	<b>634</b>	<b>961</b>	<0.001	0.0126	4040	<b>2745</b>
BH314	Kadish Bore	73	58.1	<0.001	0.0206	792	598
BH331	Clevedale House Bore	<b>464</b>	229	<0.001	0.0108	2920	<b>2032</b>
BH337	House Bore	<b>1472</b>	<b>806</b>	<0.001	0.035	7050	<u><b>4272</b></u>
BH441	House Bore	<b>860</b>	483	<0.001	0.0501	3730	<b>2349</b>
Drinking Water Guidelines (ADWG 2004)		<b>250<sup>a</sup></b>	<b>500</b>	<b>0.01</b>	<b>3<sup>a</sup></b>	NA	<b>1000<sup>a</sup></b>
Irrigation (ANZECC 2000)		<b>700<sup>b</sup></b>	NA	<b>2<sup>c</sup>/5<sup>d</sup></b>	<b>2<sup>c</sup>/5<sup>d</sup></b>	5,200 <sup>e</sup>	NA
Livestock (ANZECC 2000)		NA	<u><b>2000<sup>f</sup></b></u>	<u><b>0.1</b></u>	<u><b>20</b></u>	NA	<u><b>3000</b></u>

Notes: all results are expressed as milligrams per litre (mg/L) unless otherwise indicated.

Results in **bold** exceed relevant drinking water criterion (ADWG, 2004)

Results in *italics* exceed relevant irrigation criterion (ANZECC, 2000)

Results underlined exceed relevant livestock criterion (ANZECC, 2000)

<sup>a</sup> denotes aesthetic guideline for ADWG (2004) provided as no health-based criterion exists.

<sup>b</sup> concentration above which only salt tolerant plants are supported (ANZECC 2000).

<sup>c</sup> denotes long term trigger value (LTV; 100 years) criterion from ANZECC, 2000.

<sup>d</sup> denotes short term trigger value (STV; 20 years) criterion from ANZECC, 2000.

<sup>e</sup> EC value above which only very salt tolerant plants are supported (ANZECC 2000).

<sup>f</sup> concentration above which acute or chronic health effects may occur (ANZECC, 2000).

<sup>g</sup> lowest concentration above which loss of production and a decline in animal condition and health is expected to occur (chickens: 3,000; dairy cattle: 4,000; beef cattle: 5,000; horses and pigs: 6,000; sheep: 10,000) (ANZECC, 2000).

The results of the groundwater quality study indicate that the groundwater resource associated with the bedrock aquifer is generally unsuitable for human consumption and crop irrigation, and is marginal for stock watering. Electrical conductivity values for groundwater in the vicinity of Broken Hill are posted on Figure 9, the water is suitable mostly for only very salt tolerant crops (where  $EC > 5,200 \mu S/cm$ ); and if used for stock watering may result in loss of productivity for most animals (if  $TDS > 3,000 mg/L$ ). The average EC and TDS values in the area are from the bedrock are  $7,150 \mu S/cm$  and  $4,650 mg/L$ , respectively (Ruperto and Caritat, 2006).

## **4.0 POTENTIAL SENSITIVE RECEPTORS**

The potential receptors evaluated with regards to risk posed by dewatering include the following:

- groundwater users in the immediate vicinity of the lease area (defined as being within 2 km of the site);
- surface water features in close proximity to the mine lease;
- groundwater dependent ecosystems (GDEs) in the proximity of the mine lease; and
- Town water supply for Broken Hill.

Each of these is evaluated in the following sections.

### **4.1 Groundwater Users**

As previously discussed, there are only two registered wells within 2 km of the mine lease, both of which are installed in shallow sediments, and are separated from the proposed mining zone by the Globe Vauxhall sheer zone, a significant structural feature running parallel to the western lease boundary. The history of mining within this lease dates back over 100 years, and water levels within the mine lease workings have been maintained at approximately 500 mbgl for the past ten years as a safety measure for operations on the south adjacent property. The nature of the structural features in the bedrock suggests that drawdown or depressurisation associated with the dewatering program would propagate preferentially in a NE – SW direction with the regional trend of the structural feature (Figure 7). Little if any influence is expected to propagate westward, perpendicular to the structural features.

If significant impacts to the groundwater resource being accessed by these shallow wells were to occur, they would have already been realised due to the dewatering program on site. Standing water levels of approximately 10-20 mbgl were reported for these wells at installation, and a groundwater level of 500 mbgl is being maintained within the mine lease, at a distance of approximately 2 km from these wells. The dewatering program would have by now influenced the groundwater levels in the bores if there was a direct hydraulic connection.

The future development of the local groundwater resource is considered unlikely, because of the generally poor quality and low yields. To date, the thick sedimentary sequences of the Mundi Mundi plains have been the target of local water supply schemes, and it is expected that this will remain the case in the foreseeable future.

### **4.2 Surface Water Features**

The surface water features in proximity to the site are presented in Figure 11, along with a regional regolith base map. The closest surface water feature to the site is a minor creek located approximately two to three km to the east of the site, which drains to the Stevens Creek Reservoir located approximately 15 km northeast of the mine lease area. Whilst there may be potential for vertical leakage of perched groundwater associated with surface water features into bedrock structural features, previous research has suggested that the connection between bedrock and perched aquifers is likely to be limited. In addition, the creek line is located perpendicular to the regional trend of structural features, and there is at least one significant shear zone separating the mine lease area from the creek. Finally, there is a well installed in the alluvial sediments adjacent to the creek (approximately 5 km from the lease

area), with a water level reported at approximately 20 mbgl, which is what would be expected from a perched groundwater resource that has not been impacted by drainage. It is noted that water quality information was not available with respect to that well. Stevens Creek reservoir itself is considered to be too remote from the site to be affected by dewatering activities within the lease area, even if a hydraulic connection did exist. Given this, it is considered that it would be unlikely that extension of mine dewatering activities will directly impact on surface water features.

#### **4.3 Groundwater Dependent Ecosystems**

Advice provided by ERM suggested that groundwater dependent ecosystems (specifically river red gums) could potentially be present along creek lines and should be conservatively assessed as such. There are no river red gum communities present within the mine lease area, and, considering the hydraulic separation provided by the local geological structure between the mine lease area and the closest creek line, the mining activities are considered unlikely to impact on perched groundwater resources that are potentially sustaining river red gum ecosystems.

#### **4.4 Town Water Supply**

The primary water source for Broken Hill is the Menindee Lakes Scheme, for which a licensed allocation of 10 GL/year is held. Advice from Mike Schulzer, Manager for Assets, Planning and Maintenance with Country Water, indicated that current water consumption for Broken Hill ranges from approximately 7 to 8 GL/year. Mr Schulzer further indicated that the estimated requirement from town water supply in the mine water plan (approximately 230 ML/year: 231 ML/year as raw water and 9 ML/year as potable water) was available and would not impact on the security of the town water supply for Broken Hill.

## 5.0 CONCLUSIONS

The review of the available hydrogeological reports and published groundwater quality data indicate that:

- The hydrogeological environment associated with the Proterozoic bedrock formations of Broken Hill have been characterised as being generally low yielding;
- The occurrence and flow of groundwater is controlled by distinct structural features present across the region, with the rock mass itself having negligible capacity for storage or transmission of groundwater; and
- Groundwater quality in the Broken Hill area is generally unsuitable for human consumption and crop irrigation, and is marginal for stock watering.

The potential impact of additional dewatering associated with the proposed western mineralization mining has been evaluated with regard to the surrounding groundwater users, surface waters and groundwater dependant ecosystems. On the basis of the data available and our current understanding of the CHM, the potential impacts are summarised as follows:

- Groundwater users in the vicinity of the mine lease are considered unlikely to be affected by mine dewatering. Water level data from wells installed in perched groundwater systems proximal to the site (but separated by structural features) indicate that the effects of historical and current dewatering have not propagated across the structural features;
- Assuming that Perilya continues to dewater SW of the site, it is estimated that steady state groundwater inflow with mining at 800 m depth at the site may be around 6 to 6.5 L/s. The actual inflow could be greater if high permeable zones within the rock mass are encountered during mining, but this is considered unlikely according to the current mine plan;
- The deepening and extension of mining within the site area will cause steepening of the drawdown cone at depth. There is expected to be very little if any change in the drawdown cone near the surface; and
- Groundwater quality associated with the bedrock is poor and is unsuitable for most uses due to high salinity and high natural concentrations of trace metals;
- It is generally considered that the hydraulic connection between the shallow surface aquifers and bedrock groundwater is poor to non-existent, therefore, mine dewatering is not expected to directly impact surface water quality or quantity in the vicinity of the mine lease;
- Groundwater dependent ecosystems, if present along nearby creeks, are considered to be at low risk from the proposed mining operations as a result of the structural features (i.e. major shear zones) that are present between the mine lease area and the surface water systems closest to the mine lease; and
- Advice from Country Water indicates that the estimated water contribution from town water supply in the mine water plan is available and will not impact on the security of the water supply for Broken Hill.



In summary, the results of the hydrogeological assessment suggest that the groundwater resource in the vicinity of the mine lease area is characterised by low yields, poor quality, and is hydraulically isolated from potential sensitive receptors identified in the vicinity of the mine lease. As such the proposed mining operations are considered to represent a low risk to the groundwater resources in the vicinity of the mine lease area.

## 6.0 REFERENCES

ADWG, 2004. Australian Drinking Water Guidelines, National Health and Medical Research Council (NHMRC) and Natural Resource Management Ministerial Council (NRMMC).

ANZECC and ARMCANZ, 2000. Australian and New Zealand Guidelines for Fresh and Marine Water Quality, Australian and New Zealand Environment and Conservation Council and Agriculture and Resource Management Council of Australia and New Zealand, Paper No 4.

Blampain, P. and Plimer, I. 2006. The Western Mineralisation – Rasp Mine. BHE Conference Broken Hill, 26-28 September, 8-13.

BHGD, 2002. Broken Hill Geoscience Database. NSW Department of Mineral Resources. Version 2.

Corbett, G.J., Phillips, G.N., 1981. Regional retrograde metamorphism of a high grade terrain: the Willyama Complex, Broken Hill, Australia. *Lithos*, 14, 59–73.

Caritat, P. de, Kirste, D., Carr, G. and McCulloch, M. 2005. Groundwater in the Broken Hill region Australia: recognising interaction with bedrock and mineralization using S and Sr and Pb isotopes. *Applied Geochemistry*, 20, 767-787

Caritat, P. de, Kirste, D., Dann, R., Hutcheon, I., 2002. Groundwater composition in the Broken Hill area: salinity and mineral exploration applications. In: Phillips, G.N., Ely, K.S. (Eds.), *Proceedings and Field Guide, Victoria Undercover* (Benalla, VIC, 30 April–2 May 2002). CSIRO Publishing, Collingwood, pp. 275–278.

Forbes, C.J., Betts, P.G. and Lister, G.S. 2005. Synchronous development of Type 2 and Type 3 fold interference patterns: evidence for recumbent sheath fold in the Allendale Area, Broken Hill, NSW, Australia. *Journal of Structural Geology*, 26, 113-126.

Haydon, R.C. and McConachy, G.W. 1987. The stratigraphic setting of the Pb–Zn–Ag mineralisation at Broken Hill. *Economic Geology*, 82, 826–856.

Laing, W.P., Majoribanks, R.W. and Rutland, R.W.R. 1978. Structure of the Broken Hill mine area and its significance for the genesis of the ore bodies. *Economic Geology*, 73, 1112-1136.

Majoribanks, R.W., Rutland, R.W.R., Glen, R.A. and Laing, W.P. 1980. The structure and tectonic evolution of the Broken Hill region, Australia. *Precambrian Research*, 13, 209-240.

NRAtlas, 2008. NSW National Resource Atlas, available online <http://www.nratlas.nsw.gov.au/>

NZG, 2006. The potential of groundwater supply and aquifer storage and recovery in the Broken Hill area. 39 p. available online: [http://www.brokenhill.nsw.gov.au/files/4196/File/AppendixB\\_Groundwater\\_Consultant.pdf](http://www.brokenhill.nsw.gov.au/files/4196/File/AppendixB_Groundwater_Consultant.pdf)

Rothery, E. 2001. Tectonic origin of the shape of the Broken Hill lodes supported by their structural setting in a high grade shear zone. *Australian Journal of Earth Sciences*, 48, 201-220.

Ruperto, L., and de Caritat, P., 2006. Geological review of the southern Curnamona region. CRC LEME Open File Report 183.

Stevens, B.P.J., Barnes, R.G., Brown, R.E., Stroud, W.J., Willis, I.L., 1988. The Willyama Supergroup in the Broken Hill and Euriowie Blocks, New South Wales. *Precambrian Research*, 40/41, 297–327.

Williams, P.F. and Vernon, R.H. 2001. Origin of vertical lineation in conjugate transcurrent shear-zones at Broken Hill, Australia. *Tectonophysics*, 335, 163-182.

Willis, I.L., Brown, R.E., Stroud, W.J., Stevens, B.P.J., 1983. The early Willyama Supergroup; stratigraphic subdivision and interpretation of high to low grade metamorphic rocks in the Broken Hill Block, New South Wales. *J. Geol. Soc. Aust.* 30, 195–224.

## **7.0 LIMITATIONS**

Your attention is drawn to the following limitations, which must be read in conjunction with this report. This report has been prepared in accordance with the agreement between Broken Hill Operations Pty Ltd and Golder Associates Pty Ltd (Golder Associates). The services performed by Golder Associate have been conducted in a manner consistent with the level of quality and skill generally exercised by members of its profession and consulting practice. No warranty or guarantee of site conditions is intended.

This report is solely for the use of the client and any reliance of this report by third parties shall be at such party's sole risk and may not contain sufficient information for purposes of other parties or for other uses. This report shall be presented in full and may not be used to support any other objective than those set out in the report, except where written approval with comments are provided by Golder Associates.

The information in this report is considered to be accurate at the date of issue in accordance to the current conditions of the site. It is based solely on the site conditions encountered at the time of the site visit, supplemented by the historical information and data described in the report. No assurance is made regarding changes in conditions subsequent to the time of the site visit or issue of this report.

In evaluating the study area, Golder Associates has relied in good faith on information provided by individuals as noted in this report. We believe that the information provided by the various personnel interviewed and information from documents cited is accurate and has been accurately interpreted; however Golder does not provide any guarantees in this regard.

We accept no responsibility for any deficiency, misstatements or inaccuracies contained in this report as a result of omissions, misinterpretation or fraudulent acts of the persons interviewed or contacted. This assessment was carried out using information available from various agencies and no assurance is made regarding the accuracy or completeness of this information.

No sampling or chemical analysis of any kind at or in the vicinity of the subject site was conducted as part of this assessment.

## 8.0 IMPORTANT INFORMATION

Your attention is drawn to the document - "Important Information about your Environmental Site Assessment", which is included in Appendix C of this report. The statements presented in this document are intended to advise you of what your realistic expectations of this report should be, and to present you with recommendations on how to minimise the risks associated with this project. The document is not intended to reduce the level of responsibility accepted by Golder Associates, but rather to ensure that all parties who may rely on this report are aware of the responsibilities each assumes in so doing.

We would be pleased to answer any questions about this important information from the reader of this report.

### GOLDER ASSOCIATES PTY LTD

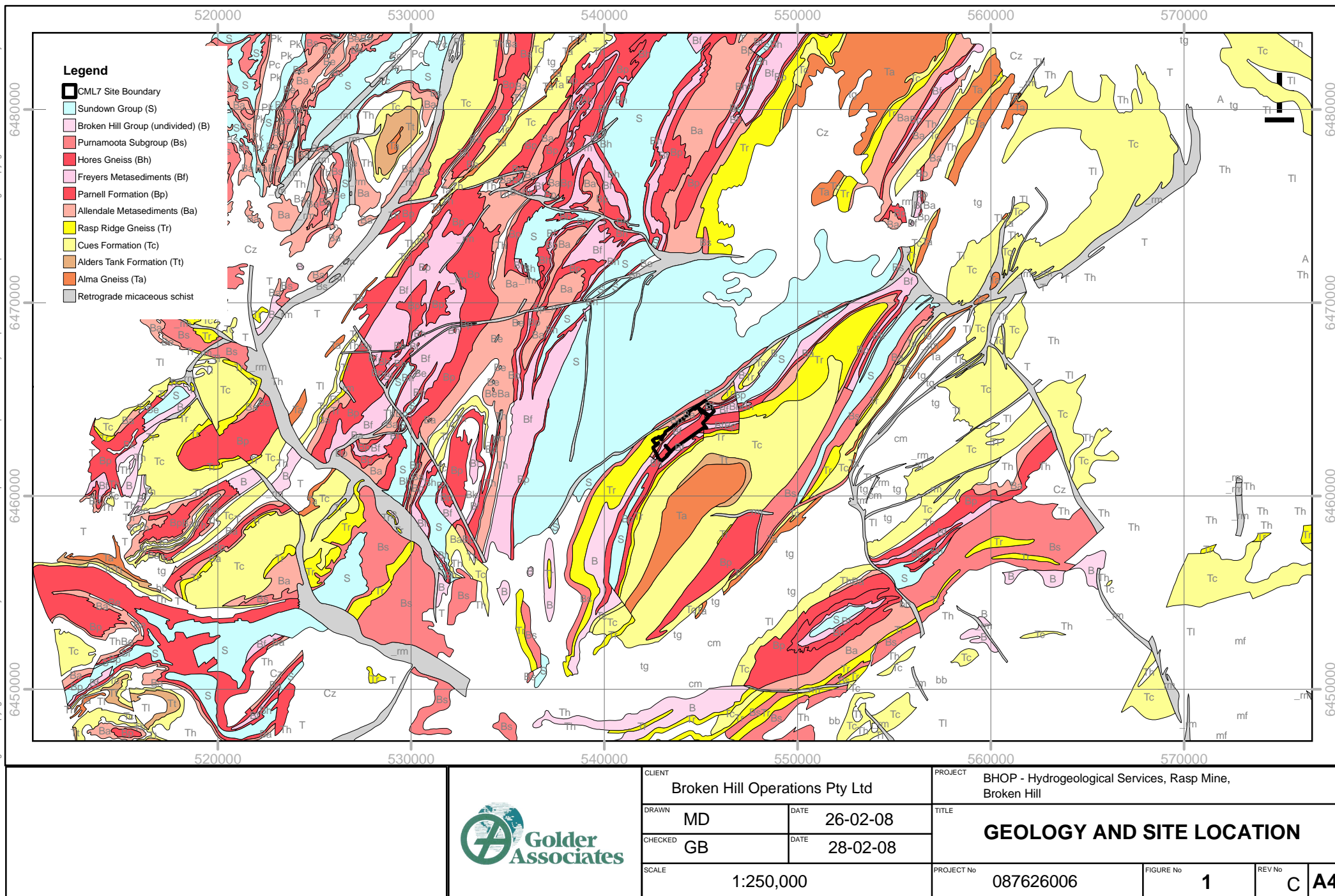


Dr Lange Jorstad  
Senior Hydrogeologist

LBJ,MD,JRB,RF/gb,ikh,cpm/lbj,md,jrb  
J:\hyd\2008\087626006\_BHOP\_Rasp Mine\Correspondence Out\Report\_Draft\_Final\087626006\_003\_R\_Rev0\_Draft.doc

## Figures

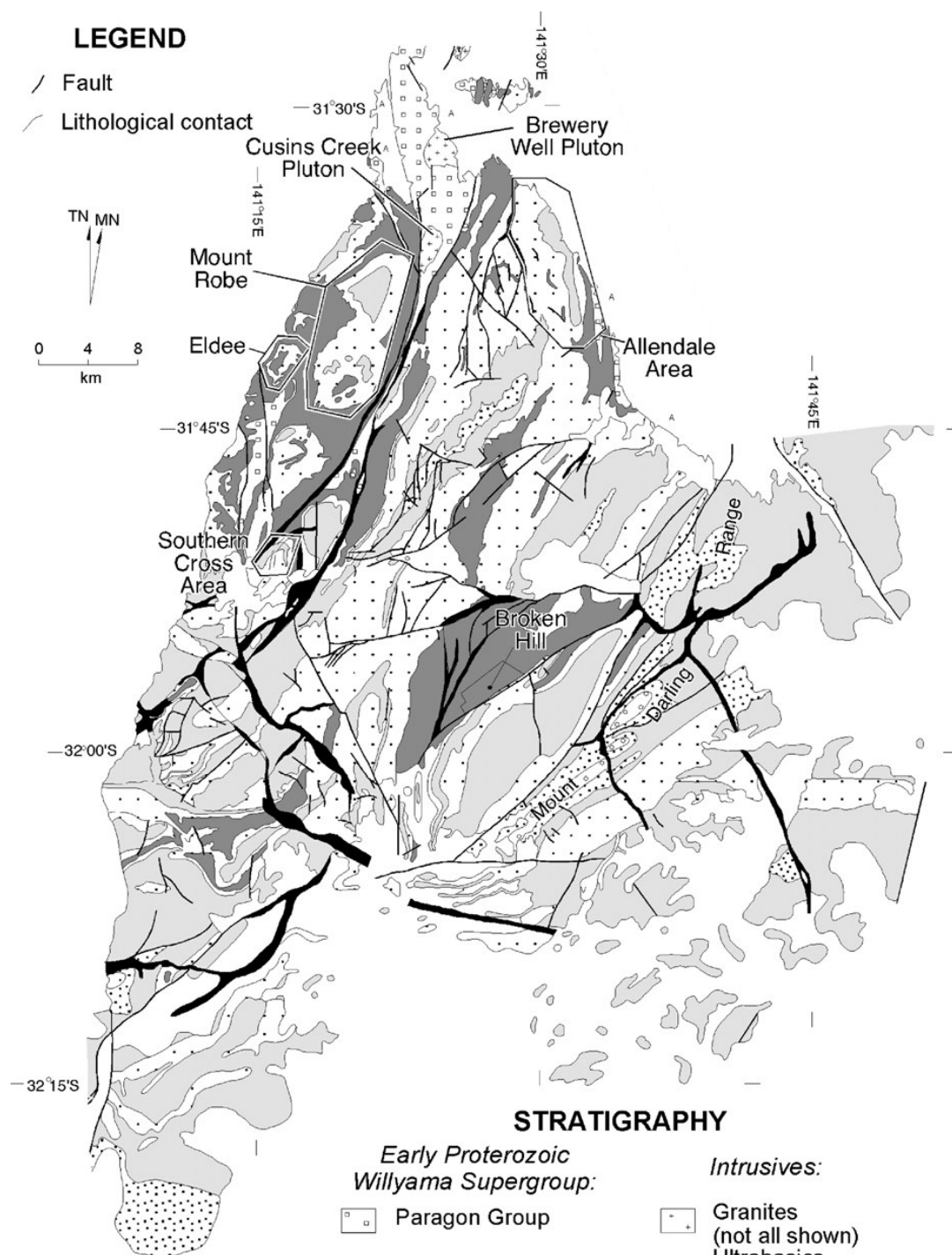
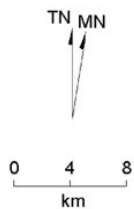
Information contained on this drawing is the copyright of Golder Associates Pty. Ltd. Unauthorised use or reproduction of this plan either wholly or in part without written permission infringes copyright. © Golder Associates Pty. Ltd.



File Location:  
Note: The \* beside the typed initials denotes the original drawing issue was signed or initialed by that respective person.

## LEGEND

- / Fault
- Lithological contact



## STRATIGRAPHY

### Early Proterozoic Willyama Supergroup:

- Paragon Group
- Sundown Group
- Broken Hill Group
- Thackaringa Group
- Thorndale Composite Gneiss
- Clevedale Migmatite

### Intrusives:

- Granites (not all shown)
- Ultrabasics (not all shown)

### Late Proterozoic:

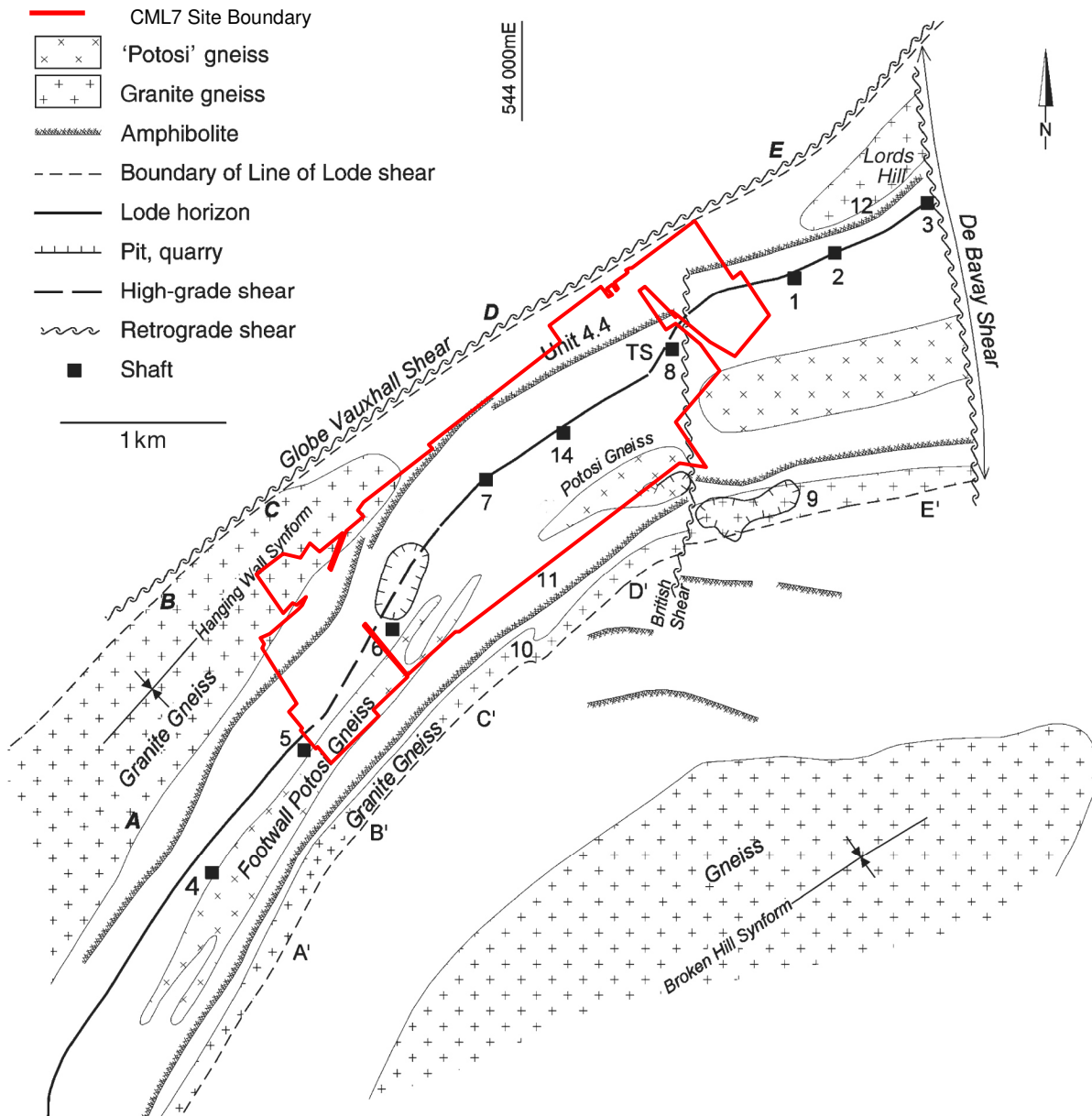
- Adelaidean
- No outcrop
- Broad shear zone

Source: Forbes et al., 2005




CLIENT Broken Hill Operations Pty Ltd		PROJECT BHOP – Hydrogeological Services, Rasp Mine, Broken Hill	
DRAWN MD	DATE 25.02.2008	TITLE <b>Geological Map of Broken Hill</b>	
CHECKED LBJ	DATE 27.02.2008		
SCALE N.T.S		PROJECT No 087626006	FIGURE No <b>2</b>
		REV No <b>C</b>	<b>A4</b>

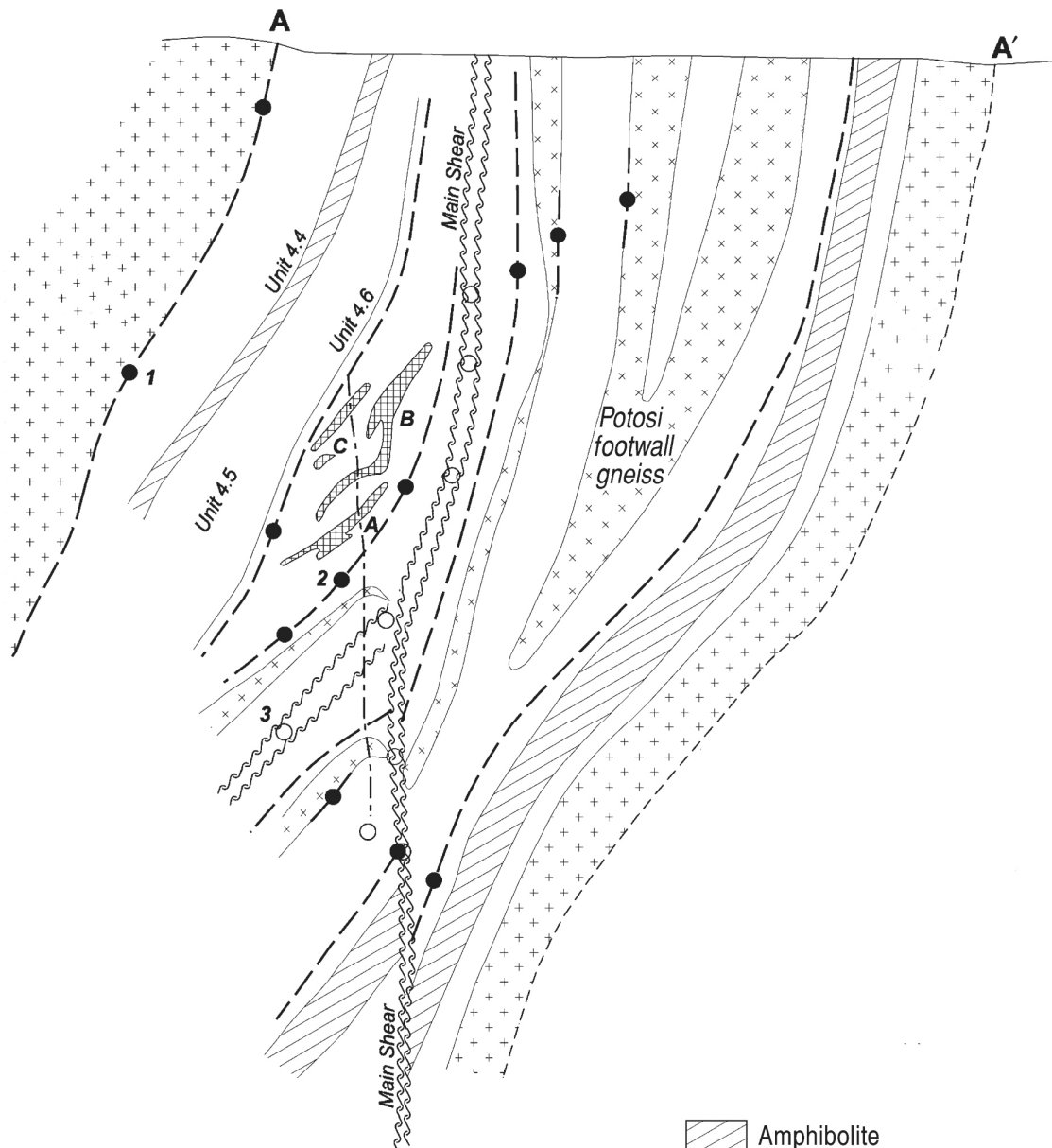




- 1 - Pasminco North Mine No. 1 Shaft
- 2 - Pasminco North Mine No. 2 Shaft
- 3 - Pasminco North Mine No. 3 Shaft
- 4 - NBHC Shaft at Pasminco Southern Operations
- 5 - ZC Old Main Shaft
- 6 - Kintore Shaft
- 7 - Delprat's Shaft
- 8 - Thompson's Shaft
- 9 - Readymix Main Quarry
- 10 - Otto's Hill
- 11 - Amphibolite
- 12 - De Bavay Quarry
- 14 - Block 14 Shaft

Modified after: Rothery, 2001; and Haydon & McConachy, 1987

	CLIENT Broken Hill Operations Pty Ltd		PROJECT BHOP – Hydrogeological Services, Rasp Mine, Broken Hill			
	DRAWN MD	DATE 25.02.2008	TITLE <b>Geology of the Broken Hill Line of Lode</b>			
	CHECKED LBJ	DATE 27.02.2008				
	SCALE N.T.S		PROJECT No 087626006	FIGURE No <b>3</b>	REV No <b>C</b>	<b>A4</b>

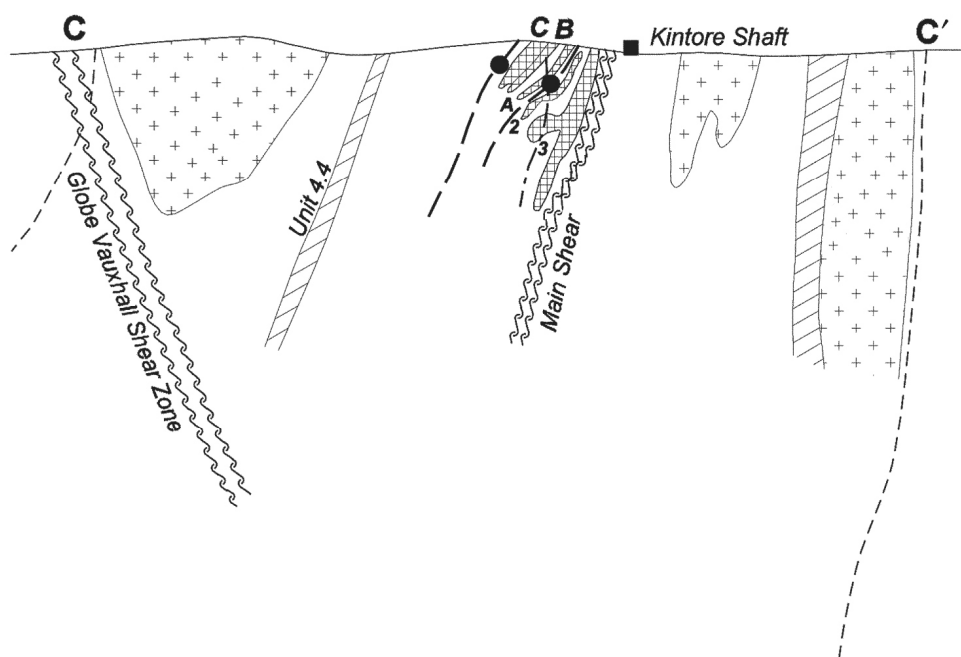
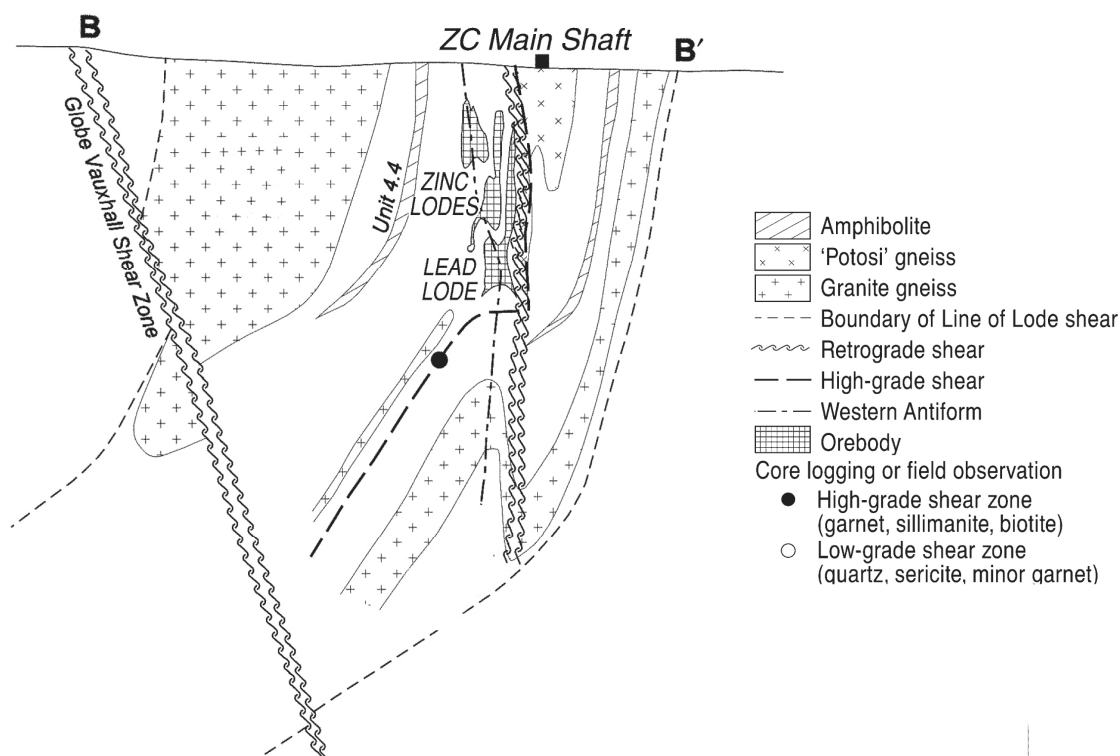


- Amphibolite
- 'Potosi' gneiss
- Granite gneiss
- Boundary of Line of Lode shear
- Retrograde shear
- High-grade shear
- Western Antiform
- Orebody
- Core logging or field observation
  - High-grade shear zone (garnet, sillimanite, biotite)
  - Low-grade shear zone (quartz, sericite, minor garnet)

Modified from: Rothery, 2001



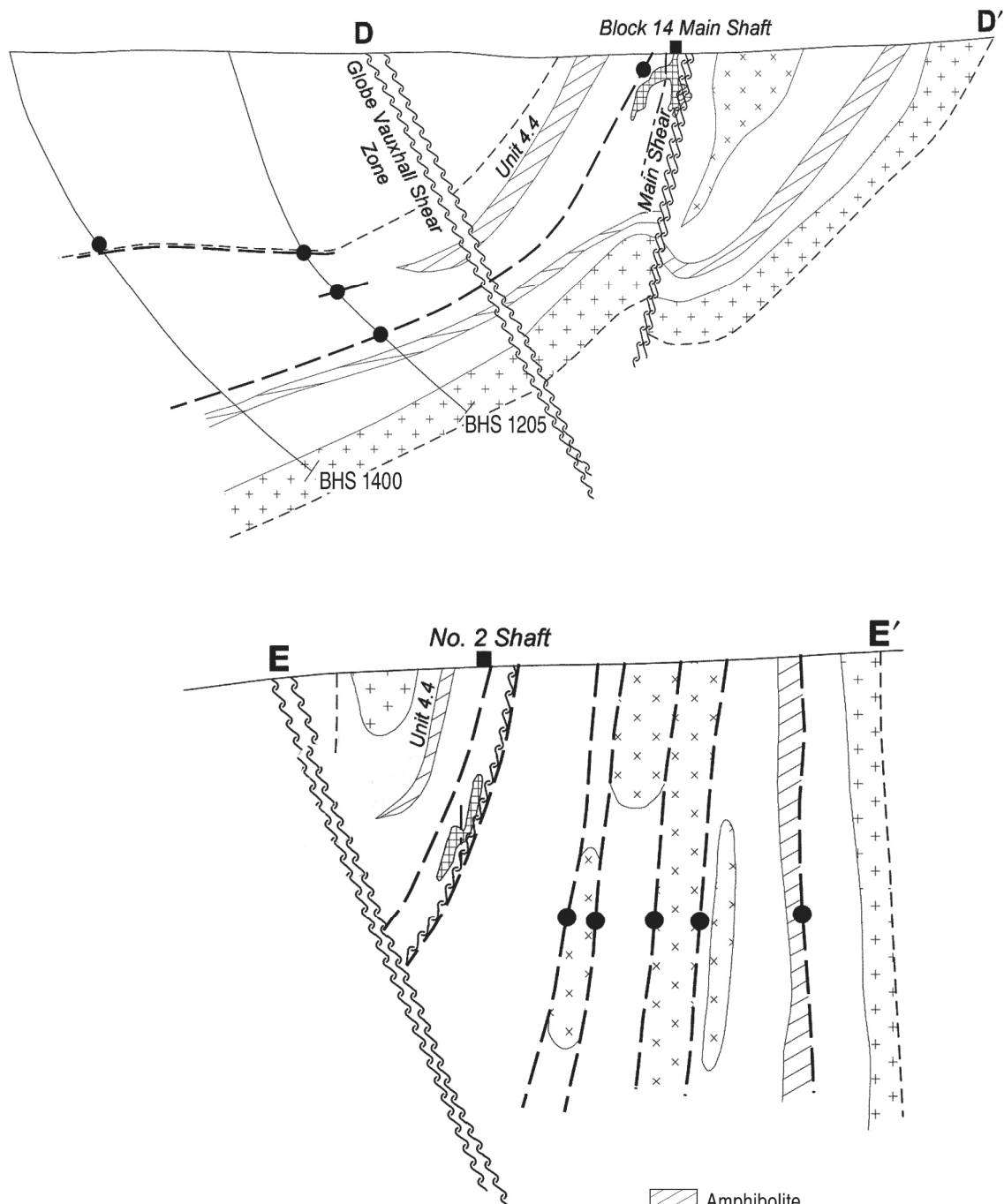
CLIENT Broken Hill Operations Pty Ltd		PROJECT BHOP – Hydrogeological Services, Rasp Mine, Broken Hill	
DRAWN MD	DATE 25.02.2008	TITLE <b>Cross-section A-A'</b>	
CHECKED LBJ	DATE 27.02.2008		
SCALE N.T.S	PROJECT No 087626006	FIGURE No <b>4</b>	REV No <b>C</b> <b>A4</b>




Modified from: Rothery, 2001



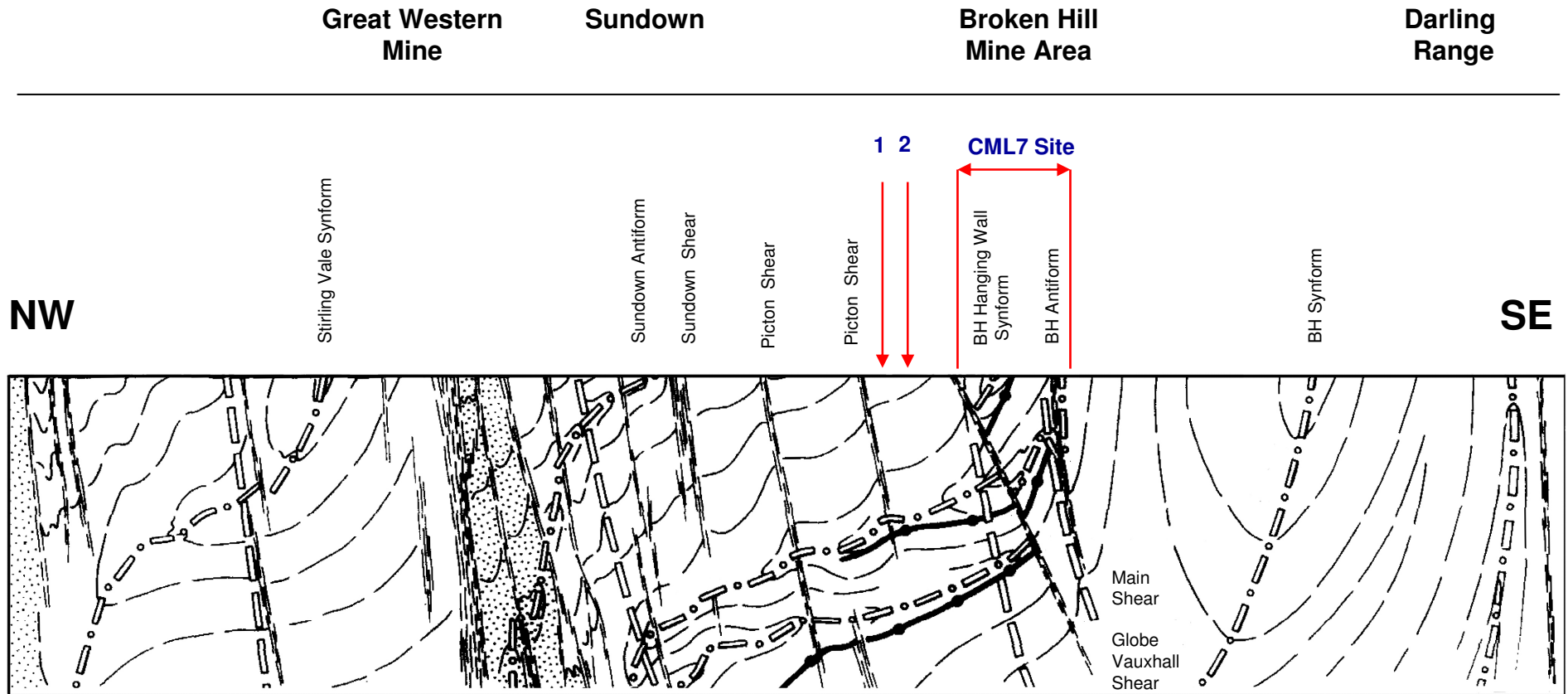
CLIENT Broken Hill Operations Pty Ltd		PROJECT BHOP – Hydrogeological Services, Rasp Mine, Broken Hill	
DRAWN MD	DATE 25.02.2008	TITLE <b>Cross-sections B-B' and C-C'</b>	
CHECKED LBJ	DATE 27.02.2008		
SCALE N.T.S		PROJECT No 087626006	FIGURE No <b>5</b>
		REV No <b>C</b>	<b>A4</b>



Modified from: Rothery, 2001

	CLIENT Broken Hill Operations Pty Ltd		PROJECT BHOP – Hydrogeological Services, Rasp Mine, Broken Hill			
	DRAWN MD	DATE 25.02.2008	TITLE <b>Cross-sections D-D' and E-E'</b>			
	CHECKED LBJ	DATE 27.02.2008				
	SCALE N.T.S		PROJECT No 087626006	FIGURE No 6	REV No C	A4

Information on this drawing is the copyright of Golder Associates Pty Ltd. Unauthorized use or reproduction of this plan either wholly or in part without written permission infringes copyright. © Golder Associates Pty. Ltd.



Modified after: Majoribanks et al., 1980

1 - GW 03404

2 - GW 600132

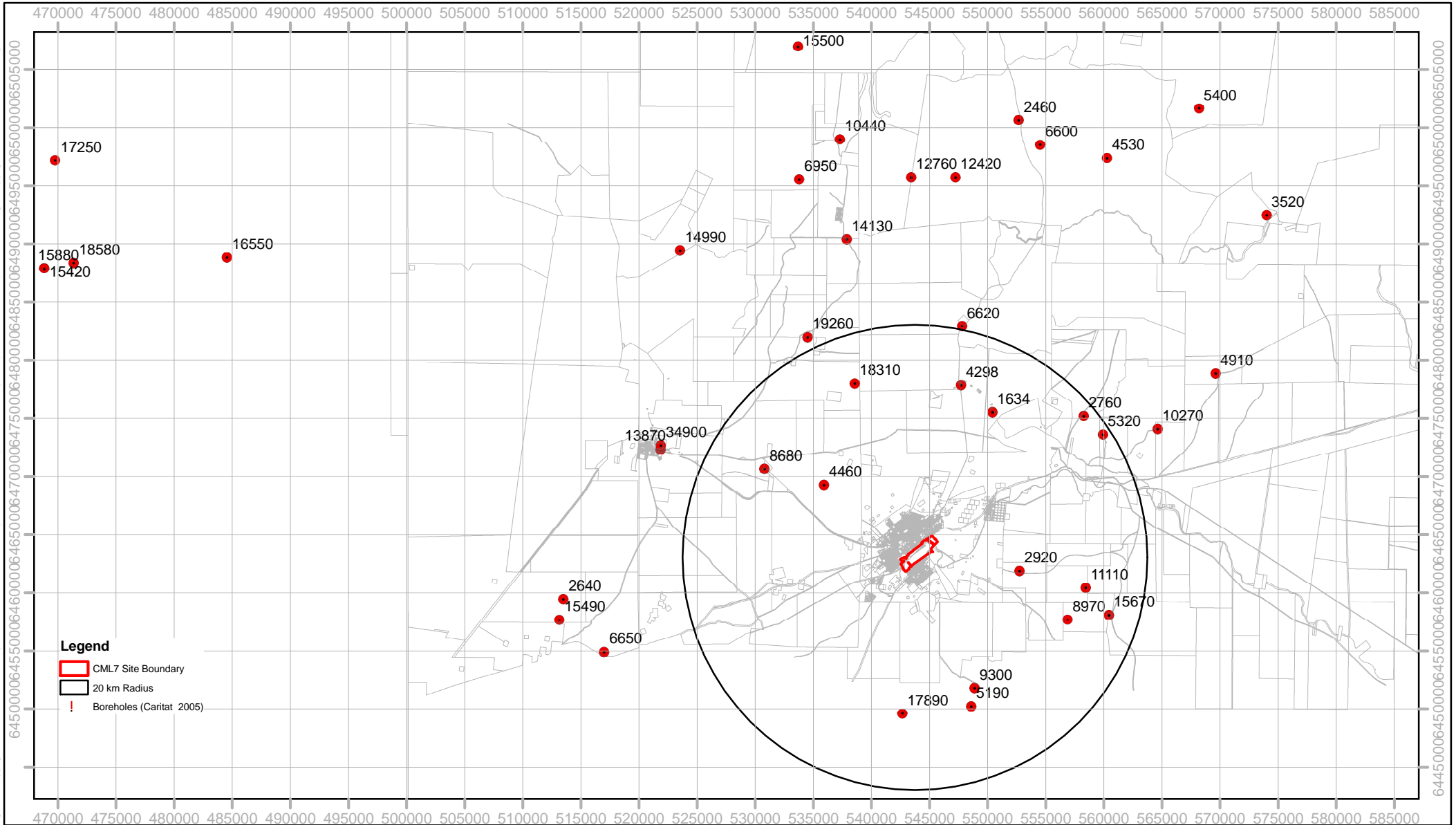



CLIENT Broken Hill Operations Pty Ltd		PROJECT BHOP – Hydrogeological Services, Rasp Mine, Broken Hill	
DRAWN MD	DATE 25.02.2008	TITLE <b>Extended Cross Section</b>	
CHECKED LBJ	DATE 27.02.2008		
SCALE N.T.S		PROJECT No 087626006	FIGURE No 7
		REV No C	A4





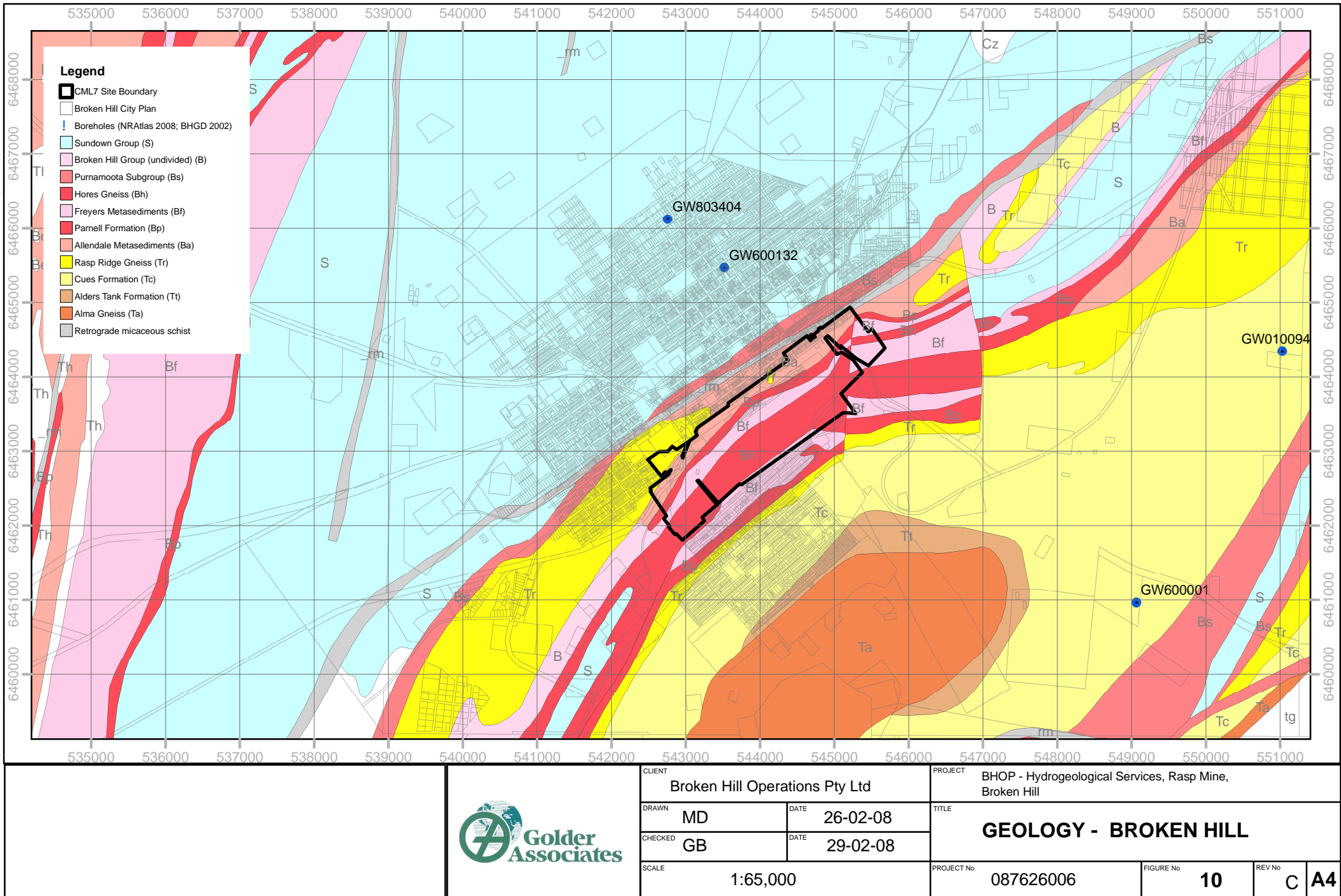
Information contained on this drawing is the copyright of Golder Associates Pty. Ltd. Unauthorised use or reproduction of this plan either wholly or in part without written permission infringes copyright. © Golder Associates Pty. Ltd.



		CLIENT Broken Hill Operations Pty Ltd		PROJECT BHOP - Hydrogeological Services, Rasp Mine, Broken Hill				
		DRAWN MD	DATE 26-02-08	TITLE <b>ELECTRICAL CONDUCTIVITY (µS/cm)</b>				
		CHECKED GB	DATE 29-02-08					
		SCALE 1:450,000		PROJECT No 087626006		FIGURE No 9	REV No C	A4

File Location:  
Note: The \* beside the typed initials denotes the original drawing issue was signed or initialled by that respective person.

Information contained on this drawing is the copyright of Golder Associates Pty. Ltd. Unauthorised use or reproduction of this plan either wholly or in part without written permission infringes copyright. © Golder Associates Pty. Ltd.

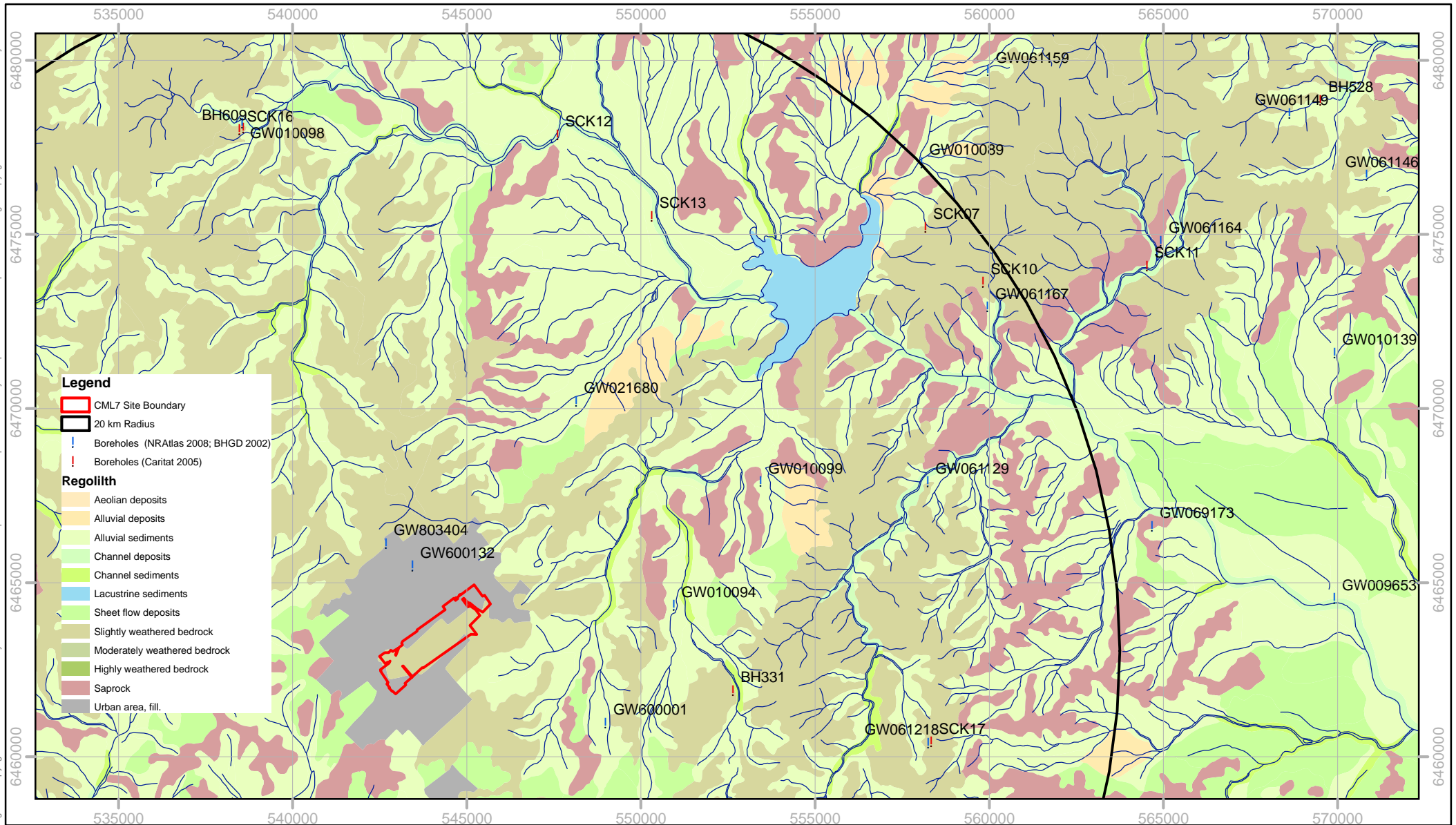


File Location:

Note: The \* beside the typed initials denotes the original drawing issue was signed or initialled by that respective person.



Information contained on this drawing is the copyright of Golder Associates Pty. Ltd. Unauthorised use or reproduction of this plan either wholly or in part without written permission infringes copyright. © Golder Associates Pty. Ltd.



#### Legend

- CML7 Site Boundary
- 20 km Radius
- ! Boreholes (NR Atlas 2008; BHGD 2002)
- ! Boreholes (Caritat 2005)

#### Regolith

- Aeolian deposits
- Alluvial deposits
- Alluvial sediments
- Channel deposits
- Channel sediments
- Lacustrine sediments
- Sheet flow deposits
- Slightly weathered bedrock
- Moderately weathered bedrock
- Highly weathered bedrock
- Saprock
- Urban area, fill.



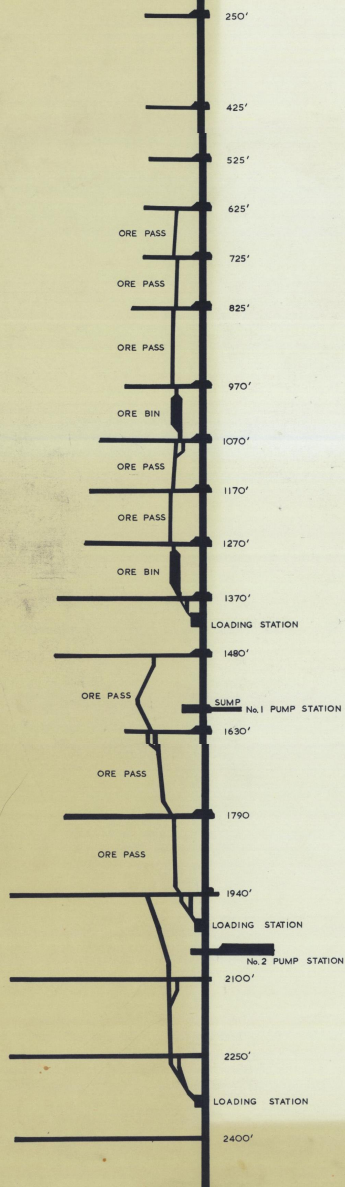
CLIENT Broken Hill Operations Pty Ltd		PROJECT BHOP - Hydrogeological Services, Rasp Mine, Broken Hill		
DRAWN MD	DATE 26-02-08	TITLE <b>SURFACE WATER FEATURES</b>		
CHECKED GB	DATE 28-02-08			
SCALE 1:150,000		PROJECT No 087626006	FIGURE No 11	REV No C A4

File Location:  
Note: The \* beside the typed initials denotes the original drawing issue was signed or initialled by that respective person.

**Appendix A**  
**Background Figures for Groundwater Inflow Estimate**



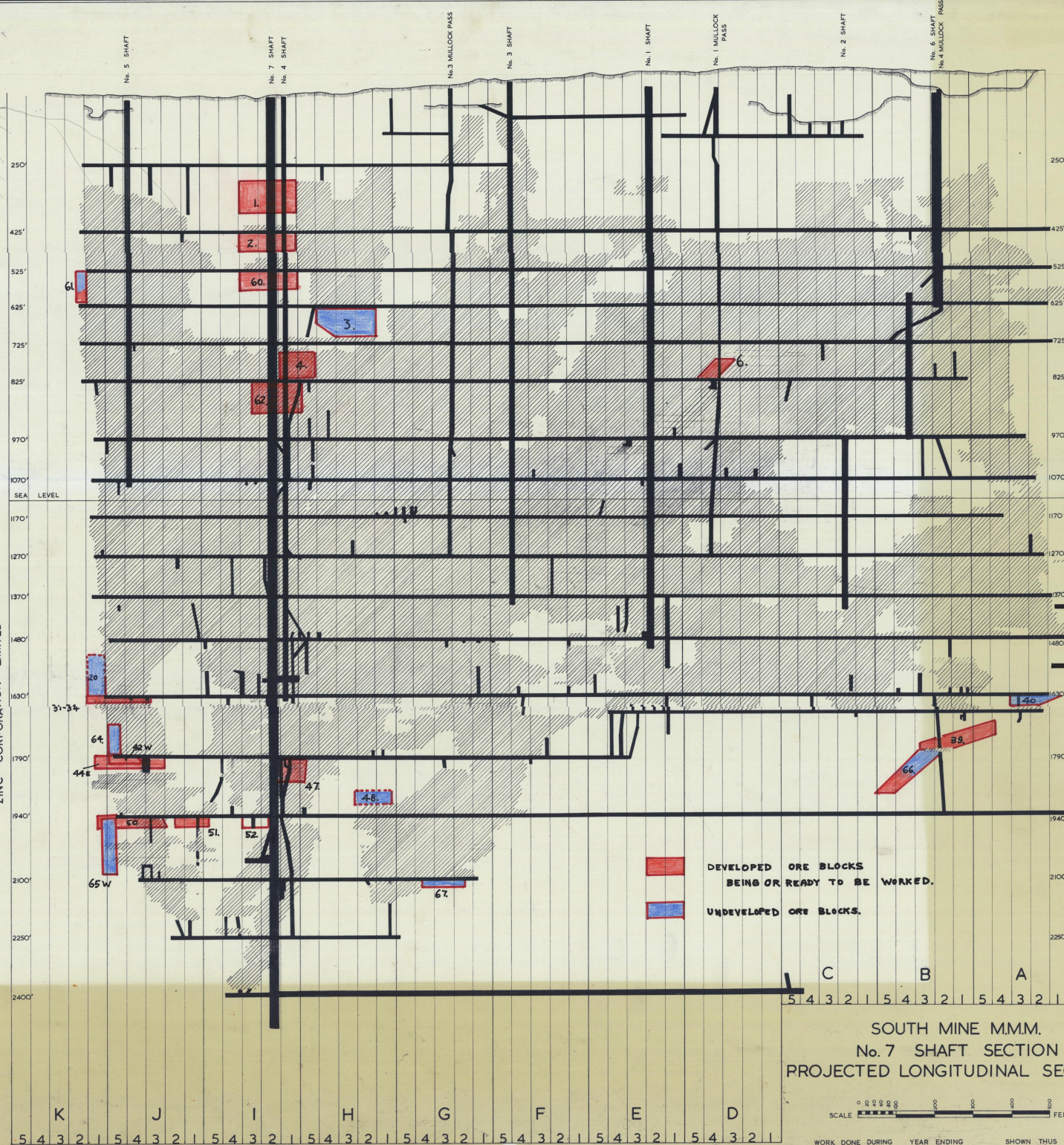
CRUSHER STATION WINDER HOUSE



### No. 7 SHAFT

PROJECTED SECTION ON LINE 11-2

ZINC CORPORATION LIMITED



KINTORE SHAFT SECTION

SOUTH MINE M.M.M.  
No. 7 SHAFT SECTION  
PROJECTED LONGITUDINAL SECTION





## **Appendix B**

### **Compendium of Reference Documents**



Cooperative Research Centre for  
Landscape Environments  
and Mineral Exploration



Australian Government  
Geoscience Australia



OPEN FILE  
REPORT  
SERIES

# GEOLOGICAL REVIEW OF THE SOUTHERN CURNAMONA REGION

*Luisa Ruperto and Patrice de Caritat*

**CRC LEME OPEN FILE REPORT 183**

**January 2006**

CRCLEME

CRC LEME is an unincorporated joint venture between CSIRO-Exploration & Mining, and Land & Water, The Australian National University, Curtin University of Technology, University of Adelaide, Geoscience Australia, Primary Industries and Resources SA, NSW Department of Primary Industries and Minerals Council of Australia, established and supported under the Australian Government's Cooperative Research Centres Program.





**Australian Government**  
**Geoscience Australia**



# **GEOLOGICAL REVIEW OF THE SOUTHERN CURNAMONA REGION**

*Luisa Ruperto and Patrice de Caritat*

**CRC LEME OPEN FILE REPORT 183**

January 2006

© CRC LEME 2006

---

CRC LEME is an unincorporated joint venture between CSIRO-Exploration & Mining, and Land & Water, The Australian National University, Curtin University of Technology, University of Adelaide, Geoscience Australia, Primary Industries and Resources SA, NSW Department of Primary Industries and Minerals Council of Australia.

*Headquarters:* CRC LEME c/o CSIRO Exploration and Mining, PO Box 1130, Bentley WA 6102, Australia

This report presents a brief geological overview of the southern Curnamona Region in South Australia and New South Wales. This project commenced July 2004 and was completed July 2005. A complementary document entitled “Three-dimensional model of the Callabonna Sub-Basin sequence, southern Curnamona Region” by Luisa Ruperto and Malcolm Nicoll (2006) is recommended to be read in conjunction with this report.

**Copies of this publication can be obtained from:**

The Publications Officer, CRC LEME, c/- CSIRO Exploration & Mining, PO Box 1130, Bentley WA 6102, Australia. Information on other publications in this series may be obtained from the above, or from <http://crcleme.org.au>

**Cataloguing-in-Publication:**

Ruperto, L.

Geological review of the southern Curnamona Region

ISBN 1 921039 18 3

1. Geology – South Australia/New South Wales

2. Regolith – South Australia/New South Wales

I. Ruperto, L.

CRC LEME Open File Report 183.

ISSN 1328-4768

**Addresses and affiliations of authors**

**Luisa Ruperto**

Cooperative Research Centre for Landscape  
Environments and Mineral Exploration  
c/- Geoscience Australia  
GPO Box 378  
Canberra ACT 2601  
Australia

**Patrice de Caritat**

Cooperative Research Centre for Landscape  
Environments and Mineral Exploration  
c/- Geoscience Australia  
GPO Box 378  
Canberra ACT 2601  
Australia

© Cooperative Research Centre for  
Landscape Environments and Mineral Exploration  
2006



## CONTENTS

ABSTRACT.....	viii
INTRODUCTION.....	1
PALAEO- TO MESOPROTEROZOIC.....	3
NEOPROTEROZOIC (Adelaidean).....	7
PALAEOZOIC (Cambrian).....	7
MESOZOIC (Cretaceous).....	11
CAINOZOIC (Tertiary).....	12
CAINOZOIC (Quaternary).....	18
CONCLUSION.....	20
REFERENCES.....	22

## LIST OF FIGURES

		Page
Figure 1	General location and spatial relationships between outcropping major geological units of the southern Curnamona Region	2
Figure 2	Major sub-surface geology (including inliers), outcrop areas and faults of the Curnamona Region.	4
Figure 3	Stratigraphic comparison between the three major cratons in central Australia. The relationships described here compare deposition, metamorphism, intrusion, regional deformation and mineralisation (IOCG = iron-oxide copper-gold) events.	6
Figure 4	Extent of Arrowie Basin and location of Benagerie Ridge, Moorowie and Yalkalpo synclines; and Poontana Fracture Zone.	9
Figure 5	3D representation of the depth to base of Cambrian surface. Numbers represent contour values in kilometres.	10
Figure 6	Highly irregular limits of the Eromanga Basin within the Curnamona Region of South Australia. Noted is the Denison-Willouran Divide and its location relative to the structurally prominent Birdsville Track Ridge. The contours depict the base of the Mesozoic.	11
Figure 7	Palaeochannels within Tertiary Callabonna Sub-basin.	14
Figure 8	Schematic sketch of Eyre Formation as it exists today north-south across the 1:250 000 CURNAMONA map sheet. The alternating clay and sand layers are evident particularly in the incised Yarramba palaeochannel displayed here.	15
Figure 9	Schematic cross-section showing the main components of the Namba Formation at Beverley. The Beverley Sands are important as host units to the economic uranium mineralisation here.	17
Figure 10	Diagram showing the complex stratigraphy in the vicinity of the Lake Eyre Basin and adjacent areas (comprising the Eyre and Namba Formations and overlying Willawortina Formation as seen in the western portion of the study area).	19

## LIST OF TABLES

		Page
Table 1	Spatial context of Cainozoic geology between the Callabonna Sub-basin and equivalent units in adjacent basins.	13

## **ABSTRACT**

This report reviews the subsurface geology of the southern Curnamona region, as background information to the associated 3D model of the Cainozoic Callabonna Sub-basin.

The geological setting of this region incorporates multiple basins with complex inter-relationships across the region. Proterozoic basement units are assigned to the Willyama Supergroup, including the Benagerie Ridge basement high. The overlying Arrowie Basin records a significant period of deformation when the Benagerie Ridge served as a structural divide between the Moorowie and Yalkalpo synclinal depocentres during the Late Cambrian. The Mesozoic Eromanga Basin sediments are distinguished based on their spatial relationship to the Denison-Willouran Divide. This predominantly marine succession is overlain by Tertiary Lake Eyre Basin units comprising the Eyre and Namba Formations. These comprise an alternating sequence of lacustrine and fluvial sediments with depositional environments dominated by river channels and/or a lack of major structural relief. Significant drying of the environment during the Quaternary has led to the development of sequences dominated by regolith materials.

## INTRODUCTION

The purpose of this report is to describe the sub-surface geological environment of the Curnamona Region in eastern South Australia and western New South Wales (Figure 1). The region of interest occupies a large arid to semi-arid area located between the geographic coordinates: 139°E/33°S and 143°E/30°S. The relevant 1:250 000 map sheets are OLARY SI54-2, CURNAMONA SH54-14, BROKEN HILL SH54-15, FROME SH54-10 and COBHAM LAKE SH54-11. This review aims to serve as background information to the associated 3D model of the Cainozoic sedimentary fill (Ruperto and Nicoll, 2005).

The Curnamona Region has a complex geological history, including the development of several sedimentary basins that herald distinct depositional events in the area (Figure 2). In the broadest sense, the region can be subdivided into:

- (1) Palaeo- to Neoproterozoic metamorphic basement, which encompasses the Willyama Supergroup, the 'Bimbowrie supersuite' and the Adelaidean sequence;
- (2) Cambrian marginal marine/shelf facies of the Arrowie Basin;
- (3) Mesozoic Frome Embayment of the Eromanga Basin;
- (4) Cainozoic sedimentary fill of the Callabonna Sub-basin of the Lake Eyre Basin, including the fluvio-lacustrine Eyre and Namba Formations; and
- (5) Recent sediments locally hosting gypsum, siliceous, ferruginous and carbonate regolith materials.

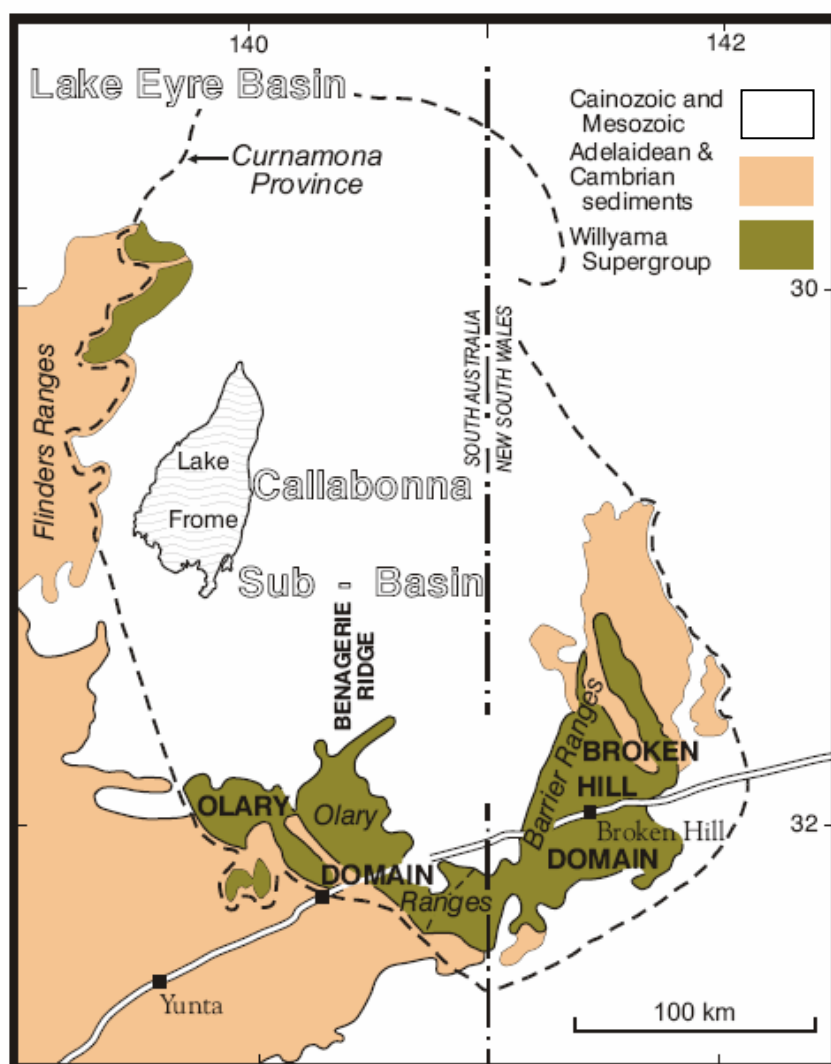
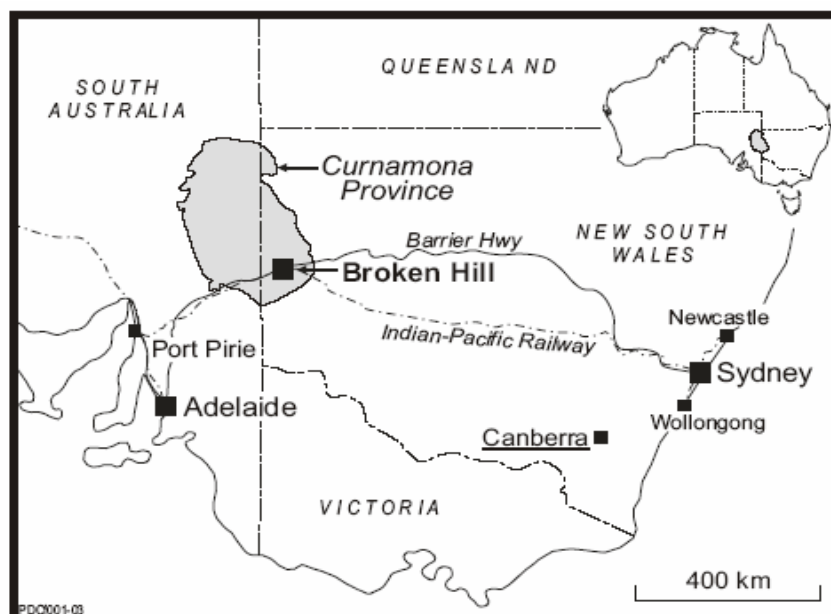


Figure 1. General location and spatial relationships between outcropping major geological units of the southern Curnamona Region. Source: Leyh and Conor (2000).

The high mineral prospectivity of the Curnamona Region arises primarily from the numerous base metal deposits in the Proterozoic basement, including the world-class Pb-Zn-Ag Broken Hill line of lode orebody hosted by the Willyama Supergroup. Other important mineral commodities in the region are Cu-Au, Au, polymetallic mineralisation, Co, rare earth elements, W, Sn and U. The latter mineralisation occurs both in the basement rocks and in the sedimentary sequence of Tertiary palaeovalley fills within the Callabonna Sub-basin as roll-front U deposits.

The prime focus of this study is the mid-late Cainozoic Callabonna Sub-basin, which represents the uppermost 250 m or so of sediments.

### **PALAEO- TO MESOPROTEROZOIC**

The Curnamona Region encompasses a high-grade metamorphic and complexly deformed basement (Stevens et al., 1988; Stevens and Corbett, 1993; Stevens and Burton, 1998). The basement is generally described in the literature as pre-Adelaidean or Palaeoproterozoic to early Mesoproterozoic in age and evolved from a series of rifting events. It crops out in the Willyama Inliers (Olary and Broken Hill Domains) in the southern part of the Region, and at Mt Painter and Mt Babbage in the northwest (Burt et al., 2004). The complex distribution of Palaeo- to Meso-Proterozoic units is illustrated in Figure 2.

The Curnamona Region abuts the Nackara Arc system within the Olary Ranges (Paul et al., 1999). The southernmost of the Proterozoic inliers, the Willyama Inlier, originated as a result of four phases of deformation culminating in high grade metamorphism and syn-tectonic plutonism associated with the Olarian Basin phase (~1700-1600Ma) (Teasdale et al., 2001).

One of the dominant features of this basement is the now-buried Benagerie Ridge, a north-south trending basement high situated to the east of Lake Frome (Figure 2). The ridge is composed of Willyama Supergroup metasediments and 'Bimbowrie Supersuite' felsic and mafic intrusives and bimodal volcanics (Burt et al., 2004).

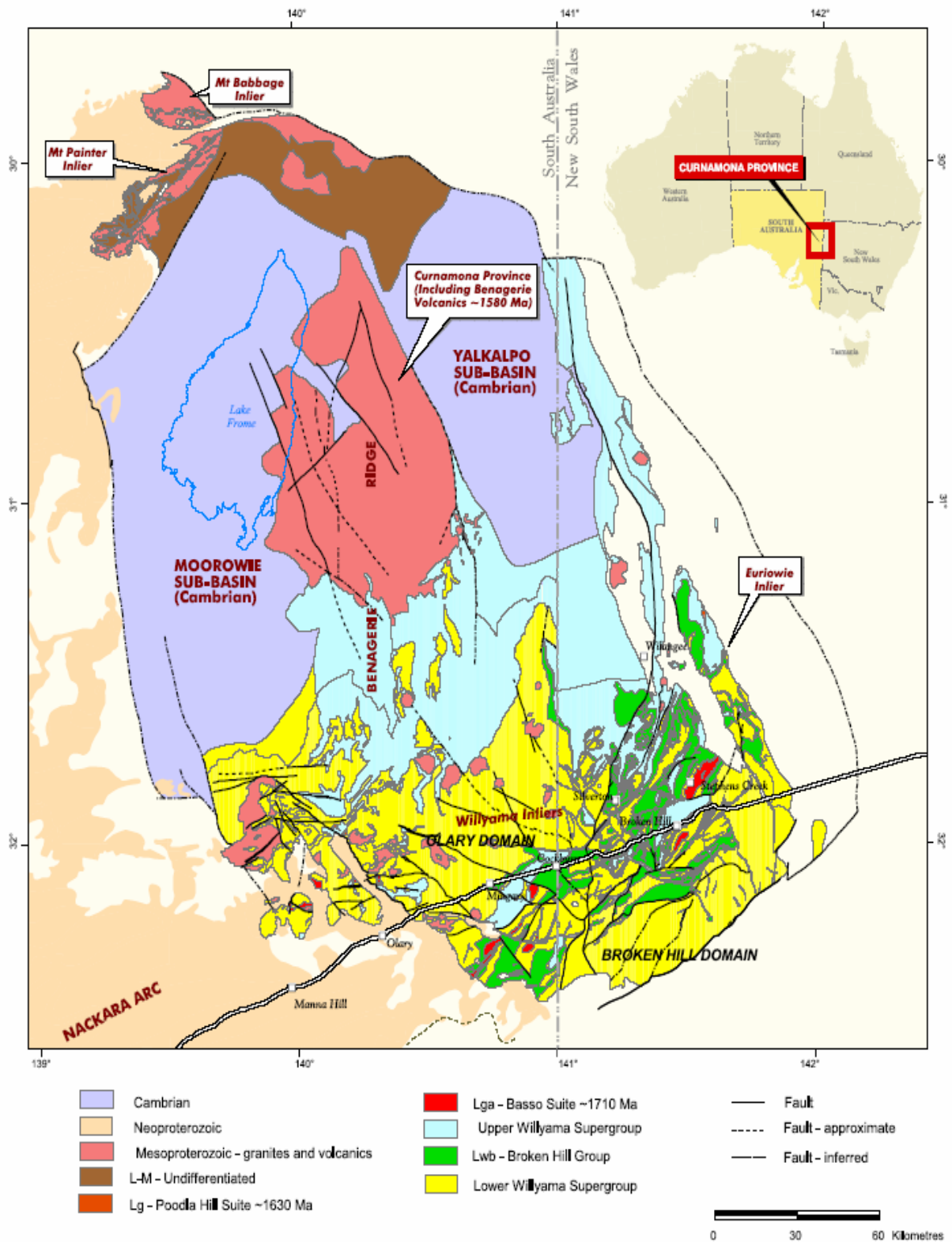


Figure 2. Major sub-surface geology (including inliers), outcrop areas and faults of the Curnamona Region.  
 Source: PIRSA Image AV201310\_014  
[http://www.pir.sa.gov.au/pages/minerals/geology/curnamona/curnamona\\_geology.htm](http://www.pir.sa.gov.au/pages/minerals/geology/curnamona/curnamona_geology.htm).



Burt et al. (2004) have summarised the stratigraphy and tectonic elements of the Curnamona Region as understood to date (see Figure 3). The Province encompasses two major groups of rocks, the Willyama Supergroup and the younger 'Bimbowrie Supersuite', which are recognised within the Olary and Broken Hill Domains and correlate reasonably well across them. Both groups comprise metasedimentary and metavolcanic rocks intruded by various gneiss/granitoid bodies. The Willyama Supergroup hosts the Broken Hill Pb-Zn-Ag deposit in the Broken Hill Group (Figure 2).

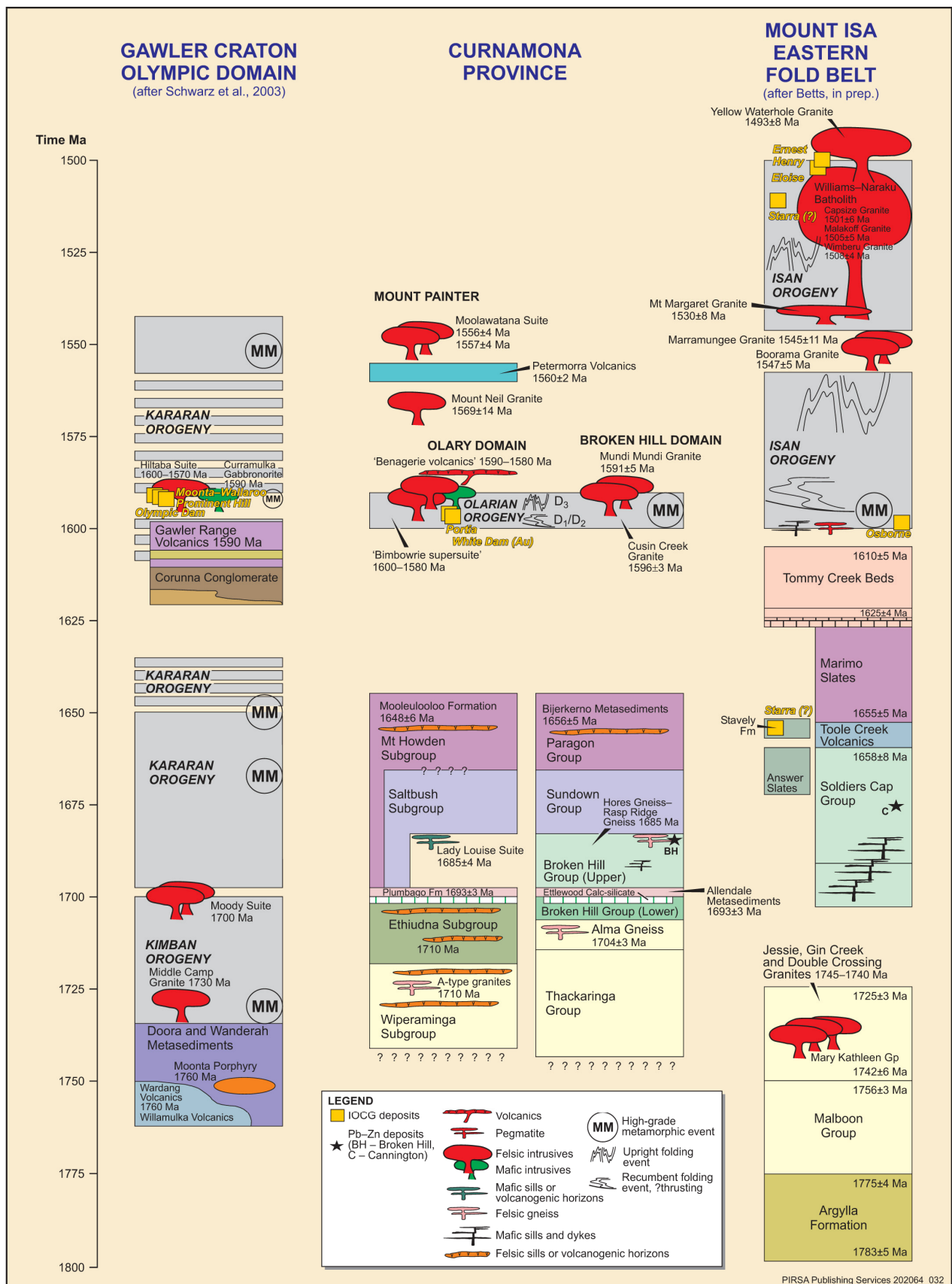


Figure 3. Stratigraphic comparison between the three major cratons in central Australia. The relationships described here compare deposition, metamorphism, intrusion, regional deformation and mineralisation (IOCG = iron-oxide copper-gold) events. Source: Burt et al. (2004).

## **NEOPROTEROZOIC (ADELAIDEAN)**

Neoproterozoic sedimentary rocks record deposition in cratonic, craton-margin and rift-basin settings, with relatively minor associated igneous activity (Preiss et al., 1993; Preiss, 2000), particularly to the west of the Curnamona Region. Sediments of Adelaidean age were deposited mainly in the Adelaide Geosyncline and fall within the Neoproterozoic. The sediments have been subdivided into four chronostratigraphic units: Willouran (oldest), Torrensian, Sturtian and Marinoan (youngest) (Preiss et al., 1993). The Adelaidean sequence is thickest in the Flinders Ranges (forming the western boundary of the Curnamona Region) and in the Mount Lofty Ranges.

The Adelaidean sequence records a transition from

1. mafic volcanism and dyke emplacement followed by deposition of a mixed sequence of evaporitic clastic/ carbonate sediments and minor mafic volcanics with rift basins (Willouran);
2. to minor mafic and local felsic volcanism followed by terrestrial to shallow marine clastics and minor carbonates, proximal clastic wedges interfingering with more distal fine-grained clastic and carbonate sediments, followed by the precipitation of dolomite and sedimentary magnesite in marginal marine and lagoonal environments and coarse sandy facies in source-proximal zones during the first major marine inundation of the Geosyncline (Torrensian);
3. to a phase of basin uplift followed by marine transgression, deposition of glacial sediments during a rifting episode (Sturtian);
4. to a low then rising sea level during which products of the waxing, maximum then waning stages of glaciation were deposited (Marinoan) (Preiss, 2000).

Subsurface Adelaidean units of the Curnamona Region commonly consist of quartzite, quartzite conglomerate, limestone, siltstone, sandstone, shale, dolomite and diamictite forming various groups (Willis et al., 1983; Stevens et al., 1988; Stevens and Corbett, 1993).

## **PALAEOZOIC (CAMBRIAN)**

Up to 5 km of Early to mid Late Cambrian sediments of the vast Arrowie Basin crop out in the Flinders Ranges, unconformably overlying the Curnamona craton, Adelaide Geosyncline and Stuart Shelf basement rocks (Gravestock and Cowley, 1995; PIRSA, 2002). Within the study area, the Arrowie Basin consists of depocenters, the Moorowie and Yalkalpo synclines

or depressions (Figures 4 and 5) separated by the Benagerie Ridge basement high. These two depocenters contain up to 2300 m of Cambrian strata (PIRSA, 2002; Zang, 2002). The Moorowie depocenter is bisected by the Poontana Fracture Zone, a northerly trending wrench fault complex subparallel to the Benagerie Ridge (Callen, 1990; Gravestock and Cowley, 1995). Granitic intrusions were emplaced within the Arrowie Basin sediments only in the Moorowie depocenter (PIRSA, 2002).

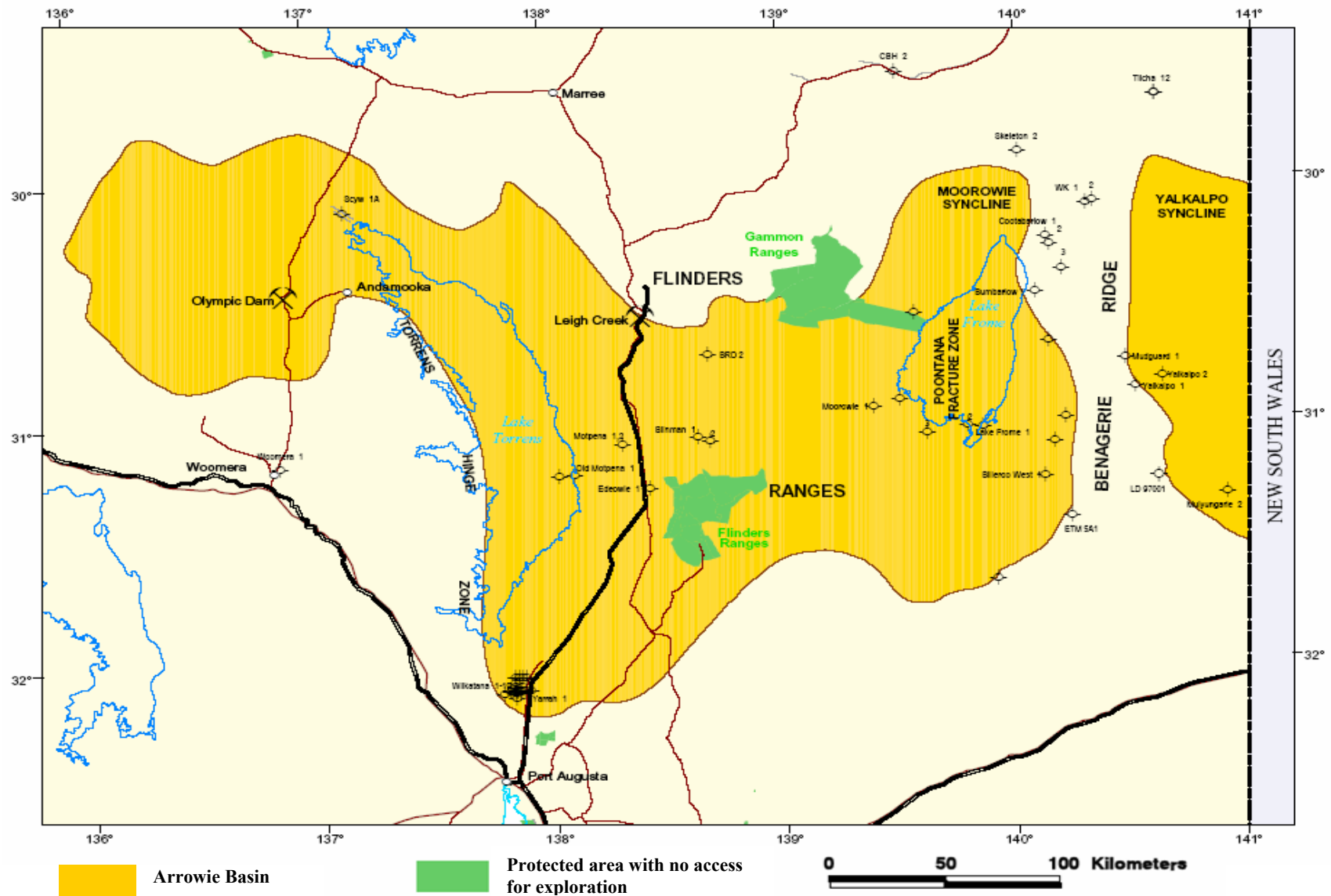


Figure 4. Extent of Arrowie Basin and location of Benagerie Ridge, Moorowie and Yalkalpo synclines, and Poontana Fracture Zone. Source:PIRSA (2002)

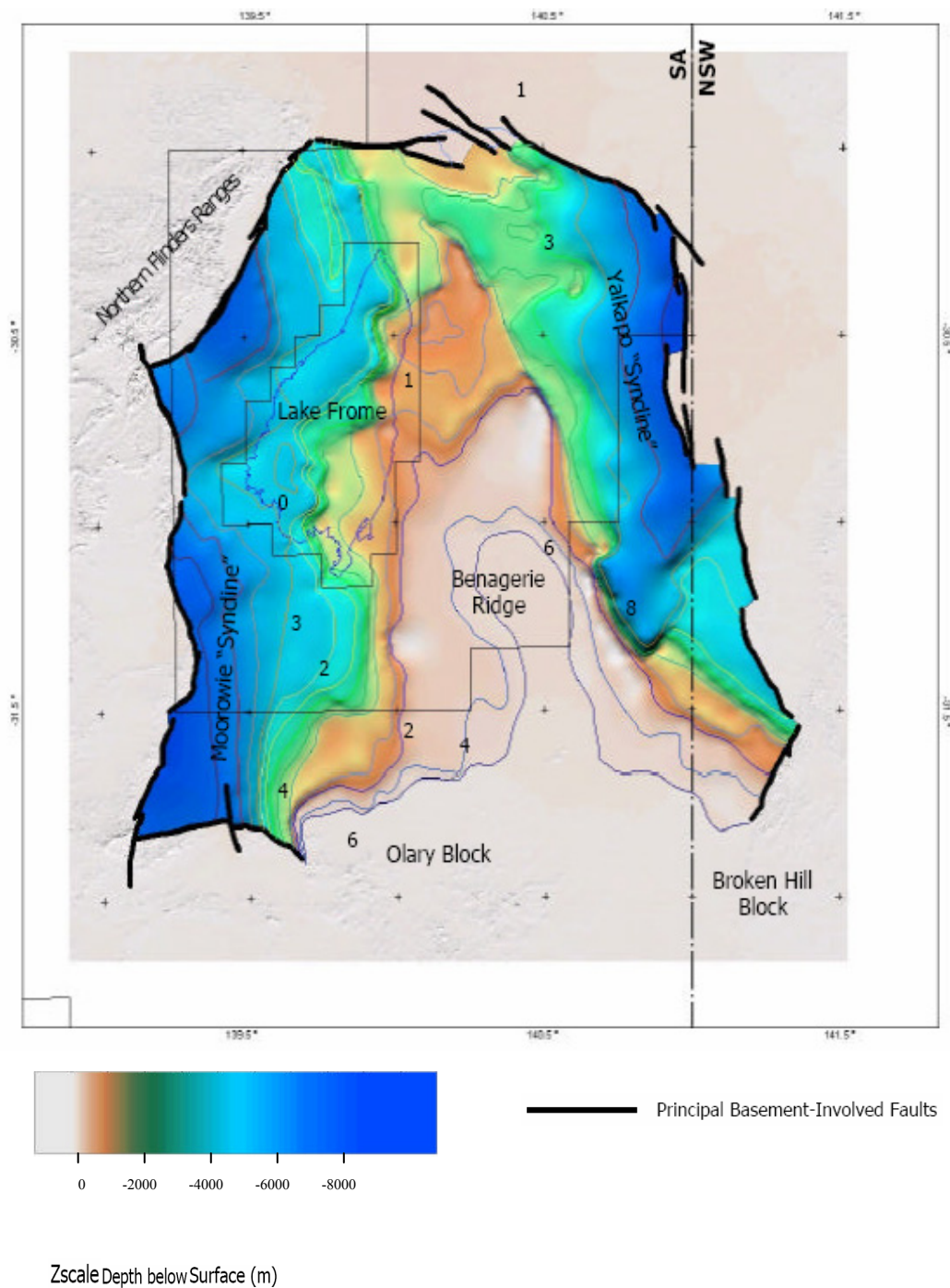


Figure 5. 3D representation of the depth to base of Cambrian surface. Source: Teasdale et al. (2001).

The predominantly subsurface Cambrian Arrowie Basin includes bedded limestone, shales and sandstones deposited within a regressive near-shore to shelf-deltaic marine environment (Callen, 1990). Overlying the Arrowie Basin is the Mesozoic Frome Embayment, a large-scale feature representing a south-eastern depocenter of the Eromanga Basin.



## MESOZOIC (CRETACEOUS)

Evidence of global climate change within the southern Curnamona Region is visible in the Jurassic and Cretaceous geological sequences. Intra-plate tectonism throughout the Early Jurassic was the precursor for the formation of the epicratonic Jurassic-Cretaceous Eromanga Basin in a predominantly terrestrial freshwater environment (Krieg et al., 1995). It is the far south-western portion of this basin that overlies the Curnamona Region and is represented by a thin, variable cover. The structurally faulted Denison-Willouran divide (Figure 6) serves as a predominant partition of the South Australian portion of the Eromanga Basin including a small thin lobe situated beneath Lake Frome. Due to the irregular limits of the Eromanga Basin, it is difficult to definitely determine its spatial extent in the study area.

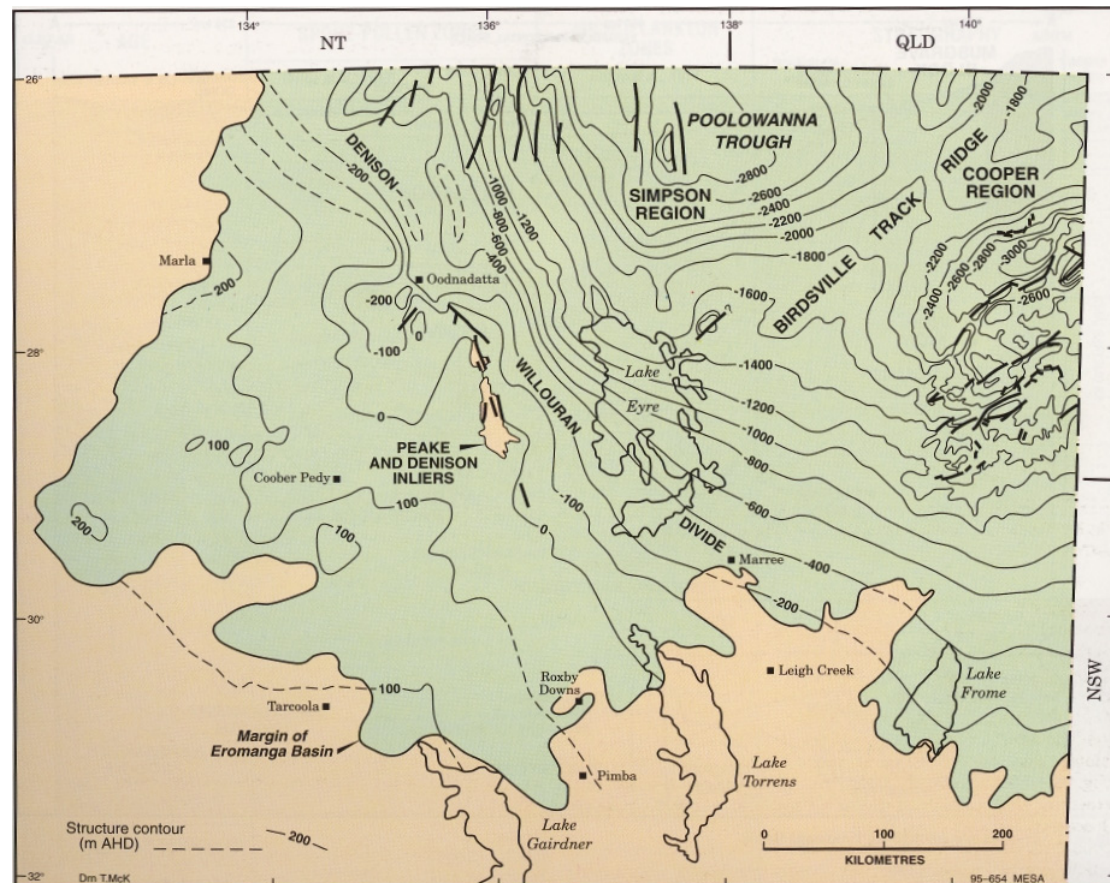


Figure 6. Highly irregular limits of the Eromanga Basin within the Curnamona Region of South Australia. Note the Denison-Willouran Divide and its location relative to the structurally prominent Birdsville Track Ridge. The contours depict the base of the Mesozoic. Source: Krieg et al. (1995)

According to Ker (1958) shale of Late Jurassic Maree Subgroup (of the Neales River Group) and Cadna-Owie Formation represents the Frome Embayment of the Mesozoic Eromanga Basin in this area. The Lower Cretaceous shales appear to be fairly widespread over the area and tend to accumulate to the east of the Benagerie Ridge, in the Yalkalpo syncline (Ker, 1958). The mostly sandstone Cadna-Owie Formation is identified through a fining upward sand sequence with a pebble bed, roughly marking the base of the Mesozoic at a maximum topographic height of 81 metres above sea level (Callen, 1990). Indicative of marginal and shelf marine conditions (Callen, 1990), this thickly laminated, often pebbly formation represents a minor succession of the Eromanga Basin and is significant as the last major transgression onto the continent (Krieg et al., 1995). Within this unit there is widespread evidence for shoreline oscillations along the basin margins (such as in the study area), whilst the central parts of the Eromanga Basin experienced much broader scale transgressive and tectonic effects at this time (Krieg et al., 1995). The Marree Subgroup includes the Bulldog Shale, Coorikiana Sandstone and Oodnadatta Formations with the distribution of these units within the Curnamona Region limited this far south in the Eromanga Basin.

The overlying Cainozoic basins are significantly more complex offering various examples of sedimentation and evidence of shifting depositional environments.

### **CAINOZOIC (TERTIARY)**

Within the study area the broad regional Lake Eyre Basin is subdivided into two smaller basins – the Tirari Sub-basin (formerly known as the Tarkarooloo Sub-basin) and the Callabonna Sub-basin (Callen, 1990), separated by the Birdsville Track Ridge structural divide (Figure 6). Sediments in the Lake Eyre Basin were deposited in three phases:

- i. Late Palaeocene - Mid Eocene (Eyre Formation),
- ii. Late Oligocene - Pliocene (Etadunna and Namba Formations), and
- iii. Pliocene - Quaternary (modern sands).



It is important to note that some units within the Callabonna Sub-basin also occur in adjacent basins. These spatial relationships are described in Table 1.

Lake Eyre Basin	Torrens Basin	Callabonna Basin (includes CURNAMONA)	Murray Basin
Katipiri Formation Tirari Formation	Motpena Palaeosol	Billeroo or Moko Palaeosols	
	Lake Torrens Formation; Pooraka Formation of Port Augusta area	Coonarbine Formation	
	Wilkatana Palaeosol	Moko or Pinpa Palaeosols	
	Pooraka Formation on COPLEY	Eurinilla Formation	
	Hindmarsh Clay and Telford Gravel	Coomb Spring and Millyera Formations	
		Conglomerates of the Pasmore River (Willawortina Fm.)	
	?Avondale Clay	Willawortina Formation	
?Mampuwordu sand		Silcrete and mottled iron palaeosols	Karoonda and Ardrossan Palaeosols
Etadunna Formation		Namba Formation	Geera Clay (in part)
Eyre Formation	Eyre Formation	Eyre Formation	

Table 1. Spatial context of Cainozoic geology between the Callabonna Sub-basin and equivalent units in adjacent basins. Source: Callen, (1990).

The most widespread unit across this broad region is the Late Palaeocene - Mid Eocene Eyre Formation. This comprises a basal pebbly lag, fine to very coarse-grained pyritic and carbonaceous sands, lignite beds and montmorillonitic to kaolinitic clays. These are arranged in two spatially distinct facies: a multilayered aquifer/aquitard system within a formerly active braided river palaeochannel complex (Figure 7) and a blanket cover of fine-grained laminated swamp deposits (Callen, 1990; Callen et al., 1995; Krieg et al., 1990). At the base of this unit are numerous gravel horizons containing rounded quartz, chert and woody fragments that appear to have been sourced from underlying Mesozoic rocks (Krieg et al., 1990).

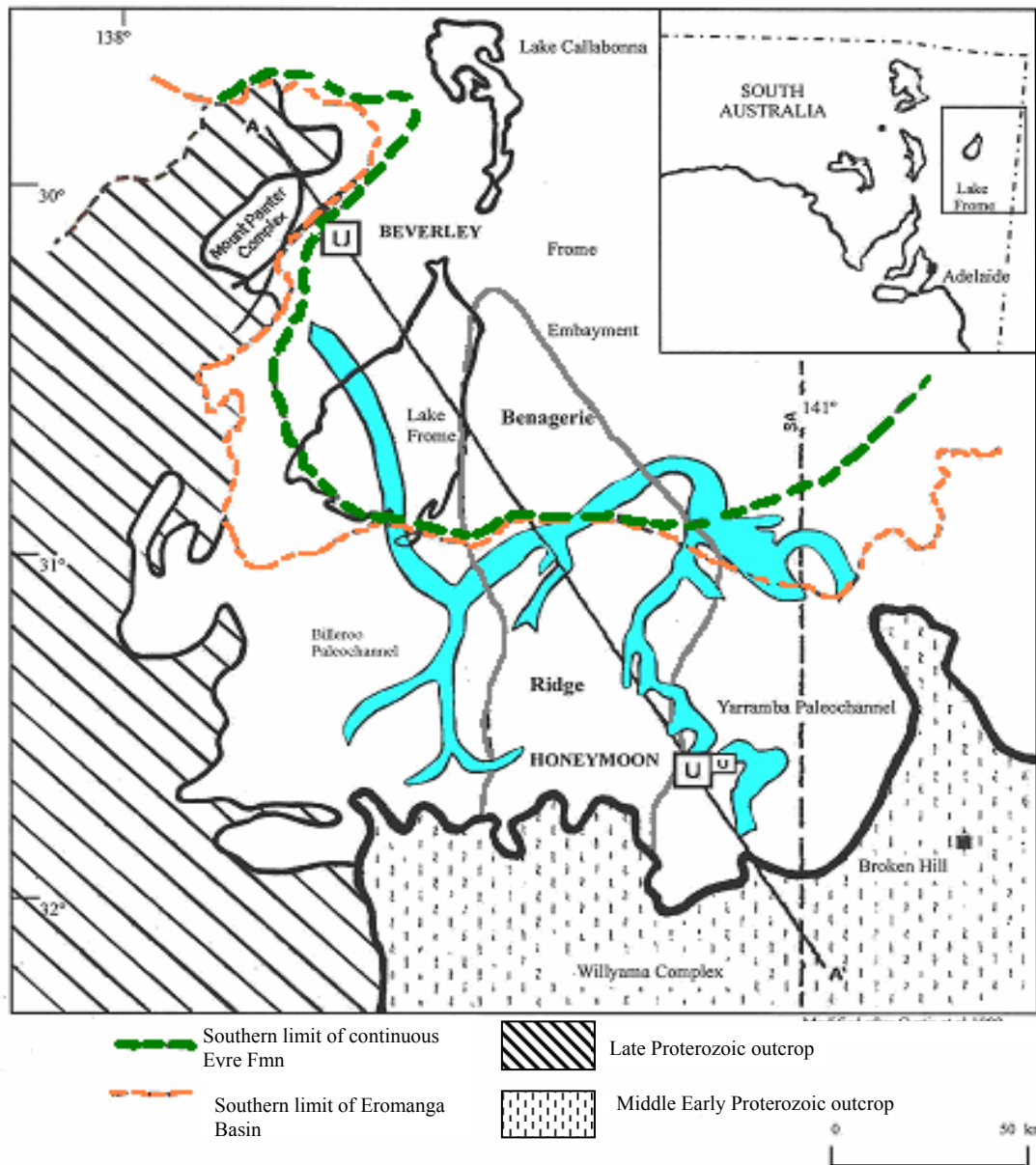


Figure 7. Palaeochannels within Tertiary Callabonna Sub-basin. Source: Modified after Curtis et al. (1990).

A series of alternating clay and sand layers of the Eyre Formation (Figure 8) have been deposited in a large-scale complex incising the Proterozoic basement. This effectively infills the sinuous Yarramba and Billeroo palaeochannels within the southern Curnamona region. The Yarramba palaeochannel containing ~50 m of fluvatile Eyre Formation sediments is situated 70 km south east of Lake Frome, with the base of the palaeochannel approximately 100-120 m below the modern-day land surface (Habermehl, 2000). It comprises a confined multi-layered aquifer system incorporating sandy units of the Upper, Middle and Lower Members of the Eyre Formation, each separated by relatively thin clay seals that separate each aquifer as confining beds (Callen, 1990). The channel sequence can be traced for ~100

km to the north where it connects to a more laterally extensive remnant blanket of Eyre Formation sediments (Habermehl, 2000).

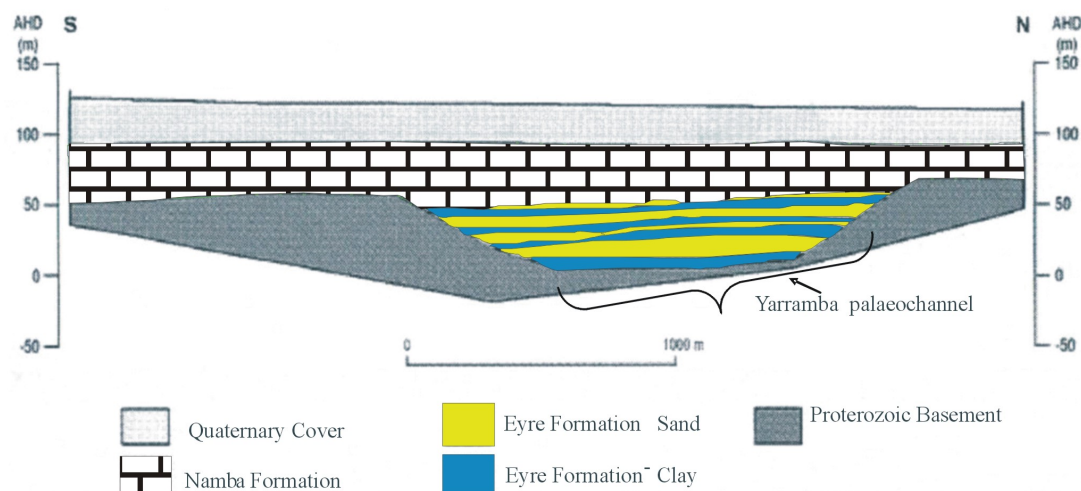


Figure 8. Schematic sketch of the Eyre Formation as it exists today north-south across the 1:250 000 CURNAMONA map sheet. The alternating clay and sand layers are evident particularly in the incised Yarramba palaeochannel displayed here. Source: Habermehl (2000).

Numerous sand bars, ripples and scour marks are buried within the area and are interpreted to reflect a humid environment possibly linked to two distinct depositional phases of Late Palaeocene to early Miocene (Krieg et al., 1990), and the Mid Miocene to Pliocene age. The former coincided with deposition of the Lake Eyre Basin. The latter consists of sandstones, carbonaceous clastics and conglomerates overlain by clays and fine-grained sands and carbonate. This configuration is largely due to incision by younger fluvial action and subsequent deposition of younger, finer-grained materials.

Regional tectonism during the Oligocene and Early Miocene led to the formation of a series of structural domes preceding the configuration of the Birdsville Track Ridge (BTR) (Figure 6), followed later by early Tertiary uplift of the BTR's western portion, the Lake Eyre Basin and the eastern Callabonna Sub-basin (Krieg et al., 1990). Eyre Formation deposited throughout the Palaeocene-Eocene is overprinted by silcrete development. The Cambro-Ordovician Benagerie Ridge to the east of Lake Frome is concealed beneath a thin sequence of micaceous silts of Eyre Formation affinity (Callen, 1990). Krieg et al. (1990) suggested that this may be related to Eocene erosion while the Mid-Late Miocene succession may represent a lacustrine phase within this area, expressed as laminated lacustrine clays in the south-western Callabonna region.

The Eyre Formation is broadly covered by the Miocene Namba Formation (Figure 8), which was deposited in a low-energy lacustrine and braided fluvial environment. This unit forms sheet deposits in the north and is confined to channels to the south-east of Lake Frome (Callen 1990), with the thickest sequences lying east and west of the Benagerie Ridge (Callen et al., 1995). It can be loosely sub-divided into an upper dolomite/smectite unit and a lower kaolinite/illite rich unit. (Callen, 1977; Callen, 1990). The environment at the time of deposition of the Namba Formation was one of fresh to brackish water with distinct channels and floodplain facies which spanned all over the Eyre Formation including the Benagerie Ridge (Callen, 1990).

The widely distributed Namba Formation is generally clastic and carbonaceous with sandy deposits in the channels, and dolomite horizons confined to the western side of the Benagerie Ridge (Callen, 1990). In the vicinity of the Beverley palaeochannel complex, the Namba Formation consists of an interbedded sequence of aquitards and aquifers comprising the basal Alpha Mudstone, overlying Beverley Clay and uppermost Beverley Sands (Figure 9). The latter is a prominent aquifer occupying palaeochannels approximately 120 m below the topographic land surface (Habermehl, 2000). Significantly, these channels have eroded into the Alpha Mudstone restricting water movement between the underlying Cadna-Owie Formation (aquifer) and the overlying Beverley Clay (Habermehl 2000).

The Cainozoic units of the Callabonna Sub-basin have undergone various degrees of weathering as discussed in Tonui and Caritat (2003) and Tan et al. (2004).

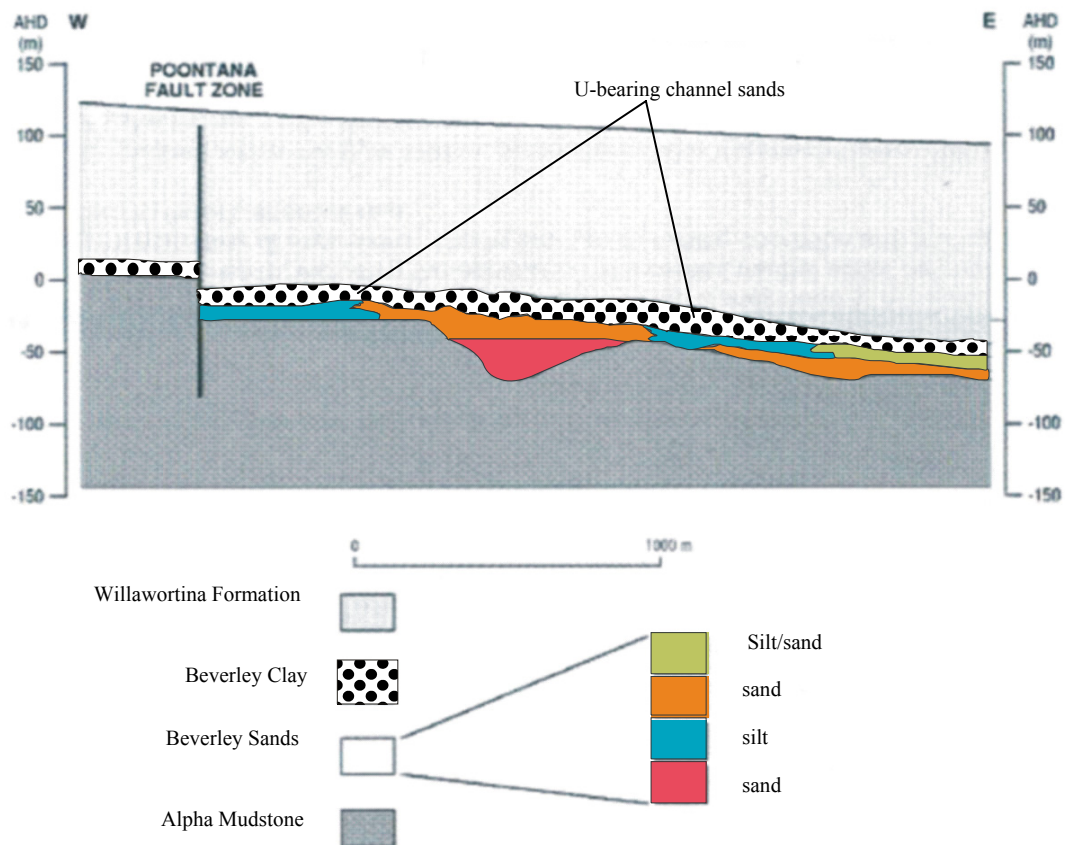


Figure 9. Schematic cross-section showing the main components of the Namba Formation at Beverley. The Beverley Sands are important as host units to the economic uranium mineralisation here. Source: Habermehl (2000).

Towards the end of the Late Neogene period, a significant drying phase resulted in a transition from predominantly lacustrine conditions to the development of dunefields and beach ridges. Silicification of sediments occurred in inter-ridge areas resulting in localised indurations of sands and carbonates. Widespread silcretes and silcrete horizons are a prominent feature and reflect the impact of groundwater or fluctuations in lake levels on the sediments (Krieg et al., 1990). The Late Quaternary period in this region is characterised by major flooding events at about 25-40 ka possibly displaying coastal-like features (Krieg et al., 1990). As well as playa, fan and aeolian deposits, stream networks also appear to have become disconnected at this stage probably as a consequence of the climate drying during the last glacial period (~18 ka) up until the present. A significant phase of dune construction followed (until ~13 ka) with large-scale transverse, longitudinal dune development and even reactivation of older dunes (Krieg et al., 1990).

## **CAINOZOIC (QUATERNARY)**

Sediments deposited over the Callabonna Sub-basin are represented by Quaternary units shown on the 1:250 000 CURNAMONA map sheet. This fluvial upward-fining sequence incorporates dune-dominated fan-like deposits in the west and centre, and laterally extensive undifferentiated brown sands in the east (Callen, 1995).

Overlying the Namba Formation is the ~100 m thick fluvial Willawortina Formation in the western portion of the study area, adjacent to the Flinders Ranges (Habermehl, 2000) (Figures 9 and 10). Associated with anastomosing/single low-sinuosity channels situated in the western and eastern parts of the CURNAMONA 1:250 000 map sheet, this unit is known to extend beneath Lake Frome and crops-out in the Pasmore River in the far west where it is dominated by channel deposition (Callen, 1986). Both fine and a coarse facies appear to be represented, the former comprising a fining-upward cyclical sequence of sandy mud and silty dolomite (Callen et al., 1995). Carbonate-cemented channel conglomerates are overlain by a more gypsiferous variant representing a debris flow derived from braided fan gravels (Callen et al., 1995).



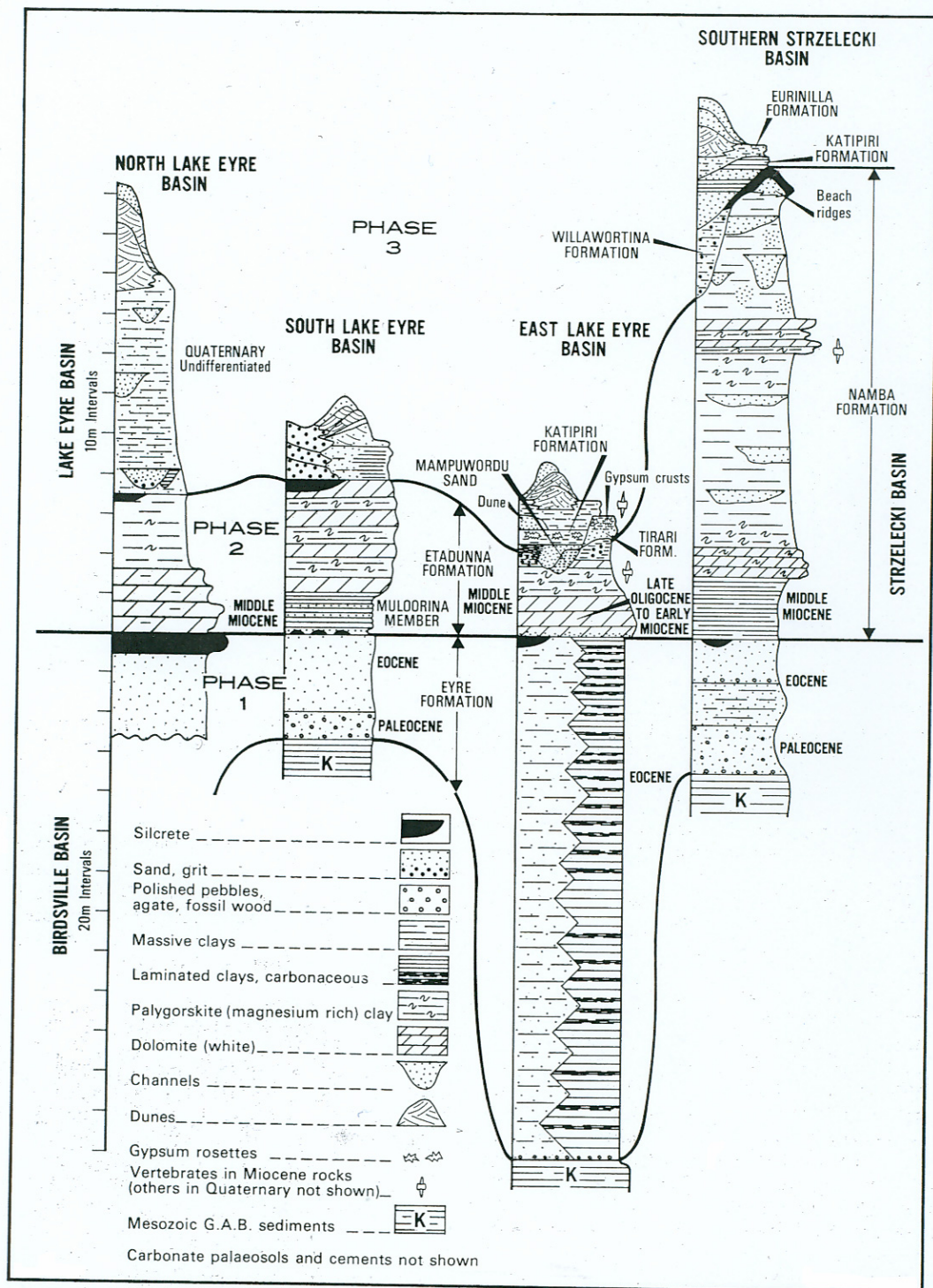


Figure 10. Diagram showing the complex stratigraphy in the vicinity of the Lake Eyre Basin and adjacent areas (comprising the Eyre and Namba Formations and overlying Willawortina Formation as seen in the western portion of the study area). Source: Krieg et al. (1990).

The Millyera (lacustrine) and Coomb Spring (shoreline) Formations, which are the predominant units covering the central parts of the CURNAMONA sheet area (where the Willawortina Formation is absent), interfinger with each other and comprise laminated green clays and sands, respectively. The Coomb Spring Formation is represented by coarse-grained

well-sorted nearshore sandy beach deposits adjacent to Lake Frome and consists of sands (Callen, 1990), while the Millyera Formation represents the lacustrine floodplain depositional phase expressed as green coloured clays, sands and algal limestone (Callen and Benbow, 1995). The spatial distribution of the Millyera Formation is variable and typically overlies the Namba Formation (Callen, 1990).

Fine-grained aeolian sands/clays of the Eurinilla Formation (inclusive of the Moko and Billeroo Palaeosols) overlie the Coomb Spring and Millyera Formations. Channels incised into the Willawortina Formation contain aeolian fill of the Eurinilla Formation typically towards the western edge of Lake Frome which has a broad, thin, almost sheet-like distribution across the basin as gravels derived from overbank deposits and intermittent streams (Callen and Benbow, 1995).

The Late Pleistocene - Holocene Coonarbine Formation is an aeolian unit spatially associated with falling sea levels where dune construction was prominent and in which distinct palaeofeatures such as lunette sands, marine faunal artefacts and gypsum dunes are well preserved (Callen, 1990). Aeolian sands are often disconformable over the Late Pleistocene alluvial and lacustrine sediments and tend to display features of several (older) dune building phases associated with the last glacial maximum and subsequent temperature stabilisation (Callen and Benbow, 1995). The mobile Holocene sands and clays tend to be red-brown in colour and often are found proximal to watercourses, fan deposits, playas and terraces (Callen, 1986).

## **CONCLUSION**

This report reviews the geology of the southern Curnamona Region. This region presents evidence of considerable depositional, deformation and incision events in its complex basin configuration. Comprising sediments and structures spanning from Palaeoproterozoic to Recent in age, the southern Curnamona Region is subdivided into five separate local and regional entities (namely depositional basins) each representative of a significant geological phase in the region's compilation. These five entities include the Palaeo- to Mesoproterozoic Willyama Supergroup basement which is spatially limited to the southern ranges and is demonstrative of numerous phases of deformation. Unconformably overlying this unit is the marine influenced Cambrian Arrowie Basin. The Benagerie Ridge was a basement high that influenced deposition within the Moorowie and Yalkalpo synclines at this time. Mesozoic sediments of the Eromanga Basin, which formed as a result of intra-plate tectonic activity,



and its southeastern Frome Embayment, recorded a transgressive depositional phase. The overlying Lake Eyre Basin, comprising Cainozoic Callabonna Sub-basin sediments describes a somewhat intricate pattern of facies deposition. The spatially continuous fluvial Eyre Formation forms the basal unit within the Callabonna Sub-basin and is incised into the Proterozoic basement. Miocene in age, the overlying Namba Formation almost replicates the Eyre Formation in that its sequential arrangement of interbedded sands and clays is discriminated by age but is marginally thicker and more continuous throughout the region. Although it may be argued that the Quaternary sediments within this region should be inclusive of the Callabonna Sub-basin, this largely fluvial sequence is dominated by the Willawortina Formation and in its absence, the Millyera and Coomb Spring Formations dominate. Conformably overlying these units are the Eurinilla followed by the Coonarbine Formations all significant in demonstrating an environment of gradually increasing aridity.

The framework outlined in this geological overview forms the basis of ongoing project work centered on a 3D model of the Callabonna Sub-basin, Southern Curnamona Region (Ruperto and Nicoll, 2005). The present document supplements the 3D model which facilitates visualisation of the uppermost units described in this text.

## REFERENCE

- Burt, A., Connor, C. & Robertson, S., 2004. Curnamona — an emerging Cu-Au province. *MESA Journal* (Quarterly Earth Resources Journal of Primary Industries and Resources South Australia), 33: 9-17.
- Callen, R.A., 1977. Late Cainozoic environments of part of northeastern South Australia. *Journal of the Geological Society of Australia*. 24:151-169.
- Callen, R.A., 1986. *Curnamona Map Sheet, South Australia and New South Wales: topographic map 1:250 000 scale. SH54-14*. Australian Surveying and Land Information Group.
- Callen, R.A. 1990. Curnamona, South Australia: 1:250 000 Geological Series – Explanatory Notes. SH/54-14. Department of Mines and Energy South Australia.
- Callen, R.A., Alley, N.F., Greenwood, D.R., 1995 Lake Eyre Basin. in Drexel, J.F. and Preiss (eds), W.V. Chapter 10 Tertiary. The Geology of South Australia Volume 2 – The Phanerozoic.
- Callen, R.A. and Benbow, M.C., 1995. The Deserts – Playas, Dunefields and Watercourses in Drexel, J.F. and Preiss (eds), W.V. Chapter 11 Quaternary. The Geology of South Australia Volume 2 – The Phanerozoic.
- Curtis, J.L., Brunt, D.A. and Binks, P.J., 1990. Tertiary palaeochannel uranium deposits of South Australia, in *Geology of the Mineral Deposits of Australia and Papua New Guinea* (Ed F.E. Hughes), pp. 1631-1636 (*The Australasian Institute of Mining and Metallurgy: Melbourne*).
- EA, 2001. Environment Australia Public Notifications Report (January 2001) *Assessment of the Environmental Impact Statement for the Proposed Honeymoon Uranium Project*.  
<http://www.deh.gov.au/assessments/epip/notifications/honeymoon/assessmentreport/report5.html>  
 accessed on 15-11-2004
- Gravestock, D.I. & Cowley, W.M., 1995. Arrowie Basins. In: Drexel, J.F. & Preiss, W.V. (Eds), The Geology of South Australia. Vol. 2, The Phanerozoic. *South Australia Geological Survey Bulletin*, 54: 20-34.
- Habermehl, M.A. (2000). *Comparison of the Hydrogeology of the Beverley and Honeymoon Uranium Deposits*. Land and Water Sciences Division, Bureau of Rural Sciences, Canberra ACT.  
<http://www.deh.gov.au/assessments/epip/notifications/honeymoon/assessmentreport/brs.html>  
 accessed on 15-11-2004
- Ker, D.S. 1958. *The Hydrology of the Frome Embayment in South Australia, 010780*. Department of Mines South Australian Geological Survey no.27.
- Krieg, G.W, Callen, R.A, Gravestock, D.I. and Gatehouse, C.G. 1990. 1: Geology. In Natural History of the North East Deserts edited by Tyler, M.J, Twidale, C.R, Davies, M. and Wells, C.B (eds).
- Krieg, G.W., Alexander, E.M. and Rogers, P.A. 1995 Chapter 9 – Mesozoic. In: Drexel, J.F. & Preiss, W.V. (eds), The Geology of South Australia. Vol. 2, The Phanerozoic. *South Australia Geological Survey Bulletin*, 54: 20-34.
- Leyh, W.R. & Connor, C.H.H., 2000. Stratigraphically controlled metallogenic zonation associated with the regional redox boundary of the Willyama Supergroup – Economic implications for the

- southern Curnamona Province. *MESA Journal* (Quarterly Earth Resources Journal of Primary Industries and Resources South Australia), 16: 39-47.
- Paul, E., Flöttmann, T., Sandiford, M. (1999) Structural geometry and controls on basement-involved deformation in the northern Flinders Ranges, Adelaide Fold Belt, South Australia. *Australian Journal of Earth Sciences* 46: 343-354
- PIRSA, 2002. Arrowie Basin (and central Adelaide Geosyncline). Anonymous report, [http://www.pir.sa.gov.au/pages/petrol/prospectivity/prospectivity\\_arrowie.pdf](http://www.pir.sa.gov.au/pages/petrol/prospectivity/prospectivity_arrowie.pdf)
- PIRSA. Image AV201310\_014, Geological Map of the Curnamona Province. [http://www.pir.sa.gov.au/pages/minerals/geology/curnamona/curnamona\\_geology.htm](http://www.pir.sa.gov.au/pages/minerals/geology/curnamona/curnamona_geology.htm) Accessed 18-05-2005.
- Preiss, W.V., Belperio, A.P., Cowley, W.M. & Rankin, L.R., 1993. Neoproterozoic. Chapter 6 in: Drexel, J.F., Preiss, W.V. & Parker, A.J. (Eds), *The Geology of South Australia. Vol. 1, The Precambrian. South Australia Geological Survey Bulletin*, 54: 171-203.
- Preiss, W.V., 2000. The Adelaide Geosyncline of South Australia and its significance in Neoproterozoic continental reconstruction. *Precambrian Research* 100:21-63.
- Ruperto, L., Nicoll, M., 2005. Three Dimensional Model of the Callabonna Sub-basin Sequence, Southern Curnamona Region – Methods and Documentation. CRC LEME Open File Report 191.
- Stevens, B.P.J., Barnes, R.G., Brown, R.E., Stroud, W.J., Willis, I.L., 1988. The Willyama Supergroup in the Broken Hill and Euriowie Blocks, New South Wales. *Precambrian Research* 40/41:297-327.
- Stevens, B.P.J., Corbett, G.J., 1993. The Redan Geophysical Zone, part of the Willyama Supergroup? Broken Hill, Australia. *Australian Journal of Earth Sciences* 40:319-338.
- Stevens, B.P.J., Burton, G.R., 1998. The Early to Late Proterozoic Broken Hill Province, New South Wales. *AGSO Journal of Australian Geology & Geophysics* 17:5-86.
- Tan, K.P., Caritat, P. de, Scott, K., Eggleton, R.A. & Kirste, D., 2004. The controls on element distribution in the regolith at the Portia and North Portia prospects, Curnamona, South Australia. PacRim 2004 Congress (Adelaide, SA, 19-22 September 2004), Proceedings Volume, *The Australasian Institute of Mining and Metallurgy Publication Series*, 5/2004:273-281.
- Teasdale, J., Pryer, L., Etheridge, M., Romine, K., Stuart-Smith, P., Cowan, Jun., Loutit, T., Henley, P. 2001. *Eastern Arrowie Basin SEEBASE\* Project*. SRK Consulting and Primary Industries and Resources SA – South Australian Govt.
- Tonui, E. & Caritat, P. de, 2003. Composition, diagenesis and weathering of sediments and basement of the Callabonna Sub-basin, Central Australia: Implications for landscape evolution. *Journal of Sedimentary Research*, 73:1036-1050.
- Willis, I.L., Brown, R.E., Stroud, W.J., Stevens, B.P.J., 1983. The Early Proterozoic Willyama Supergroup: stratigraphic subdivision and interpretation of high to low-grade metamorphic rocks in the Broken Hill Block, New South Wales. *Journal of the Geological Society of Australia* 30:195-224.

Zang, W., 2002. Sequence analysis and petroleum potential in the Arrowie Basin, South Australia.  
*South Australia. Department of Primary Industries and Resources. Report Book, 2002/024.*

# Tectonic origin of the shape of the Broken Hill lodes supported by their structural setting in a high-grade shear zone

E. ROTHERY

PO Box 1161, Subiaco, WA 6904, Australia.

Recent studies have claimed structural support for a syngenetic model of ore formation at Broken Hill. The structural features of the Line of Lode—foliation, lineation, boudinage, folding and shearing—are re-evaluated and new data presented from several locations in and around the Line of Lode, including the Kintore Opencut and Readymix Quarries. Although deformation partitioning preserves areas of low strain, especially in the hangingwall, that exhibit primary features, the deformation history described shows a history of high-strain on the Line of Lode. Gneisses in the wall rocks of the orebody show extreme extension in places, with destruction of primary layering and imposition of transposed tectonic fabrics. Sulfide bodies would have been softer than the wall rocks during deformation and any layering in the lodes is likely to be a result of tectonic processes rather than preserved bedding. The geometry of the orebody is described and its setting is revealed as a low-strain site, a minor fold pair, that developed early in a major high-grade shear zone. The orebody probably acquired its linear shape first as a result of mass transport of sulfides to this structural site and then by extension within the shear zone, an epigenetic process. Previous fold models for the Line of Lode are rejected, along with the application of regional stratigraphic units to the orebody footwall. Deformation of the Line of Lode before peak metamorphism is obscured by recrystallisation. Subsequent minor deformation occurred at both high metamorphic grade and under retrograde conditions to produce the range of features previously quoted in support of syngensis. Sulfides were remobilised during both the post-peak metamorphic high-grade, and later low-grade, deformation events.

**KEY WORDS:** Broken Hill, deformation history, kinematics, lineation, ore genesis, structure.

## INTRODUCTION

The Proterozoic Broken Hill deposit in western New South Wales, has been mined since 1883 and originally contained approximately 300 Mt of ore grading in excess of 15% combined lead and zinc (Haydon & McConachy 1987). Current thinking on Broken Hill ore genesis is still divided, although most authors appear to favour syngenetic chemical or exhalative sedimentation (Morland & Webster 1998; Oliver *et al.* 1998; Stevens 1998; Wyborn *et al.* 1998) after the work of King and Thomson (1953) and colleagues, especially Stanton (1976b,c, d). Some (Morland & Webster 1998) claim structural support for this view and it is the purpose of this paper to examine the structural features along the Broken Hill Line of Lode, such as geometry, layering, lineation, folds, shear zones and kinematics, to see whether such support is warranted. Particular reference is made to previous work, as Broken Hill is unique in having had considerable geological attention for over 100 years. The Broken Hill orebody is made up of several distinctive Lead Lodes (2 and 3 lens) and Zinc Lodes (1 lens, A, B, C lodes) stacked above one another in an *en echelon* manner over a strike length of 8 km (Figures 1, 2). Hodgson (1974) recognised five main rock types that could occur in several or all of the lodes: (i) Calcitic Ore—calcite, sulfides, rhodonite, bustamite, knebelite; (ii) Quartzitic Ore—sulfides, minor quartz; (iii) Pyroxene Sub-ore—massive rhodonite, or

hedenbergite, bustamite, quartz, garnet rock; (iv) Garnet Sandstone or pure garnet; and (v) Pyrrhotite Sub-ore—pyrrhotite, quartz, garnet, Fe-rich pyroboles. Recently, Webster (1993) distinguished several distinct ore types that owe their texture to shear or movement: (i) Massive Equigranular Sulfide-Dominated Ore or Pebble Ore with milled quartz inclusions and *durchbewegung* textures [these textures were previously recognised at Broken Hill by Maiden (1975) and are common in sulfide deposits as described by Marshall and Gilligan (1989)]; (ii) Homogeneous Ore grading to Saccharoidal Ore, essentially a foliated sulfide mylonite; and (iii) Sulfide Veins either brecciating wall rocks or massive gangue bodies. Webster (1993) claimed that Calcitic Ore and Pyroxene Sub-ore, which he called Banded Carbonate Ore and Massive Manganese Silicate Ore preserved original layering. Morland and Webster (1998) followed this up by claiming that this original layering was in part syndepositional. Previously, Maiden (1975) had pointed to preserved foliation and lineation parallel to layering in calcite ore as evidence of plastic flow of ore during deformation. Are the orebodies originally stratiform and metamorphosed in place? Alternatively, have they moved to their present position, preserving no primary features? This paper, after describing the geological setting and the geometry of the orebodies, considers each structural element in turn (layering, foliation, lineation, boudinage, folding and shear zones)

with published work being supplemented by new observations at Kintore Opencut and Readymix Quarries (Figure 1). The orebodies are then placed in this context and an attempt is made to build a deformation history from the evidence.

## GEOLOGICAL SETTING

The Broken Hill Line of Lode and its enclosing rocks strike northeast-southwest and generally dip northwest, and the ore is contained in a fold pair, consisting of the Western Antiform and the Eastern Synform, which together make up the Main Drag Fold that verges towards the southeast (Figures 1, 2). The stratigraphy in the Broken Hill Mine area (Figure 3) has been defined by Haydon and McConachy (1987) and consists of three suites, equivalent to three groups in the formal stratigraphy for the Willyama Block (Stevens *et al.* 1983; Willis *et al.* 1983): these are Suite 3 (Thackaringa Group), Suite 4 (Broken Hill Group, which hosts the orebodies) and Suite 5 (Sundown Group), respectively oldest to youngest. As described from the mine sequence (Haydon & McConachy 1987; Haydon *et al.* 1993), these can then be further broken down into lithostratigraphic units, numbered in the case of Suite 4 from Unit 4.1 to 4.8. The spatially highest unit of the mine sequence is the Hanging Wall or Upper Granite Gneiss (Figures 1, 3, 4), which has been assigned to Suite 3 (Haydon & McConachy 1987), i.e. Rasp Ridge Gneiss Formation (Willis *et al.* 1983). Going east the next marker is the amphibolite

of Unit 4.4, which can be traced with minor breaks for the length of the Line of Lode (Figures 1, 2), followed by the psammities and pelites of Unit 4.5 (Figure 4). A pelitic sequence with banded iron-formation (Unit 4.6) lies in the immediate hangingwall of the lode horizon that hosts the orebodies (Figures 2a, 4). The lode horizon consists of a mixed package of rocks (Unit 4.7 of Haydon & McConachy 1987) that includes quartz gahnite and garnet quartzite. In the footwall, the stratigraphy is less clear: a sequence of metasediments (Figures 2, 4) separates the lode horizon from the Footwall Potosi Gneiss and amphibolite (Figures 1–4). Potosi Gneiss is a textural term for distinctive gneiss spotted by garnet with biotite halos (King & Thomson 1953). The footwall sequence has been assigned suite and unit numbers from 4.8 to 5 and back down through 4 to 3 (Haydon & McConachy 1987), the last and spatially lowest being the Lower Granite Gneiss (Figures 1–3), which like the Upper Granite Gneiss has been assigned to the Rasp Ridge Formation (Willis *et al.* 1983). The local names are used here to distinguish structurally separate bodies of gneiss units that have been grouped into formal stratigraphic units by Willis *et al.* (1983). The stratigraphic numbers for the footwall sequence are not shown in this paper as they depend on the acceptance of a Broken Hill Antiform, which is rejected below.

Deformation in the Broken Hill area has been divided into four or five major tectonic events,  $D_1$ – $D_4$  (Olarian) and the Delamerian retrograde reactivation of shear zones (Laing *et al.* 1978; Marjoribanks *et al.* 1980; Hobbs *et al.* 1984; Stevens 1986). The Olarian deformation took place under

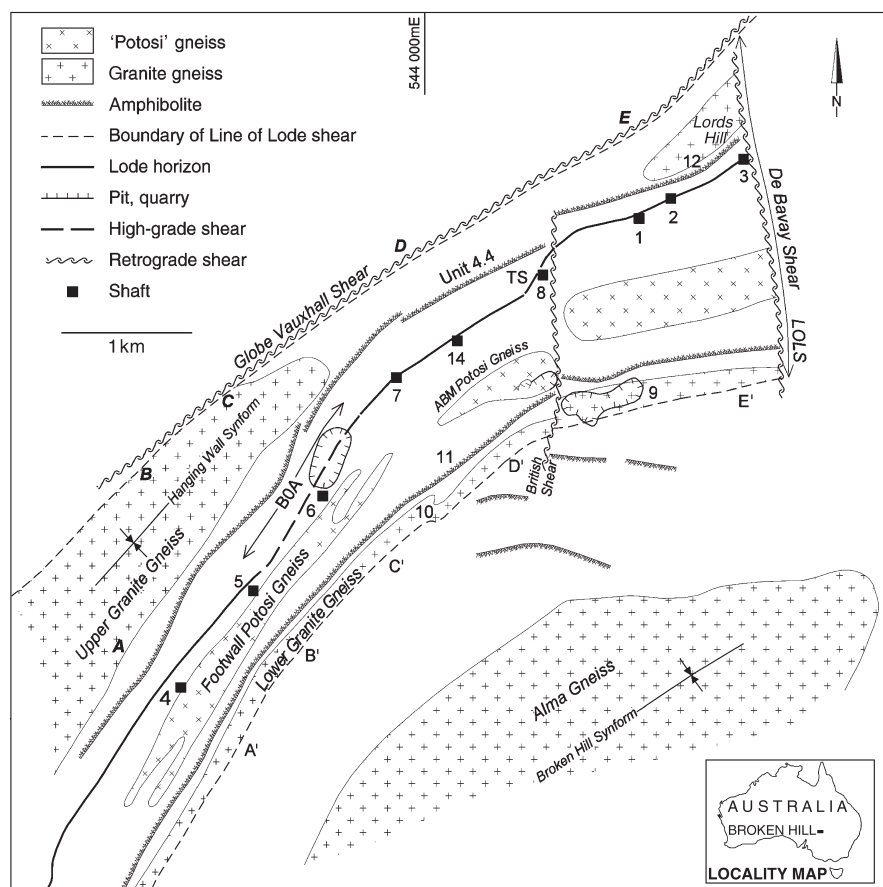


**Figure 1** Schematic geology of the Broken Hill Line of Lode (after Haydon & McConachy 1987) showing: 1, Pasmenco North Mine No. 1 Shaft; 2, No. 2 Shaft; 3, No. 3 Shaft; 4, NBHC Shaft at Pasmenco Southern Operations; 5, ZC Old Main Shaft; 6, Kintore Shaft; 7, Delprat's Shaft; 8, Thompson's Shaft; 9, Readymix Main Quarry; 10, Otto's Hill; 11, Alma Amphibolite; 12, De Bayay Quarry; 14, Block 14 Shaft; BOA, Belt of Attenuation; TS, Thompson Shear (both marked with a dashed line); LOLS, Line of Lode Shear. AMG coordinates on the Australian Geodetic Datum 1966. A–A', B–B', C–C', D–D' and E–E' are section lines shown in Figure 2.

mostly granulite to amphibolite conditions ( $M_1/M_2$ ,  $D_1/D_2$ ), with significant greenschist facies retrogression accompanying  $D_3$  (Marjoribanks *et al.* 1980; Hobbs *et al.* 1984). Peak metamorphic conditions attained along the Line of Lode were granulite facies, approximately 800°C and a pressure of 550 MPa or approximately 18 km burial (Phillips 1978; Stevens 1986). Similar peak conditions prevailed at the time of both  $D_1$  and  $D_2$  (Laing 1977). The effects of  $D_1$  have been controversial, but it may have imposed a regional layer-parallel foliation and involved isoclinal folding with inversion of large areas (Marjoribanks *et al.* 1980; Hobbs *et al.* 1984; Laing 1996), or alternatively is of more local origin in high-strain zones (White *et al.* 1995). The major fold and thrust system probably formed during  $D_2$ , with a strong southwest-plunging lineation ( $L_2$ ) developing in the Broken

Hill area (Laing *et al.* 1978; White *et al.* 1995). A retrograde foliation developed in shear zones and in the axial surfaces of related folds during  $D_3$  (Laing *et al.* 1978; White *et al.* 1995). A study of these shear zones (White *et al.* 1995) found evidence for shear-zone development under six recognisable temperature conditions as indicated by different transient mineral assemblages from peak metamorphism through retrogression to near-surface gouge rocks. The absolute timing of each deformation event has been uncertain;  $D_1$  and  $D_2$  were originally assigned to  $ca$  1660  $\pm$  10 Ma (various sources relying on Rb–Sr and mass zircon dating, summarised in Stevens 1986), and then revised by SHRIMP zircon dating to 1600 Ma (Page & Laing 1992; Page *et al.* 2000). Other work by Nutman and Ehlers (1998) has proposed at least three thermal events accompanied by

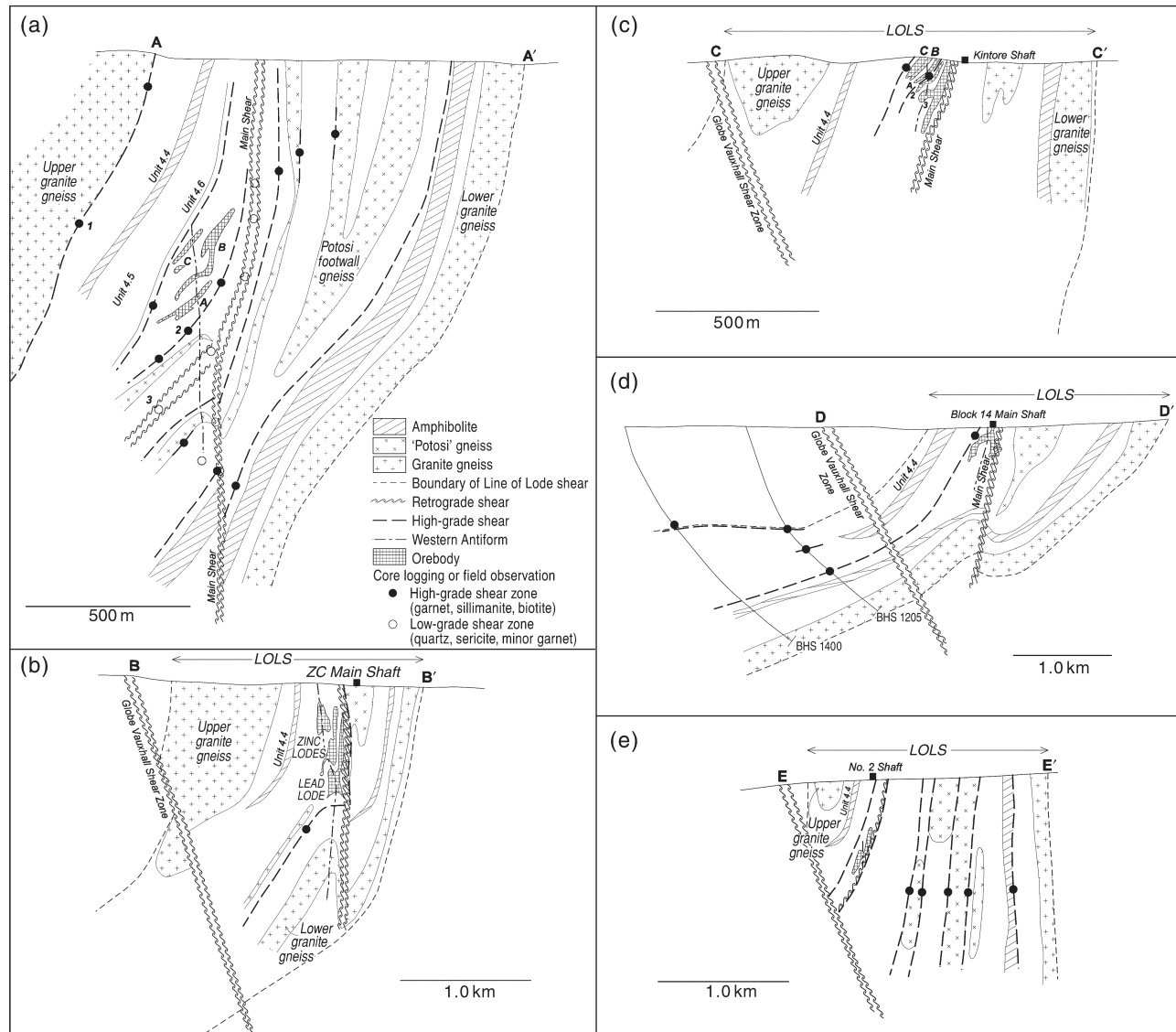


**Figure 2** Serial sections through the Line of Lode (see Figure 1 for location of section lines). The Main Drag Fold is made up of the Western Antiform (trace shown), visible in the lode and gneiss units in the footwall, and the Eastern Synform (trace not shown as it is mostly coincident with the Main Shear). The width of the Line of Lode Shear (LOLS) is indicated diagrammatically. (a) NBHC Shaft section, with A, B, C, marking individual zinc lodes. 1, location of Figure 10a; 2, location of Figure 11b; 3, minor retrograde shear zone linking to, but not part of, the Main Shear. (b) ZC Main Shaft section. (c) Kintore Shaft section with A, B, C, 2 and 3 marking individual zinc and lead lodes. Note that this section is within the Belt of Attenuation, which has the effect of rotating and stretching the ore and host rocks in this area. (d) Block 14 Shaft section. (e) North Mine No. 2 Shaft section.



high-grade deformation, two prior to 1640 Ma (one possibly as old as 1690 Ma) and one syn- or post-1600–1570 Ma identified as  $D_2$ . This latter date conflicts with another date for  $D_2$  presented in the same paper (Nutman & Ehlers 1998) at 1658 Ma. Reassigning this 1658 Ma date to an earlier high-grade event—broadly  $D_1$ —leaves the balance of evidence appearing to point to deposition at *ca* 1690 Ma,  $M_1/D_1$  at *ca* 1650 Ma,  $M_2/D_2$  at *ca* 1600 Ma and  $M_3/D_3$  at *ca* 1570 Ma (see Table 1).

### Geometry of the orebodies

The orebodies have the dimensions of several long ribbons within fold hinges. A typical dimension is approximately 7000 m  $\times$  300 m  $\times$  100 m (2 lens). The long dimension is parallel to the local mineral elongation direction. Andrews (1922) described a pipe of garnet sandstone 100 feet (30.4 m) in length, 50–100 feet (15.2–30.4 m) in width, that could be traced for 700 feet (213.4 m) along the pitch of the lode. The Western Mineralisation, down dip from the main orebodies, is also shaped like a ‘very elongated pipe’ (Gentle 1968 p. 181). The occurrence of pipes of rhodonite was also noted by Andrews (1922). As they appear in long section at North Mine (Henderson 1953) these rhodonite bodies occur as *en echelon* bodies within Lead Lode, all plunging around 15° steeper than Lead Lode itself. Similar rhodonite bodies at North Broken Hill Consolidated (NBHC) were described by O’Driscoll (1968a), but here the *en echelon* bodies plunge parallel to the plunge of Lead Lode. These same rhodonite bodies have been described as: ‘in cross section, these are ragged, rounded to ellipsoidal bodies which are elongate parallel to the axial planes of the orebody folds’ by Webster (1993 p. 138). Maiden (1972, 1975) proposed that the manganese silicate masses were drawn out into boudins, and Webster (1993) suggested that originally these boudins were joined to form a layer within Lead Lode. However, such a layer, within markedly linear or ribbon orebodies, must have been a very long, thin layer. As depicted in unfolded cross-section by Mackenzie (1968 figure 4) the rhodonite mass appears like a pipe enclosed within a teardrop-shaped Lead Lode. This kind of geometry led Gustafson *et al.* (1950 p. 1388) to comment that ‘if the

sedimentary hypothesis is valid, one must assume that...[the lodes occupied] an extremely elongated channel of sedimentation which later became the Western anticline’. It is this peculiar shape and coincidence with the folding that needs explanation.

### LAYERING AND FOLIATION

In unravelling the geology of the Line of Lode, one of the most important issues is the extent to which compositional layering represents a metamorphosed primary layering. The Broken Hill Block is folded into tight to isoclinal  $F_2$  folds, with most of the rocks being on limbs with a strong foliation  $S_2$  parallel and indistinguishable from  $S_1$ , with a few  $F_2$  hinges where  $S_2$  foliation can be observed parallel to the  $F_2$  axial plane, with  $S_1$  parallel to the  $S_0$  layering (Laing *et al.* 1978). Significant metamorphic segregation is seen on  $S_1$ , with regularly alternating quartzo-feldspathic and mafic laminae in granite gneiss (Laing *et al.* 1978). Both  $S_1$  and  $S_2$  are high-grade metamorphic foliations, being defined by growth of new sillimanite and biotite (Laing *et al.* 1978). A later penetrative foliation is defined by muscovite and related to regional retrogression and shear-zone activity (Laing *et al.* 1978; White *et al.* 1995). In the wall rocks of the Broken Hill orebody, especially in pelitic to psammitic sillimanite gneisses, most early workers (Andrews 1922) assumed that the compositional layering ( $S_0$ ) represented metamorphosed bedding. Condon (1959) recognised cross-bedding, ripple marks and scour features, but the sedimentary origin was disputed (Thomson 1959; Williams 1959). It was not until the 1970s (Glen & Laing 1975; Hopwood 1976; Laing 1977; Stevens 1978) that the essentially sedimentary origin of the sillimanite gneisses and the primary layering for the bulk of pelitic to psammitic gneisses in the Broken Hill Block was accepted. However, there is local evidence that some layering has been derived from tectonic processes such as transposition (Hobbs & Vernon 1965; Williams 1967; Dewar 1968; Ransom 1968; Hodgson 1975a; White *et al.* 1995; Leyh 2000; Webster 2000). A detailed description of the process, citing a local example from the Broken Hill South Mine is given

Regional stratigraphy (Stevens <i>et al.</i> 1983, Willis <i>et al.</i> 1983)		Mine sequence stratigraphy (Haydon & McConachy 1987)		Local rock unit names (as used in this paper)
Sundown Group		Suite 5		
Broken Hill Group	Hores Gneiss (Silver King Formation in other areas)	Suite 4	Unit 4.8	
			Unit 4.7	Zinc Lodes; Lead Lodes; Footwall Potosi Gneiss; ABM Potosi Gneiss
			Unit 4.6	
			Unit 4.5	
	Freyers Metasediments		Unit 4.4	Upper Amphibolite; Alma Amphibolite/Main Lower Amphibolite (Laing <i>et al.</i> 1978)
	Parnell Formation		Units 4.1–4.3	
	Allendale Metasediments			
Thackaringa Group	Rasp Ridge Gneiss (Himalaya Formation in other areas)	Suite 3	Unit 3.10	Upper Granite Gneiss also known as Hanging Wall Gneiss (Lewis <i>et al.</i> 1965) or the Auger Gneiss (Andrews 1922); Lower Granite Gneiss

**Figure 3** Relationships of local rock names to Line of Lode stratigraphy.



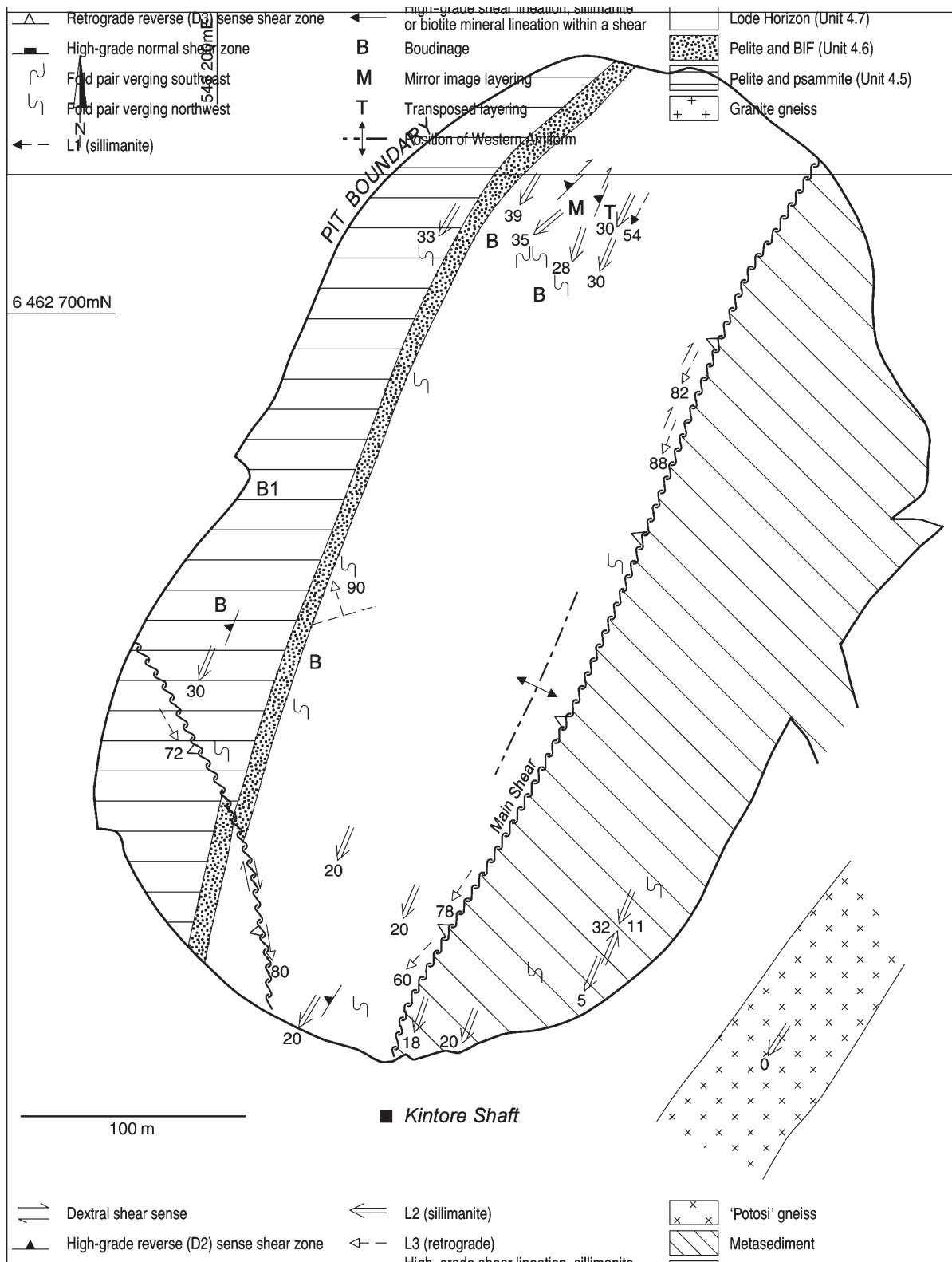


**Figure 4** Structural features at Kintore Opencut. Note that the lineations in shear zones are expressed as pitch (drawn parallel to shear plane or perpendicular for 90° lineations).

in Hobbs (1966 p.321). Transposition has recently been mapped by White *et al.* (1995) in a zone on either side of the Lead Lode orebodies at North Mine. Outside the zone,  $S_0/S_1$  foliation in a gneiss (psammopelitic compositionally) is folded around a  $D_2$  fold, with sillimanite defining the axial planar  $S_2$  foliation. As the orebodies

are approached a well-defined banding is developed parallel to the  $S_2$  foliation and the  $S_0/S_1$  fabric is lost. This rock was regarded by White *et al.* (1995) as a tectonically transposed and altered gneiss or protomylonite in a lower strain envelope around the shears hosting the orebody. These observations suggest that, locally in or near the ore

**Table 1** Line of Lode deformation history.

Observation	Interpretation	Event
Compositional layering in pelites-psammmites.	Bedding (Condon 1959; Stevens 1998).	
Potosi Gneiss dated at 1690 Ma (Page & Laing 1992).	Volcanic eruption (Stevens 1998).	
Rasp Ridge Gneiss dated at 1690 Ma (Love 1992).	Synvolcanic intrusion (Stevens 1998).	
Dating of pre- $D_2$ high-grade structures at approximately 1650 Ma (Nutman & Ehlers 1998, see text for discussion).	Preservation of $D_1$ thermal event.	
Bedding parallel foliation ( $S_1$ ).	High-grade layer parallel foliation developed in $D_1$ .	$D_1$
Oldest preserved sillimanite lineation ( $L_1$ ) observed at North Mine (Laing <i>et al.</i> 1978) and Kintore (this paper).	Early transport direction of the Line of Lode Shear.	$D_1$
Orebody parallel to $L_1$ at North Mine (Laing <i>et al.</i> 1978).	Orebody originally all aligned parallel to $L_1$ .	$D_1$
Layering in orebody (Hodgson 1974; Maiden 1975; Webster 1993) and evidence for partial melting of sulfides (Maiden 1975) and gangue (Hodgson 1974).	Transposed layering by preferential movement of sulfides as against gangue during high-grade deformation (Maiden 1975).	$D_1$
Main Drag Fold affects ore interface with garnet quartzite (Hodgson 1974). Main Drag Fold, in part, parallel to $L_1$ and overprinted by later high-grade events.	Garnet quartzite pre-dates Main Drag Fold.	$D_1$ – $D_2$
SW-plunging sillimanite lineation ( $L_2$ ), regional folding and shears (Laing <i>et al.</i> 1978; White <i>et al.</i> 1995).	Main Drag Fold probably initiated during $D_1$ .	
Development of foliation and lineation in high-grade ore (Maiden 1975).	Fold and thrust tectonic deformation event at high metamorphic grade (White <i>et al.</i> 1995).	$D_2$
1600 Ma dates from metamorphic zircon overgrowth $D_2/M_2$ (Page & Laing 1992, Love 1992).	Orebody preserves $D_2$ (at least) deformation, with strong $L_2$ (SW plunge).	$D_2$
Sulfide movement continues after folding has ceased, plucking wall rock from its position (Maiden 1975).	Timing of peak metamorphism synchronous with deformation (Page & Laing 1992).	
Later, overprinting high-grade foliations in sulfide ore, e.g. droppers, belt of attenuation (Hodgson 1974; Maiden 1975; Webster 1993).	Sulfides mobile during $D_2$ (Maiden 1975)	$D_2$
Sulfides are coarse with unstrained crystals (Hodgson 1974; Maiden 1975).	Orebody preserves second high-grade deformation (Hodgson 1974; Maiden 1975).	$D_2$
East-dipping minor folds oblique to lode that produce plunge reversals in $L_2$ (Webster 1993).	Dynamic recrystallisation by dislocation creep as described by Duckworth and Rickard (1993).	$D_2$
Sinistral shear along Line of Lode Shear producing Belt of Attenuation and Thompson Shear (Webster 1993) along with minor horizontal dextral shear noted by Hodgson (1974).	Consistent with a phase of west block up movement on the Line of Lode Shear (NW-SE principal compression with vertical extension).	$D_2$
Boudinage extends layering and deforms $L_2$ lineation.	Period of NW-SE directed principal compression with NE-SW extension. This event produced a high-grade foliation (Hodgson 1974; Webster 1993) and overprints above fold event (Webster 1993).	$D_2$
Sulfides in droppers show evidence of recrystallisation at high metamorphic grade (Hodgson 1974; Maiden 1976).	Vertical and horizontal extension within the plane of the foliation: consistent with both the above events.	$D_2$
Temperature drops below 500°C (Stevens 1986) at 1570 Ma.	Droppers exploit vertical fold axes, consistent with layer parallel principal compression / NW-SE extension or NE-SW compression parallel to the Line of Lode.	$D_2$
Retrograde foliation, lineation and kinematics on Main Shear.	Most retrograde activity post-dates this, but shears may have been initiated before (Stevens 1986).	
Minor regional retrograde shear with the British, De Bavay and Globe Vauxhall Shears cutting the Line of Lode Shear. Coincident with greenschist metamorphism.	Retrograde Main Shear movement was west block up with vertical extension.	$D_3$
Intrusion of post-tectonic Mundi Mundi Granite and related pegmatites dated at 1490 Ma (Stevens 1986).	Further period of NW-SE compression (White <i>et al.</i> 1995). These retrograde shears may have been initiated during this event. Movement sense may have been NW directed (Gibson 2000).	$D_3$
Deposition of Adelaidean sediments at approximately 1100 Ma with subsequent uplift and erosion, followed by emplacement of ultrabasic plugs (Stevens 1986).	Bulk of deformation has ceased.	
Thermal pulse and brittle fault formation in Delamerian at 520 Ma (Stevens 1986). Sulfides remobilised in retrograde shears and veins (Morland & Webster 1998).	Minor brittle extension of Willyama Group metamorphics.	
	Minor reactivation of some retrograde shears with development of pug zones etc. Note that sulfides are remobilised once again.	$D_4$

zone, layering in the wall-rock gneisses may be of tectonic origin.

The origin of layering in lode rocks and in the sulfide orebodies themselves is not as clear. Layering in banded iron-formation 'appears, quite unequivocally, to be bedding' (Stanton 1976a p. B34). The fine lamination that is distinctive in garnet quartzite lode rock was suggested as being of sedimentary origin by Condon (1959) and rejected by Williams (1959) and later by Haydon *et al.* (1993) who pointed out that the apparent sedimentary structures often give conflicting younging directions. Garnet quartzite and garnet sandstone, which is a garnet-rich garnet quartzite, occur as a selvage (or rim) at the contact of Lead Lode with pelitic gneiss (Hodgson 1975b). Similar garnet rims, up to 45 cm across, have been described as metasomatic (Jones 1968) from evidence of transitional chemical change across the contact, and continuity and uniform width on ore contacts. Hodgson (1975b) suggested that garnet quartzite was produced from a reaction between pelitic sediments and manganese-rich solutions during metamorphism (post- $S_1$ ), and so any layering would be from alteration effects. Most of the orebodies are hosted in garnet quartzite (Morland & Webster 1998) and this garnet quartzite envelope was regarded as wall-rock alteration in the early work (Gustafson *et al.* 1950). The garnet quartzite geometry led Stevens (1998) to suggest that the garnet quartzite is the metamorphic product of a manganiferous quartz-chlorite rock formed by early hydrothermal alteration. If the garnet-bearing rocks are the products of either metasomatism or alteration (pre- or synmetamorphic) the banding could be a result of these processes and need not reflect depositional layering. Similar garnetiferous selvages around the Broken Hill-type Pegmont mineralisation in Queensland have been interpreted as epigenetic wall-rock alteration zones (Binns 1993). A recent Australian example of alteration banding comes from alteration studies of lode gold deposits metamorphosed at amphibolite to granulite facies, where proximal alteration is 'clearly marked by the appearance of...mono- and bi-mineral banding' (Eilu *et al.* 1999 p. 35). Other possibilities for the

origin of layering are suggested by the occurrence of mirror-image layering, which have been recorded from garnet- and gahnite-bearing psammitic rocks at Kintore (Figure 4) and Readymix (Figure 5); the repetition of layer types about a central plane suggests that either veining or intense isoclinal folding are responsible for the layering. An epigenetic origin for some occurrences of quartz gahnite lode rock has recently been suggested by Leyh (2000).

As for the sulfide orebodies, in calcite ore Maiden (1975) recorded a well-developed compositional layering with preferred orientations of crystals or mineral aggregates defining foliations and lineations. Recent work by Webster (1993) has mapped similar layering in Lead Lode, and essentially primary ore (sulfide and gangue minerals) layering parallels the ore-wall-rock contact. Webster (1993) and Morland and Webster (1998) regarded the layering in the ore as evidence of synsedimentary origin and drew a distinction between these and other sulfide textures that occur, such as *durchbewegung*, which are indicative of mobilisation. However, Maiden (1976) recognised that sulfide minerals are among the first to undergo plastic flow with increasing metamorphism and that fold crests were a zone of weakness where this flow might preferentially occur. With increasing temperature and pressure, galena deforms in a ductile manner first, followed by pyrrhotite, chalcopyrite and sphalerite (Maiden 1976; Marshall & Gilligan 1987; Duckworth & Rickard 1993). Even pyrite (though not a common mineral species in Broken Hill) can develop banding at temperatures as low as 400°C (Duckworth & Rickard 1993). This ductility of sulfide minerals at relatively low temperatures compared to metamorphic conditions of up to 800°C at Broken Hill suggests that sulfide minerals were mobilised early, during prograde metamorphism, and were still mobile until well after peak metamorphism. Indeed, partial melting of both sulfides and gangue minerals may have occurred (Maiden 1975; MacIntosh & Mavrogenes 1998). Mobilisation during prograde metamorphism is likely to have imposed a tectonic layering on the sulfide orebodies, as has been described from many other, lower grade, regions (McClay

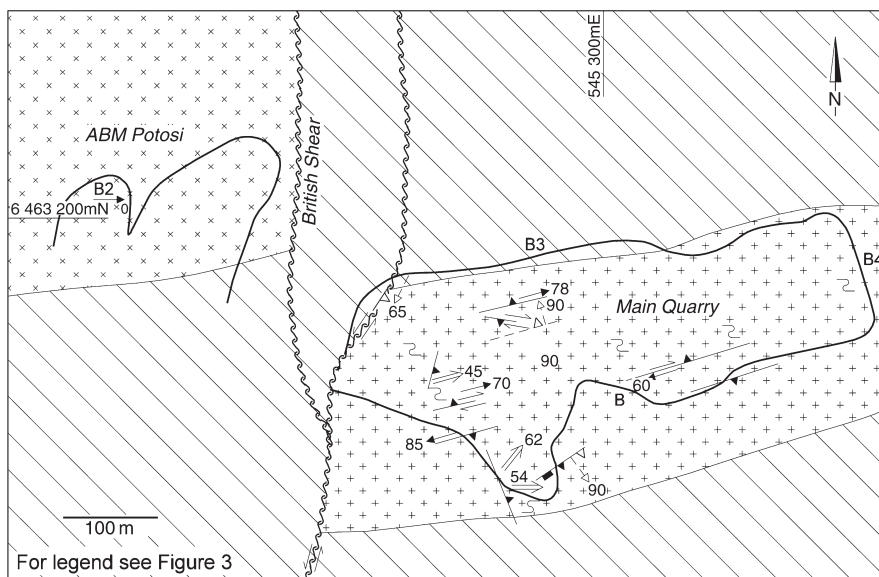


**Figure 5** Structural features at Readymix Quarries.

For legend see Figure 3

1991; Duckworth & Rickard 1993). In other less mobile rock types, early deformation imposed a strong lineation and a bedding parallel foliation ( $L_1$ ,  $S_1$ ). Evidence of transposition occurring shows that, at least locally, primary layering has been obliterated from some gneissic rock types (Hobbs 1966; Williams 1967; Dewar 1968; Ransom 1968; Hodgson 1975a; White *et al.* 1995; Leyh 2000). Given that sulfides could be expected to be more ductile or mobile than gneisses, it is reasonable to suggest that primary layering was obliterated in sulfide orebodies, as it is in some of the wall rocks. Such transposition could have led to separation of sulfide layers from gangue layers. None of the other evidence quoted in support of primary layering based on compositional differences, such as sharp boundaries, zoning, lack of evidence for metamorphic reactions, nor differing proportions of volatiles (Stanton 1976b), are unequivocal evidence that layering is a preserved sedimentary structure. Several authors have pointed to recrystallisation during the high-grade event (Ramdohr 1950; Hodgson 1975a,b; Webster 1993; Morland & Webster 1998), which post-dates the imposition of linearity and could have removed any evidence of early kinematics and differentiation. This is probably dynamic recrystallisation by dislocation creep as described in sulfide ores by Duckworth and Rickard (1993).

## LINEATION

Rocks in the Broken Hill area often exhibit a high-grade lineation. The most common lineation is a prominent sillimanite lineation ( $S_2$  of Laing *et al.* 1978) in pelites, which plunges dominantly to the southwest (Hobbs & Vernon 1965). A local occurrence of Potosi Gneiss, known as the ABM (named after the Australian Blue Metal company) Potosi Gneiss (Figures 5, 6) has a pronounced  $L$  tectonite fabric plunging northeast (also termed  $L_2$  by Laing *et al.* 1978), where the quartzo-feldspathic segregations are drawn out into rods that have dimensions in excess of 10:1:1 (Hobbs & Vernon 1965). Laing (1977) recognised two high-grade lineations at the De Bavay Quarry on Lords Hill (Figure 1) and other locations near the North Mine with the older steep northeast-plunging lineation ( $L_{1a}$ ) consisting of sillimanite that was crenulated by folds, with a second shallow southwest-plunging ( $L_{2a}$ ) sillimanite growth parallel to the axial surfaces of the new folds. A photograph of the above outcrop, which lies a few metres east of the contact with the Upper Granite Gneiss, is featured in Laing *et al.* (1978 figure 11b). Laing (1977) used this discovery of two lineations to propose that at North Mine the orebody was parallel to the older lineation, while in the south of the Line of Lode the orebody was parallel to the later or

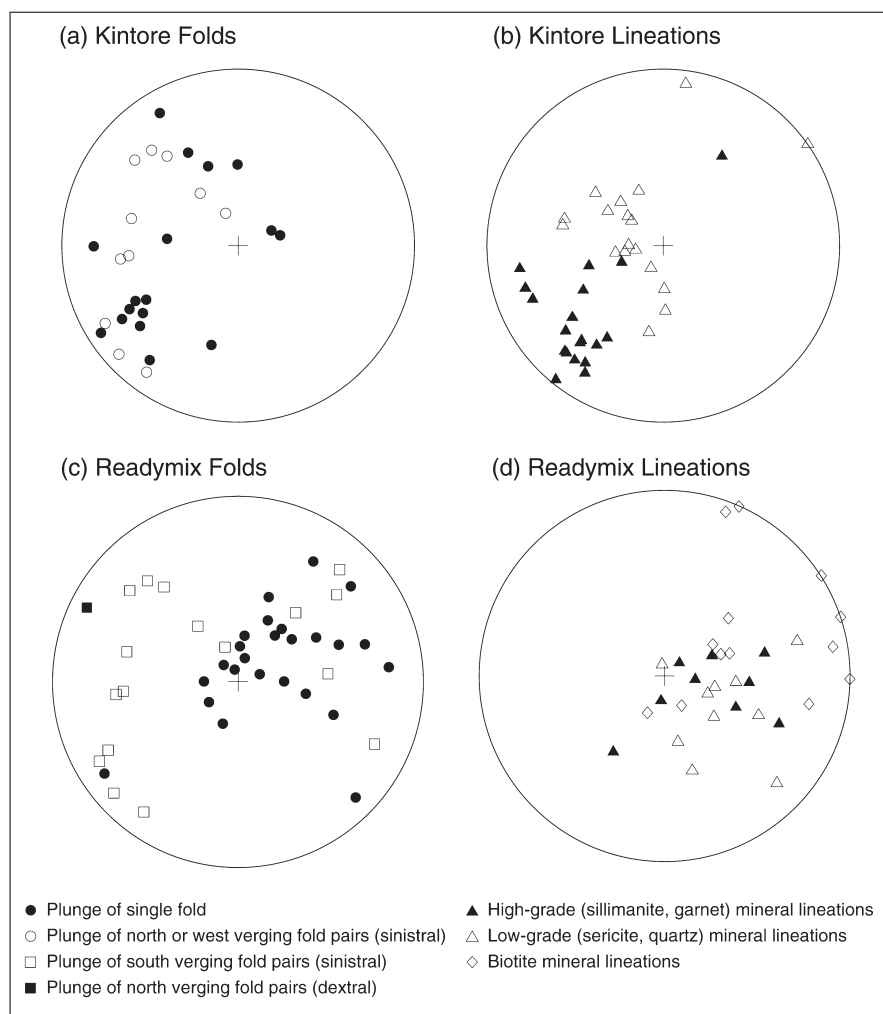


**Figure 6** Fold plunge and lineation orientation data (true north). (a) Kintore fold plunges. (b) Kintore mineral lineations. (c) Readymix Main Quarry fold plunges. (d) Readymix Main Quarry mineral lineations. All lineations are shown as plunge (pitch shown on maps). Vergence is recorded perpendicular to the fold axial plane, as viewed down the plunge of the fold axis (sinistral or dextral). Broad directions are given.

composite southwest-plunging lineation. However, the lineation is not always composite in the southern part of the field, as two sillimanite lineations have recently been discovered at Kintore (Figures 4, 6), with  $L_1$  plunging  $54^\circ$ SW, steeper than  $L_2$ , which plunges  $30^\circ$ SW.

Minor fold axes along the Line of Lode are commonly subparallel to the prominent lineation  $L_2$  (Laing *et al.* 1978). This is confirmed by data from Kintore (Figure 6a) where most folds are subparallel to the southwest-plunging sillimanite lineation, although some fold axes trend notably more northwest. Retrograde lineations at Kintore are steeper (Figure 6b) and consistent with reverse movement indicated by kinematic indicators, such as shear bands and C-S fabric (Hanmer & Passchier 1991) recorded on the Main Shear at several localities. Data from the Readymix Quarries (Figure 6c, d) are more complex, with a group of south-verging folds having variable plunge. Other folds generally tend to plunge east, subparallel to both high-grade and low-grade mineral lineations (Figure 6d).

## BOUDINAGE

Boudinage as an explanation for barren spots along the Line of Lode was first suggested by Andrews (1922) who noted that lenses of ore may have caused the planes of bedding or of crush to gape, and the gaping planes were themselves closed at the end of the lens. Boudinage occurs largely as a result of competency contrast. Many instances of such contrasts are available in the lodes, between gangue and sulfides (see discussion of rhodonite boudins above) and many workers have recorded boudinage (Hobbs & Vernon 1965; Ransom 1968; Webster 1993). Boudinage at the Kintore Opencut (Figure 4) extends the layering when viewed perpendicular to the southwest-plunging high-grade lineation (Figure 7a). Boudinage at the Readymix Quarries (Figures 5, 7) is either horizontal (parallel to the local stretching direction) or vertical, in the plane of the foliation. A distinctive example of 'fish mouth' symmetric foliation boudinage (Lacassin 1988 figure 5a) occurs in the ABM Potosi Gneiss (Figures 7b, 8), parallel to the dominant lineation fabric. Other extreme versions of foliation boudinage occur, including one example on the north wall of the Readymix Main Quarry (Figure 5) where layering is drawn into a narrow east-dipping surface for several metres, while layers in the footwall are gently warped, then undisturbed further away (Figure 7c). The deformation of the strong sillimanite lineation ( $L_2$ ) in boudin necks suggests that boudinage post-dates the primary linearity rather than produces it as suggested by Findlay (1994), and was a later manifestation of along-strike extension.

## LINE OF LODGE FOLDING

Andrews (1922) made the correlation between presence and size of drag folds and the presence and size of the orebody (Figure 2). Not only are the orebodies generally hosted by a large fold pair (termed the Main Drag Fold) consisting of the Western Anticline and the Eastern Syncline, but on a local basis ore position appears to be determined by smaller *en echelon* folds (Gustafson *et al.* 1950; Lewis *et al.*

1965; Laing *et al.* 1978). The opposing fold plunge of both ends of the orebody (steep to the northeast and moderate to the southwest) is reflected in minor folds (Gustafson 1939; O'Driscoll 1964, 1968b; Hobbs & Vernon 1965). Changes in fold plunge along the Line of Lode have been recorded by many authors and attributed to a wide variety of causes including refolding (Gustafson 1939), development of *en echelon* fold style (Lewis *et al.* 1965), interference by cross folds (Webster 1996a), a swap in the principal strain axes during the deformation history (O'Driscoll 1968a), strike changes (Both & Rutland 1976), high-angle shear zones (Ransom 1968), and parallelism with different lineations (Laing *et al.* 1978). The development of early ideas about Broken Hill structural setting is neatly summarised by Both and Rutland (1976) and by Haydon and McConachy (1987). The first workers said that the Broken Hill lodes were hosted by parasitic folds on a limb of an antiform between the Hanging Wall and Broken Hill Basins (Andrews 1922; Gustafson *et al.* 1950). A proposal that the orebody transgressed layering (Hobbs 1966; Hobbs *et al.* 1968) did not survive the recognition of more than one high-grade foliation and lineation (Rutland & Etheridge 1975; Laing 1977), and the erection of the Mine stratigraphy (Laing *et al.* 1978). Lewis *et al.* (1965) concluded that the Broken Hill lodes occurred on a limb between older (Lower) and younger (Upper) granite gneiss bodies. This was accepted by later workers (Johnson & Klingner 1976), but not by Rutland and Etheridge (1975) who reintroduced the Hanging Wall and Broken Hill synforms despite the postulated tight anticline not being supported by the layering-schistosity relationships. They proposed that  $F_1$  dislocations,  $F_2$  antiforms or  $F_2$  thrusts separated these  $F_2$  synforms. Laing *et al.* (1978) then resurrected the  $F_2$  Broken Hill Antiform as a structural necessity between two  $F_2$  synforms, although commenting that 'the axial trace probably corresponds to a symmetamorphic slide rather than a fold hinge' (Laing *et al.* 1978 p. 1124).

## Broken Hill Antiform

Several lines of evidence, including sedimentary (graded bedding), structural (minor fold pairs) and lithological correlation have been used to support the presence of the Broken Hill Antiform (Laing *et al.* 1978). None of the evidence stands up well to re-examination. Laing *et al.* (1978) showed four drillholes on sections through the Line of Lode where supporting graded-bedding evidence had been recorded. Relogging, by the author, of one example, DD508, which traversed part of the orebody footwall on the No. 2 Shaft Section (North Mine), recorded nine significant shear zones (Figure 2e) and confirmed local reversals across three of these, but was unable to substantiate any consistent younging evidence (White *et al.* 1996). Efforts by other workers along the Line of Lode since 1977 to locate the Broken Hill Antiform have also failed (Haydon & McConachy 1987).

Most mesoscopic fold pairs on the Line of Lode verge towards an antiform to the northwest, i.e. are dextral on a southwest plunge (Gustafson 1939; Laing *et al.* 1978). The structural evidence to support a vergence change across the Broken Hill Antiform quoted by Laing *et al.* (1978) is a corresponding vergence change in mesoscopic  $F_2$  fold pairs



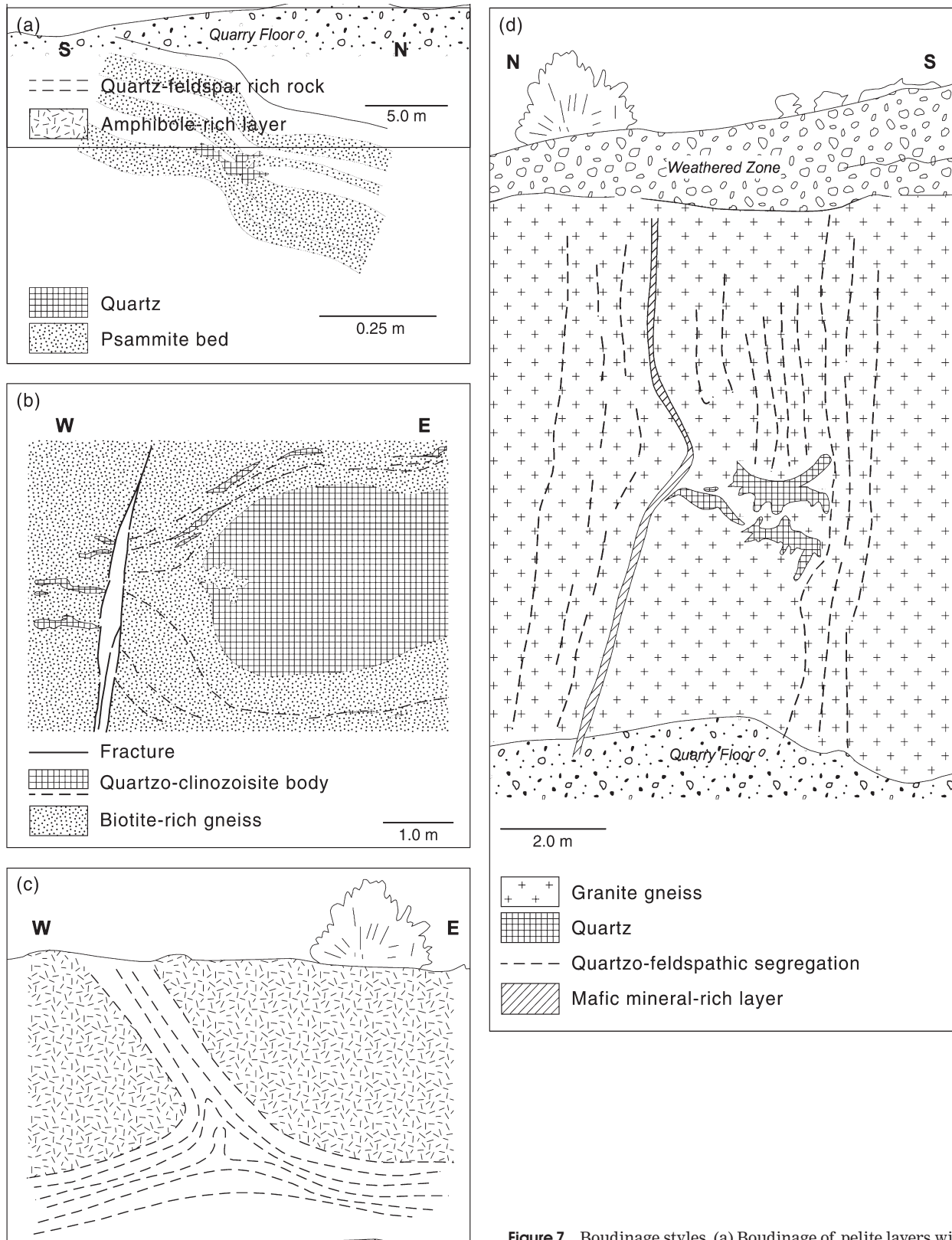


**Figure 7** Boudinage styles. (a) Boudinage of pelite layers with flow of incompetent psammite into the boudin neck, at Kintore, point B1. (b) Fish-mouth boudinage of large quartz-clinzoisite body at ABM Potosi Quarry point B2. (c) Foliation boudinage of amphibolite layer, with quartz-feldspathic gneiss intruding the neck at Readymix Main Quarry point B3. (d) Boudinage necking in granite gneiss at Readymix Main Quarry point B4. See Figures 4 and 5 for locations of points B1–B4.

in the Kintore area, where the Broken Hill Antiform was regarded as coincident with the Main Shear. Today, the outcrops in question have probably been destroyed by open-cut mining and the area is now dominated by the Kintore Opencut. However, rather than simple opposed vergence across the Broken Hill Antiform, many mesoscopic fold pairs recorded in this area verge towards the northwest, north and northeast (Figure 4). In the north part of the Kintore Opencut opposing vergence occurs in the same outcrop (Figure 9). Layering in banded gneiss contains fold pairs that verge northwest, while folds in subparallel quartz veins in the same outcrop verge southeast. Shear strain in the layering may have started to unfold the asymmetry of the first-formed folds before the introduction of the quartz veins and further fold formation. Such opposing and conflicting vergence is to be expected in progressive shear deformation (Hanmer & Passchier 1991). An alternative explanation is that, since these mesoscopic folds are incongruent to the Hanging Wall Synform and Main Drag Fold, they are part of a later, unrelated deformation event. The northwest-verging folds in Figure 9 could then represent  $D_1$ , the southeast-verging folds in the same outcrop (and the Main Drag Fold) could represent  $D_2$ , and most of the mesoscopic folds observed could be  $D_3$  or  $D_4$ . The latter appear similar to folds with pegmatite melts in the axial plane called  $F_4$  by Laing *et al.* (1978 p. 1121), which 'have no known macroscopic effects'. Whatever the explanation, the simple picture of a vergence change in mesoscopic fold pairs across the position of, and supporting, the Broken Hill Antiform does not occur in the present-day exposures at Kintore Opencut.

Correlation of the two granite gneisses, the Upper Granite Gneiss and the Lower Granite Gneiss (Figures 1, 2) is critical to antiformal fold models for the Line of Lode, such as that of Laing *et al.* (1978). Both gneiss units have been assigned to the Rasp Ridge Gneiss Formation in the Geological Survey of New South Wales mapping and stratigraphic definitions (Willis *et al.* 1983). Early workers (Andrews 1922; Gustafson 1939) also equated the two, before Carruthers and Pratten (1961) proposed that they were different and cited evidence from the Hanging Wall Synform that it was right way up. Fold vergence recorded in the Lower Granite Gneiss (Figure 5) is towards the south, or away from the position of the supposed antiform. Whole-



**Figure 8** Photograph of fish-mouth boudinage illustrated in Figure 7b; hammer (lower left) for scale.

rock analyses (Shaw and colleagues reported in Brown *et al.* 1983) show that the Lower Granite Gneiss is closer to Potosi Gneiss than the Upper Granite Gneiss (higher FeO,  $\text{Fe}_2\text{O}_3$  and Ca). Johnson and Klingner (1976) reported subtle differences between the two and pointed out the resemblance to Potosi Gneiss where garnet is present. The Lower Granite Gneiss has in fact been mapped in part, at Otto's Hill (Figure 1), as Potosi Gneiss by Brown (1983). These observations do not make the Lower Granite Gneiss Potosi Gneiss, but they cast doubt on its correlation with the Upper Granite Gneiss. The possibility that these granite gneisses are intrusive sills (Vernon & Williams 1988; Nutman & Ehlers 1998; Stevens 1998) makes their stratigraphic correlation less likely and not advisable (Vernon 1996), as sills could have intruded at different points in the stratigraphic rock sequence. The most recent geochronological work (Page *et al.* 2000) appears to confirm that bodies of Rasp Ridge Gneiss are indeed later intrusions with an age of  $1682 \pm 3$  Ma.

Similar correlation difficulties apply to other rock units on either side of the Broken Hill Antiform. Laing

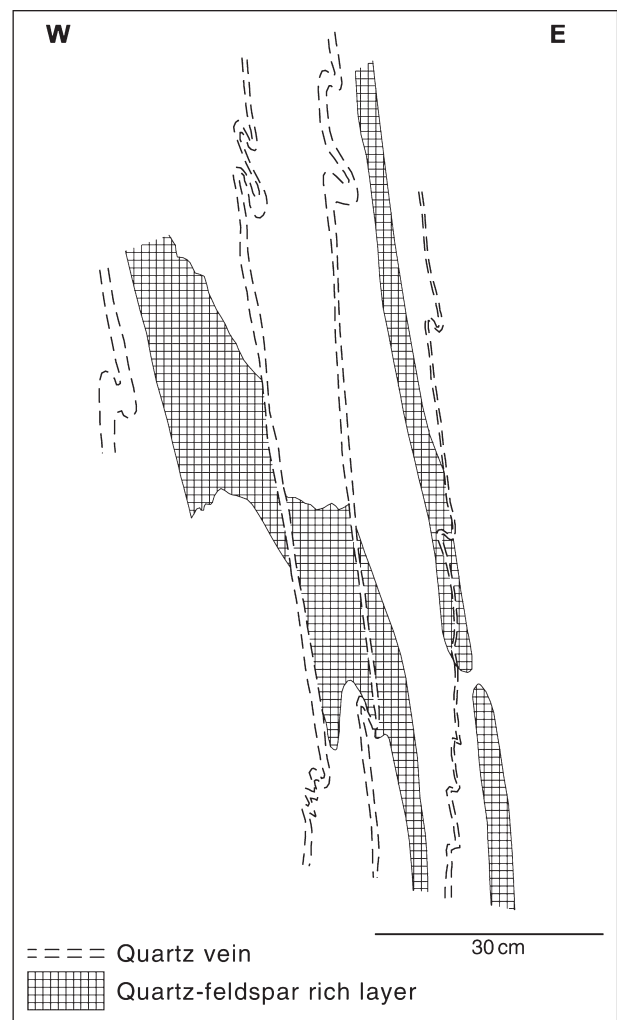


**Figure 9** Opposing fold asymmetry at Kintore Opencut. Sketch is of a vertical face located beside the ramp where it turns east at the northern end of the pit, shown by the opposing vergence symbols on Figure 4.

*et al.* (1978), when they reintroduced the antiform, did not attempt a correlation, but drew attention to the structural complexity of the east limb, and the possibility of facies changes or 'tectonic thinning'. Examination of published maps and sections of the Line of Lode show considerable differences in the number and position of different rock units across the inferred anticline (e.g. Laing *et al.* 1978 figures 1, 2, 4; Haydon & McConachy 1987 figures 5, 6). Considering the evidence above, the presence of a Broken Hill Antiform in the footwall of the Line of Lode is rejected on the basis of: (i) lack of mesoscopic structural evidence, such as fold vergence to support it; (ii) unreliability of way-up evidence in these high-grade metamorphic rocks; and (iii) lack of correlation of rock types across the supposed antiform, in particular, lack of confidence in the correlation of the two granite gneiss bodies. Here the stratigraphy proposed by Haydon and McConachy (1987) is supported by field logging only in the Line of Lode hangingwall (Figures 2, 4). Rocks in the footwall could not be assigned to stratigraphic units, but are mapped simply as rock type.

### Main Drag Fold

A critical feature of the deformation history presented in Table 1 is the timing of initial fold development. The Broken Hill orebody is located in the hinge zones and common limb of the Main Drag Fold (the Western Antiform and Eastern Synform) for its entire length (Gustafson 1939), although Webster (2000) has pointed to some complications and lack of continuity along the structure. Nevertheless, examination of serial sections, such as presented here (Figure 2) or by other authors (Hodgson 1974; Laing *et al.* 1978; Haydon & McConachy 1987) shows that a fold pair is indeed present on all sections, folding the orebodies and verging towards the southeast. This observation does not support the claims of Morland and Webster (1998) that there is no relationship between the linear form of the deposit and fold structure or that  $F_2$  folds transgressed the linearity of the lode horizon. Morland and Webster (1998) still included the Western Antiform and Eastern Synform in their deformation history (as  $F_2$ ). Hodgson (1974) recognised the difference in orientation of minor fold axes to that of the Main Drag Fold, while accepting that both existed.

On the basis of detailed structural mapping of minor folds around Lead Lode, Hodgson (1974) concluded that the Main Drag Fold was post the early layering ( $D_1$ ), but synchronous with the Belt of Attenuation during high-grade metamorphism—essentially  $D_2$ . Webster (1993) recorded two generations of minor folds in the Lead Lode and on the Lead Lode footwall contact, and assigned one to  $F_2$  high-grade deformation and one to  $F_3$  retrograde folding in the same area. As mapped by Webster (1993) and observed by Hodgson (1974), the  $F_2$  folds clearly deform the Main Drag Fold as defined by the ore-wall rock contact of Lead Lode. Therefore, the Main Drag Fold pre-dates Webster's  $F_2$ . Laing *et al.* (1978) assigned the Main Drag Fold to  $F_2$ , coaxial to  $L_1$  in the northern part of the field, but observed a retrograde schistosity in the axial surface of the Main Drag Fold and so assigned it to  $F_3$  in the southern part of the Line of Lode. However, while the retrograde fabric is probably  $S_3$ , this fabric is probably related to the later minor folds as mapped by Webster (1993) or movement on the Main Shear,

and is probably unrelated to the formation of the Main Drag Fold.

In assigning the Main Drag Fold to  $F_3$  in the south Laing *et al.* (1978) noted that it affected the Lower Granite Gneiss and because it was thought that the Lower Granite Gneiss was folded around the  $F_2$  Broken Hill Synform and that therefore the two folds were incongruous with the Main Drag Fold being formed later. However, as White *et al.* (1995, 1996, 1997) have shown, the Lower Granite Gneiss or Eastern Gneiss may not be folded around the Broken Hill Synform (see also Figure 2d). The Broken Hill Synform does not have the same 'banana-bend' plunge culmination or dome as the Hanging Wall Synform or the Line of Lode do in their central part. In fact the Broken Hill Synform is hosted in a different thrust sheet (the Airport Thrust Sheet) and is reclined, whereas the folds along the Line of Lode have variable plunge, but are mostly upright (White *et al.* 1995). This difference in fold style, which was first picked up in mapping by Brown (1983), the lack of evidence for the Lower Granite Gneiss being folded around the Broken Hill Synform, the fold timing relationships of Hodgson (1974) and Webster (1993), the assignment of the Main Drag Fold to  $F_2$  rather than  $F_3$  in the northern part of the field by Laing *et al.* (1978), and its parallelism to  $L_1$  in this area, all suggest that the Main Drag Fold formed either late in  $D_1$  or possibly early  $D_2$ , prior to the main phase of  $D_2$  deformation. So, the Main Drag Fold is early, and this early fold development may have been critical to the creation of a

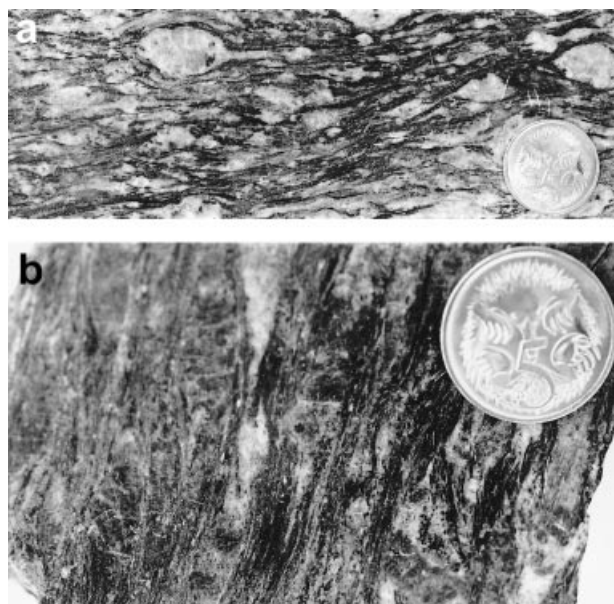


**Figure 10** Mylonitic rocks from unoriented drillcore from NBHC Shaft Section. Kinematics in both samples shown by  $\sigma$  type clast asymmetry and shear bands (Hanmer & Passchier 1991). (a) Protomylonite from granite gneiss at point 1 on Figure 2a [Drillhole N250 at 512 m (1680 feet)]. Large crystals are K-feldspar; matrix is made up of biotite, garnet and quartz. Asymmetry is sinistral in this view. (b) Mylonite with pelitic composition from point 2 on Figure 2a [Drillhole N250A at 954 m (3132 feet)]. Dark K-feldspar augen sit in a matrix of sillimanite (white) and biotite (black). Garnet is spotted throughout. Asymmetry is left-hand-side towards the top (dextral) in this view. Coin is 2 cm in diameter in both photographs.



structural site to attract mass transport of sulfides and gangue. There is evidence from fold mechanisms that minor drag or parasitic folds form prior to differential shear on major fold limbs (Ramsay & Huber 1987), as there is no tendency to form minor folds in the flexural slip process. Such minor folds probably form earlier through buckling of a competent layer under layer-parallel shortening (Ramsay & Huber 1987). Note that it is not clear which units were more or less competent at this time. In Kintore, boudinage in Unit 4.5 (Figures 4, 7a) is largely of pelitic units, with psammitic and banded iron-formation layers acting incompetently and being drawn into boudin necks. Relative competence could change during deformation as water content decreased.

### LINE OF LODE SHEAR ZONES

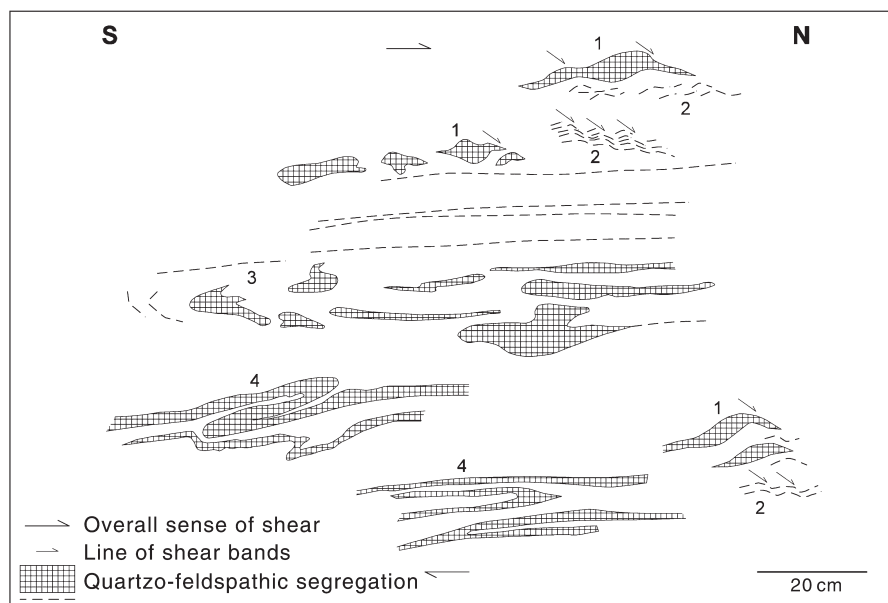
The basic geometry of the Line of Lode was recognised early. The Line of Lode occurs between two synforms, and no antiformal trace is obvious. Rocks outside the Line of Lode are relatively undeformed, while deformation increases towards the orebodies and the area where the trace of the antiform should occur. The importance of the high-strain zone around the orebodies is a contentious issue. Both high-grade (Belt of Attenuation, Thompson Shear) and retrograde shears (Main Shear) are recognised to occur along the Line of Lode. In the following section the development of ideas about shear deformation on the Line of Lode are traced with a view to establishing that high strain is indeed of prime importance along the Line of Lode.

Andrews (1922) described the Hanging Wall Basin as separated from the Broken Hill Basin by the Broken Hill Lode and a zone of rock crush and flowage. He regarded this shear zone to be a separate, mineralised type to the wide zones of coarse schist, such as the barren Thackaringa-Pinnacles. The mineralised shears were identified by associated narrow zones of sericite schist, silicified laminae, drag folding and visible faulting. The divergence of the Line of Lode (Figure 1) with respect to the Footwall

(Potosi) Gneiss and the Alma amphibolite on the footwall side and a corresponding convergence of the Upper Granite (Augen) Gneiss and what was later identified as the Unit 4.4 amphibolite (Parnell Formation) on the hangingwall side was noted by Andrews (1922 p. 175) and attributed to 'dislocation or rock flowage' along the Line of Lode trend. Two shear zones, in particular, have been prominent in any discussion of shearing along the Line of Lode. These are the Belt of Attenuation and the Main Shear, both terms being introduced by Gustafson (1939). The Belt of Attenuation was thought to be generally coincident with the Eastern Syncline. The Main Shear was defined as 'merely the most conspicuous (plastic) shear plane at any place within the Belt of Attenuation' (Gustafson 1939 p. 58). 'Schisting', or as we understand today 'retrograde', was clearly regarded as later by Gustafson (1939) and Gustafson *et al.* (1950). In later works (Laing *et al.* 1978; Webster 1993) there has been a tendency to regard the term Main Shear as describing the retrograde shear often found on the eastern side of the Line of Lode (Figure 2), with the term Belt of Attenuation reserved for the high-grade ductile zone that affects the ore horizon between ZC (Zinc Corporation) and Delprat's Shafts (Figure 1).

As well as the Belt of Attenuation described above, many authors have alluded to other high-grade shearing along the Line of Lode. Rutland and Etheridge (1975) proposed an  $F_1/F_2$  thrust or antiform between the Hanging Wall and Broken Hill Basins. A divergence of the lode horizon and the Lower Granite Gneiss was noted by Both and Rutland (1976). Hodgson's (1975a) ideas of a 5-stage shear modification of Lead Lode are based on the recognition that the ore is surrounded by high-grade shears and cut by low-grade ones. Major  $D_1$  shear zones were proposed for the eastern side of the orebody by Archibald (1978), their location determined by changes in facies. Laing *et al.* (1978 figure 11a) showed the lode horizon bounded by high-grade shears and identified the zone east of the orebody as a zone of dislocation and high strain. High-grade shearing has also been identified on the hangingwall of Lead Lode—the Western Zone of Folding and Transposition—by

**Figure 11** Composite sketch of structural features in mylonite at Kintore Opencut (near location M on Figure 4). 1, asymmetric quartzo-feldspathic segregations; 2, shear bands; 3, truncation of layering; 4, isoclinal folds. Small arrows indicate shear sense of individual shear bands. Overall shear sense is dextral/thrust on the southwest-plunging lineation [the view is perpendicular to the lineation (X) and the main compression direction (Z)].



Webster (1993). In much of the early work, the term 'shear' became synonymous with 'retrograde shear' or even 'cataclasite' to many workers. High-grade mylonites were recognised in the Broken Hill area by White *et al.* (1995) as having a well-developed stretching lineation formed by aligned and stretched sillimanite or garnet set in a recrystallised matrix, and asymmetric internal structures, such as shear bands, C-S or C-C' fabric (Hanmer & Passchier 1991). This study, through core relogging and fieldwork using similar criteria, has identified discrete high-grade mylonites and protomylonites in the Line of Lode. Several locations are indicated on Figures 2 and 4, while specific examples are illustrated in Figures 10 and 11. The examples from unoriented drillcore (Figure 10) on the NBHC Shaft Section (Figure 2a) come from the Upper Granite Gneiss and a pelite assigned to Unit 4.8 (compare the same section in Haydon & McConachy 1987 figure 12). The latter occurs in the immediate footwall of A lode. The high-grade deformation features at Kintore Pit, which are illustrated in Figure 11, come from a shear zone between Zinc and Lead Lodes.

All the evidence presented above points to the possibility that in fact the orebody is contained within or bounded by a high-grade shear zone for its entire length. High-grade shearing is not confined to the Belt of Attenuation or the Thompson Shear—these are simply strands, analogous to shear bands (Hanmer & Passchier 1991), slightly more northeast–southwest-oriented than the main lode direction, across which the Line of Lode is shifted in a sinistral sense (Figures 1, 12). Note that there is no dislocation of the Line of Lode across the Belt of Attenuation or Thompson Shear: the offset is ductile, resulting in Line of Lode changing direction and moving more to the north as it runs northeast. The angle of the Thompson Shear relative to the main Line of Lode is rather large at between 30 and 60°, but it may have been rotated by movement on the later retrograde British shear, which was east-block-up and dextral on a stretching lineation that plunges 60°S at Readymix (Figure 5). The effect is similar to a riedel shear in brittle wrench tectonics (Wilcox *et al.* 1973). The high-grade shearing next to the ore horizons in both hangingwall and footwall at Kintore, Block 14 and No. 1 Opencut (Figure 2) are all outside the Belt of Attenuation or the Thompson Shear and are part of a Line of Lode shear system, called here the Line of Lode Shear. This shear broadly corresponds to the Broken Hill Thrust Sheet of White *et al.* (1996). It is not clear precisely how wide the Line of Lode Shear is, as the footwall area is less well-exposed. On the hangingwall side, the Mine Sequence (Units 4.1–4.5) appears to preserve good sedimentary features. Deformation rapidly increases from Unit 4.5 eastwards into the lode horizon and continues strongly into the footwall side in the No. 1 Opencut (White *et al.* 1995) and Kintore (Figure 4). High-grade mylonitic rocks occur throughout the footwall (Laing *et al.* 1978) to the Lower Granite Gneiss (Figures 2, 4). On either side, the Sundown and Airport Thrust sheets (White *et al.* 1995) appear to have lower strain, although as part of the same fold and thrust belt they share many of the same structural features (White *et al.* 1995). Deformation style in the ore horizon itself is often described as plastic (Gustafson *et al.* 1950; King & Thomson 1953; Carruthers 1965; Ransom 1969). This

could be due to higher shear strains, fluid pressures or competency contrast. Clearly the Line of Lode Shear has undergone deformation partitioning with some horizons more sheared than others that preserve sedimentary features. As the shearing is subparallel to layering, which has large compositional differences (pelite–psammite–amphibolite) and sharp boundaries, bedding-plane reactivation probably played a major role. On a broad scale the Line of Lode Shear dislocates geological units: there is truncation of amphibolite horizons along its footwall (Andrews 1922; Both & Rutland 1976; White *et al.* 1995, 1996, 1997).

## Kinematics

The two overprinting sillimanite lineations at Lords Hill and Kintore described above probably relate to transport or extension directions. The Line of Lode Shear shares  $L_2$  with the regional deformation, as do many of the shears in the Broken Hill area (White *et al.* 1995). At Kintore (Figure 12) sillimanite-bearing mylonites occur with kinematic indicators, such as shear bands, that suggest oblique dextral and northwest-block-up reverse movement on the southwest-plunging lineation. At Readymix Quarries, kinematic indicators are less clear, with strike-parallel high-grade and low-grade shears both showing evidence of movement towards the south as well as to the north. The preponderance of south-verging minor fold pairs is consistent with north to south movement. Kinematics on the British Fault are clearer, with thrust/sinistral movement indicated on a moderate south-plunging stretching lineation. The Belt of Attenuation and Thompson Shear are synthetic (shears at a small angle to the main shear direction with the same movement sense)

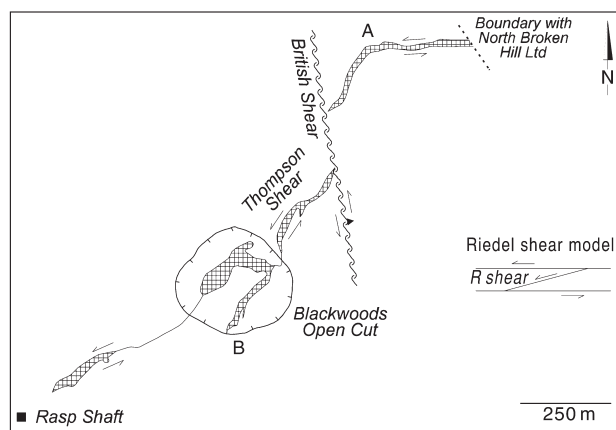


**Figure 12** Thompson Shear as a synthetic structure during northeast–southwest sinistral shear along the Line of Lode. The Thompson Shear is a ductile shear zone that sinistraly offsets No. 3 lens (hatched) between points A and B: the change in strike at point A is the most obvious effect. The Line of Lode is further offset and probably rotated by later sinistral movement on the British Shear. The Thompson Shear may have developed as a riedel type shear (illustrated by inset) or shear band (Hanmer & Passchier 1991) during bulk sinistral shear along the Line of Lode. The geometric pattern of No. 3 lens in Blackwoods Opencut is affected by the Western Antiform. Diagram after van der Heyden and Edgecombe (1990).

high-grade shears that cause minor sinistral offsets in the lodes (Morland & Webster 1998). An antithetic east–west dextral ductile shear was described from Lead Lode by Hodgson (1974). These conjugate shears and the obliquity of *en echelon* folds are consistent with sinistral movement along the Line of Lode Shear, as originally suggested by O'Driscoll (1968b). During retrograde conditions, movement direction on the Line of Lode Shear changed to west-block-up reverse, indicated by vertical mullions of ore on the Main Shear (Gustafson 1939) and modern kinematic indicators (Webster 1993; White *et al.* 1995) (Figure 4). Combining the observations of the occurrence of high-grade shears, stretching lineations and the kinematics along the Line of Lode it must be concluded that movement on the Line of Lode Shear has been complex (Table 1) and needs more work and documentation. Early work, prior to the recognition of kinematic indicators, understandably proposed conflicting movement directions to that described above (O'Driscoll 1964, 1968a, b; Hodgson 1974).

## SULFIDE MOBILITY

To a structural geologist, the linear to ribbon shape of the orebodies and their parallelism to fold plunge, sillimanite lineations and gneissic L tectonites (ABM Potosi) in the wall rocks clearly suggest that the shape is imposed by deformation. The linear shape is disrupted by the high-grade shears of the Belt of Attenuation and the Thompson Shear, placing the development of linearity in the early part of the high-grade metamorphic event(s) at the latest. Carruthers (1965) suggested that the presence of sulfide could have acted as a locus of weakness that localised the deformation. Laing *et al.* (1978) recognised that the orebodies' linearity has been at least strongly accentuated during deformation or is entirely tectonic, but favoured an original sedimentary linearity. Note that this would have to be coaxial with, not only later  $F_1$ ,  $F_2$ ,  $F_3$  and  $F_4$  folds, but, in part, both early sillimanite lineations. This line of argument had been discounted earlier by Lewis *et al.* (1965 p. 331) who dismissed a sedimentary origin for the ore on the basis that it becomes necessary 'to assume that the fold pattern was precisely determined by the original metal content of the bed. This possibility because it is one of extreme coincidence, . . . seems unlikely'. Instead, many workers (Both & Rutland 1976; Laing *et al.* 1978) have suggested mass transport of sulfides (and gangue minerals) during deformation to generate the linear shape. The work of Ramdohr (1950), Hodgson (1974, 1975a, b), Laing *et al.* (1978) and Webster (1993) restricts this possible mass transport to the earliest period of high-grade metamorphism and deformation. Pb and Zn are soluble, hence mobile, at high temperatures (above 300°C) in metamorphic fluids, and galena and sphalerite are mechanically soft relative to silicate minerals (Oliver *et al.* 1998). Transport would probably have been by fluids infiltrating the area (Marshall *et al.* 1999; Williams *et al.* 1999), which may have also delivered the gangue components (Ca,  $O_2$ ,  $CO_2$ , Mn, Si). Alternatively, transport may have been a solid-state reworking of a pre-existing orebody—high strain and high strain gradients will allow the 'squeezing' of sulfides into a relatively low-strain site (Oliver *et al.* 1998). Textures in the

sulfide ores of the main orebodies that owe their origin to further movement, post-primary development, or emplacement have been defined and mapped by Webster (1993). For instance, the outer parts of Lead Lode are characterised by deformed sulfide ore types, such as Pebble Ore, with durchbewegung structure and Saccharoidal Ore (Webster 1993). The sulfide lodes show evidence of remobilisation from high-grade metamorphic conditions through to relatively low-temperature retrograde conditions (Carruthers 1965; Lewis *et al.* 1965; Webster 1993, 1996b). The clearest examples of remobilised sulfide bodies are the droppers, which are described in the next section.

## Droppers

Droppers are narrow, usually tabular, sheets of ore that cut across lithological boundaries in the crests of synclines (and anticlines, where they have been called uppers). They have been known for a long time (King & O'Driscoll 1953). They consist of fragments of wall rock and silicate-rich ore in a matrix of coarse, recrystallised sulfides (Hodgson 1974, 1975b; Maiden *et al.* 1986), such as galena, sphalerite and pyrrhotite. The clasts sometimes contain an earlier mineralogy and recrystallised texture (e.g. polygonal garnet grains now fractured and injected by sulfides), suggesting that the main part of the orebody had recrystallised prior to dropper formation (Maiden 1976). Droppers can be considered similar to piercement veins, which are formed by layer-parallel extension (Marshall & Gilligan 1989). Given that the layers are usually in flattish fold hinges, this suggests that compression was essentially steep to vertical during dropper formation. Dropper formation is thought to have been initiated during high-grade metamorphism, synchronous with the development of the Belt of Attenuation (Hodgson 1974). Wall-rock fragments can be replaced by garnet sandstone, sulfides, quartz–calcite–hedenbergite or epidote–quartz–garnet (Maiden 1976). Most clasts are altered, with few retaining the mineralogy and texture of neighbouring wall rocks. The droppers themselves are enriched in sulfides relative to gangue minerals as well as in lead and silver compared to the main lodes (Maiden 1976), suggesting preferential mobility of galena. A similar differentiation of sulfides was proposed by Webster (1996b) to account for the formation of silver-rich pegmatitic galena veins that cut the lodes and garnet quartzite bodies. The presence of a fluid phase, which could have acted as a transport medium during dropper formation, is suggested by the occurrence of veins originating from droppers that contain quartz, hydrous minerals and terminated crystals of silicates (Maiden 1976), and by the occurrence of euhedral pyrrhotite in droppers (Ogierman 1984). Textures within droppers suggest ductile deformation: development of foliation parallel to the margins (Hodgson 1974; Maiden *et al.* 1986), brecciation, entrainment and injection of sulfides into wall-rock clasts (Maiden 1976). Most droppers are bounded by zones of retrograde schist (Maiden 1976), which suggests that either some dropper formation continued during the retrograde event or that these contacts were preferentially exploited by later shear zones.

Several critical timing relationships can be used to time the formation of droppers. Droppers cut across the

gneissosity or layering indicating that their formation post-dates  $S_1$  (Hodgson 1974). Similarly, the localisation of droppers at fold crests of the Main Drag Fold indicates that their formation post-dates this episode of folding. Because droppers themselves contain high-grade minerals, this also shows that the Main Drag Fold was in place before the end of high-grade metamorphism. Furthermore, evidence of relict recrystallisation textures preserved in clasts in droppers (Maiden 1976) and evidence of dropper ore being derived from ore in the main bodies through alteration at high metamorphic grade (Hodgson 1974, 1975b), suggests that droppers were formed after the main orebodies had already been metamorphosed to high-grade (granulite) facies. In summary, droppers were initiated during high-grade metamorphism, but post-date some high-grade metamorphism,  $S_1$  and the Main Drag Fold. Dropper formation exploited crests and axial planes, suggesting that the principal compressive stress may have moved from a position at a high angle to the fold axial planes to one more subparallel or parallel. This could be consistent with either northwest-block-up reverse or strike-slip shear along the Line of Lode.

## DEFORMATION HISTORY OF THE LINE OF LODGE

The above sections have described the geometry and structural features of the Broken Hill Line of Lode. The following discussion attempts to interpret these features as part of the deformation history, looking in particular at the timing of development of the main features. The kinematics presented above allow a picture to be built of the deformation history of the Line of Lode Shear (Table 1), which contrasts with that recently proposed by Morland and Webster (1998). No evidence has been recorded of any movement events that may have occurred before high-grade metamorphism.

### Discrete deformation phases

The deformation history of the Broken Hill Line of Lode is here proposed to be the history of a shear zone. As such, regionally identified events  $D_1$ – $D_3$  can only be broadly correlated with events in the shear. Progressive deformation and rotation of structural elements has led to a more complex deformation history than might be expected in other parts of the Willyama Block: although the Line of Lode has seen the most work, it is not the best place to determine the regional deformation history. Shear-zone-hosted progressive deformation may have also lead to misidentification of fold and foliation phases in the past. In a polyphase deformation event in a shear zone it is very difficult to separate discrete phases. Indeed, in the Broken Hill Block in general, Hobbs *et al.* (1984 p. 359) found that 'isolated folds or schistosity could not always be assigned to a specific deformation event'. Geochronology (Nutman & Ehlers 1998) may point to at least one discrete metamorphic/structural event (called here  $D_1$ ) prior to the main event (called here  $D_2$ ) at 1600 Ma. Annotation of structural features as  $L_1$ ,  $S_1$  etc. in this paper represents the recognition that these features are older than the main phase of  $D_2$ , but may simply be part of an early phase of

$D_2$  Line of Lode Shear movement. Peak metamorphism occurred during  $D_1$  or early  $D_2$  and it is important to note that it is most unlikely that significant deformation occurred only after peak metamorphism and not before. Hence,  $D_1$  is simply the earliest deformation recorded and may post-date earlier deformation between sedimentation and peak metamorphism.

It is accepted by most workers that the lower temperature retrograde shear zones that are so common in the Broken Hill Block belong to one or more later deformation events than most of the high-grade deformation. This has been termed  $D_3$  (Laing *et al.* 1978), but was assigned to a later event than  $F_4$  folding by Hobbs *et al.* (1984). However, both Laing (1977) and Marjoribanks *et al.* (1980) claimed to have discovered  $S_3$  of sillimanite grade, and other workers refer to three high-grade deformation events (Gibson 2000; Leyh 2000). Overprinting high-grade foliations could be expected to develop as part of a progressive shear event (during  $D_1$  or  $D_2$ ) and there would be no need to number each foliation as a different deformation event. Similarly, the presence of higher temperature minerals, such as sillimanite or kyanite, in some shear zones could reflect an earlier higher temperature history of the shear zone, rather than providing evidence of high temperature during  $D_3$ . In this paper the term  $D_3$  is applied to the lower temperature deformation event (or events) that gave rise to the retrograde mineralogy of the shears.

### $D_1$

Marjoribanks *et al.* (1980) and Hobbs *et al.* (1984) both assigned a major nappe-forming event to this deformation phase, while disagreeing about the coaxiality of  $F_1/F_2$  and the resultant interference patterns.  $D_1$  on the Line of Lode could be represented by the recognisably early features, such as bedding-parallel foliation and rare isoclinal folds in the layering (Hodgson 1974), or the earliest sillimanite lineation,  $L_1$  (Laing *et al.* 1978). Alternatively, such features could represent an early phase of  $D_2$  fold and thrust development. The sulfide orebodies are parallel to  $L_1$ , as is the Main Drag Fold, at the North Mine (Laing *et al.* 1978). This area may represent a window to the early event. The kinematics of early deformation also remain obscure due to overprinting. Both  $L_1$  and  $L_2$  could represent stretching or transport directions from different phases of the same progressive shear event during  $D_2$  or shear during  $D_1$  overprinted by  $D_2$ .

### $D_2$

The parallelism of the strong sillimanite lineation ( $L_2$ ) with major folds regionally and within the Line of Lode Shear places this event firmly in what has been termed  $D_2$  (Laing *et al.* 1978). At North Mine, the  $L_2$  lineation overprints  $L_1$  (Laing *et al.* 1978) as do shear zones (White *et al.* 1995) and minor folds (termed  $F_4$ , 'coaxial with  $L_2$ ' by Laing *et al.* 1978 p. 1121), with pegmatite melts along the fold axial plane, that share  $L_2$ . At Readymix Quarries, which is generally in the northeast-plunging domain (Laing *et al.* 1978), two groups of folds occur (Figure 6), one plunging west and verging south, the other plunging steeply east. These could be either more- and less-rotated folds in the Line of Lode Shear, or a



west-plunging group ( $D_2$ ) overprinting an east-plunging group ( $D_1$ ). Several features (see Kinematics section and Table 1) have now been defined that occurred at high-grade and appear to post-date  $D_1$  structures:  $F_2$ ,  $L_2$ ,  $S_2$ , droppers, boudinage, and minor folds in Lead Lode that deform  $L_2$ . These all broadly belong to  $D_2$ . All of these structures generally share northwest-southeast or northeast-southwest principal strain axes that are consistent with thrust transport to the southeast (White *et al.* 1995). During such movement on a southwest-plunging sillimanite lineation, oblique dextral and northwest-block-up reverse movement on the northeast-southwest Line of Lode Shear would have taken place. The plunge culmination could have developed during this phase (White *et al.* 1995). The Line of Lode was later overprinted at high-grade by northeast-southwest sinistral shear along the Belt of Attenuation and Thompson Shear (Figure 12), with minor conjugate east-west dextral shear (Hodgson 1974).

### $D_3$

The retrograde schist zones are a prominent feature of the Broken Hill Block due to the formation of wide zones of chlorite, biotite or quartz-sericite schist, although often with only minor displacement (White *et al.* 1995). This event, accompanied by greenschist-facies metamorphism, appears to have had only minor influence on the Line of Lode, although a retrograde foliation is widely developed. New shears, such as the Globe Vauxhall, British and De Bavay, were formed, cutting across the Line of Lode, while the pre-existing Main Shear was reactivated, probably as a back-thrust to the general northwest-directed transport direction of White *et al.* (1995).  $F_3$  folds are rarer: retrograde folding ( $F_3/F_4$ ) is described by Hobbs *et al.* (1984) to be largely confined to the northwestern part of the Broken Hill Block. The reclassification, above, of the Main Drag Fold from  $F_2$ - $F_3$  (Laing *et al.* 1978) to late  $F_1$  or early  $F_2$  leaves  $D_3$  without a major mesoscopic fold on the Line of Lode. Folds described as  $F_4$ , with pegmatite melts on the axial plane (Laing *et al.* 1978), probably belong to the earlier, higher temperature deformation phase  $D_2$ .

### Later deformation

Prominent, but minor in terms of offset, cataclastic fault zones on the Line of Lode, such as the Central Fault (Webster 1993), belong to a later phase of brittle deformation, possibly Delamerian (Morland & Webster 1998). Evidence of Delamerian reactivation of the retrograde shear zones was provided by a study on a shear zone at the ABM Quarry (just east of point B2 on Figure 4) by Etheridge and Cooper (1981).

### ORE GENESIS

Consideration of the structural features of the Broken Hill Line of Lode reveals support for epigenetic models as the ore appears to occupy a low-strain dilational site in a major shear zone to which fluids could have been expected to flow. This conclusion is in contrast to the suggestion of Marjoribanks *et al.* (1980) that the Broken Hill orebody does

not have a unique structural position in the region. The association of the Broken Hill orebody with a low-strain fold hinge, high-grade shear zone, skarn mineralogy and carbonate support an epigenetic model of ore formation by syntectonic carbonate replacement (Huston *et al.* 1998). Initial delivery of sulfides and gangue minerals to the structural site could have been by fluid movement at high temperature (Oliver *et al.* 1998; Marshall *et al.* 1999), while transposition and metamorphic differentiation probably imposed the layering and accentuated the linearity by solid-state processes, similar to those described by Duckworth and Rickard (1993), later in the prograde metamorphic history.

No support for syngenetic models can be gained from the structural evidence. Other evidence to support syngeneses, such as sharp compositional boundaries, zoning, lack of evidence for metamorphic reactions, and differing proportions of volatiles (Stanton 1976b), could equally have been imposed by metamorphic differentiation, or tectonic processes during  $D_1/D_2$  with dynamic recrystallisation at peak metamorphism. Evidence is emerging that calls into question the occurrence of exhalites other than banded iron-formation in the Broken Hill Block: Stevens (1998) suggested that garnet quartzites may be metamorphosed alteration products, quartz gahnites may have been formed by lateral fluid flow along permeable horizons and tourmalinites may have formed by replacement. Although envisaged as early (i.e. synsedimentation) it is unlikely that such processes could achieve the fine layering quoted in support of sedimentary models of ore formation. Recently, Leyh (2000) has described quartz gahnite rocks as epigenetic. A remobilised model of exhalative or other origin, with subsequent transport of sulfide as well as gangue constituents *en masse* during prograde deformation, and prior to transposition and metamorphic differentiation, could be used to fit a syngenetic model to the structural evidence. This model is less attractive as it requires two ore-forming events instead of one.

### CONCLUSIONS

The evidence of transposition and high strain in the wall rocks of the Broken Hill orebodies leaves little doubt that any compositional layering in the softer orebodies is derived from high-grade metamorphic or tectonic processes, rather than sedimentary processes. Similarly, there can be little doubt that the linear/ribbon shape of the Broken Hill orebodies is not a preserved pre-tectonic shape, but one which is derived from their intimate association with fold hinges and their parallelism to strong tectonic lineations. Structural evidence, mainly from field evidence of high-grade mylonites (Figures 10, 11), suggests that the Main Drag Fold in which the orebodies are located is itself contained in a Line of Lode Shear for its entire length. Examination of the deformation history of this shear zone shows that the Main Drag Fold formed early in the structural history, and so may have acted as a low-strain locus for the deposition of sulfides and gangue minerals, probably from a fluid phase. There is no structural support for models of deformed pre-metamorphic sulfide accumulation, or that such accumulations had an original linear

shape. However, the pre-peak metamorphic history of the Line of Lode is obscured by dynamic recrystallisation, so some uncertainty must remain as to the origin of the sulfide orebodies. As a consequence of the recognition of the Line of Lode Shear, the presence of a Broken Hill Antiform is rejected, along with previous lithological correlation of rock units from the orebody hangingwall to the footwall.

## ACKNOWLEDGEMENTS

This work was carried out mostly while I was employed by Pasminco Exploration. The figures were drawn by Val Preedy at Great Central Mines Ltd (now Normandy Yandal Operations Ltd), Perth. The primary supporters and mentors to me for this work were Stan White, Terry Barclay, Tom Eadie, Thella Burford, Bob Haydon and Ron Morland. The most helpful in crystallising ideas through spirited debate were Barney Stevens, Mike Schuler and Tony Webster. This work also benefited from discussions with Kevin Capnerhurst, Linda Dobe, Nathan Duhig, Ken Hickey, Terry Lees, Dave Larsen, Wolf Leyh, Gordon Lister, John Stockfeld, John Vinar, Barry Murphy and Ian Oppy. I would like to thank Geoff McConachy of Normandy Ltd and staff at Readymix Quarries for access to their opencuts. I would also like to thank Andrew Aitchison, Mike Bartholomeus, Doug Brewster, Jeff Burford, Gary Burton, Brian Casey, Cath Chalmers, Ian Cook, Deryn Enderby, Donna Grillett, Mike Hicks, Natalie Hiddlestone, Steve Hinde, Heidi Hohnberg, Mike Hudson, Andor Lips, Jon Moore, Mike Powell, Lachlan Reid, Bruce Somerville, Annette Wilson and John Wickham who all contributed in some way to this work. The reviewers, Chris Wilson and Barney Stevens, hammered the text into a much more coherent story from the early ramblings.

## REFERENCES

- ANDREWS E. C. 1922. The Geology of the Broken Hill District. *Geological Survey of New South Wales Memoir* 8.
- ARCHIBALD N. J. 1978. Stratigraphic controls on Pb–Zn sulphide mineralisation in the Proterozoic Willyama Supergroup. Report to the Broken Hill Mine Managers Association (unpubl.).
- BINNS R. A. 1993. Is Pegmont a stratiform-exhalative base metal sulfide deposit? In: *Symposium on Recent Advances in the Mount Isa Block, Sydney, May 21 1993*, pp. 55–56. Australian Institute of Geoscientists Bulletin 13.
- BOTH R. A. & RUTLAND R. W. R. 1976. The problems of identifying and interpreting stratiform orebodies in highly metamorphosed terrains: the Broken Hill example. In: Wolf K. H. ed. *Handbook of Stratabound and Stratiform Ore Deposits*, Vol 4. pp. 261–325. Elsevier, New York.
- BROWN R. E. 1983. *Broken Hill 1:25 000 Geological Sheet, 7134-II-S*. Geological Survey of New South Wales, Sydney.
- BROWN R. E., STEVENS B. P. J., WILLIS I. L., STROUD W. J., BRADLEY G. M. & BARNES R. G. 1983. Quartz-feldspathic rocks. *Geological Survey of New South Wales Record* 21, 127–226.
- CARRUTHERS D. S. 1965. An environmental view of the Broken Hill ore occurrence. In: McAndrew J. ed. *Geology of Australian Ore Deposits*, pp. 339–351. Proceedings of the 8th Commonwealth Mining and Metallurgical Congress 1. Australasian Institute of Mining and Metallurgy, Melbourne.
- CARRUTHERS D. S. & PRATTEN R. D. 1961. The stratigraphic succession and structure in The Zinc Corporation Limited and New Broken Hill Consolidated Limited, New South Wales. *Economic Geology* 56, 1088–1102.
- CONDON M. A. 1959. Sedimentary structures in the metamorphic rocks and orebodies of Broken Hill. *Australasian Institute of Mining and Metallurgy Proceedings* 189, 47–65.
- DEWAR G. J. A. 1968. Detailed geological mapping north-east of No. 3 Shaft, North Broken Hill Limited. In: Radmanovich M. & Woodcock J. T. eds. *Broken Hill Mines—1968*, pp. 137–153. Australasian Institute of Mining and Metallurgy Monograph 3.
- DUCKWORTH R. C. & RICKARD D. 1993. Sulphide mylonites from the Renstrom VMS deposit, Northern Sweden. *Mineralogical Magazine* 57, 83–91.
- EILU P. K., MATHISON C. I., GROVES D. I. & ALLARDYCE W. J. 1999. Atlas of alteration assemblages, styles and zoning in orogenic lode-gold deposits in a variety of host rock and metamorphic settings. *Centre for Strategic Mineral Deposits and University of Western Australia Extension Publication* 30.
- ETHERIDGE M. A. & COOPER J. A. 1981. Rb/Sr isotopic and geochemical evolution of a recrystallized shear (mylonite) zone at Broken Hill. *Contributions to Mineralogy and Petrology* 78, 74–84.
- FINDLAY D. 1994. Boudinage, a reinterpretation of the structural control on the mineralisation at Broken Hill. *Australian Journal of Earth Sciences* 41, 387–390.
- GENTLE L. V. 1968. Geology of the western limb and Western Mineralisation at Broken Hill South Limited. In: Radmanovich M. & Woodcock J. T. eds. *Broken Hill Mines—1968*, pp. 179–183. Australasian Institute of Mining and Metallurgy Monograph 3.
- GIBSON G. M. 2000. Tectonic evolution of the Palaeoproterozoic Willyama Supergroup, Broken Hill: the early years. *Australian Geological Survey Organisation Record* 2000/10, 45–47.
- GLEN R. A. & LAING W. P. 1975. The significance of sedimentary structures in the Willyama Complex, New South Wales. *Australasian Institute of Mining and Metallurgy Proceedings* 256, 15–20.
- GUSTAFSON J. K. 1939. Geological investigations in Broken Hill. Final Report to the Mine Managers Association Volume 1 (unpubl.).
- GUSTAFSON J. K., BURRELL H. C. & GARRETTY M. D. 1950. Geology of the Broken Hill ore deposit, Broken Hill, New South Wales. *Geological Society of America Bulletin* 61, 1369–1414.
- HANMER S. & PASSCHIER C. 1991. Shear-sense indicators: a review. *Geological Survey of Canada Paper* 90–17.
- HAYDON R. C. & MCCONACHY G. W. 1987. The stratigraphic setting of the Pb–Zn–Ag mineralisation at Broken Hill. *Economic Geology* 82, 826–856.
- HAYDON R. C., MCCONACHY G. W. & WRIGHT J. V. 1993. Broken Hill ore environment—examples of critical guides to ore location. In: Matthew I. G. ed. *Proceedings of the International Symposium on Zinc*, pp. 131–149. Australasian Institute of Mining and Metallurgy, Melbourne.
- HENDERSON Q. J. 1953. North Broken Hill Mine. In: Edwards A. B. ed. *Geology of Australian Ore Deposits*, pp. 627–649. 5th Empire Mining and Metallurgy Congress Australia and New Zealand 1.
- HOBBS B. E. 1966. The structural environment of the northern part of the Broken Hill orebody. *Journal of the Geological Society of Australia* 13, 315–338.
- HOBBS B. E., ARCHIBALD N. J., ETHERIDGE M. A. & WALL V. J. 1984. Tectonic history of the Broken Hill Block, Australia. In: Kroner A. & Greiling R. eds. *Precambrian Tectonics Illustrated*, pp. 353–368. E. Schweizerbartische, Stuttgart.
- HOBBS B. E., RANSOM D. M., VERNON R. H. & WILLIAMS P. F. 1968. The Broken Hill orebody—a review of recent work. *Mineralium Deposita* 3, 293–316.
- HOBBS B. E. & VERNON R. H. 1965. The structural and metamorphic history of the area around the northern half of the Broken Hill Lode. In: McAndrew J. ed. *Geology of Australian Ore Deposits*, pp. 1419–1428. Proceedings of the 8th Commonwealth Mining and Metallurgical Congress 6. Australasian Institute of Mining and Metallurgy, Melbourne.
- HODGSON C. J. 1974. The geology and geological development of the Broken Hill Lode in the New Broken Hill Consolidated Mine, Australia, Part I: Structural Geology. *Journal of the Geological Society of Australia* 21, 413–430.
- HODGSON C. J. 1975a. The geology and geological development of the Broken Hill Lode in New Broken Hill Consolidated Mine, Australia, Part II: Mineralogy. *Journal of the Geological Society of Australia* 22, 33–50.

- HODGSON C. J. 1975b. The geology and geological development of the Broken Hill Lode in the New Broken Hill Consolidated Mine, Australia, Part III: Petrology and petrogenesis. *Journal of the Geological Society of Australia* **22**, 195–213.
- HOPWOOD T. P. 1976. The geology of the Northern leases and its relationship to the North Broken Hill orebody. Report to North Broken Hill Limited (unpubl.).
- HUSTON D. L., WYBORN L. A. I. & STEVENS B. P. J. 1998. Pb–Zn–Ag mineral systems: an example from Broken Hill. *Australian Geological Survey Organisation Record* **1998/25**, 59–63.
- JOHNSON I. R. & KLINGNER G. D. 1976. The Broken Hill ore deposit and its environment. In: Knight C. L. ed. *Economic Geology of Australia & Papua New Guinea*, Vol 1. pp. 476–495. Australasian Institute of Mining and Metallurgy Monograph 5.
- JONES T. R. 1968. Garnet sandstone and garnet rims at orebody contacts, Broken Hill. In: Radmanovich M. & Woodcock J. T. eds. *Broken Hill Mines—1968*, pp. 171–178. Australasian Institute of Mining and Metallurgy Monograph 3.
- KING H. F. & O'DRISCOLL E. S. 1953. The Broken Hill Lode. In: Edwards A. B. ed. *Geology of Australian Ore Deposits*, pp. 578–600. 5th Empire Mining and Metallurgy Congress Australia and New Zealand 1.
- KING H. F. & THOMSON B. P. 1953. The geology of the Broken Hill district. In: Edwards A. B. ed. *Geology of Australian Ore Deposits*, pp. 533–577. 5th Empire Mining and Metallurgy Congress Australia and New Zealand 1.
- LACASSIN R. 1988. Large-scale foliation boudinage in gneisses. *Journal of Structural Geology* **10**, 643–647.
- LAING W. P. 1977. Structural and metamorphic geology of a critical area adjacent to the Broken Hill orebody. PhD thesis, University of Adelaide, Adelaide (unpubl.).
- LAING W. P. 1996. Nappe interpretation, palaeogeography and metallogenic synthesis of the Broken Hill – Olary Block. In: Pongratz J. & Davidson G. J. eds. *New Developments in Broken Hill Type Deposits*, pp. 21–52. CODES, University of Tasmania, Special Publication 1.
- LAING W. P., MARJORIBANKS R. W. & RUTLAND R. W. R. 1978. Structure of the Broken Hill mines area and its significance for genesis of the orebodies. *Economic Geology* **73**, 1112–1136.
- LEWIS B. R., FORWARD P. S. & ROBERTS J. B. 1965. Geology of the Broken Hill lode, reinterpreted. In: McAndrew J. ed. *Geology of Australian Ore Deposits*, pp. 319–332. Proceedings of the 8th Commonwealth Mining and Metallurgical Congress 1. Australian Institute of Mining and Metallurgy, Melbourne.
- LEYH W. R. 2000. Detailed lithostructural mapping of Broken Hill type mineralization in the Broken Hill Block, NSW. *Australian Geological Survey Organisation Record* **2000/10**, 63–66.
- LOVE S. 1992. Possible ages and origins of some rocks of the Willyama Supergroup, New South Wales. BSc(Hons) thesis, Australian National University, Canberra (unpubl.).
- MCCLAY K. R. 1991. Deformation of stratiform Zn–Pb (–barite) deposits in the northern Canadian Cordillera. *Ore Geology Reviews* **6**, 435–462.
- MACINTOSH I. W. & MAVROGENES J. A. 1998. Experimental studies in the system PbS–FeS–ZnS ± Ag<sub>2</sub>S: implications for the Broken Hill Orebody, NSW. *Australian Geological Survey Organisation Record* **1998/25**, 76–79.
- MACKENZIE D. H. 1968. Lead lode at New Broken Hill Consolidated Limited. In: Radmanovich M. & Woodcock J. T. eds. *Broken Hill Mines—1968*, pp. 161–169. Australasian Institute of Mining and Metallurgy Monograph 3.
- MAIDEN K. J. 1972. Studies of the effects of high-grade metamorphism on the Broken Hill orebody. PhD thesis, University of New South Wales, Sydney (unpubl.).
- MAIDEN K. J. 1975. High-grade metamorphic structures in the Broken Hill orebody. *Australasian Institute of Mining and Metallurgy Proceedings* **254**, 23–26.
- MAIDEN K. J. 1976. Piercement structures formed by metamorphic mobilisation of the Broken Hill Orebody. *Australasian Institute of Mining and Metallurgy Proceedings* **257**, 1–8.
- MAIDEN K. J., CHIMIMBA L. R. & SMALLEY T. J. 1986. Cuspate ore – wall rock interfaces, piercement structures and the localization of some sulfide ores in deformed sulfide deposits. *Economic Geology* **81**, 1464–1472.
- MARJORIBANKS R. W., RUTLAND R. W. R., GLEN R. A. & LAING W. P. 1980. The structure and tectonic evolution of the Broken Hill region, Australia. *Precambrian Research* **13**, 209–240.
- MARSHALL B. & GILLIGAN L. B. 1987. An introduction to remobilization: information from ore-body geometry and experimental considerations. *Ore Geology Reviews* **4**, 175–210.
- MARSHALL B. & GILLIGAN L. B. 1989. Durchbewegung structure, piercement cusps and piercement veins in massive sulfide deposits: formation and interpretation. *Economic Geology* **84**, 2311–2319.
- MARSHALL B., LAROCQUE A. C. L. & VOKES F. M. 1999. Extensive remobilisation in massive sulphide deposits: a fluid affair! In: Stanley C. J. et al. eds. *Mineral Deposits: Processes to Processing*, pp. 955–958. Balkema, Rotterdam.
- MORLAND R. & WEBSTER A. E. 1998. Broken Hill lead–zinc–silver deposit. In: Berkman D. A. & Mackenzie D. H. eds. *Geology of Australian and Papua New Guinean Mineral Deposits*, pp. 619–626. Australasian Institute of Mining and Metallurgy, Melbourne.
- NUTMAN A. P. & EHLERS K. 1998. Evidence for multiple Palaeoproterozoic thermal events and magmatism adjacent to the Broken Hill Pb–Zn–Ag orebody, Australia. *Precambrian Research* **90**, 203–238.
- O'DRISCOLL E. S. T. 1964. Cross fold deformation by simple shear. *Economic Geology* **59**, 1061–1093.
- O'DRISCOLL E. S. T. 1968a. The tectonic setting of the Broken Hill lode and its relationship to regional lineaments in the Australian continental structure. Report to Broken Hill Mine Managers Association (unpubl.).
- O'DRISCOLL E. S. T. 1968b. Notes on the structure of the Broken Hill lode and its tectonic setting. In: Radmanovich M. & Woodcock J. T. eds. *Broken Hill Mines—1968*, pp. 87–102. Australasian Institute of Mining and Metallurgy Monograph 3.
- OGERMAN J. A. 1984. A study of the petrology, geochemistry and fluid inclusions of dropper structures in the Zinc Corporation Ltd. Mine, Broken Hill, New South Wales. BSc(Hons) thesis, University of Adelaide, Adelaide (unpubl.).
- OLIVER N. H. S., RUBENACH M. J. & VALENTA R. K. 1998. Precambrian metamorphism, fluid flow, and metallogeny of Australia. *AGSO Journal of Australian Geology & Geophysics* **17**, 31–53.
- PAGE R. W. & LAING W. P. 1992. Metavolcanics related to the Broken Hill orebody, Australia: geology, depositional age and timing of high-grade metamorphism. *Economic Geology* **87**, 2138–2168.
- PAGE R. W., STEVENS B. P. J., GIBSON G. M. & CONOR C. H. H. 2000. Geochronology of Willyama Supergroup rocks between Olary and Broken Hill, and comparison to northern Australia. *Australian Geological Survey Organisation Record* **2000/10**, 72–75.
- PHILLIPS G. N. 1978. Metamorphism and geochemistry of the Willyama Complex. PhD thesis, Monash University, Melbourne (unpubl.).
- RAMDOHR P. 1950. The ore deposit of Broken Hill in New South Wales in the light of new geological knowledge and ore-microscopic investigations. *Heidelberger Bietrage Zur Mineralogie und Petrographie* **2**, 291–333.
- RAMSAY J. G. & HUBER M. I. 1987. *The Techniques of Modern Structural Geology, Volume 2: Folds and Fractures*. Academic Press, London.
- RANSOM D. M. 1968. The relationship of orebody shape to country rock structure in the southern half of the Broken Hill Lode. *Journal of the Geological Society of Australia* **15**, 7–64.
- RANSOM D. M. 1969. Structural and metamorphic studies at Broken Hill. PhD thesis, Australian National University, Canberra (unpubl.).
- RUTLAND R. W. R. & ETHERIDGE M. A. 1975. Two high-grade schistositys at Broken Hill and their relation to major and minor structures. *Journal of the Geological Society of Australia* **22**, 259–275.
- STANTON R. L. 1976a. Petrochemical studies of the ore environment at Broken Hill, New South Wales, 1—constitution of 'banded iron formation'. *Transactions of the Institution of Mining and Metallurgy* **85**, B33–B46.
- STANTON R. L. 1976b. Petrochemical studies of the ore environment at Broken Hill, New South Wales, 2—regional metamorphism of banded iron formations and their immediate associates. *Transactions of the Institution of Mining and Metallurgy* **85**, B118–B131.
- STANTON R. L. 1976c. Petrochemical studies of the ore environment at Broken Hill, New South Wales, 3—banded iron formations and sulphide ore bodies: constitutional and genetic ties. *Transactions of the Institution of Mining and Metallurgy* **85**, B132–B141.



- STANTON R. L. 1976d. Petrochemical studies of the ore environment at Broken Hill, New South Wales, 4—environmental synthesis. *Transactions of the Institution of Mining and Metallurgy* **85**, B221–B233.
- STEVENS B. P. J. 1978. The geological environment of mineralization in the Centennial-Great Western area, Broken Hill. MSc thesis, University of Sydney, Sydney (unpubl.).
- STEVENS B. P. J. 1986. Post-depositional history of the Willyama Supergroup in the Broken Hill Block, NSW. *Australian Journal of Earth Sciences* **33**, 73–98.
- STEVENS B. P. J. 1998. The origins of Broken Hill rock types and their relevance to mineralisation. *Australian Geological Survey Organisation Record* **1998/25**, 109–114.
- STEVENS B. P. J., WILLIS I. L., BROWN R. E. & STROUD W. J. 1983. The Early Proterozoic Willyama Supergroup: definitions of stratigraphic units from the Broken Hill Block, New South Wales. *Geological Survey of New South Wales Record* **21**, 407–442.
- THOMSON B. P. 1959. Discussion on sedimentary structures in the metamorphic rocks and orebodies of Broken Hill, by M. A. Condon. *Australasian Institute of Mining and Metallurgy Proceedings* **191**, 201–211.
- VAN DER HEYDON A. & EDGEcombe D. R. 1990. Silver–lead–zinc deposit at South Mine, Broken Hill. In: Hughes F. E. ed. *Geology of the Mineral Deposits of Australia and Papua New Guinea*, pp. 1073–1077. Australasian Institute of Mining and Metallurgy, Melbourne.
- VERNON R. H. 1996. Structural evidence of parent rocks in high-grade metamorphic areas—especially Broken Hill. In: Pongratz J. & Davidson G. J. eds. *New Developments in Broken Hill Type Deposits*, pp. 17–20. CODES, University of Tasmania Special Publication 1.
- VERNON R. H. & WILLIAMS P. F. 1988. Distinction between intrusive and extrusive or sedimentary parentage of felsic gneiss: examples from the Broken Hill Block, NSW. *Australian Journal of Earth Sciences* **35**, 379–388.
- WEBSTER A. E. 1993. Sulphide orebodies and structure: mapping within an orebody and what it can tell you. An example from Broken Hill, NSW. In: Robertson I., Shaw W., Arnold C. & Lines K. eds. *Proceedings of the International Mining Geology Conference*, pp. 133–141. Australasian Institute of Mining and Metallurgy, Melbourne.
- WEBSTER A. E. 1996a. Delamerian refolding of the Palaeoproterozoic Broken Hill Block. *Australian Journal of Earth Sciences* **43**, 85–89.
- WEBSTER A. E. 1996b. A detailed description of the Broken Hill deposit—lessons from ore fabrics. In: Pongratz J. & Davidson G. J. eds. *New Developments in Broken Hill Type Deposits*, pp. 95–103. CODES, University of Tasmania, Special Publication 1.
- WEBSTER A. E. 2000. Structures in the Broken Hill Orebodies. *Australian Geological Survey Organisation Record* **2000/10**, 105–108.
- WHITE S. H., ROTHERY E., LIPS A. W. & BARCLAY T. J. R. B. 1995. Broken Hill base-metal deposit: a tectonically transported and modified basinal deposit within the Proterozoic Willyama Fold and Thrust Belt. *Transactions of the Institution of Mining and Metallurgy* **104**, B1–B17.
- WHITE S. H., ROTHERY E., LIPS A. W. & BARCLAY T. J. R. B. 1996. Reply to discussion. *Transactions of the Institution of Mining and Metallurgy* **105**, B90–B98.
- WHITE S. H., ROTHERY E., LIPS A. W. & BARCLAY T. J. R. B. 1997. Reply to discussion. *Transactions of the Institution of Mining and Metallurgy* **106**, B56–B58.
- WILCOX R. E., HARDING T. P. & SEELY D. R. 1973. Basic wrench tectonics. *American Association of Petroleum Geologists Bulletin* **57**, 74–96.
- WILLIAMS E. 1959. Discussion on sedimentary structures in the metamorphic rocks and orebodies of Broken Hill, by M. A. Condon. *Australasian Institute of Mining and Metallurgy Proceedings* **189**, 77–79.
- WILLIAMS P. F. 1967. Structural analysis of the Little Broken Hill area, New South Wales. *Journal of the Geological Society of Australia* **14**, 317–331.
- WILLIAMS P. J., GUOYI D., PRENDERGAST K. & POLLARD P. J. 1999. Metasomatism and metal mobility in Broken Hill-type deposits. In: Stanley C. J. et al. eds. *Mineral Deposits: Processes to Processing*, pp. 999–1002. Balkema, Rotterdam.
- WILLIS I. L., BROWN R. E., STROUD W. J. & STEVENS B. P. J. 1983. The early Proterozoic Willyama Supergroup: stratigraphic subdivision and interpretation of high to low-grade metamorphic rocks in the Broken Hill Block, New South Wales. *Journal of the Geological Society of Australia* **30**, 195–224.
- WYBORN L. A. I., BUDD A. R., STEVENS B. P. J., ASHLEY P. M., CONOR C. H. H. & BASTRAKOVA I. V. 1998. Major felsic igneous units of the Broken Hill – Olary region and their metallogenic potential. *Australian Geological Survey Organisation Record* **1998/25**, 123–126.

Received 21 June 1999; accepted 18 November 2000

**NZG**

**GROUNDWATER  
CONSULTANT**

*Specialist Consulting Services*

*Aquifer Storage and Recovery*

*Groundwater Investigation and  
Assessment*

*Groundwater Contamination Sites*

*Sedimentary and Fracture Rock*

*Groundwater Education and Seminar*

# THE POTENTIAL OF GROUNDWATER SUPPLY AND AQUIFER STORAGE AND RECOVERY IN THE BROKEN HILL AREA

by

**NZG GROUNDWATER CONSULTANT**

February 2006

**NZG GROUNDWATER**

**CONSULTANT**

**1 Shamrock Rd. Hallett Cove SA 5158**

**Tel: 041356803**

**Email: [gergesnz@iprimus.com.au](mailto:gergesnz@iprimus.com.au)**

1. INTRODUCTION .....	4
2. PROJECT OBJECTIVES.....	4
3. GEOLOGY .....	6
<b>3.1 Structural Elements.....</b>	<b>7</b>
<b>3.2 Lineaments.....</b>	<b>8</b>
<b>3.3 Retrograde Schist Zones .....</b>	<b>9</b>
<b>3.3.1 The Globe-Vauxhall Schist Zone.....</b>	<b>10</b>
4. HYDROGEOLOGY .....	15
<b>4.1 Willyama Supergroup Rocks .....</b>	<b>17</b>
<b>4.2 Quaternary aquifer .....</b>	<b>19</b>
Colluvial sediments.....	19
Alluvial sediments.....	19
Sand dunes aquifer .....	19
<b>4.3 Quaternary and Tertiary aquifers in Darling floodplain and Lake Menindee area .....</b>	<b>19</b>
<b>4.3.1 Quaternary Aquifer .....</b>	<b>20</b>
<b>4.3.2 Tertiary aquifers.....</b>	<b>21</b>
5. RECOMMENDATIONS .....	22
<b>5.1 Locally in Broken Hill .....</b>	<b>22</b>
<b>5.2 Utilizing existing Lake Menindee pipeline.....</b>	<b>23</b>
<b>5.3 Proposed Field Investigations .....</b>	<b>23</b>
6. REFERENCES .....	26

## TABLES

## Page

<b>Table 1</b> Summary of water boreholes known from recent date obtained from DIPNR for a 15 -kilometers radius around Broken Hill (adapted from C.M Jewell, 2004)	16
<b>Table 2</b> Summary of the regional hydrogeology in the Darling floodplain and Menindee Lake area	20

## FIGURES

## Page

<b>Figure 1</b> Location of Broken Hill City	5
<b>Figure 2</b> General geology of the area from Broken Hill geological map 1:25,000	11
<b>Figure 3</b> Major structures in the area interpretative structure and stratigraphic map	12
<b>Figure 4</b> Detailed structural analysis throughout the Broken Hill Block	13
<b>Figure 5</b> Lineaments in Broken Hill 1:25,000 sheet area interpreted from 1:60,000 photographs	14
<b>Figure 6</b> Interpreted distribution of retrograde schist zones in Broken Hill 1: 25,000 sheet area	14
<b>Figure 7</b> Location of the lode horizon areas	25

## **APPENDICES**

## **Page**

### **APPENDIX A** Selected examples of ASR in South Australia

35

# **ASSESSMENT OF BROKEN HILL TOWNSHIP POTENTIAL GROUNDWATER SUPPLY AND AQUIFER STORAGE AND RECOVERY (ASR)**

## **1. INTRODUCTION**

NZG Groundwater Consultant was engaged by Tonkin Consulting to provide assessment of the potential for groundwater resources and Aquifer Storage and Recovery (ASR) of stormwater in aquifers in the Broken Hill area (refer Figure 1). This briefing covers the preliminary investigative work and includes assessment of the geology and hydrogeology of the concerned area in relation to the potential of groundwater supply and ASR.

The briefing is based on the most recent information interpreted from geological maps, hydrogeological data, previous reports and data from existing wells in the area. Regions and/or major features that exhibit the greatest potential have been highlighted for future in depth investigation. The area of interest includes the Broken Hill Township and the area surrounding Menindee Lake, located approximately 90 to 100 km south-east of Broken Hill.

Previous studies by several sources including John Wilson and Partners Pty Ltd (May 2004), covered a large area of approximately 100 km radius surrounding Broken Hill, however it did not elaborate specifically on potential of groundwater supply in the township. However, this report investigates in depth the hydrogeology of the area and the prospect of groundwater use in the immediate area of Broken Hill.

## **2. PROJECT OBJECTIVES**

The objective of this study was to assess the potential for groundwater to be used as a resource in the area, either independently or conjunctively with ASR techniques.

The following report aims to:

- Summarise the potential for groundwater in the Broken Hill area to provide suitable water for irrigation purposes;
- Summarise the feasibility of ASR locally in the Broken Hill and Menindee Lake areas.

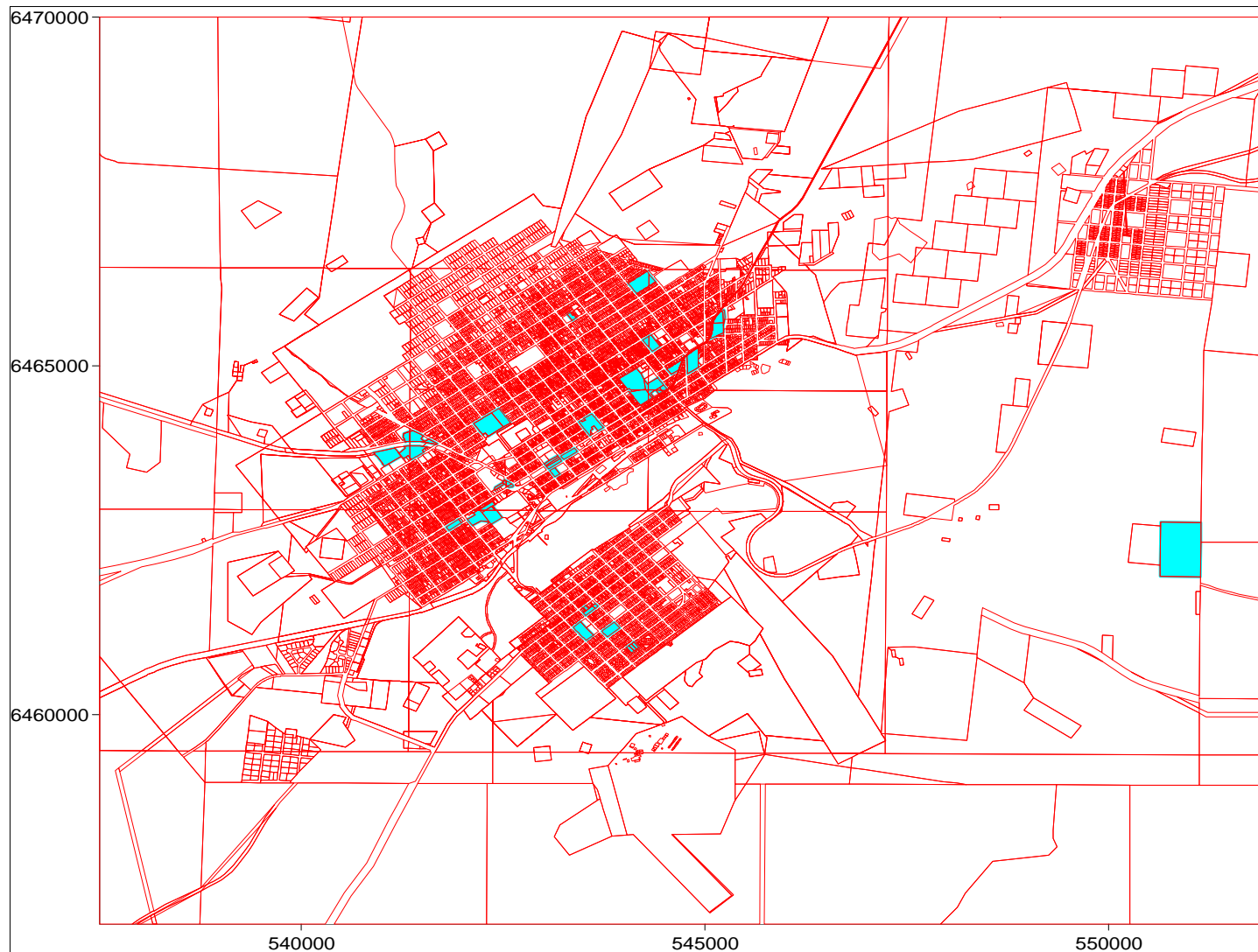


**Figure 1** Location of Broken Hill City (Council greenspace marked in blue)

### 3. GEOLOGY

The Broken Hill area is covered with a thin veneer of Cainozoic Sediments (undifferentiated Cainozoic deposits), which overlay the occasionally outcropping prograde metamorphic rocks. The Cainozoic deposits include alluvial, aeolin and lateritic sediments. Alluvial deposits are probably the most abundant in the area and they are poorly sorted and are typical of braided stream sediments. The colluvial deposits are restricted to the base of ridges and hills. Aeolian sediments are minor with occasional thick deposits formed on the southern flanks of many steep ridges. The Cainozoic sediments also contain occasionally a veneer of calcrete which is up to several meters thick.

The high grade metamorphic rocks and igneous rocks of the Broken Hill sheet area are of Early Proterozoic age (approximately 1800 million years old), and constitute part of the Willyama Complex (a subdivision of the Adelaide Fold Belt). In NSW the Willyama Complex is recognised in two main cratonic blocks, the Broken Hill Block and the Euriowie Block. The Broken Hill sheet area lies within the Broken Hill Block (refer Figure 2).

The Broken Hill sheet area lies within an amphibolite to granulite facies terrain, which has undergone at least one major prograde metamorphic event with several generations of folding. Subsequent retrograde metamorphism on a regional scale, with more intense retrograde metamorphism in retrograde schist zones, has produced a variety of new structures and mineral assemblages and textures of lower amphibolite facies to upper green schist facies. Dykes of granite, pegmatite, dolerite, and hornblendite intruded after the prograde metamorphic event and were altered by retrograde metamorphism.

The Broken Hill sheet area comprises prograde metamorphic rocks such as basic granulite and amphibolite, as well as metasediment, quartzo-felspathic gneiss, composite gneiss and mimetite, leucocratic K-feldspar rich and plagioclase rich quartzo-felspathic rocks, and calc-silicate rocks. A variety of



less abundant rocks generally associated with or located close to Pb-Zn (Lead-Zinc) mineralisation include quartz-gahnite rock, garnet-quartz rock, garnet-hematite/magnetite rock, manganese oxide rock, banded magnetite-garnet rock and quartz-magnetite rock.

Regional retrograde metamorphism has produced staurolite, sericite, muscovite, chlorite, kyanite, and pinite in the quartzo-felspathic rocks and metasediments of this sheet area; fibrous amphibole, epidote, sericite, muscovite, chlorite, kyanite and pinite in the quartzo-felspathic rocks; and sericite, chlorite, zoisite, clinozoisite and idiomorphic garnet in amphibolite or basic granulite.

To the east of the Barrier Range, the Darling plains are covered by Quaternary-age sediments. These sediments (which include alluvium, playa deposits, sand dunes and sand plains) locally reach thicknesses greater than 200 metres, but are generally less than 30 metres thick. Further east they extend across the boundary of the Murray-Darling sedimentary basin, where they are underlain by a thick succession of Tertiary-age sediments that form major regional aquifers.

The Broken Hill sheet area is traversed by several major retrograde schist zones and an abundance of minor schist zones. Some of the major schist zones are responsible for large scale dislocations of the stratigraphy and structure of the region. Schist zones are identified by abundant sericite schist and intense sericite schistosity, or where outcrop is scarce or absent by abundant quartz float.

### ***3.1 Structural Elements***

In hard rock environments fractures, schist zones and cleavage are generally associated with faults, lineaments, and folds. These are the most important features in groundwater investigation as they may contain potential for groundwater supply/injection. The aquifers within the hard rock can be classified as compartment, strip, or fracture aquifers.

Structurally the dominant trend is the north to north-east regional structures, mostly as anticlines, synclines and monoclines (refer Figure 3). The rocks have been heavily deformed by multiple phases of folding, and are also faulted. Two main groups (Group 1 folds, which have deformed the lithologic layering and generated the regional schistosity; and Group 2 folds, which have deformed the regional schistosity) and two minor groups of folds have been mapped in the area.

Major folds in the Broken Hill sheet area are first and second generation structures. F2/1 folds are rare and tight to isoclinal. F2 folds are upright, open to tight, and relatively abundant. These include the Stirling Vale synform, Great western antiform, and the major folds in the Broken Hill mine area. Folds contain high fractures zones particularly along their axis, and are an important feature in groundwater storage and movements.

The stratigraphy of the Broken Hill sheet area comprises metamorphic rocks of suites 3, 4, and 5. Suite 4 rocks are most widespread throughout the area, which is host for the Broken Hill Main Lode. The Main Lode generally contains various amounts of Broken Hill type “lode” rocks (e.g. quartz-gahnite) and is consequently of prime interest to base metal exploration companies. Suite 5 rocks are predominantly found in a broad belt extending from the north to the west of the Broken Hill township. Except for a few very minor occurrences, this belt is devoid of mineralization.

Structural analysis in the Broken Hill mines area has recognised two main styles of deformation; Group 1 folds with axial plane schistosity and a lineation parallel to their axes, and Group 2 folds which folded with the same schistosity and lack axial plane schistosity. Detailed structural analysis throughout the Broken Hill Block is shown in Figure 4.

### **3.2 Lineaments**

The majority of lineaments interpreted from 1:60,000 aerial photographs are

orientated in sets trending north-north-west to north-west or north-north-east (refer Figure 5). The trend of these lineament sets corresponds with the trend of sets of retrograde schist in schist zones. Other lineaments whose trends do not fall into any one of the two sets listed above possibly represent lithological trends, fold structures, unidentified schist zones or fracture systems, or coincidental alignment or surface features.

The Broken Hill Synform is an open, overturned, south plunging anticline whose axial plane dips north-west and passes through the core of outcrop of the “alma” augen gneiss.

The Hanging Wall Synform is a relatively tight, overturned, south-west plunging fold whose axial plane dips steeply north-west. This synfold is well defined by lithological symmetry.

The Broken Hill Antiform is inferred to exist between the Broken Hill Synform and the Hanging Wall Synform. The antiform is a tight inverted syncline, dipping steeply to the north-west and plunging to the south-west.

### **3.3 Retrograde Schist Zones**

Retrograde schist zones have previously been referred to as “crush zones”, “shear zones” or “faults”, and are localised (refer Figure 6). These schist zones are characterised by a strong micaceous schistosity which is generally parallel to the margins of the zone.

Some degree of transcurrent displacement is evident in some schist zones. At least one period of movement in these schists zones is indicated by:

- Relative displacement of adjacent blocks separated by the schist zones;
- The development of f4 folds within schist zones and post-f4 folds along the margins of some zones;
- Well developed cleavage in quartz veins injected during or prior to the

generation of s4.

Generally, larger zones occupy several sets of regional trends, with each set having an individual sense of transcurrent movement. These sets can be grouped as:

1. North-easterly to easterly trending; north block moved relatively eastward. Includes the Globe-Vauxhall, Stephens Creek, and limestone schist zones.
2. Northerly to north-north-easterly trending; east block moved relatively northward.

### ***3.3.1 The Globe-Vauxhall Schist Zone***

The Globe-Vauxhall Schist Zone extends along strike for many kilometres and in this sheet are intersections with the De Bavay, British, and Picton Schist Zones. The Globe-Vauxhall Schist Zone crops out very poorly within and to the west of the Broken Hill township area, but is well exposed to the east of Broken Hill. The schist zone attains a maximum width of 100 metres and dips to the south-east at 60 to 70 degrees. As this schist zone approximately parallels lithological layering, it is difficult to estimate horizontal movement along the zone. Laing et al (1978) concluded that strike-slip movements were not very large.

Horizontal dislocation of the Burke Street Lode is estimated at approximately 600 metres. Vertical movement is tentatively estimated at greater than 500 metres. This structural feature contains fractures, and if the fractures intersect the water table it may represent a potential source of groundwater supply.

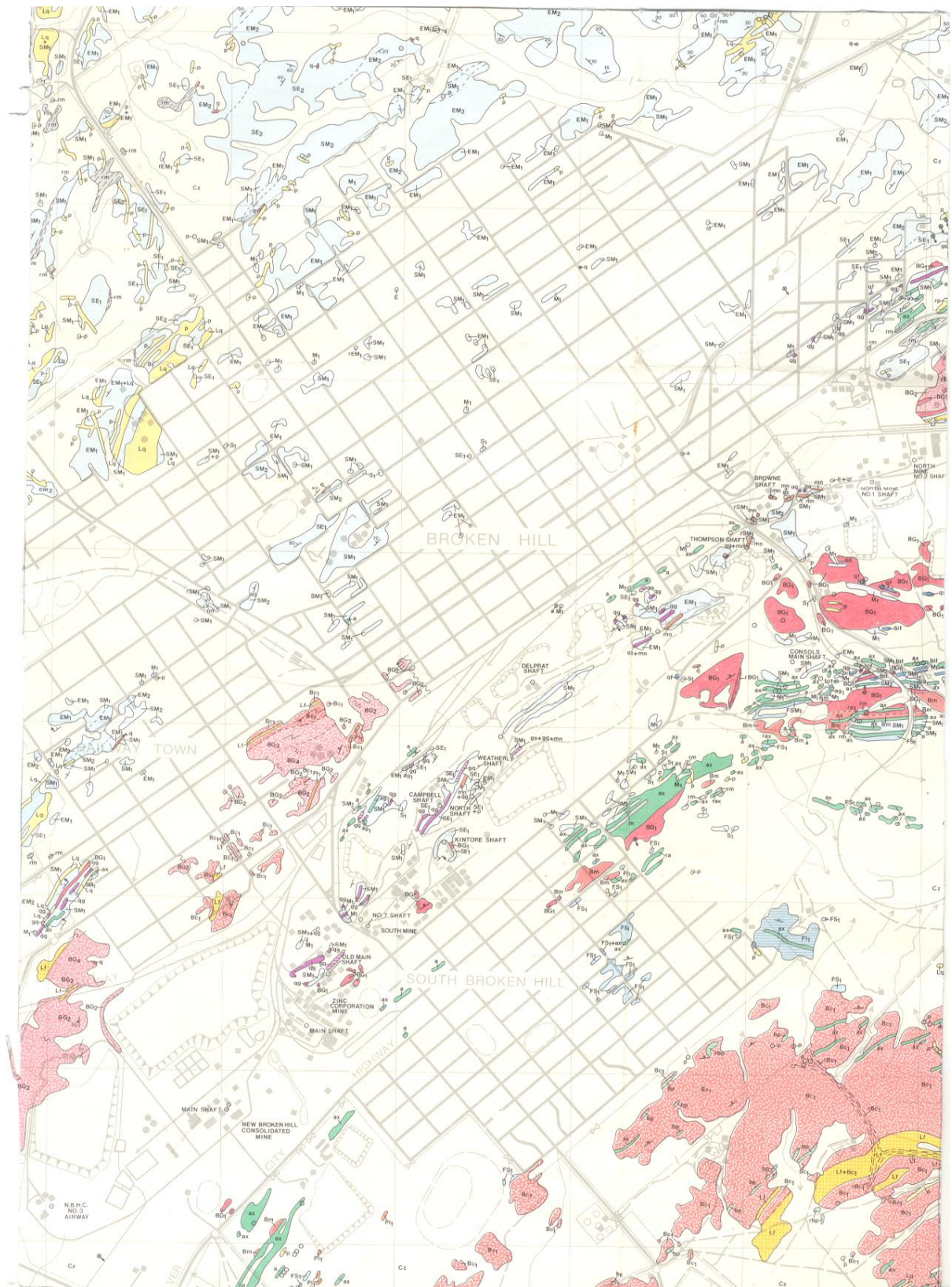


**Figure 2** General geology of the area from Broken Hill geological map 1:25,000



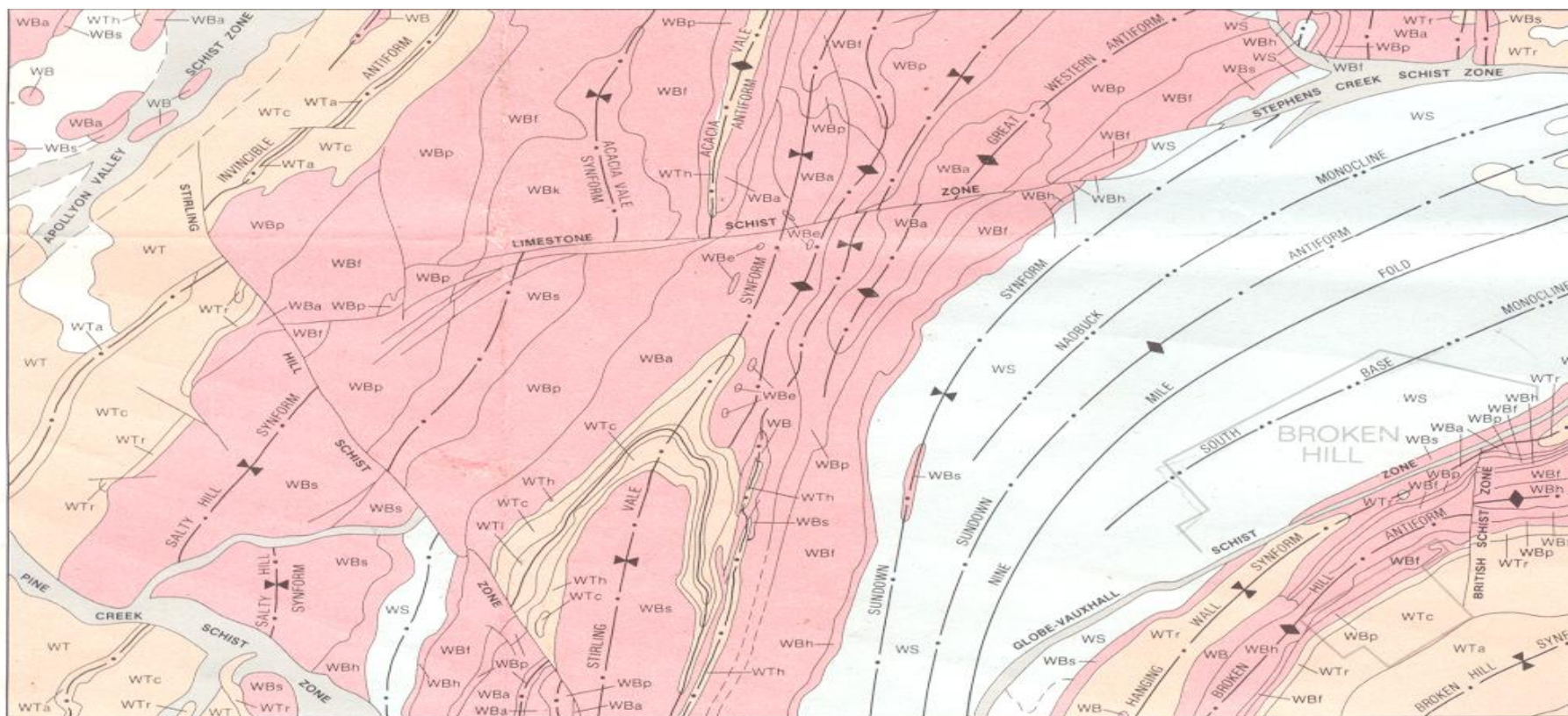


**Figure 3** Major structures in the area – Interpretative structure and stratigraphic map

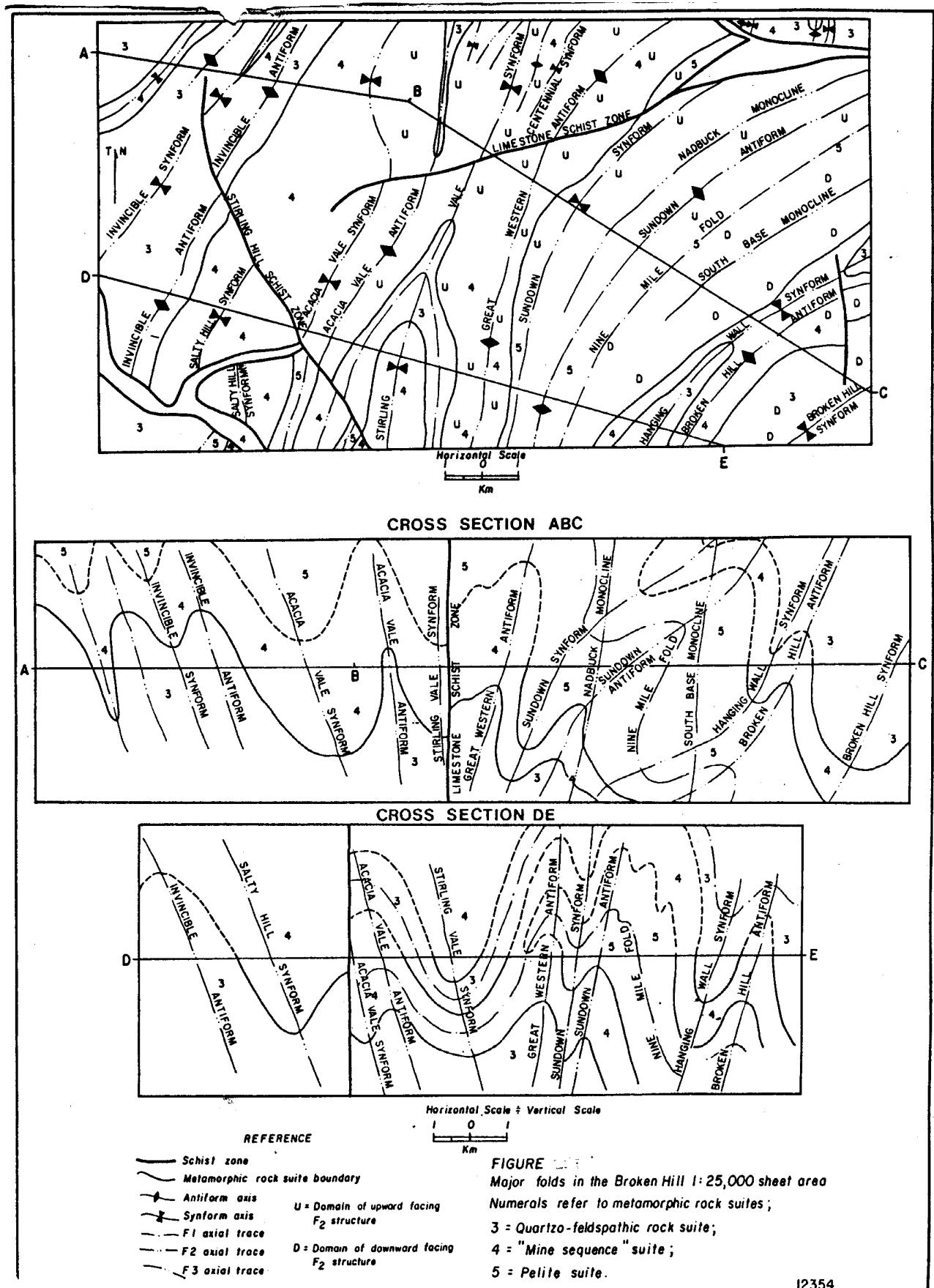


**Figure 4** Detailed structural analysis throughout the Broken Hill Block – showing main



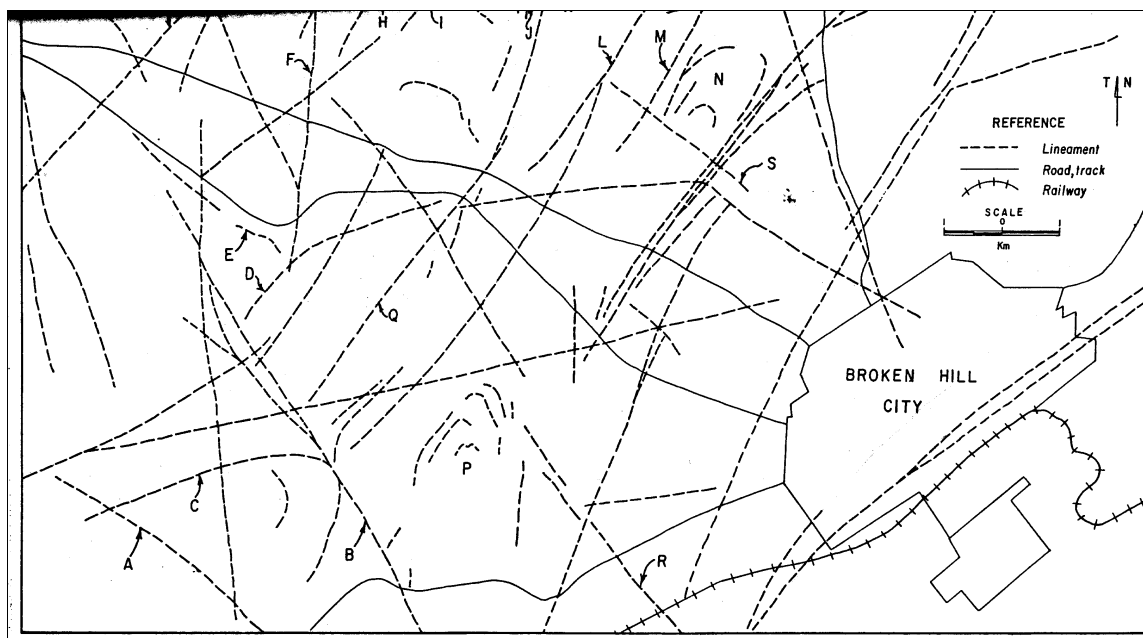


**Figure 5** Lineaments in Broken Hill 1:25,000 sheet area interpreted from 1:60,000 photographs  
– Upper case letters correspond to lineaments

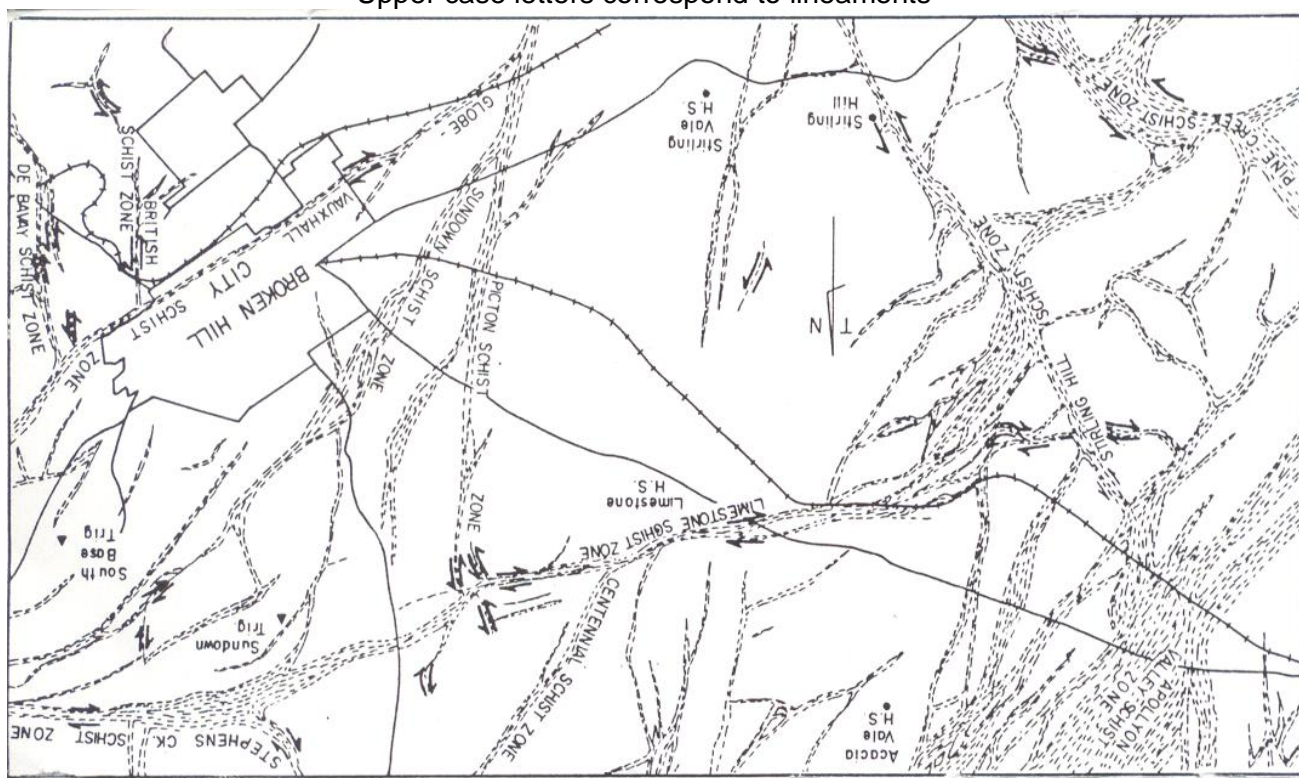


**Figure 6** Interpreted distribution of retrograde schist zones in Broken Hill 1:25,000 sheet area.  
Arrows show interpreted direction of displacement

## 4. HYDROGEOLOGY

The following description of hydrogeology is extracted from reports compiled by C.M. Jewell & Associates (2004) and R.W. Corkery (2005).

Previous work and data from the NSW Department of Infrastructure, Planning and Natural Resources (DIPNR) shows relatively little use of groundwater in the Broken Hill area. There are no known municipal or potable domestic abstractions, however a number of boreholes, wells and mine shafts provide useful groundwater information for stock and non-potable domestic use.

Many of the water wells and boreholes in the Broken Hill area are completed in Cainozoic sediments of regolith, and others abstract from the Torrowangee Group. Some are completed in the Willyama Supergroup.

Table 1 (adapted from C.M Jewell & Associates, 2004) provides a summary of water boreholes known at the time of publication, obtained from the DIPNR for a 15 kilometre radius around Broken Hill. Few of the borehole records held by DIPNR include borehole logs, or indeed any geological data. However, C.M. Jewell & Associates (2004) use the methods of plotting the AMG coordinates of the borehole on the 1:100,000 geological maps to obtain an indication of the stratigraphic unit from which water is drawn. They claim that the grid coordinates are not sufficiently reliable to identify individual lithological or structural units, but it is possible to identify the group. The table shows that the total depth of the wells varies from 10 to 131 metres, and yield varies between 0.1 and 10 L/s, but generally averages 1.5 L/s which is considered very low for the intended purpose.

Observations made during mining operations have also provided a reasonable indication of groundwater occurrence in the Willyama Supergroup Rocks.

TABLE 2 Broken Hill Regional Groundwater Bore Data								
DIPNR No.	Bore Log		Depth to Top of Aquifer (m)	Supply (m <sup>3</sup> /day)	S.W.L. (m)	S.W.L. R.L. (m)	Quality	Other
	Total Depth (m)	Summary						
4297	-	-	-	-	-	-	-	-
9812	22.3	-	-	112.32	7.0	258.0	-	Adjacent to fault
9653	131.1	-	-	0.0	-	-	-	-
9782	21.3	-	-	6.912	18.3	291.7	Brackish	-
9785	-	-	30.5	2.592	10.7	244.3	Good	-
10089	15.5	-	-	13.824	9.1	245.9	Good	Adjacent to fault
10090	54.94	-	-	65.664	-	-	Stock	-
10091	27.4	-	-	Poor	18.3	276.7	Good	Adjacent to fault
10094	19.8	-	-	112.32	17.4	247.6	Good	-
10095	30.5	-	-	112.32	21.3	243.7	Good	-
10096	21.3	-	-	Good	17.7	242.3	Good	-
10097	15.2	-	-	Fair	7.6	322.4	Good	-
10098	15.2	-	-	Fair	6.1	328.9	Good	-
10099	18.3	-	15.2	54.432	12.2	227.8	Good	-
10136	27.4	-	-	4.4064	11.6	223.4	Very good	-
10139	18.3	-	12.2	65.4912	12.2	192.8	Good	-
10244	15.2	-	-	224.64	2.7	272.3	Good	-
17685	42.7	0-42.7 m grey shale	-	0.0	-	-	-	-
18521	20.7	0-3.3 m clay & gravel 3.3-15.9 m schist 15.9-18.3 m pegmatite 18.3-20.7 m schist	18.3	19.872	7.6	207.4	Stock	Fractured aquifer T=1.67 m <sup>3</sup> /day/m (S=0.001)
20084	15.3	0-1.2 m sand red clay 1.2-7.9 m yellow sandstone 7.9-15.2 m grey rock 15.2-15.3 m coarse gravel	-	25.92	10.1	-	-	-
21680	24.4	0-4.3 m clay 4.3-24.4 m rock	18.3	32.832	16.8	243.2	Stock	T=19.4 m <sup>3</sup> /day/m (S=0.001)
21882	67.1	0-1.8 m soil 1.8-61.0 m granite 61.0-67.1 m coarse gravel	61.0	27.648	45.7	244.3	Stock	-
61218	213.4	-	-	-	-	-	-	-
500290	10.0	-	-	864.0	5.0	-	Domestic, Stock	-
600001	44.3	-	-	61.344	19.0	-	Domestic, Stock	-

**Table 1** Summary of water boreholes known from recent date obtained from DIPNR for a 15 -kilometers radius around Broken Hill (adapted from C.M Jewell)

#### **4.1 Willyama Supergroup Rocks**

These rocks transmit water only through secondary features such as fractures and joints. Generally, the total rock mass permeability, including transmission through fractures, is low. Locally, where fracturing is intense, flows may be higher. The main lode horizons tend to be significantly more fractured than the surrounding rocks and therefore function as low-permeability compartment aquifers.

A few water boreholes are known to have been constructed into the Willyama Supergroup Rocks, and these generally provide low to moderate yields of water (yields range between 20 and 500 m<sup>3</sup>/day).

Experience over many years of mining in the Broken Hill area has confirmed these observations. Most mines have made some water, with locally higher and sometimes usable inflows, but water in the mines has never been a significant constraint on mining activities. The largest groundwater inflows have occurred in the southern mining leases.

Similarly, the rock quarry to the south-west of Broken Hill experiences low-volume groundwater seepage inflows from a depth of 15 metres along the southern and south-western faces.

Recharge to the Willyama Supergroup Rocks may occur by direct infiltration of rainfall, but the volume is not known and is most likely to be low. However, the high evaporation in this environment, coupled with low rainfall and steep slopes, all suggest a low recharge rate. In addition, some of the recharge occurs as downward leakage from the overlying Quaternary alluvium sediments.

Reports from mining operations reveal that the lode horizon in the southern leases has a well developed fracture system oriented parallel to the main rock contacts (striking north-south and dipping to the west at about 70 degrees), with a secondary fracture system at right angles to this. Reports also suggest

the presence of a brecciate hanging-wall aquifer between the lode horizon and the granite-gneissic country rock.

Existing information suggests that the lode horizon aquifer transmissivity ranges between 20 and 80 m<sup>2</sup>/day, which is considerably low. However, given that there is no documentation of draw down, the type of the aquifer, and whether or not recovery tests were carried out, this information must be treated with great caution. It is assumed that the aquifer is unconfined and a value of specific yield can be assumed to be in the range 0.001 to 0.01.

Results of a pumping test carried out at a Rising Sun shaft (C.M Jewell & Associates, 2004) have indicated that with pumping rates of 520 L/sec the draw down was about 20 metres, while the White Leads shaft yielded less than 100 m<sup>3</sup>/day for three months with about 57 metres draw down. Exploration boreholes in the southern leases have yielded up to 500 m<sup>3</sup>/day. Groundwater is pumped from the former Daydream Mine, north of Broken Hill, for non-potable domestic and garden irrigation use.

Borehole records from the Willyama Supergroup Rocks show that water quality is generally 'good' to brackish, and mostly suitable for irrigation and stock. Most groundwater analysis suggests that the calcium-magnesium sulphate content is relatively high.

A groundwater sampling program carried out from exploration boreholes in the southern leases indicated total dissolved solids generally in the range 8000 to 10,000 mg/L, with sulphate typically 1500 to 2800 mg/L (C.M Jewell & Associates, 2004). Heavy metal concentrations in groundwater derived from the lode horizons were evaluated, and the data indicate that cadmium, manganese, lead, zinc and iron are present at significant concentrations. Cadmium concentrations exceed those considered suitable for stock use.

A sample of water obtained from the quarry sump was sampled and showed salinity (TDS) of 7000 mg/L, with sulphate of 1160 mg/L and chloride of 2310 mg/L.

## ***4.2 Quaternary aquifer***

The types of aquifer present in the Broken Hill Township and immediate surroundings:

### ***Colluvial sediments***

Possibly contain a thin aquifer, but uneconomic for either extraction or injection and overall it is poorly documented.

### ***Alluvial sediments***

Located primarily along water courses with the coarser material confined to areas in the immediate surrounding of creeks. These sediments generally consist of gravel, sand, and silt interbedded with clay material. Yields are generally low, probably reflecting low permeability due to the poorly sorted nature of these sediments, and the presence of clay layering.

The distribution of these sediments is poorly documented, and given that they are confined to surface water drainage their capability to store and release water is considerably limited. However because this aquifer is located in close proximity to surface water drainage, natural recharge occurs during winter and therefore water quality is expected to be generally good and usable.

### ***Sand dunes aquifer***

This aquifer is scarce in the Broken Hill area but is located in the surrounding region. It contains groundwater at its base. The yield and salinity is not known but is expected to be negligible for the intended purpose.

## ***4.3 Quaternary and Tertiary aquifers in Darling floodplain and Lake Menindee area***

This area was included in the study because of its significance in implementing ASR. The area is well known as it contains Quaternary and Tertiary aquifers.

These aquifers are located approximately 90 to 100 kilometres south-west of

Broken Hill, but were included in this study as the Broken Hill water supply is partly supplemented from Lake Menindee. The lake is located within the Murray-Darling Basin.

**Table 2** Summary of the regional hydrogeology in the Darling floodplain and Menindee Lake area

<i>Alluvial Aquifer- includes Blanchetown Clay</i>	Generally unconsolidated fine to medium sands, interbedded with clays, silty and sandy in parts
<i>Pliocene Sand Aquifer Parilla Sand</i>	Partly cemented shelly limestone with sand matrix and unconsolidated fine to coarse sand
<i>Upper Confining Layer</i>	Silt, clays and sand, fossiliferous and glauconitic, marl
<i>Murray Group Limestone Aquifer</i>	Consolidated, highly fossiliferous fine to coarse limestone
<i>Lower Confining Layer</i>	Consolidated glauconitic and fossiliferous marl
<i>Lower Renmark Group Aquifer</i>	Unconsolidated carbonaceous sands, silt and clay

#### **4.3.1 Quaternary Aquifer**

Most of the Quaternary aquifer systems are located adjacent to the Darling River. The sediments covering the Darling floodplain have in some places higher permeability and storage, but it was also documented that they generally contain groundwater of higher salinity. The Quaternary sediments are up to 30 metres thick and consist of floodplain deposits which include silts and clay, interbedded with relatively thin sands and rare gravel layers forming the Quaternary aquifer(s).

The shallow sand layer forms a water-table aquifer system which is claimed to have a hydraulic connection to the surface water drainage system of the Darling and the underlying Tertiary aquifers. This shallow groundwater is recharged from rainfall on the floodplain, but mostly from the Darling River during flood flows. In some places close to the River the groundwater is of potable quality, but during low flows there is slow discharge back to the surface system. The supply from this aquifer is considered negligible for the intended purpose. However, it is possible to investigate its potential in close proximity to the River in future drilling.



The lacustrine Blanchetown Clay forms a discontinuous confining bed at the base of the Quaternary deposits.

#### **4.3.2 Tertiary aquifers**

The Tertiary sediments host thick, permeable and high-yielding aquifers, but the volume of fresh water in storage is not well known and is thought to be limited.

Conversely, the thick sediments covering the Darling floodplain have higher permeability and storage, but generally contain groundwater of much higher salinity. These deposits probably receive a small amount of recharge from direct rainfall infiltration, but also from surface and subsurface flows at the foot of the Ranges. Recharge is also derived by infiltration from the Darling River in times of flood.

The uppermost Tertiary aquifer is the Pliocene Sand (Parilla Sand), which is a composite aquifer unit made up of several different stratigraphic units and facies. It includes the Shepparton formation, which is argillaceous. Salinity levels in the groundwater from this aquifer are generally too high for the intended purpose. However, groundwater salinity of 1000 mg/L or less has been recorded around the Darling River area suggesting a direct recharge from the River.

Underlying the sand an upper confining layer consists of silt, clays and sand which is generally fossiliferous, glauconitic and marly. Most of the concerned area shows that the Upper Renmark aquifer immediately underlies the Pliocene Sand. This aquifer is separated from the Lower Renmark aquifer by a confining bed. This confining bed consists of clay and silt, mostly glauconitic and calcareous. In some areas, the Murray Group Limestone aquifer occupies the interval equivalent to the middle of the Renmark Group. This limestone group consists of well to moderately cemented limestone, generally highly fossiliferous fine to coarse limestone.

Tertiary aquifers are considered reliable for performing ASR. The aquifer can

be used for purifying the injected water and extracting it for the intended purpose. The previous works in South Australia by the author at several locations (Gerges 1996a - d, 1999a, 1999a – d, 2001 and 2003 and Gerges et al 1994, 1996a – g, 1997a – f and 1998a - e ) prove the feasibility of the ASR technique. A summary of examples of ASR work carried out by the author including work in town of Clayton, located on the edge of Lake Alexandrina (S.A) is included in Appendix A.

This technology was successfully applied at the township of Clayton, to improve the quality of River Murray water supplied for domestic and potable purposes in towns located in the lower River Murray region. This concept relies in essence on a suitable aquifer to accept and filter untreated River Murray water to a level suitable for domestic and potable purposes.

A recent desktop study undertaken by the author for SA Water has qualitatively assessed the potential for ASR at a number of towns in the lower River Murray as potential candidates for Aquifer Filtration Scheme (AFS) trials (ie. using the aquifer as a storage and filter medium). The potential of ASR in this formation should be investigated.

## **5. RECOMMENDATIONS**

Several options are available for groundwater supply and implementing ASR both locally in Broken Hill, and the surrounding region.

### ***5.1 Locally in Broken Hill***

The location of potential sites to obtain groundwater and implement ASR are mainly associated with major structures in the Willyama Supergroup, and can be summarised below:

- South Base Monocline;
- Global Vauxhall City Schist Zone;
- Hanging Wall synform;
- Broken Hill Synform;

- Broken Hill Antiform.

Areas that may be worth further investigations are located along the lode horizon shown on Figure 7.

### ***5.2 Utilizing existing Lake Menindee pipeline***

The existing infrastructure for pumping surface water from Lake Menindee to Broken Hill represents a good opportunity to use it for the application of ASR techniques.

The presence of thick Tertiary aquifers near Lake Menindee represents a good opportunity for the injection of surplus winter water in one well, and extraction from another well. This concept relies in essence on a suitable aquifer to accept and filter untreated River Murray water to a level suitable for domestic and potable purposes. This technology has been successfully applied at the township of Clayton to improve the quality of River Murray water supplied for domestic and potable purposes in towns located in the lower River Murray region.

### ***5.3 Proposed Field Investigations***

It is recommended to drill exploration wells to total depth of 150 metres using a small hummer drilling technique, and if the exploration well is successful then it can be converted into an injection/extraction well.

A careful study of local geology and site mapping by a hydrogeologist is required prior to drilling. Drilling supervision by a qualified hydrogeologist is important for the success of the project. Pump testing must be conducted according to specification from a hydrogeologist.

Indicative costing for drilling an exploration well in the fracture rock aquifer to total depth of 150 metres is approximately \$40,000 to \$50,000, excluding water courtage and hydrogeological supervision, and also providing that

overburden does not exceed 10 metres. This costing is serving as an indication only, and the actual costs could be considerably higher depending on the availability of drilling rigs and operators.

The pump testing consists of three stages; injections of 100 minute duration, long term draw down tests and long term recovery tests. An indicative cost to carry out this exercise is approximately \$14,000. The long term recovery test is important in the fracture rock environment as it will indicate the type of aquifer (either strip or compartment aquifer) and give some indication of the boundary condition of the aquifer. Drilling permits are required to carry out such works in NSW, and an EPA license may be required for injection.

If drilling and pump testing prove to be successful a conceptual scheme design is required which identifies the following parameters:

- Type of aquifer;
- Boundary condition;
- Injection rates and potential, and this includes impact of clogging and treatment;
- Recovery efficiency of injected water;
- EPA License if required.

The second stage of the conceptual design process requires the following:

- Injection/extraction well design (includes number of wells, if applicable);
- Injection pumps and delivery pipeline;
- Process control;
- Monitoring requirements.

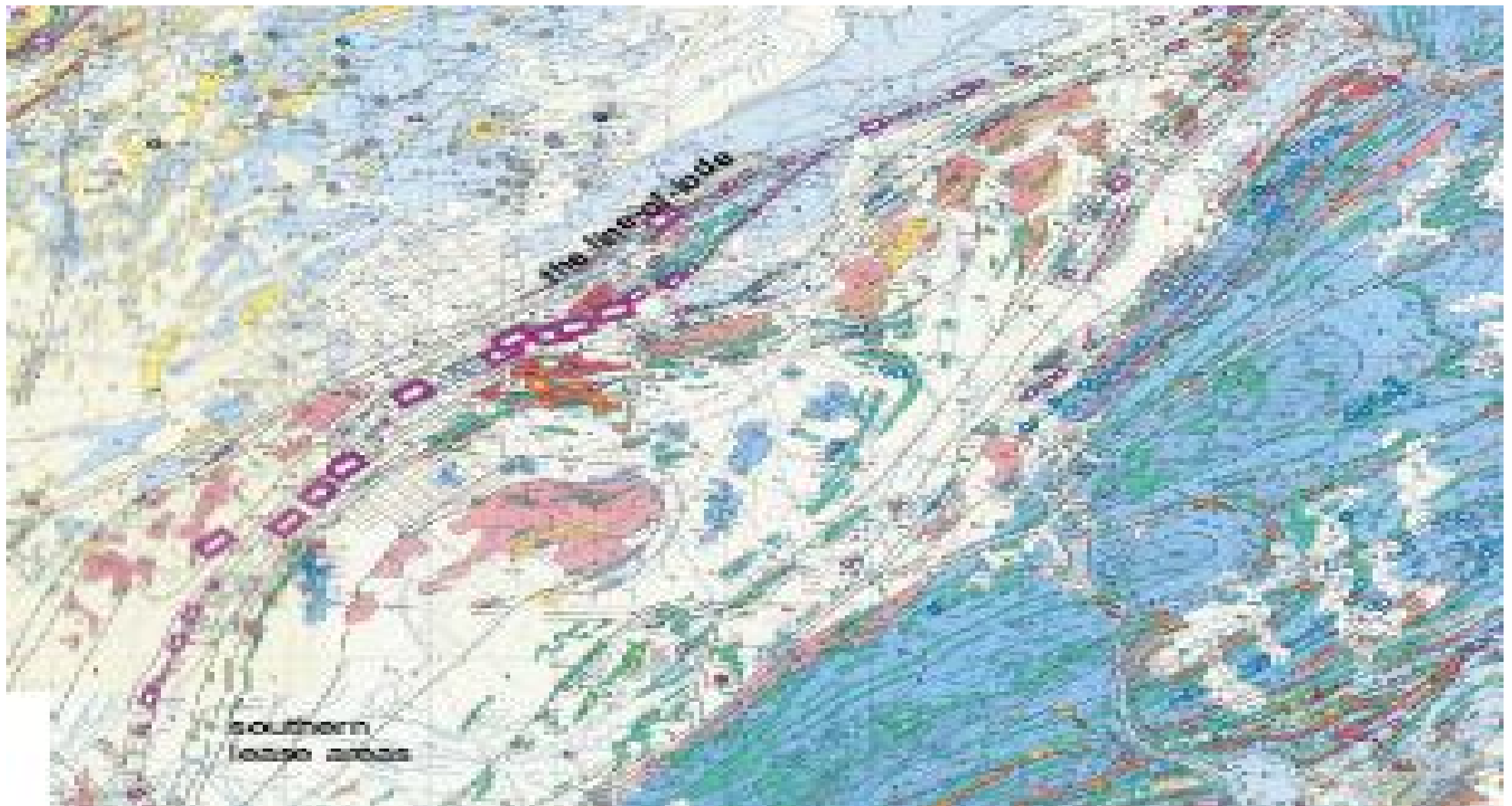


**Figure 7** Location of the lode horizon areas

## 6. REFERENCES

Brown, R.E., The Geology of the Broken Hill 1:25,000 Sheet area, Broken Hill, New South Wales, Geological Survey of New South Wales, Department of Mineral Resources, Geological Survey Report No: 1980/143 .

Corkery, R.W. & Co. PTY LIMITED in LEMP (2005) Broken Hill Landfill Site, Report No.438/02.

Gerges, N. Z., 1987, Underground water resources of the Adelaide metropolitan area with the latest understanding of recharge mechanism, *Proceedings of the international conference on groundwater systems under stress, Brisbane, AGPS May 1987*, AWRC conference series no. 13, pp. 165-75.

Gerges, N. Z., 1991, River Torrens Linear Park aquifer recharge investigations – Athelstone–Highbury zone, South Australian Department of Mines and Energy, Adelaide, Report book no. 91/80 (unpublished).

Gerges, N. Z., 1992, A preliminary assessment of artificial recharge potential, with reference to the Northern Adelaide Plains irrigation area, South Australian Department of Mines and Energy, Adelaide, Report book no. 92/40 (unpublished).

Gerges, N. Z., 1995, Virginia Pipeline Committee Bolivar – Virginia refuse project technical memorandum no.12, aquifer storage and recovery, South Australian Department of Mines and Energy, Adelaide, Report book no. 95/18 (unpublished).

Gerges, N. Z., 1996a, Overview of the hydrogeology of the Adelaide metropolitan area, South Australian Department of Mines and Energy, Adelaide, Report book no. 97/3 (unpublished).

Gerges, N. Z., 1996b, Adelaide and Northern Adelaide Plains Examples,

*Proceeding to Aquifer Storage and Recovery “CGS” Workshop, Adelaide, South Australia, 1996.*

Gerges, N. Z., 1996c, Clogging Mechanism, *Proceeding to Aquifer Storage and Recovery “CGS” Workshop, Adelaide, South Australia, 1996.*

Gerges, N. Z., 1996d, Proposals for injecting effluent for aquifer storage and recovery scheme, (Eds Kivimaki A. L and Suokko, T), In: Artificial recharge of groundwater. *Proceedings of the international symposium on groundwater artificial recharge Helsinki, Finland, June 3-5, 1996 Nordic Hydrologic Program NHP Report no 38. pp 65-74.*

Gerges, N. Z., 1999a, Northern Adelaide Plains potential for aquifer storage and recovery, South Australian Department of Primary Industry and Resources, Adelaide

Gerges, N. Z., 1999b, Northern Adelaide Plains Groundwater Review, Adelaide, S. A., Dept. Water Resources. Report 2001/013

Gerges, N. Z., 1999c, Andrews Farm T2 aquifer tests and ASR tests site Northern Adelaide Plain Area, South Australian Department of Primary Industry and Resources, Adelaide,.

Gerges, N.Z., 1999d. The Geology and Hydrogeology of the Adelaide Metropolitan Area. Flinders University of S.A. PhD Thesis.

Gerges N.Z., 2001. Virginia Pipeline Scheme Drilling Observation Wells for the Irrigation Management Plan Progress Report No. 1 – NZG Groundwater Consultant

Gerges. N Z., 2003. Edinburgh Park Aquifer Storage and Recovery Wells Completion and Aquifer Tests Result (a report for the City of Salisbury) – NZG Groundwater Consultant.



Gerges, N. Z., Sibenaler, X. P. and Armstrong, D., 1994, Experience in injecting stormwater into aquifers to enhance irrigation water supplies in South Australia, (Ed A. I. Johnson and R.D. G. Pyne.). *Proceedings of the international symposium on the artificial recharge of groundwater 2, Orlando, Florida, 1994*, pp 436-45.

Gerges, N. Z. and Howles, S. R., 1996a, Aquifer types and confining beds, *proceeding to Aquifer Storage and Recovery "CGS" Workshop, Adelaide, South Australia, 1996*.

Gerges, N. Z. and Howles, S. R., 1996b, Groundwater quality consideration, *Proceeding to Aquifer Storage and Recovery "CGS" Workshop, Adelaide, South Australia, 1996*.

Gerges, N. Z. and Howles, S. R., 1996c, Methods of artificial recharge, *Proceeding to Aquifer Storage and Recovery "CGS" Workshop, Adelaide, South Australia, 1996*.

Gerges, N. Z. and Howles, S. R., 1996d, Types of well completion, *Proceeding to Aquifer Storage and Recovery "CGS" Workshop, Adelaide, South Australia, 1996*.

Gerges, N. Z. and Howles, S. R., 1996e, Where is ASR the preferred form of artificial recharge, *Proceeding to Aquifer Storage and Recovery "CGS" Workshop, Adelaide, South Australia, 1996*.

Gerges, N. Z., Howles, S. R. and Dennis, K. J., 1996f, Clayton water supply – aquifer storage and recovery investigation, South Australian Department of Mines and Energy, Adelaide, Report book no. 96/14 (unpublished).

Gerges, N. Z., S. R., Sibenaler X. P, and Howles, 1996g, South Australia Experience in aquifer storage and recovery, (Eds Kivimaki A. L and Suokko), T.,.In: Artificial recharge of groundwater. *Proceedings of the international symposium on groundwater artificial recharge Helsinki, Finland, June 3-5, 1996*

Gerges, N. Z. and Howles, S. R., 1997a, Aquifer storage and recovery technique in a highly saline aquifer as a novel solution for a town water supply, *AWWA Proceedings of the 17th Federal Convention, Melbourne, Victoria, 1997*, pp. 432-437.

Gerges, N. Z. and Howles, S. R., 1997b, Briefing – 1 on the feasibility of aquifer injection using reclaimed water at Port Adelaide, South Australian Department of Mines and Energy, Adelaide, Report book no. 97/41 (unpublished).

Gerges, N. Z. and Howles, S. R., 1997c, Briefing on Adelaide South Parklands aquifer storage and recovery potential, South Australian Department of Mines and Energy, Adelaide, Report book no. 97/45 (unpublished).

Gerges, N. Z. and Howles, S. R., 1997d, Briefing on the potential for ASR at the MFP, The Levels site, South Australian Department of Mines and Energy, Adelaide, Report book no. 97/47 (unpublished).

Gerges, N. Z., Howles, S. R. and Dennis, K. J., 1997e, The Paddocks ASR investigation, South Australian Department of Mines and Energy, Adelaide, Report book no. 97/54 (unpublished).

Gerges, N. Z., Howles, Dennis, K.J, and, S. R., 1997f, Morphettville Racecourse aquifer storage and recovery potential, South Australian Department of Mines and Energy, Adelaide, Report book no. 97/55 (unpublished).

Gerges, N. Z. and Howles, S. R., 1998a, Groundwater resource abuse and management in South Australia, (Eds Weaver T. R, Lawrence C. R.), *Paper presented to International Groundwater Conference, Groundwater: Sustainable Solutions IAH*. Melbourne, Australia, 1998. pp 645-51.

Gerges, N. Z. and Howles, S. R., 1998b, Aquifer storage and recovery in a highly saline aquifer as a solution for town water supply, South Australian

Department of Mines and Energy, Adelaide, Report book no. 98/6 (unpublished).

Gerges, N. Z., Howles, S. R. and Dennis, K. J., 1998c, Clayton Water Supply ASR Investigation, South Australian Department of Primary Industry and Resources, Adelaide, Report book no. 96/14 (unpublished).

Gerges, N. Z., Howles, Dennis, K.J, 1998d, ASR, hydraulic and salinity response in unconfined/confined aquifers,(Eds.Peters, J. H., et. al.). Proceeding to the 3rd International Symposium on Artificial Recharge of Groundwater, TISAR. Amsterdam, Netherland 21-25 September 1988. pp. 269-73.

Gerges, N. Z., Sibenaler, X. P. and Howles, S. R., 1998e, South Australian experience in aquifer storage and recovery, South Australian Department of Mines and Energy, Adelaide, Report book no. 98/7 (unpublished).

Jewell, C.M., and Associates Pty Ltd (2004), Broken Hill Groundwater Resources Study for John Wilson and Partners Pty Ltd. Report No. J0958.1R-rev2.

Laing, W.P., Marjoribanks, R.W. and Rutland, R.W., 1978. Structure of the Broken Hill mine area and its significance for the genesis of the ore bodies. Economic Geology, 73 (6), 1112-1136.

Pavelic P, **Gerges N Z** and Dillon P J (1995). "Draft guidelines on the quality of stormwater and treated wastewater for injection into aquifers for storage and reuse", Centre for Groundwater Studies Report No 63, November 1995.

Pavelic, P., Dillon P., Barry, K.E., Herczeg, A.L., Rattray, K.J., Hekmeijer, P., & **Gerges, N.Z.** (1998) Well clogging effects determined from mass balances and hydraulic response at a stormwater ASR site. *In* Artificial Recharge of Groundwater, Peters et al (eds) Balkema, Rotterdam, p.61-66.

Pavelic, P; Dillon, P; **Gerges, N.Z.** 1998. Restoring heterogeneous brackish

aquifer through aquifer storage and recovery TISAR '98: Proc. 3rd Int. Symp. on Artificial Recharge of Groundwater, 12-25 September, 1998, Amsterdam (this volume).

## **APPENDIX A**

### **SELECTED EXAMPLES OF ASR IN SOUTH AUSTRALIA**

## **ASR IN SOUTH AUSTRALIA**

Although limited experience with ASR exists within Australia, South Australia has recently developed the expertise of aquifer injection in various hydrogeological environments. This has been demonstrated at various other sites. Experimental injection into the shallow coastal highly saline aquifers will have wide implication throughout Australia and possibly South-East Asia.

ASR has the potential to enhance the State's water resources and relieve the pressure on traditional sources. In the broader sense, opportunities exist to use ASR to rethink our traditional water management and distribution policies, and to provide cost-effective and innovative alternatives to current methods of water supply and stormwater management. In irrigation areas, surplus winter runoff can be harvested for summer re-use, and assist in reducing the stress on groundwater basins.

ASR has the greatest potential in those regions, which are approaching full development of the water resource, have degraded or low quality groundwater, and have a surplus of suitable quality alternative water resources, such as stormwater.

ASR offers opportunities for both government and the private sector to increase management options for greater use of the State's water resources.

The obvious application is temporary storage of stormwater, which would normally flow to waste. Other options could include the use of existing pipelines to take advantage of "off-peak" opportunities to store quality water at a re-use location. It can also enhance degraded aquifers and assist in improving or maintaining existing irrigation developments.

Research and development work undertaken in South Australia indicates that ASR will be a key conjunctive surface and groundwater resource management tool in the near future. Well construction is critical to the success of injection, in particular where water compatibility problems exist and clogging may occur. Wells completed



in sedimentary aquifers are more susceptible to clogging than fractured rock aquifers. Controlled acidisation experiments in carbonate aquifers demonstrate the effectiveness of this method for enhancing well performance.

The results of using ASR in South Australia will be restoration of aquifer pressures, localised reduction in salinity of groundwater where traditionally groundwater was unsuitable for irrigation and the creation of low salinity lenses/bubbles within saline aquifers for town water supply. Consequently infrastructure costs associated with mains water supply will be reduced, in particular to country towns, and there will be less reliance on imported water.

Currently, ASR projects are being developed in Adelaide Metropolitan area and Northern Adelaide Plain area with the intention in most cases of using stormwater for irrigation, and these include:

- Andrews Farm - irrigation supply in confined limestone saline aquifer,
  - Greenfields - irrigation supply in confined limestone saline aquifer,
  - The Paddocks - irrigation supply in confined limestone saline aquifer,
  - Regent Gardens - irrigation supply in confined fractured rock saline aquifer,
  - Clayton Township - town water supply in unconfined limestone highly saline aquifer, Strathalbyn - town water supply in unconfined limestone saline aquifer,
  - South Parklands - irrigation supply in complex confined aquifer,
  - Morphettville Racecourse - irrigation supply in confined limestone saline aquifer,
  - Heynes Nursery - irrigation supply in confined limestone saline aquifer,
  - Salisbury development - irrigation supply in confined limestone saline aquifer,
  - The Pines—irrigation supply in confined limestone aquifer,
  - Northfield development—irrigation Fracture rock aquifer,
  - Parafit Square housing state, irrigation supply unconfined aquifer,
  - Brompton housing state irrigation supply unconfined Quaternary aquifer,
  - Scotch College- Irrigation supply, unconfined fractured rock aquifer,
  - Numerous research and development sites, such as Glengowrie, Marine Land.
- In addition. Responsible for conceptualising and initiating the injection of 10,000

ML/y <sup>1</sup> of treated effluent from Bolivar pipeline during winter in to the Limestone aquifer in NAP,

- Parafield air port ASR project capable of supplying 1000 ML/year,
- Cheltenham race course ASR project,
- ASTR project in Greenfield-Parafield area,
- Edinburgh Park South ASR,
- Edinburgh Park North ASR,
- Pooraka ASR site,
- Glenelg Golf course,
- Royal Adelaide Golf Course,
- Grange Golf Course,
- Virginia Nursery ASR site,
- Cooper Brewery ASR site,
- Parker inlet ASR site.

Reuse of effluent on land is becoming a common way to reduce nutrient discharges to coastal and surface water bodies. However, storage of effluent is needed in the wet or winter season to protect both coastal or surface waters and groundwater from contamination and supply irrigation in the dry season. Surface water dams are normally expensive. If the effluent is given appropriate treatment an injection and extraction wells can be used to restore saline and brackish aquifers. This concept combines water that would otherwise be wasted with an unproductive aquifer to add value to both. In South Australia at a site near Bolivar, Adelaide's, a multi-disciplinary research project is underway to assess technical viability, environmental sustainability, and commercial/economic feasibility of ASR. The project team seeks to extend this work to other sites and expand the range of applications and scientific knowledge of aquifer processes.

## **SELECTED EXAMPLES OF ASR PROJECTS IN SOUTH AUSTRALIA**

Among the numerous investigation sites the two most complex sites are at The Paddocks, Salisbury and Andrews Farm in the Northern Adelaide Plains and at Clayton adjacent to Lake Alexandrina. All sites required investigation of a nature previously not undertaken by any other organisation in Australia. In particular, the Clayton project is the first investigation of its kind on an international basis and the outcome of the work will have wide application in similar coastal aquifers throughout Australia. Other sites have been summarised for reference.

### ***A). ANDREWS FARM***

The Northern Adelaide Plains, a market gardening area 40 km north of Adelaide, is underlain by confined Tertiary limestone. Irrigators have depended entirely on groundwater from the second Tertiary aquifer over the last 25 years which has resulted in depletion of elastic storage and the development of a large cone of depression (75 m deep in the centre). Urbanisation of the surrounding area has resulted in increasing stormwater runoff. A trial project assessing the potential of the second Tertiary aquifer system to support ASR has been successful.

An injection well was drilled to a total depth of 180 m and three deep observation wells were drilled and completed in the second Tertiary aquifer. The injection well was completed open hole from 107 - 125 m producing a yield of 20 L/s with a salinity of 2,200 mg/L and depth to water of 20 m below ground.

During testing the response of the injection well and the 25 m observation well were almost identical in time and magnitude indicating a high degree of connection between both wells. Inter-connection is believed to be due to the removal of sand from the naturally occurring limestone aquifer fractures as a result of well development.

Several gravity injection tests with storm water (salinity 250 - 350 mg/L) were conducted at rates of 20 L/s. Some clogging of the well and near aquifer material was observed but it is believed that major clogging due to aquatic microfauna can

be avoided by filtering.

The work undertaken at this site indicates that this limestone aquifers are capable of storing and restraining (confirmed by monitoring movement of injected 260 ML over 3 years) the movement of injected waters while improving the salinity of the native groundwater locally.

### *B) GREENFIELDS*

The Greenfields wetland site 10 km north of Adelaide was developed with the long-term goal of conjunctive wetland treatment/aquifer storage of storm water. DWR is investigating the potential for ASR using the confined first Tertiary aquifer.

An investigation/injection well was drilled to a depth of 148 m, cased to 102 m, and completed open hole through the shell bed and the limestone. A final standing water level of 14 m, an airlift yield of 9 L/s and a salinity of 2,050 mg/L were measured. Instability in the shell bed required airlift development to be carried out intermittently for several weeks during which 30 to 50 tonnes of sand and shells were removed from the well. A further injection well was drilled and completed with a screen from 102 - 111 m in the shell bed, and open hole from 120 - 145 m. Preliminary pressure injection testing at a rate of 13 L/s into the well completed with screen and open hole resulted in a head of 50 m. This well's inefficiency is believed to be due to development problems over the screened interval. The well-completed open hole only is expected to operate satisfactorily under gravity injection.

### *C) THE PADDOCKS*

The Paddocks wetland site 10 km north-east of Adelaide was developed with the long-term goal of conjunctive wetland treatment/aquifer storage of storm water.

An investigation/injection well was drilled and completed open hole from 134 - 164 m in a silty sandy green grey limestone. A final standing water level of 10 m, a salinity of 1,850 mg/L and an airlift yield of 10 L/s were recorded. The well was

injection tested using both wetland and mains water. Data analysis indicated that with respect to the discharging well that injection with wetland water was 50% as efficient as discharge and injection with main water was 70% as efficient as discharge. It was apparent that there was a water compatibility problem at this site. Controlled acidisation was conducted using 5,000 L of acid. Hydraulic testing was then conducted indicating a 30% increase in efficiency.

#### *D) CLAYTON*

Clayton (80 km south-east of Adelaide) draws its water supply from the River Murray, which in summer months is suffering pollution from toxic algal blooms. Work was carried out to investigate using ASR to develop a summer water supply of 20 ML. Water will be injected into the underlying aquifer during the winter months, when toxic algal counts are low, and this water extracted during the summer.

An investigation/injection well was drilled to a depth of 115 m, cased to 22 m and completed open hole within unconfined fossiliferous sandy limestone. A final SWL of 14 m, a salinity of 37,000 mg/L and an airlift yield of 25 L/s were recorded.

Injection testing indicated that the well was readily able to accept injection of lake water, but was 40% less efficient than when the well was discharging. It was apparent that there was a water compatibility problem, although this was not considered to be a problem at this site which may be capable of accepting up to 50 L/s without pressurising the well. A lens 10 m thick and with a salinity of 4,500 mg/L developed during the injection and mixed with ambient groundwater over a period of 105 days resulting in a salinity of 6,900 mg/L.

The results are encouraging considering the unconfined nature of the limestone, the high aquifer transmissivity and the high groundwater salinity. A volume of approximately 500 ML was gravity injected in early 1996 at a rate of 50 L/s, it is expected that a lens of drinking water quality can be developed. Information gathered from this site will have a wide application in similar coastal aquifers

throughout Australia.

#### *E) REGENT GARDENS*

At Regent Gardens housing estate in Adelaide an ASR scheme was developed to reduce stormwater outflow and provide an irrigation water supply for parklands. This scheme involves piping storm water to a wetland detention basin. After treatment it is gravity injected into a saline fractured rock aquifer. Water is then extracted during the summer for irrigation of the surrounding parks and gardens. This scheme became operational in 1994 during which 10 ML was injected, followed by 40 ML in 1995.

Hydrogeological investigations were conducted by drilling an 80 m investigation/injection well. The well was completed open hole in the confined fractured rock aquifer intersected at 44 m (slate). A highly fractured quartzite was intersected at 68 m. The native groundwater had a salinity of 2,700 mg/L, depth to water was 14 m. Several hydraulic tests and injection tests using mains water (salinity 360 mg/L at 22 L/s, total volume 5 ML) resulted in a transmissivity of 70 m<sup>2</sup>/day, calculation of the yield as 24 L/s and the gravity drainage rate as 13 L/s. Following the injection of the small volume of 10 ML of storm water during 1994 some extraction occurred. During repeated pumping periods of 6 hours water quality initially started at values between 500 and 800 mg/L and rose to 1,000 - 1,100 mg/L. This trend suggested that low salinity water was initially being withdrawn from the major fracture system, and after some time additional water was being withdrawn from minor fractures and the primary porosity which yields more saline groundwater. This problem is expected to be reduced when much larger volumes of storm water are injected.



## THE STRUCTURE AND TECTONIC EVOLUTION OF THE BROKEN HILL REGION, AUSTRALIA

R.W. MARJORIBANKS<sup>1</sup>, R.W.R. RUTLAND<sup>2</sup>, R.A. GLEN<sup>3</sup> and W.P. LAING<sup>4</sup>

<sup>1</sup> *Anaconda Australia Incorporated, P.O. Box 5573, M.S.O., Townsville, Qld., 4810 (Australia)*

<sup>2</sup> *Department of Geology, University of Adelaide, Adelaide, S.A. 6000 (Australia)*

<sup>3</sup> *Geological Survey of New South Wales, Coga Centre, 8–18 Bent Street, Sydney, N.S.W. 2000 (Australia)*

<sup>4</sup> *162 Wills Street, Broken Hill, N.S.W. (Australia)*

(Received May 17, 1978; revision accepted January 29, 1980)

### ABSTRACT

Marjoribanks, R.W., Rutland, R.W.R., Glen, R.A. and Laing, W.P., 1980. The structure and tectonic evolution of the Broken Hill region, Australia. *Precambrian Res.*, 13: 209–240.

One of the world largest silver–lead–zinc sulphide orebodies occurs at Broken Hill, New South Wales. Detailed mapping and recording of small-scale structures over a large part of the Willyama Orogenic domain around Broken Hill, has enabled the evolution of the area to be seen in terms of three superposed deformational and metamorphic events. The first event was by far the most intense and produced the dominant tectonite fabrics of the area. Intense deformation accompanied by syntectonic metamorphism to granulite facies produced widespread flat-lying gravity nappes whose probable root zone lies to the southeast of Broken Hill and whose downturned noses outcrop over extensive areas to the northwest. Later deformations of lesser intensity deform the earlier structures and form the major easily recognised folds of the region. The deformation can be divided between two orogenic episodes, one terminating at ca. 1500 Ma (Willyama) and one terminating at ca. 500 Ma (Delamerian).

The Broken Hill orebody lies within the overturned limb of an extensive  $F_1$  fold nappe and has therefore been bodily transported, along with its enclosing rocks, for a distance of the order of several tens of kilometres from its original point of deposition. The orebody shows some remobilisation into locally developed structures but does not occupy a unique tectonic position within the Willyama Domain.

### INTRODUCTION

The Willyama orogenic domain is a Precambrian basement inlier outcropping over an extensive area of South Australia and New South Wales (Mawson, 1912; Thomson, 1969; Tectonic Map of Australia and New Guinea, 1971). The domain is divided into two sub-domains, the western Olary sub-domain and the eastern Broken Hill sub-domain (Fig. 1). In the Broken Hill

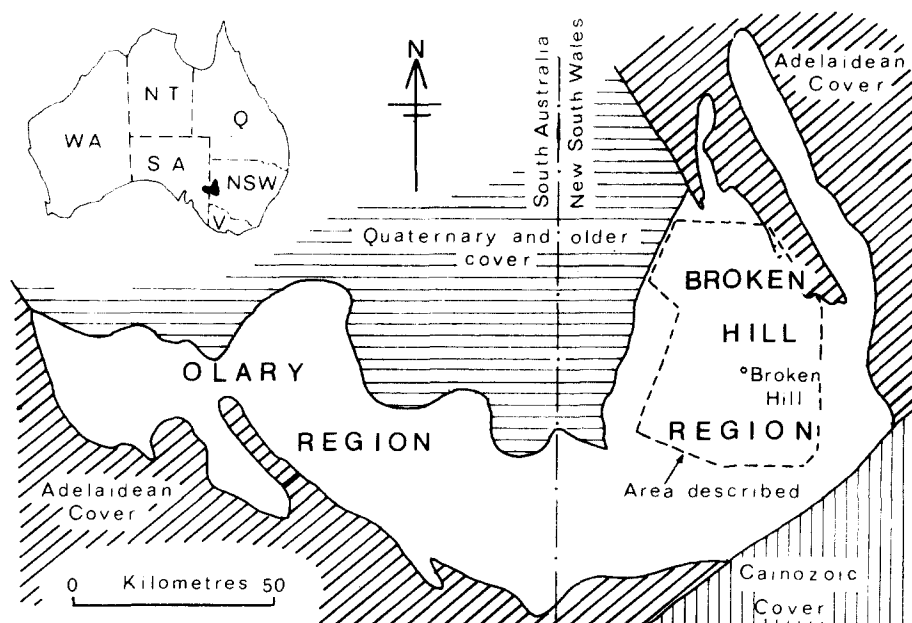


Fig. 1. Location map of Willyama orogenic domain.

sub-domain, the predominant rock-type is a coarse-grained paragneiss belonging to the almandine amphibolite and granulite facies of regional metamorphism (Binns, 1963, 1964; Vernon, 1969; Phillips, 1977). Small areas of sediments characterised by prograde, andalusite and biotite occur in the northern part of the area (see Fig. 9).

This paper describes the structural and tectonic evolution of part of the Broken Hill sub-domain, centred approximately on the town of Broken Hill (Fig. 1). The search for repetition or extension of the massive lead—silver—zinc orebody of Broken Hill has been the stimulus for many previous studies of the geology of this region. Andrews (1922) proposed that the area to the northwest of Broken Hill was the domain of open regional folds: the Great Western Fold and Great Western Basin in the west, and the Broken Hill arch in the east. Over the Mines area and to the southeast, Andrews proposed a series of much tighter folds, which he named the Hanging Wall Syncline, the Broken Hill Anticline and the Broken Hill Basin. King and Thomson (1953) subdivided Andrews' Great Western Basin and Broken Hill arch into a number of synclines and anticlines, based on the supposed repetition of conformable granite gneiss units. A more comprehensive review of this early work is given in Both and Rutland (1976). Since King and Thomson there has been no further published attempt at a systematic regional synthesis of the structure of the Broken Hill sub-domain, although speculations on the broader regional structural setting of the orebody have been published by Hodgson (1974), Katz (1976a, b), and Stanton (1976).

The structure of the Broken Hill Mines area has been the subject of a large number of papers (Gustafson et al., 1950; King and O'Driscoll, 1953; O'Driscoll, 1964; Carruthers, 1965; Lewis et al., 1965). With Hobbs (1966) and, following him, Hobbs et al. (1968), Ramson (1968) and Hodgson (1974), began the first attempts to apply modern techniques of structural analysis, based upon detailed recording of mesoscopic structures, to the Mines area. A similar structural analysis was applied by Williams (1967) to the Little Broken Hill area, southeast of the main Broken Hill Lode, and by Anderson (1966) in the Mt. Robe area N.W. of Broken Hill. These studies were based on small areas and their results had limited regional application. The earlier stages of the authors' own efforts to apply these techniques over a wider area are described by Rutland (1973) and Rutland and Etheridge (1975).

The dominant rock type of the sub-domain is a layered sillimanite-biotite-garnet gneiss which represents metamorphosed pelitic and psammopelitic sediments. This lithology may preserve bedding and sedimentary structures and is capable also of preserving the superimposed penetrative fabrics of successive deformations. This study is based upon mapping of the area, concentrating upon detailed recording and analysing the small-scale structures within this lithology in accordance with the principles of structural analysis (Hobbs et al., 1976, p. 351).

The elucidation of macroscopic geometry can make use of various criteria:

- (a) geometry of marker units;
- (b) polarity of distinctive rock sequences, i.e., distinctive elements of the stratigraphy;
- (c) bedding/schistosity relations;
- (d) use of minor-fold vergences;
- (e) mesoscopic and macroscopic evidence of overprinting of different deformation episodes.

Early structural studies at Broken Hill relied on the first of these criteria. They were unsuccessful because few distinctive marker units are available, and they lack continuity as a result of primary facies and thickness variations, extreme deformation (including dislocation by later-stage retrograde schist zones), and lack of outcrop.

At a late stage in the present work, criteria (a), (c) and (d) were combined to erect a new stratigraphy in the Mine area (Laing et al., 1978), thus allowing criterion (b) to be used elsewhere. This stratigraphy was not established when most of the mapping, on which the present study is based, was carried out. However, criteria (a) and (b) have been used to provide controls on the structural interpretation.

The first evidence of superposition of fold episodes in the region was provided by Hobbs (1966), who recognised two categories of folds: Group 1, with an axial-plane schistosity, and Group 2, which folded the schistosity. Subsequent work, however, showed that the regional schistosity, previously regarded as one element, could be separated into three separate elements on the basis of overprinting criteria: one of high metamorphic grade ( $S_1$ ), one of

variable grade ( $S_2$ ) and one consistently retrograde ( $S_3$ ) (Rutland and Etheridge, 1975, p. 259). In examining the application to the regional structure, Rutland and Etheridge also concluded that most of the mapped major folds of the region could be allocated to  $F_2$ .

These results were the starting point for the present work, but modifications have been necessary consequent upon the detailed study of the Mines area (R.W.M. and W.P.L.), and upon the provision of continuity of mapping between previously isolated areas of study (R.W.M.). The sequence of structural and metamorphic events is now best defined in the Mines area (Laing et al., 1978), and correlations are made with reference to that area.

The dislocation of structure by retrograde schist zones and lack of outcrop hamper the correlation of mesoscopic structural data over wide areas, and several problems should be noted:

(1) It is possible that  $S_1$  may not always be parallel to  $S_0$  and it may not then be possible in the absence of superposition criteria to separate  $S_1$  and  $F_1$  from  $S_2$  and  $F_2$ .

(2) Later schistosity is locally co-planar with earlier ones. The distinction of the associated fold structures may then be difficult.

## SMALL-SCALE STRUCTURES

### *Lithological layering*

Lithological layering is common throughout the sillimanite gneiss and andalusite schist of the area, and is identified as deformed but not transposed sedimentary bedding ( $S_0$ ) (Glen and Laing, 1975). In most medium- and high-grade rocks the layers typically consist of psammite bands from 1 cm to several metres thick, with generally sharp contacts against the pelitic country rock. The layers are parallel to each other and generally parallel to the contacts of the major lithological units within the domain. The overall spacing of the layers is irregular, with sections of regularly banded psammite/pelite units alternating with thicker sections of more uniform pelite. Except where affected by folds, the layers in general maintain a constant width and can be traced for the extent of the individual outcrops.

In the medium- and high-grade rocks, some psammopelite layers show a marked mineralogical gradation from a sharply defined pure quartzite base to a pelitic biotite  $\pm$  garnet  $\pm$  sillimanite  $\pm$  muscovite top (see Fig. 3,A). These graded units are considered to represent metamorphosed graded turbidite beds and to give a younging direction for the strata. This direction is consistent with younging obtained from cross-beds and flame structures where they are found together in medium-grade rocks. Such graded units were first used in regional mapping at Broken Hill by Thomson (1954) and are mentioned by Rutland and Etheridge (1975), and fully described by Glen and Laing (1975), and Laing et al., (1979).

### *First-generation structures*

In high-grade rocks, a well-developed schistosity is commonly present parallel to the bedding and to the contacts of the major lithological units. This surface is the dominant fabric element throughout the region. It is defined in pelitic rocks by planar aggregates of sillimanite and fibrolite and by the preferred orientation of sillimanite needles and biotite laths. Garnet and orthoclase porphyroblasts, and the inclusions within them, are typically flattened within the schistosity. This surface is the oldest deformational fabric that can be identified and is labelled  $S_1$ . It is most strongly developed in pelitic metasediments and is only weakly preserved within psammite units. In granite gneiss,  $S_1$  is defined by a metamorphic segregation foliation consisting of regularly alternating laminae of quartzofeldspathic and mafic minerals, and by the preferred orientation of biotite. Within amphibolite units, a similar, though generally finer, metamorphic differentiation foliation defines  $S_1$ , along with preferred orientation of biotite and the long axes of hornblende.

In pelitic metasediments, the orientation of sillimanite and fibrolite defines a prominent lineation within  $S_1$ , referred to as  $L_1$ . In granite gneiss units, this lineation is marked by a streaking of felsic-mafic material within  $S_1$  and by the preferred orientation of the long axes of feldspar augen.

It is clear that  $S_1$  and  $L_1$  are the consequence of intense strain but mesoscopic  $F_1$  folds with  $S_1$  as axial-plane schistosity are rare. However, there is good evidence from metamorphosed graded bedding, especially in the Mines area (Laing et al., 1978), that the  $F_2$  macroscopic folds are often superimposed on a pre-existing inverted stratigraphy, which is ascribed to first deformation folding. A few  $F_1$  folds have been identified on the basis of their style and superimposition upon them of structures of both  $F_2$  and  $F_3$  age. These folds have tightly appressed hinges which are the sites of local transposition of bedding and strong  $S_1$  development. As a result, it was not possible to directly measure the plunge of any  $F_1$  fold. However, it is assumed, in view of the intense strain associated with the folding and fabric development, that  $F_1$  fold axes were rotated to parallelism with the principal extension direction during deformation, a direction represented by  $L_1$ . Since  $L_1$  plunges at 30–35° to the southwest within a regionally NE-striking  $S_1$ , it follows that NE-closing  $F_1$  folds are synforms and SW-closing folds are anti-forms.

In low-grade rocks of the Mt. Franks area (see Fig. 9), the earliest penetrative fabric element is a schistosity defined by the oriented growth of muscovite and flattened quartz grains. This surface is generally parallel to bedding and is axial-plane to the regional isoclinal Kantappa-Lakes Nob Syncline (Glen, 1978b). The surface may be correlatable with  $S_1$  of adjacent high-grade rocks, although it is not possible to establish an absolute equivalence (for a discussion of this correlation, see below). The  $S_1$  surface wraps around randomly oriented andalusite porphyroblasts. The andalusites may show

partial retrogression to sericite both around their margins and within internal fractures: this sericite is oriented parallel to  $S_1$ . The andalusite hence appears to have grown during a pre- $S_1$  static metamorphic event for which there is no clear evidence within the high-grade domain.

### *Second-generation structures*

Second-generation structures can be identified by their superposition relationships with structures of the first and third deformation events. It is rare, of course, that a single mesoscopic  $F_2$  fold will show interference structures with both the earlier and the later events, but individual folds can usually be fairly confidently identified on the basis of consistent style and orientation of their structures with nearby  $F_2$  structures which do show such superposition relations. Second-generation folds ( $F_2$ ) are present at all scales and re-fold  $S_0$  and  $S_1$ . Their style ranges from tight isoclinal in the southern part of the Willyama to broad open warps in the north (Figs. 2, C, D). It should be noted, however, that this style change is dependent upon correlation of  $F_2$  structures across the Stephens Creek shear. This correlation is discussed below.

The axial-plane surface of  $F_2$  folds is labelled  $S_2$ . Where fully developed in pelitic rocks,  $S_2$  is defined by folded and flattened aggregates of fibrolite and sillimanite and by the preferred orientation of new sillimanite and biotite (Fig. 3, C). The surface is thus similar in appearance to  $S_1$ . However,  $S_2$  is typically only developed within or adjacent to  $F_2$  hinges where it is





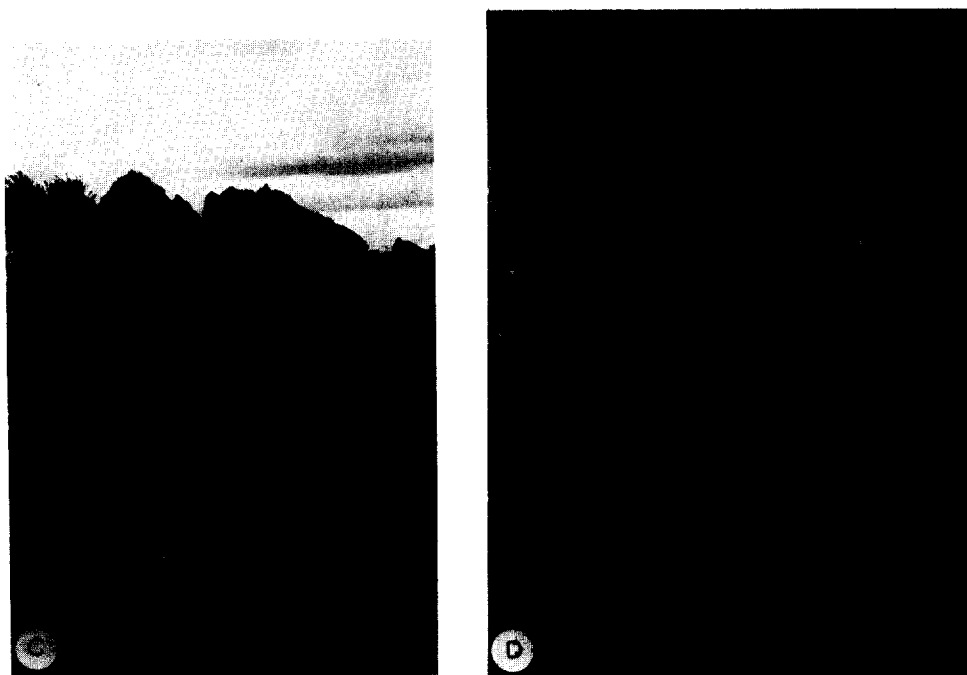


Fig. 2. Small-scale second-generation structures.

A. Layer-parallel sillimanite schistosity ( $S_1$ ) preserved in psammite bed (light colour) and oblique  $S_2$  surface in pelite bed are refolded about open  $F_3$  fold. Maybell area.

B. Horizontal profile of vertically-plunging  $F_1$  fold in pelitic sillimanite gneiss. White specks are fibrolite aggregates lying within an  $S_2$  surface cutting obliquely across the fold (parallel to page) and crenulated by  $F_3$  event. Trace of  $S_1$  can be seen in more psammitic rock in core of fold. Southern Cross area.

C. Open  $F_2$  fold with horizontal axis and shallow-dipping axial plane typical of  $F_2$  folds north of Stephens Creek Shear. A vertical  $S_2$  surface can be seen parallel to hammer handle. Maybell area.

D. Characteristic  $F_2$  fold of areas south of Stephens Creek Shear. Note strong  $S_2$  defined by knots of crenulated  $S_1$  fibrolite. 21 Level, Zinc Corporation Mine.

oblique to the layer-parallel  $S_1$ . In one common occurrence,  $S_1$  is preserved within psammite layers while being obliterated and replaced by penetrative  $S_2$  in adjacent pelite units (Fig. 2,A). Even where in hand-specimen  $S_2$  has completely overprinted  $S_1$ , the fibrolite aggregates defining  $S_2$  can often be resolved under a microscope into tightly crenulated  $S_1$  fibrolite which has been transposed into the new orientation. Sillimanite needles, which have grown during  $F_2$ , cut across this tightly folded  $S_1$  fibrolite (Fig. 3,C).

Within granite-gneiss lithologies,  $S_2$  is marked by quartzofeldspathic segregation veinlets forming a constantly oriented surface oblique to the  $S_1$  gneissosity and parallel to the axial-plane of mesoscopic  $F_2$  folds.

Over much of the southern part of the region  $F_2$  folds plunge to the south-west at moderate angles parallel to the dominant high-grade lineation,  $L_1$ . In these areas,  $L_1$  is thus probably a composite structure resulting from the

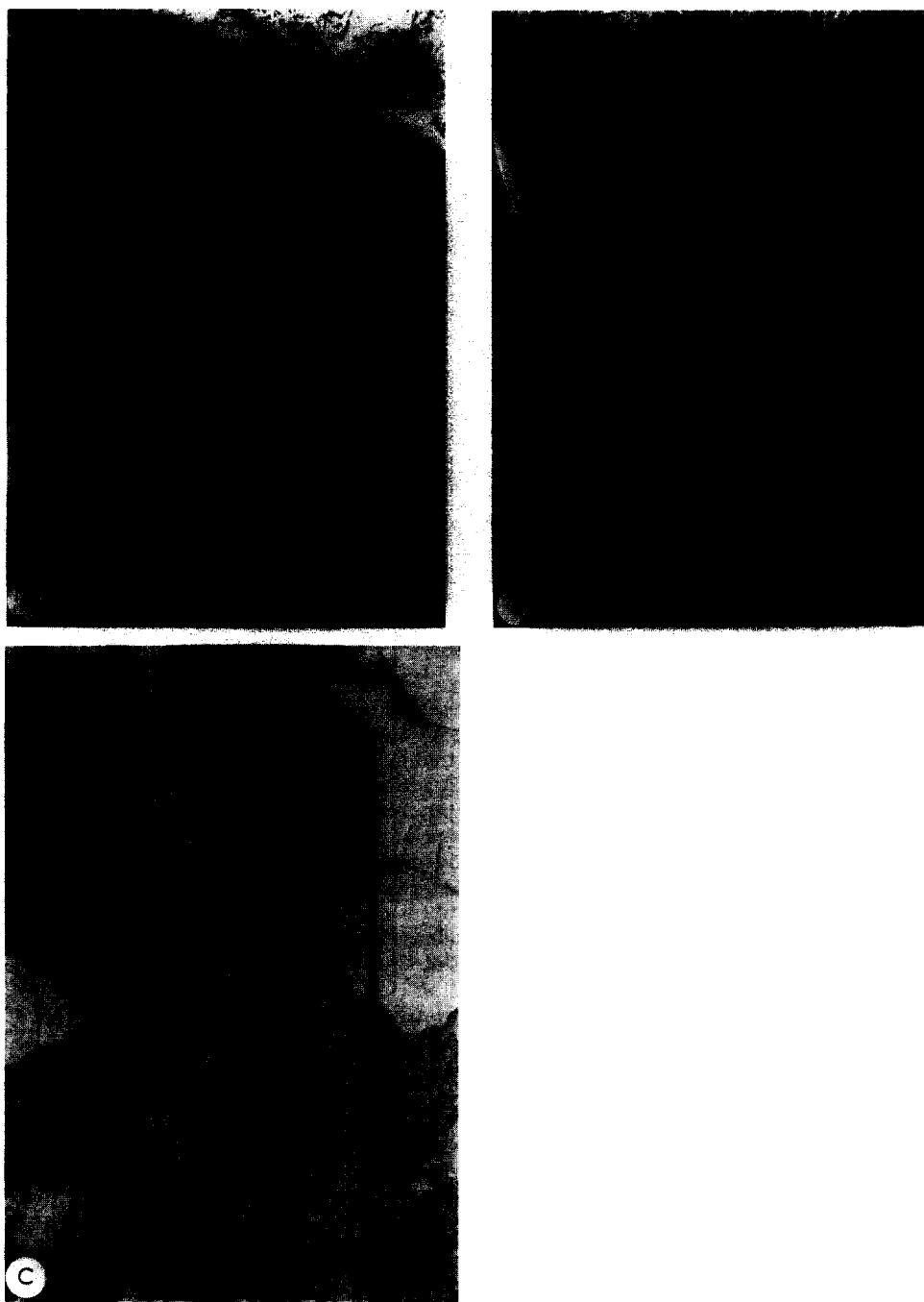


**Fig. 3. A.** Graded bed younging towards top of page. Oblique schistosity ( $S_2$ ) is crenulated by small  $F_3$  folds. Nine Mile Mine. **B.** Fold pair of  $F_1$  or  $F_2$  age affected by  $F_3$ . Note felsic segregation in hinge of late fold. Nine Mile Mine. **C.** Photomicrograph showing how a strong  $S_2$  schistosity (from top to bottom of page) can be resolved into crenulated  $S_1$  fibrolite (across the page). Note syntectonic growth of new sillimanite needle within  $S_2$ . Round Hill area.

superimposed strain of both events and is probably more accurately labelled as  $L_{1-2}$ . In places, a high-grade mineral lineation within  $S_2$  can be observed that typically plunges to the southwest parallel to adjacent  $F_2$  axes. More complex atypical lineation relationships occur in a small area northeast of Broken Hill and are described in detail in Laing et al., 1978.)

In the northern part of the region, correlatives of  $F_2$  folds (see below) have no associated linear fabric and have sub-horizontal axes which re-fold the SW-plunging  $L_1$  lineation.

### *Third-generation structures*

Structures formed during this event are present in approximately equal intensity throughout the region. The characteristic structure is a vertical schistosity ( $S_3$ ) axial-plane to an abundance of small- and large-scale, moderately open folds ( $F_3$ ).  $S_3$  formed by the crenulation of earlier schistositities and was accompanied by a retrograde metamorphism leading to the growth of oriented muscovite and chlorite  $\pm$  biotite within  $S_3$ . At its highest grade,  $S_3$  may locally contain sillimanite, and in such rocks granitic pegmatite segregations are developed in the axial planes of  $F_3$  folds (Fig. 3,B). This high-grade  $S_3$  is similar in appearance to the high-grade  $S_2$  surface and in some cases cannot be distinguished from it. In most cases, however, the consistent orientation of  $S_3$ , its congruence to macroscopic  $F_3$  folds and overprinting of  $F_2$  structures, enable it to be identified.

### CORRELATION OF DEFORMATIONAL EVENTS

The high-grade rocks of the region are subdivided by a network of linear retrograde schist zones with dominantly NE-, NW- or E.- trends. The zones may be intense narrow belts a few metres to several hundred metres wide, within which all earlier structures are obliterated, or they may be complex retrograde belts several kilometres wide. All of these wide complex belts are characterised by numerous close-spaced intense retrograde schist zones, by pervasive retrogression of intervening high-grade rocks, and by an abundance of granitoids — pegmatite, aplite, migmatite and granite — which are developed within them. The most extensive of these wide belts runs through the Apollyon Valley—Daydream areas (see Fig. 11), with the Apollyon Valley and Mt. Franks schist zones being merely the most prominent of the numerous linear retrograde schist zones within the belt. Narrower retrograde belts with similar character to the Apollyon Valley area also occur along the west-trending Stephens Creek shear in the Sundown area, and along the Darling Range.

Within the high-grade areas, structures and sequences of structures can generally be traced through closely adjacent outcrops and correlated with reasonable confidence on the basis of similarity of style and orientation. The major wide belts of retrogression, such as the Apollyon Valley area or the

Stephens Creek schist zone, represent breaks in the knowledge of the continuity of the earlier high-grade structure. Before the analysis can proceed, therefore, it is necessary to discuss correlation across these zones.

### *Correlation across the Apolloyon Valley retrograde zone*

Lithologies on either side of this zone are essentially similar and consist of well-bedded aluminous pelitic and psammopelitic metasediments. However, the zone represents a major metamorphic and tectonic break. To the west, a period of static andalusite growth was followed by a prograde syntectonic metamorphism resulting in the oriented growth of sillimanite and biotite (Glen, 1978a). This was followed by a syntectonic retrograde metamorphism resulting in the formation of a penetrative late cleavage. To the east, three deformational and metamorphic events are established, the first two ( $F_1$  and  $F_2$ ) resulting in the growth of high-grade minerals, and the last ( $F_3$ ) in a generally retrograde assemblage.

In both areas, the last tectonic event produced structures with similar orientation and style and can be correlated as  $F_3$ . It is not possible to make absolute correlations between the pre- $F_3$  structures of the two areas. There appears to be a regional decline in the intensity of  $F_2$  from southeast to northwest across the region (see below) and in the area immediately to the east of the Apolloyon Valley Zone,  $F_2$  structures are very weak. It is therefore probable that  $F_2$  is not developed to the west of the zone and that both the pre- $F_3$  events there are broadly time-equivalent to the  $F_1$  event of the main high-grade area to the southeast. Other correlations between the pre- $F_3$  structures of the two areas are, however, possible, and although the above correlation is preferred, it is far from being established with any certainty. Other possible correlations and their implications are discussed in more detail in Glen (1978a).

### *Correlation across the Stephens Creek Shear*

Three generations of folding can be independently established in the domains to the north and in the domains to the south of the Stephens Creek Shear Zone. In both areas, the earliest identifiable deformation accompanied the main high-grade metamorphic event and produced isoclinal folds and a schistosity generally parallel to layering. On this basis, the structures are correlated between both sets of areas as belonging to the  $F_1$  event. Structures belonging to the  $F_3$  event likewise can be correlated on the basis of consistent style and orientation across the Stephens Creek Shear. In both the northern and southern areas, structures are identified as  $F_2$  on the basis of their overprinting relations with  $F_1$  and  $F_3$  structures and because of their association with a second, consistently high-grade, metamorphic event resulting in crystallisation of sillimanite. For these reasons, the  $F_2$  structures can be considered to be the same age, both north and south of the Stephens Creek Shear.

On the correlation outlined above,  $F_2$  structures show a marked change in style across the shear. To the north of it,  $F_2$  folds are open with interlimb angles of  $90^\circ$  or greater (see Figs. 2,C and 8). This is in contrast to areas south of the shear where  $F_2$  folds are much tighter, with interlimb angles from  $0$  to  $90^\circ$  (Fig. 2,D). In the southern area, six major  $F_2$  folds with axial planes generally dipping steeply to the northwest can be identified. In the northern area, only one major open  $F_2$  antiform, with an axial plane dipping at a low angle to the west or southwest, is positively identified (see Fig. 10).

An alternative correlation, which cannot be excluded, is also possible. The regional  $F_2$  folds of the southern area may be present in the northern area, but have become so tight as to be indistinguishable from  $F_1$  folds. Regional isoclinal folds present in the northern area (see below) could hence be labelled  $F_2$ . This would mean that the correlation outlined above between  $F_2$  structures north and south of the Shear Zone is invalid, and that those open folds labelled  $F_2$  in the northern area, belong to a later fold generation, occurring between the  $F_2$  and what has been called the  $F_3$  event. However, this correlation is not preferred for the following reasons:

- (a) If the regional isoclinal folds north of the shear are of  $F_2$  age, then they would be expected to re-fold earlier  $F_1$  structures. In spite of careful search in the hinge area of one of these folds, no such earlier structure was found.
- (b) The regional folds repeat marker units in a consistent manner, indicating that no earlier fold phase is involved.
- (c) Ascribing the regional folds north of the shear to the  $F_2$  generation does not solve the problem of the change in  $F_2$  fold style across the Stephens Creek Shear, but necessitates postulating an additional high-grade deformational and metamorphic event, recognised only in the northern area.

Whatever correlation is adopted, the approximate line of the Stephens Creek Shear Zone must be considered to be a break of major importance separating two distinct domains of  $F_2$  deformation. In our preferred solution, strain resulting from the  $F_2$  event south of the Shear Zone was intense and a number of tight  $F_2$  folds were formed. North of the Shear Zone, strain during  $F_2$  was of lesser intensity and fewer, more open  $F_2$  folds were formed. The W-trending Stephens Creek Zone must therefore have been in existence during  $F_2$ , allowing independent deformation of the areas to the north and south. The present-day nature of the Stephens Creek Shear as a complex anastomosing retrograde schist zone is probably the result of renewed movement along it during the  $F_3$  event. In this regard, it is probably significant that the west trend of the Stephens Creek Shear Zone is abnormal for retrograde schist zones in the region, which generally strike northeast or northwest. The W-trending shear zones, of which the Stephens Creek and the Thackaringa-Pinnacles zones are the only two major examples, may thus represent fundamental structures of  $F_2$  age or older.

## REGIONAL FOLDS (Figs 4–9)

*The first-generation folds*

Within the large part of the high-grade rocks of the Willyama domain mapped by the authors, only two probable macroscopic  $F_1$  closures were identified. These are the small  $F_1$  fold in the Parnell Track area, northeast of the Southern Cross Mine (Figs. 6 and 9), and the regional  $F_1$  fold outlined by the closure of the Auger Gneiss unit south of Yanco Glen Hotel (the Yanco Glen Fold, Figs. 5 and 9). Both these folds are congruent to  $S_1$ . No definite  $F_1$  closures were mapped in the area south of the Stephens Creek Shear. However, since  $F_1$  penetrative fabrics are present throughout this area, it is reasonable to suppose that  $F_1$  closures are present but have not been identified. The failure to identify these closures is easily explained: all positively identified  $F_1$  fold closures occur north of Stephens Creek Shear where  $F_2$  folding is relatively minor and has little effect on the outcrop pattern and where strain due to the  $F_2$  event is small. South of the shear,  $F_2$  strain effects increase in intensity and major mapped closures of lithological units are the result of  $F_2$  folding.  $F_1$  fold noses are probably tight with relatively restricted hinge areas, or the hinges may be replaced by slides or thrusts. These hinge areas are either not mapped due to lack of exposure or are not identified in the outcrop because of transposition of bedding in the hinge region parallel to the  $S_1$  axial-plane surface.

If  $S_1$  in the low-grade rocks in the northwest of the area is equivalent to  $S_1$  in the high-grade rocks, then the Kantappa-Lakes Nob Syncline is also a major regional  $F_1$  fold.

Although in the southern part of the area,  $F_1$  folds cannot be directly mapped, in some areas the use of sedimentary younging directions allow structural facing to be determined for  $F_2$  folds\*. A change from downward facing to upward facing  $F_2$  structures must indicate the axis of an  $F_1$  fold. A map showing the domains of upward and downward facing  $F_2$  structures is, in effect, a map of the distribution of  $F_1$  folds. Unfortunately, as can be seen from Fig. 9, in only two areas are sufficient younging criteria available for such a map to be drawn. These areas are the Broken Hill Mines area and the Parnell Mine—Limestone Homestead area. Over large areas, no facing data are available. Nevertheless, the facing data confirm that large  $F_1$  folds are present in the southern part of the Willyama Complex even although no closures have been mapped on the surface. This facing evidence shows that the Broken Hill Mines area lies on the extensive overturned limb of a large  $F_1$

---

\*The structural facing (cf., Shackleton, 1958; Borradaile, 1976) is defined as the direction of facing measured in the axial plane normal to the fold axis. A set of upright or inclined folds produced during a first deformation episode will all be upward facing. Folds may be downward facing if they have been inverted during a previous deformation episode (or in cases of ductile folding where the axial surfaces formed during a single deformation episode are strongly curved).



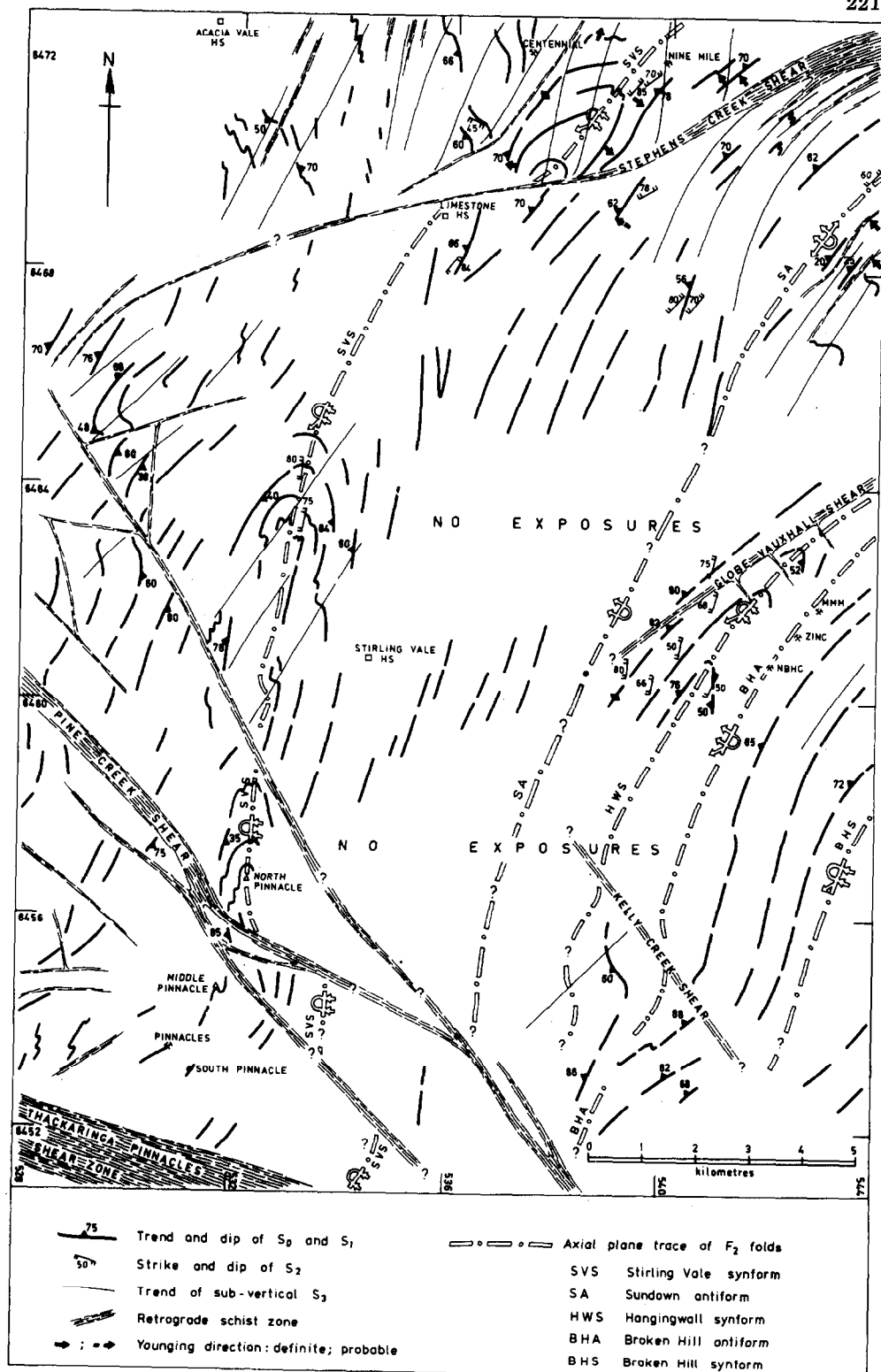


Fig. 4. Structural interpretation of Stirling Vale area showing regional  $F_2$  folds of southern part of the Broken Hill region.

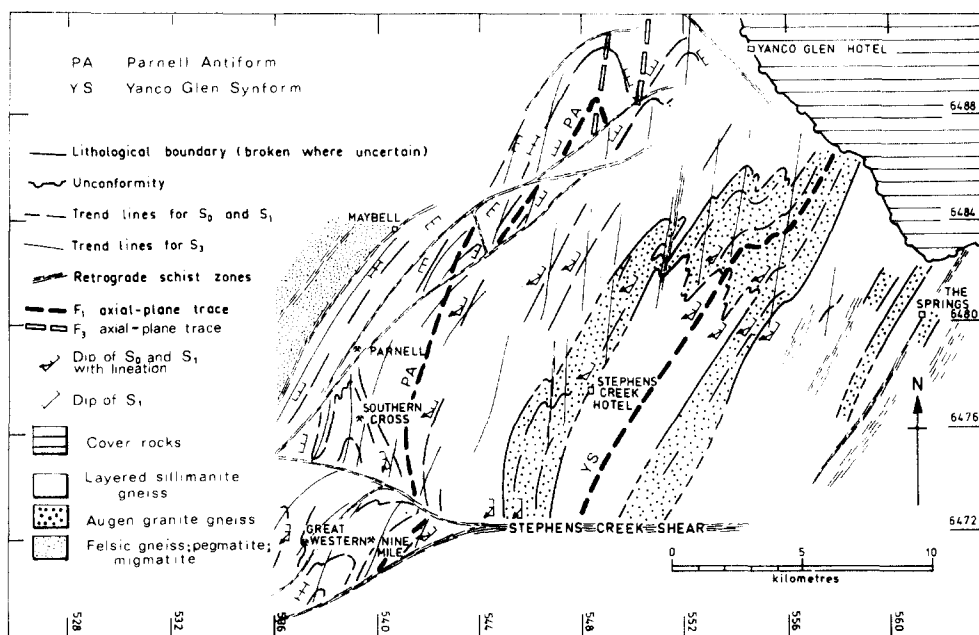


Fig. 5. Structural interpretation of Stephens Creek area showing regional  $F_1$  folds of northern part of the Broken Hill region.

fold nappe. The Parnell Mine—Limestone Homestead area is a NE-trending zone consisting of a number of relatively small  $F_1$  folds (indicated by many changes in  $F_2$  facing over a small area). This zone can be interpreted as representing the approximate hinge area of a much larger, regional  $F_1$  fold, adjacent to, and parallel with the  $F_1$  Yanco Glen Fold to the east.

Over most of the area,  $F_2$  and  $F_3$  folds are upright. The steepness of the plunge of these folds can be taken as a measure of the attitude of the beds (i.e., the attitude of  $F_1$  axial planes) prior to the  $F_2$  deformation. This, of course, ignores the possibility of reorientation of early-formed  $F_2$  fold axes during progressive strain, but on a regional basis is probably approximately correct. In the Darling Range,  $F_2$  fold axes are subvertical, suggesting that the pre-existing  $F_1$  folds there were upright. Over the remainder of the area,  $F_2$  folds have generally moderate to shallow plunges, indicating that the pre- $F_2$  folds were recumbent. The widespread inversion of stratigraphy during  $F_1$  indicates the presence of extensive fold-nappes.

North of Stephens Creek Shear, the major  $F_1$  folds which can be identified, are upright and are only slightly affected by an insignificant  $F_2$  deformation. The  $F_3$  deformation in this area, although locally intense, has not affected the attitude of the  $F_1$  folds on a regional scale. The upright attitude of  $F_1$  folds north of the shear is thus interpreted as a primary feature of the first deformation.

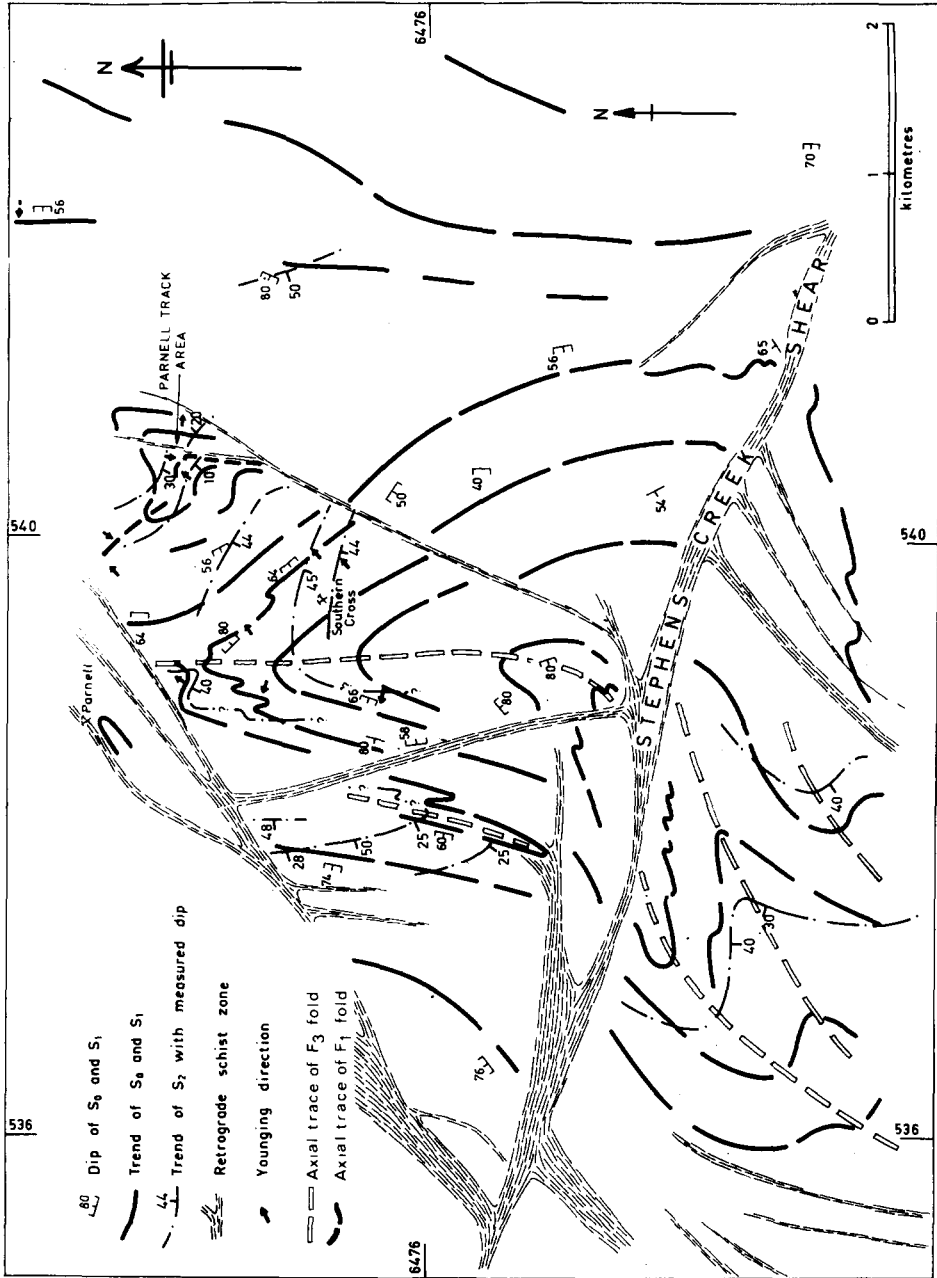


Fig. 6. Structural interpretation of Southern Cross area showing effects of  $F_1$ ,  $F_2$  and  $F_3$  deformations.

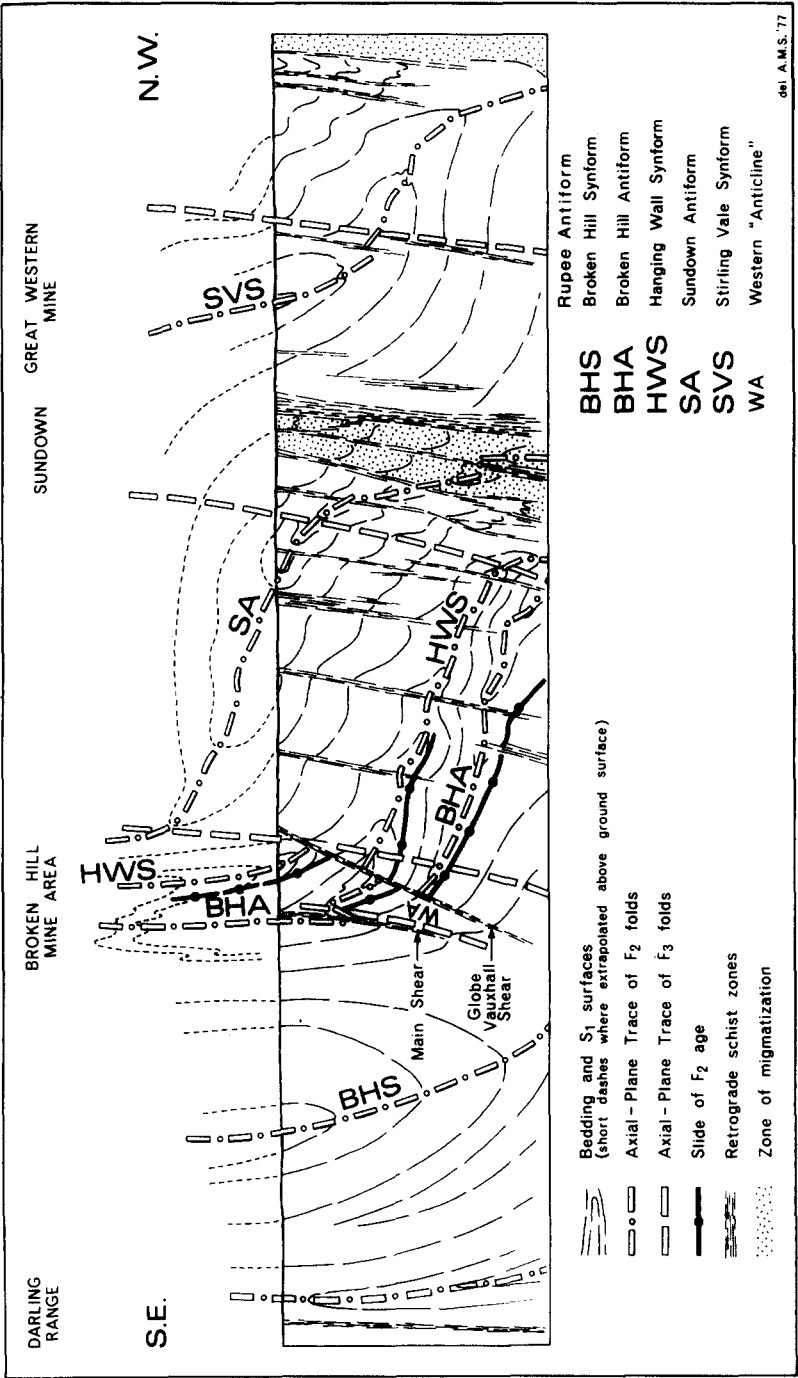


Fig. 7. NW-SE through Broken Hill Mines area showing rotation of regional F<sub>1</sub> folds about large F<sub>3</sub> monocline to the NW of the Mines.

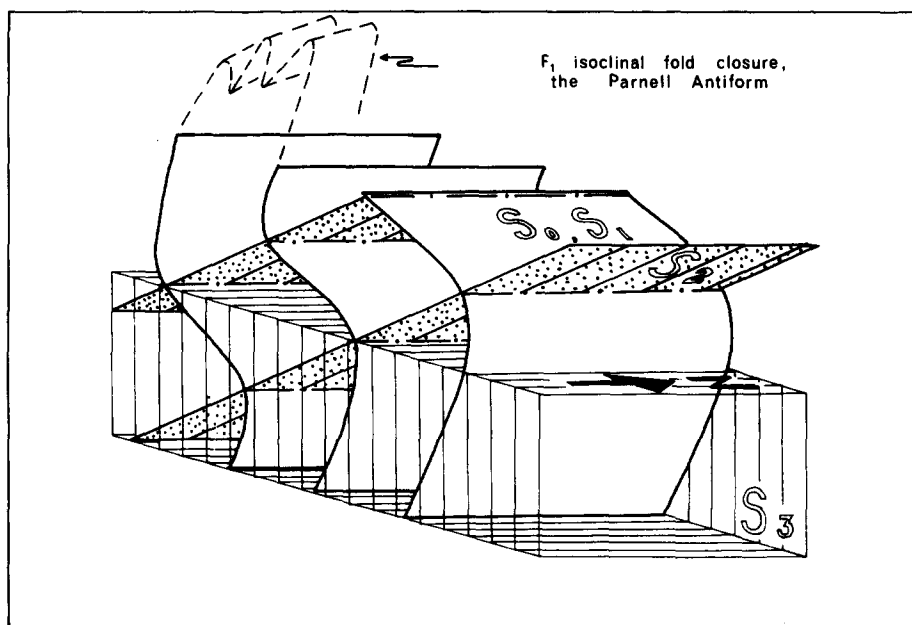
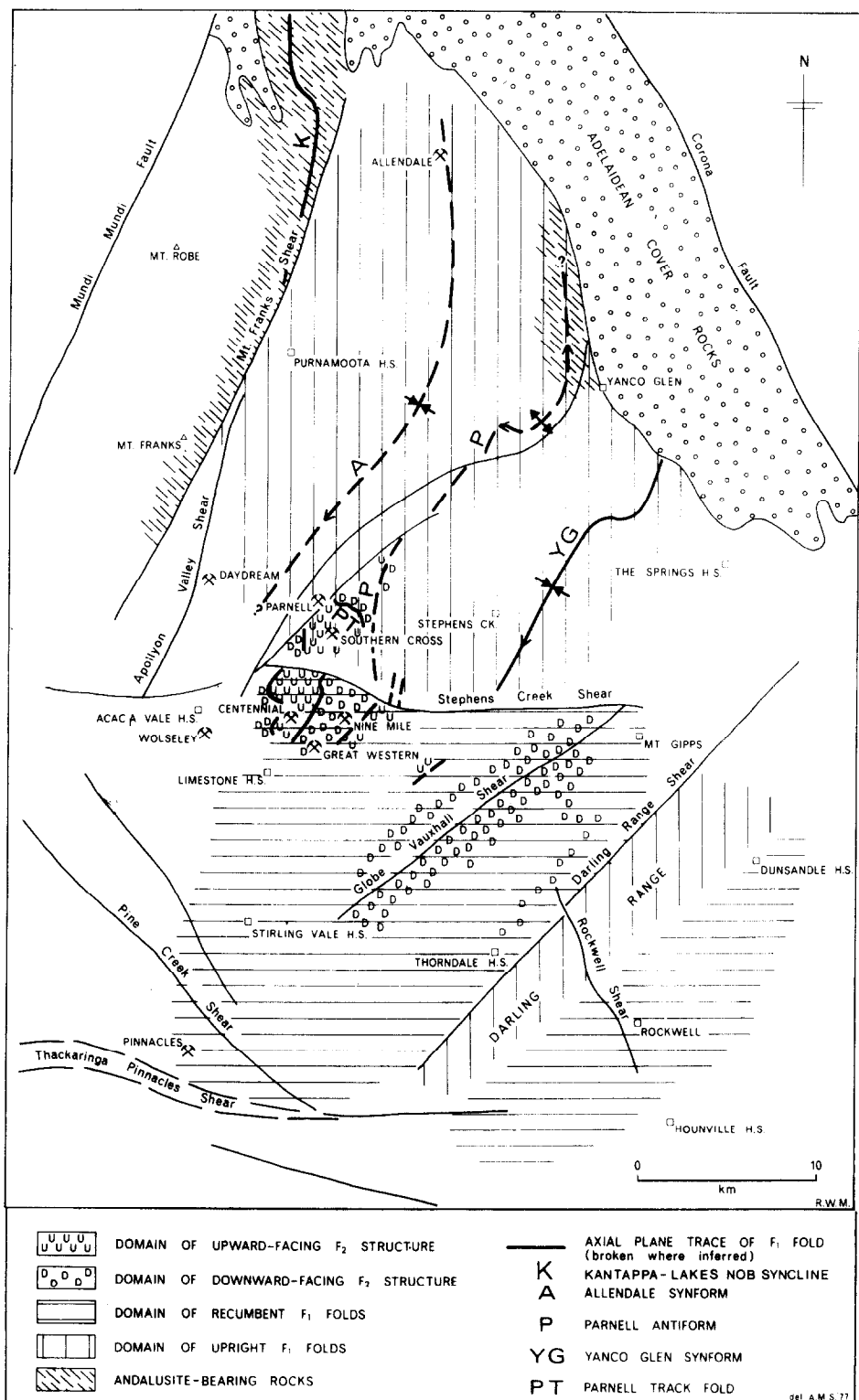


Fig. 8. Block diagram illustrating characteristic styles of  $F_1$ ,  $F_2$  and  $F_3$  foliations ( $S_1$ ,  $S_2$  and  $S_3$ ) in the area north of Stephens Creek Shear.  $S_0$  is parallel to  $S_1$ .

Fig. 9 presents a summary of available information on the location and attitude of  $F_1$  folds in the Willyama Block. In the high-grade rocks of the northern part of the block, it is proposed that three major folds are present. From northwest to southeast these are: the Allendale Fold, The Parnell Fold, and the Yanco Glen Fold. The folds are upright, have NE-trending axial planes and are probably of  $F_1$  generation. The Yanco Glen Fold has been examined and mapped by the authors. The fold is outlined by a north-closing augen granite gneiss unit. A coarse vertical gneissosity ( $S_1$ ) within the granite gneiss is axial-plane to the fold and parallel to layer-parallel schistosity in the enclosing sillimanite gneiss. A strong segregation lineation within the gneissosity plunges at moderate angles to the southwest. No  $F_2$  structures are present but a retrograde vertical  $S_3$  surface trends obliquely across both limbs of the fold. There is thus good evidence that the fold is an upright  $F_1$  fold which, if it plunges parallel to the  $L_1$  lineation, must be synformal. Limited younging evidence available suggests that the fold is downward-facing on  $S_1$ .

The nature and age of the Parnell and Allendale folds to the northwest are more speculative. The Allendale Fold has not been mapped by the authors, but a northward closure of rock units (particularly Potosi Gneiss) about a large regional fold has long been known and has recently been mapped in detail by the Geological Survey of N.S.W. (B. Stevens, pers. comm., 1976) in the area north of Allendale Mine. Potosi Gneiss occurs on both limbs of the Allendale Fold and allows the limbs to be traced for 25 km to the southwest



**Fig. 9. Synthesis of  $F_1$  structures in the Broken Hill sub-domain (retrograde schist zones and Adelaidean unconformity shown for reference only).**

of Allendale. A north-trending later fold phase is superimposed obliquely across the Allendale Fold. Structures belonging to this fold phase have been mapped by I. Symonds (pers. comm., 1976). They are upright folds with a penetrative axial-plane foliation defined by retrograde minerals. The structures are identical in style and orientation to  $F_3$  structures in the Yanco Glen and Maybell areas to the south, and they are thus identified as being of  $F_3$  age. Since only minor  $F_2$  deformation is identified north of Stephens Creek Shear, the Allendale Fold is most reasonably placed as an  $F_1$  fold analogous to the Yanco Glen Fold. Its northward closure suggests that the fold is also a synform.

Between the Allendale and Yanco Glen Synforms, it is possible to deduce the presence of an  $F_1$  antiform, which will be called the Parnell Antiform. The Antiform occurs in an area of layer-parallel  $S_1$  schistosity and so is expected to be isoclinal. No obvious closure of mappable marker units marks its hinge position but there is a symmetric repetition of Potosi Gneiss units on either side of the proposed hinge consistent with the fold. The hinge trace of the Parnell Antiform is correlated with the zone of changeable  $F_2$  structural facing which runs northeast through Parnell Mine (see above). Within the hinge area of the fold is a marked NE-trending zone of pegmatites, migmatites and leucocratic gneiss. A limited number of younging directions observed on the western limb of the Parnell Antiform indicate that it is synclinal in nature, i.e., that it contains younger rocks in its core.

In the southern and southeastern parts of the Willyama, the regional  $F_1$  folds present are presumed to be the same folds as the major  $F_1$  folds described above. The axial planes of these folds cannot be specifically located and their trace will have a complex shape due to refolding by the tight regional  $F_2$  folds of this domain. Within this region, however, there is good evidence for a marked change in the pre- $F_2$  attitude of the  $F_1$  folds between upright folds of the Darling Range and recumbent folds of the areas to the northeast and southwest of the Darling Range.

It is expected that further clarification of the distribution of  $F_1$  folds, including confirmation of the folds proposed above, will follow results of detailed lithological mapping currently being undertaken by the New South Wales State Geological Survey.

### *The second-generation Folds*

The major regional folds of the second generation are shown in Fig. 10. These folds are the characteristic structures of the southern part of the region. Most of them were recognised by earlier workers on the basis of repetition or closures of marker units (see Andrews, 1922; Gustafson et al., 1950; King and Thomson, 1953). The present survey has re-established and defined the



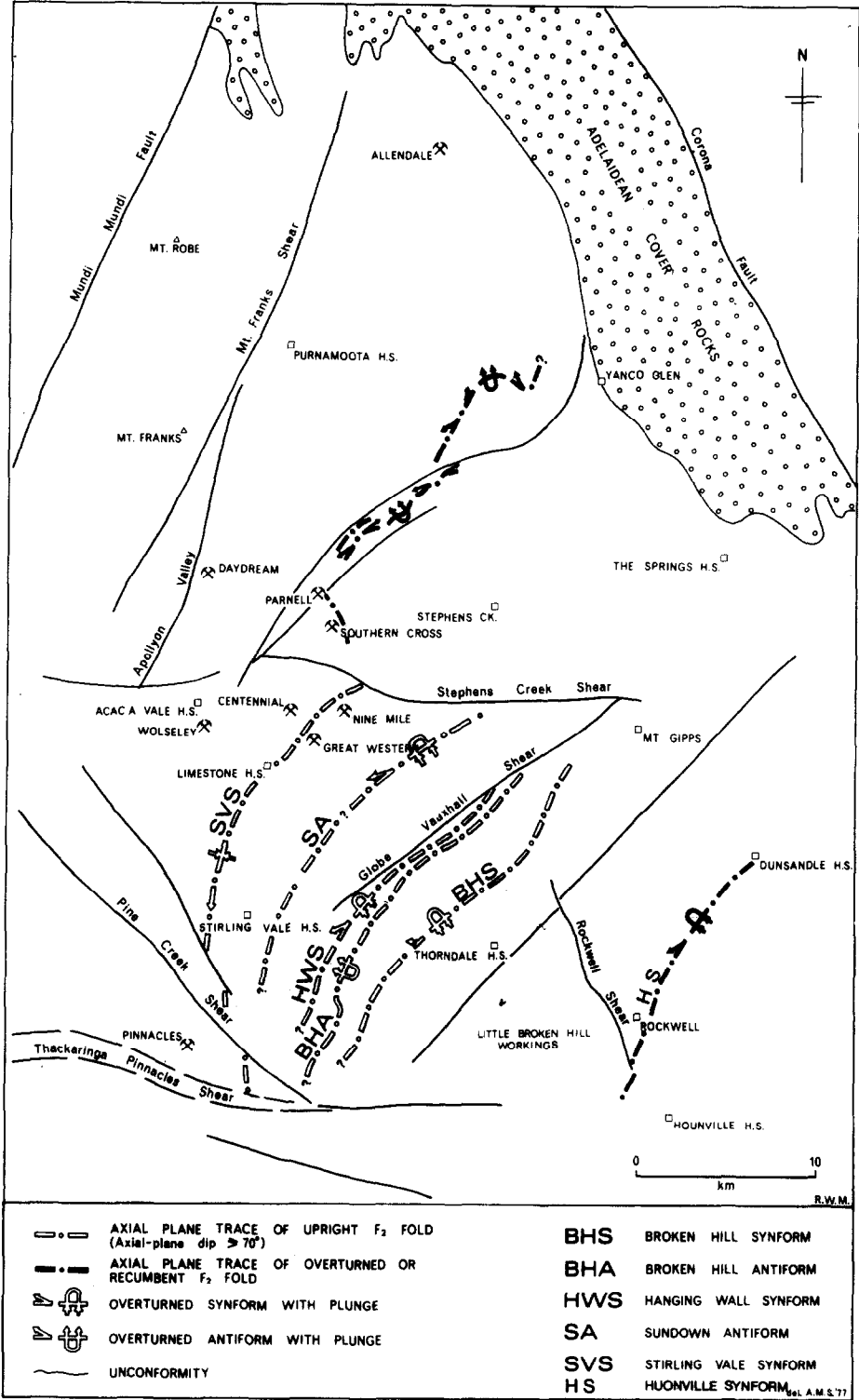


Fig. 10. Synthesis of F<sub>2</sub> structures in the Broken Hill sub-domain (retrograde schist zones and the Adelaidean unconformity shown for reference only).

extent of these folds as  $F_2$  structures. In addition, by mapping small-scale structures such as  $F_2$ -fold vergence and layering/ $S_2$  relationships, the authors have defined the previously unrecognised antiform (the Sundown Antiform) between the Stirling Vale and Hanging Wall Synforms. On the basis of mesoscopic structure it can also be shown that the Little Broken Hill area lies on the northwestern limb of a further major  $F_2$  folds, whose hinge must lie in unexposed ground to the southeast of Little Broken Hill. This synform has been tentatively called the Huonville Synform.

The Rupee Antiform (first recognised by Andrews, 1922) is established on the basis of a repetition of marker units (principally granite gneiss) about its axial trace, and a probable southern closure of amphibolite about its hinge, south of Thorndale Homestead. The age of the fold is less clear. Only layer-parallel, high-grade schistosity was identified in the vicinity of the fold and it could be either  $F_1$  or  $F_2$  in age. Graded beds from drill core show that the fold is downward-facing and it appears to match in style the isoclinal  $F_2$  Broken Hill Antiform on the opposite flank of the intervening Broken Hill Synform. For these reasons, the Rupee Antiform is provisionally ascribed to the  $F_2$  generation.

North of Stephens Creek Shear, the correlatives of the  $F_2$  folding of the Broken Hill Mines area consist of broad open folds of the steeply-dipping  $S_0$  and  $S_1$  surfaces about horizontal or sub-horizontal axes. These folds produce no closures of rock units or repetition of beds but cause the formation of extensive domains of NE- or NW-dipping  $S_0$  and  $S_1$  (Fig. 8). The presence of these domains leads to extreme variability in the plunge directions of the superimposed  $F_3$  folds.

A number of macroscopic  $F_2$  folds are present in the Darling Range area. These folds are upright and have vertical or near-vertical axes. They appear to have resulted from the action of a shear couple upon vertical NE-trending  $S_0$  and  $S_1$  surfaces. This couple was re-established during the  $F_3$  event leading to the establishment of linear zones of intense retrograde schistosity and more open dextral  $F_3$  folds. The retrograde shear zones disrupt the earlier  $F_2$  folds so that no continuous axial-plane traces can be drawn, and no vergence for the  $F_2$  folds can be defined.

### *The third-generation folds and the retrograde schist zones*

The third-generation ( $F_3$ ) produced folds at all scales throughout the Willyama Complex. These folds have a variety of attitudes consequent upon their position superimposed upon preexisting  $F_2$  folds, and upon a variation in the strike of  $S_3$  from north to northeast. A regional monocline northeast of Broken Hill (Fig. 7) is an  $F_3$  fold, and its flat limb corresponds to the Broken Hill Arch of Andrews (1922). The Western "Anticline"—Eastern "Syncline" fold pair of the Broken Hill Mines area is an  $F_3$  parasitic fold lying on the steep southeastern limb of this monocline (see Laing et al., 1978).

In the northern part of the area,  $S_3$  has a generally northerly trend and over large areas shows a dextral relationship to the NE-trending  $S_0$  and  $S_1$  surfaces. An example of this relationship is the large  $F_3$  fold pair west of Yanco Glen (Fig. 5). In the low-grade rocks northwest of the Apollyon Valley zone, large regional  $F_3$  folds, such as the Mt. Robe Synform, are present.

A notable feature of the Willyama Block is the presence of a network of retrograde schist zones. These zones have three dominant trends: NNE to NE (Darling Range, Globe Vauxhall, Apollyon Valley, Mt. Franks, Mundi Mundi); NNW (Rockwell, Pine Creek, De Bavay, British); and W (Stephens Creek, Thackaringa-Pinnacles). The relationship of the E–W Stephens Creek Shear to  $F_2$  folding indicates that it is at least as old as that event. However, the deflection of  $S_3$  trends across the shear (Fig. 11) shows that it was re-activated after  $F_3$  as a dextral shear zone. The NNW Shear Zone trends lie at a high angle to the dominant trends of  $S_0$  and  $S_1$  and a consistent sinistral horizontal component of movement can be demonstrated across them.

The shear zones are characterised by a retrograde schistosity whose strike is parallel to the zone boundaries. In the case of the NE-trending set, this schistosity is generally parallel to that of  $S_3$  in the surrounding rocks and the two retrograde surfaces are in places indistinguishable. Where  $S_3$  has a northerly trend, as it does in the central part of the region from Nine Mile to Allendale Mines, it shows a marked swing in strike into parallelism with the retrograde zones as the zones are approached. In addition, retrograde zones often form the boundaries of domains of  $F_3$  folding, with individual folds being restricted to blocks bounded by the zones. For example, the Southern Cross  $F_3$  fold (Fig. 11) is bounded to north and south by retrograde schist zones and cannot be traced beyond these zones. The large  $F_3$  folds west of Yanco Glen Hotel provide similar examples. In the Mines area, the  $F_3$  Eastern "Syncline"—Western "Anticline" cannot be traced across the British shear zone. It thus appears probable that the retrograde zones were active during early  $F_3$  deformation as planar zones of high shear strain.

Other relationships between retrograde schist zones and  $F_3$  folding can be observed in and adjacent to the Broken Hill Mines area. Between Broken Hill and Sundown, linear zones of intense retrograde schistosity are parallel to  $S_3$  in adjacent rocks and tend to occur in the antiformal position separating open  $F_3$  synforms. In the Mines area, sub-surface information from the Globe-Vauxhall shear shows that, although the shear zone boundaries cross-cut and dip more shallowly than  $S_3$ , the retrograde schistosity within the zone varies from parallel to  $S_3$  to parallel to the boundaries. An apparent systematic change in orientation of schistosity across the zone can be explained in terms of the incremental strain model of Ramsay and Graham (1970), see Laing (1977).

A marked difference between  $S_3$  and the schistosity of adjacent retrograde zones in the Broken Hill Region is that whereas the latter contains steeply-plunging intrafolial folds parallel to a steep lineation (Hobbs, 1966), the former contains no obvious mineral lineation and is axial plane to generally



shallow plunging  $F_3$  folds. This can be explained by a model involving similarly oriented strain axes for both  $S_3$  and the schistosity of the zones, but with a more intense strain in the schist zones having caused a rotation of  $F_3$  fold axes into parallelism with a steeply plunging principal extension direction, represented by the mineral lineation (cf., Sanderson, 1973; Bell, 1978).

We would thus suggest that the retrograde schist zones were initiated at an early stage of the  $F_3$  deformation, although the E-W-set in part pre-dates  $F_3$ . We recognise, however, that many of the features described above could have resulted from a later independent retrograde deformation superimposed upon, but controlled by,  $F_3$  structures. However, the fact that  $F_3$  folds are commonly not displaced by retrograde schist zones, but appear to have developed independently within blocks bounded by these zones, strongly favours the former interpretation.

#### AGE OF THE DEFORMATIONS

In the Broken Hill region, potassium-argon data from whole-rock and mica analyses (Richards and Pidgeon, 1963) indicate that the total rock system became closed at ca 500 Ma. This date can be reasonably correlated with the cessation of ductile movement on the retrograde schist zones, coinciding with the end of the Delamerian orogeny. A younger age limit to  $F_3$ , and in particular the relationship between  $F_3$  folding and folding of the Adelaidean cover rocks, is not immediately clear. Talbot (1967b), working in the Olary Province, concluded that folds in the Adelaidean cover rocks post-dated the youngest macroscopic folds of layering (our  $F_3$  folds) in the Broken Hill region. Amphibolite dykes which cut across these folds were emplaced prior to Adelaidean deposition (Talbot, 1967b).

In the Broken Hill sub-domain, a marked unconformity surface between the Willyama rocks and the Adelaidean rocks is not grossly deformed despite the presence of regional  $F_3$  folds in the former. Andrews (1922) suggested that the cover folding post-dated the main deformation in the Willyama Complex and corresponded to renewed movement in retrograde schist zones (his "crush zones"). Binns (1963) also related cover folding to strong movement on the retrograde schist zones. These conclusions have been supported by the more detailed work of Laing (1969). The evidence therefore indicates that  $F_3$  folding in the Willyama Complex was not related to folding of the Adelaidean cover rocks, but points to a long deformation history in the retrograde schist zones extending through to post-Adelaidean times.

Strong faulting was also particularly important in controlling Sturtian deposition within the cover rocks. Sturtian deposits in the Torrowangee Series show very great thickness changes across faults which appear to follow the trend of retrograde schist zones in the Willyama Complex (Laing, 1969; Thomson, 1969). It follows therefore that some zones were already established at this time. The zones, and locally the  $S_3$  schistosity, were also clearly reactivated and modified during the Delamerian Orogeny. Cleavage in the

Adelaidean rocks is commonly parallel to retrograde schistosity in their underlying basement, and examination of ERTS 1 photographs shows that extensions of some retrograde schist zones can be traced through Adelaidean rocks (cf., Scheibner, 1973). This type of evidence has led some workers to infer that  $F_3$  and the schist zones were themselves initiated during the Delamerian Orogeny, although Andrews (1922) and Talbot (1967a) recognised their pre- and post-Adelaidean history.

The deformation history of the retrograde schist zones is therefore divided between two major orogenic episodes: the Willyama Orogeny terminating ca 1500 Ma (see below), and the Delamerian Orogeny culminating ca 500 Ma ago.

It is difficult to separate the ages of the  $F_1$  and  $F_2$  deformations. Structures associated with these two events show major similarities of style and orientation. These are:

- (a) axial planes of both fold sets trend northeast.
- (b)  $F_2$  folds plunge generally to the southwest, parallel to the inferred principal extension direction (the  $L_1$  lineation) of the first deformation. If  $F_1$  folds plunge parallel to  $L_1$ , then the two fold sets will be coaxial.
- (c) Both the  $S_1$  and  $L_1$  structures, although initiated during  $F_1$ , have over wide areas been preserved and probably enhanced during second deformation.
- (d) Both deformations show maximum intensity in the southeast of the Willyama Province, with a decrease in intensity towards the west and northwest.
- (e) Both deformations were accompanied by high temperatures leading to the growth of high-grade metamorphic minerals.

From these similarities it appears probable that  $F_1$  and  $F_2$  represent pulses of a single orogenic event, and were not separated from each other by a long time interval. The orientation of the principal stress axes remained approximately the same for both events, with only the intensity and perhaps the duration of the deformation varying between the two episodes. It is therefore probable that the dating of high-grade assemblages at  $1695 \pm 21$  Ma (Pidgeon, 1967) in the Willyama Province reflects an age of metamorphism associated with one, or both, of these deformations. We know only that the age of  $F_1$  is not younger and  $F_2$  is not older than these isotopic dates. This is consistent with Shaw's (1968) suggestion that the ca 1700 Ma metamorphism took place over a protracted period or else that it was followed by a milder metamorphism prior to ca 1540 Ma, the date which he gave for the intrusion of the Mundi Mundi granite suite.

## CONCLUSIONS

The Willyama Block shows evidence of three major metamorphic and deformational events. Of these, the first was by far the most intense, producing regional isoclinal fold-nappes and the dominant high-grade metamorphic fabric of the rocks. Later events modified these first recognisable tectonic struc-

tures, but the folding and penetrative fabrics associated with the subsequent deformations are of lesser intensity, and their effects less ubiquitous, when compared to the first structures. The fundamental tectonic framework of the Willyama is thus the result of the  $F_1$  event. Due to the overlay of latter tectonisms, the detail of this earliest event is the most obscure; so, before attempting a regional synthesis, it will be useful to summarise the structures produced by this event.

When the effects of later deformations are removed, it is possible to divide the Broken Hill region into number of domains based on the style, orientation and associated metamorphic fabrics of the  $F_1$  event (Fig. 9). These domain are:

(1) *Mt. Franks—Mt. Robe area*.  $F_1$  folds are upright and isoclinal. Folding was accompanied by a prograde metamorphism, with the andalusite-sillimanite isograd located within the area and parallel to major lithological contacts. Folding was preceded by a static metamorphism resulting in andalusite growth. The regional Kantappa-Lakes Nob Syncline is upward facing on  $S_1$ .

(2) *The Allendale—Stephens Creek area*. This area is dominated by three, extensive, upright isoclinal folds, with probable shallow plunges to the south-west. The age of these folds is problematical but they are probably of  $F_1$  age and appear to be downward-facing on  $S_1$ . Syntectonic metamorphism led to the oriented growth of sillimanite, amphibole and biotite and produced strong axial schistosity and lineation. In a small area north of Yanco Glen, low-grade andalusite schist is developed in the approximate hinge position of the regional Parnell Antiform. The southern boundary of the domain is marked approximately by the line of the Stephens Creek Shear.

(3) *The Broken Hill and Little Broken Hill areas*. These areas lie between the Thackaringa-Pinnacles and Stephens Creek retrograde schist zones. The Broken Hill area is separated from the Little Broken Hill area by the NE-trending Darling Range, which forms a separate  $F_1$  domain. The areas are characterised by recumbent or near-recumbent isoclinal  $F_1$  fold-nappes. These folds were accompanied by syntectonic growth of high-grade minerals such as sillimanite or amphibole. There is an increase in metamorphic grade from the northwest of the area to the southeast, evidenced by the incoming of pyroxene in place of amphibole in the mafic lithologies (Binns, 1964; Phillips, 1977).

(4) *The Darling Range area*. The Darling Range, south of Mt. Gipps Hotel (the Darling Range north of the hotel has not been mapped by the authors), is characterised by an upright  $S_1$  schistosity. In this linear NE-trending zone, layering is over large areas transposed parallel to  $S_1$  or is obliterated. Syntectonic metamorphism reached granulite facies (Binns, 1964) and led to partial melting and the production of extensive migmatites. The area remained a zone of intense deformation through the succeeding  $F_2$  and  $F_3$  events.

With the above pattern of  $F_1$  folds in mind, a tectonic model can be envisaged for the  $F_1$  deformation. This model is presented in the serial sec-



tions of Fig. 12 and described below. It must be emphasised, however, that although the production of recumbent fold-nappes of regional extent during  $F_1$  can be demonstrated, the location of the roots and noses of these nappes is not so clearly established, and in these respects the model must be regarded as speculative. The authors have avoided the easy solution of placing the roots and noses of the  $F_1$  nappes beyond the limits of the outcropping Willyama domain, but instead have sought them in those areas that they have themselves mapped and studied.

During the  $F_1$  event the entire area underwent intense lateral compression coupled with a regional rise in geothermal gradient. Sediments, and presumably underlying basement, were folded into upright folds, trending approximately NE, with the greatest intensity of deformation and metamorphism being concentrated in a relative narrow, linear belt. At depth, within the core of this belt, isoclinal folds and high-metamorphic-grade mineral growth, oriented in directions parallel to the axial planes of these folds, were produced. With increasing distance from the centre of metamorphism, more open folds and lower-grade metamorphism were formed. In addition, with distance from the metamorphic centre, there is some evidence that the rise in geothermal gradient preceded deformation and a pre- $F_1$  static metamorphism can be identified. The centre of the metamorphic belt is preserved today in the Darling Range. The more distal  $F_1$  deformation is preserved in the West of the region in the Mt. Franks—Mt. Robe area.

As the deformation continued, coarse metamorphic fabrics were produced in the central zone, largely obscuring original sedimentary bedding. Segregation of quartzofeldspathic material and the production of felsic mobilizates took place. The principal extension direction of the deformation was vertical and ductile flow of material pushed the anticlinal crests to a high structural level, where they collapsed under gravity to form recumbent nappes disposed to the northeast and southwest of the central belt. The distal end of the northeastern nappes became overturned and are preserved today as the upright,  $F_1$ , Allendale, Parnell and Yanco Glen folds. The recumbent part of the nappes forms the  $F_1$  "flat belt" of the Broken Hill and Little Broken Hill regions.

The model described above of a root zone of intense deformation and metamorphism from which recumbent flanking fold-nappes were derived satisfactorily explains all the features of the  $F_1$  event. The pattern of deformation is a common one and has geometric analogies with the demonstrated tectonic pattern of other orogenic belts—for example, the Lower Pennine Nappe area of the Alps (Rutten, 1969); the Tay Nappe of the Southwest Highlands of Scotland (Roberts, 1974); the Carolina Slate—Charlotte belts of the Southern Appalachians (Tobisch and Glover, 1971), or the Razorback Nappe—Redbank zone of Central Australia (Marjoribanks, 1976).

It is considered that the dominant NE-trend of the Willyama Block is at least as old as the  $F_1$  event, and has controlled the orientation of later deformations. There is no evidence as to the shape of the original, depositional

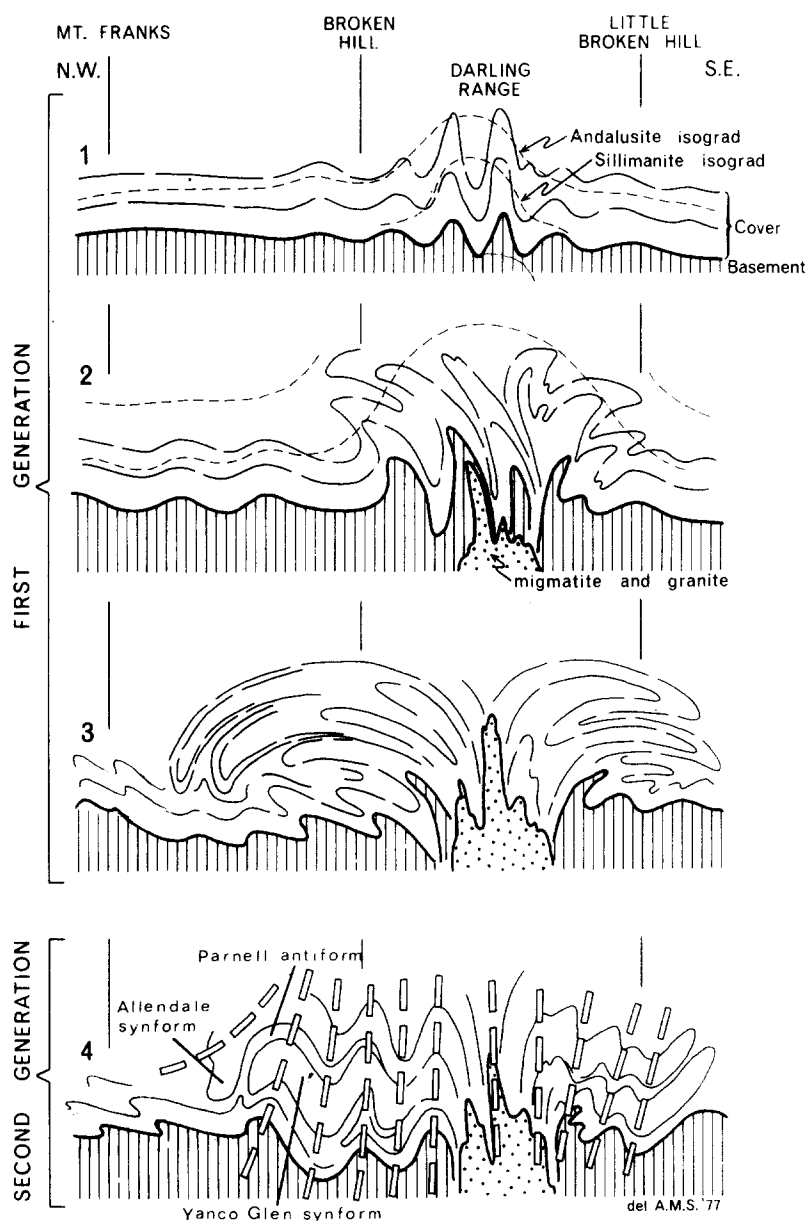


Fig. 12. Schematic sections illustrating the development of first- and second-generation structures in the Broken Hill sub-domain.

area of the sediments of the Willyama. However, correlations of these sediments of the same age in the Olary and Gawler Provinces (Glen et al., 1977) suggest that they were formed on an extensive shallow shelf with the more distal facies to the east. The  $F_1$  event can be correlated across all these prov-

inces (Glen et al., 1977) and produced structures of similar style. Deformation was, however, greatest in the eastern part of the Broken Hill region, and it is here that recumbent nappes were produced.

It is possible that the pattern of  $F_1$  deformation is related to subduction along a NE-trending plate margin situated to the southeast of the Willyama Block. The position of the Willyama Block close to the eastern edge of the Australian Proterozoic Craton (Rutland, 1976) makes this suggestion attractive, but the poor outcrop and extensive post-Proterozoic cover immediately east of the outcropping Willyama rocks make it highly speculative and outside the scope of the present paper.

### *Tectonic setting of the Broken Hill orebody*

An important result of this study is the recognition that the Broken Hill Mines area does not occupy a unique structural or tectonic position within the region. The orebody lies on the inverted limb of an  $F_1$  fold nappe of regional extent. It is remote from the hinge of the nappe and during nappe formation was bodily transported, along with its enclosing rocks, for some distance, at least of the order of several kilometres, from its original point of deposition.

$F_2$  folds in the Mines area are typical in style and orientation to  $F_2$  folds developed throughout the southern part of the region. Although the orebody lies adjacent to the axis of a tight  $F_2$  antiform, and has been remobilised into the axis of an  $F_2$  parasitic fold in North Mine (Laing et al., 1978), all of the orebody lies on one limb of the major antiform and has not been remobilised into the hinge position. Tight  $F_2$  antiforms are not unique to the Mines area but are matched by the adjacent Rupee and Sundown antiforms.

The obvious fold of the Broken Hill orebody, exhaustively described in the literature (see, for example, King and O'Driscoll, 1953) constitute a parasitic  $F_3$  fold pair developed on the steep limb of a much larger regional  $F_3$  monocline.

Because of its closeness to the orebody, the Globe—Vauxhall retrograde schist zone has had undue prominence in recent published interpretations of regional structure of the area. Katz (1976a) regarded it as a transform fault; Stanton (1976) as a graben-bounding fault contemporaneous with sedimentation; and O'Driscoll (1968) and Katz (1976b) as an expression of a fundamental crustal lineament or mega-shear. Considered regionally, however, the Globe—Vauxhall shear appears as a rather insignificant member of a set of NE-trending retrograde schist zones which were developed during the third deformational event and were superimposed upon, and hence later than, the regional  $F_2$  folds. The Globe—Vauxhall shear does not have a large throw (see Laing et al., 1978) for a full discussion) and rocks of similar lithology and metamorphic grade are present on both sides of the shear zone. Thus, although the Broken Hill orebody shows considerable localised structural control, the primary control on its position is probably syngenetic and cannot be easily related to the tectonic framework of the Broken Hill region.

## ACKNOWLEDGEMENTS

The project was set up with the co-operation of, and wholly financed by, the Mine Managers Association of Broken Hill. We wish to acknowledge the help we have gained from many discussions with and the wholehearted co-operation of the personnel of the Mines, particularly D. Klingner, G. Scott and T. McConaghie of C. R. A. Exploration Pty. Ltd., and W. Widdop, R. Burkett, D. Archibald and W. Leyh of North Broken Hill Ltd.

Numerous students, completing Honours degrees at the University of Adelaide, greatly contributed to the early part of the survey. In addition, we have benefited from many discussions with officers of the Geological Survey of New South Wales.

## REFERENCES

- Anderson, D.E., 1966. Structural and Metamorphic Studies in the Mt. Robe Area, Broken Hill, N.S.W. Ph.D. thesis, Univ. Sydney. (unpubl.)
- Andrews, E.C., 1922. The geology of the Broken Hill District. Mem. Geol. Surv. N.S.W., 8.
- Bell, T.H., 1978. Progressive deformation and reorientation of fold axes in a ductile mylonite zone: the Woodroffe Thrust. *Tectonophysics*, 44: 285–320.
- Binns, R.A., 1963. Some observations on metamorphism at Broken Hill, N.S.W. *Proc. Aust. Inst. Min. Metall.*, 207: 239–261.
- Binns, R.A., 1964. Zones of progressive regional metamorphism in the Willyama Complex, Broken Hill District, N.S.W. *J. Geol. Soc. Aust.*, 11: 283–330.
- Borradaile, G.J., 1976. "Structural facing" (Shackleton's rule) and the Palaeozoic rocks of the Malaguide Complex, near Velez Rubio, S.E. Spain. *Proc. K. Ned. Akad. Wet. Ser. B*, 79: 330–336.
- Both, R.A. and Rutland, R.W.R., 1976. The problem of identifying and interpreting stratiform orebodies in high metamorphosed terrains: the Broken Hill example. In: K.H. Wolf (Editor), *Handbook of Strata-Bound and Stratiform Ore Deposits*, 4, Elsevier, Amsterdam, pp. 261–325.
- Carruthers, D.S., 1965. An environmental view of Broken Hill ore occurrences. 8th Commonwealth Min. Metall. Congr., 1: 339–351.
- Glen, R.A., 1978a. Structural and Metamorphic Relations Between Low, Medium- and High-Grade Rocks in the Mt. Franks-Mundi Mundi Area, Broken Hill, N.S.W. Ph. D. thesis, Univ. Adelaide. (unpubl.)
- Glen, R.A., 1978b. Large-scale early folding and tectonic levels in the northwestern part of the Willyama Complex, New South Wales. *Notes Geol. Surv. N.S.W.*, 31: 4–15.
- Glen, R.A. and Laing, W.P., 1975. The significance of sedimentary structures in the Willyama Complex, N.S.W. *Proc. Australas. Inst. Min. Metall.*, 256: 15–20.
- Glen, R.A., Laing, W.P., Parker, A.J. and Rutland, R.W.R., 1977. Tectonic relationships between the Proterozoic Gawler and Willyama orogenic domains, Australia. *J. Geol. Soc. Aust.*, 24: 125–150.
- Gustafson, J.K., Burrell, H.C. and Garretty, M.C., 1950. Geology of the Broken Hill ore deposit, Broken Hill, N.S.W., Australia. *Bull. Geol. Soc. Am.*, 61: 1369–1438.
- Hobbs, B.E., 1966. The structural environment of the northern part of the Broken Hill orebody. *J. Geol. Soc. Aust.*, 13: 315–338.
- Hobbs, B.E., Ransom, D.M., Vernon, R.H. and Williams, P.F., 1968. The Broken Hill orebody, Australia: a review of recent work. *Miner Deposita*, 3: 293–316.

- Hobbs, B.E., Means, W.D. and Williams, P.F., 1976. *Outline of Structural Geology*. Wiley, New York, N.Y.,
- Hodgson, C.J., 1974. The geology and geological development of the Broken Hill Lode in the New Broken Hill Consolidated Mine, Australia: structural geology. *J. Geol. Soc. Aust.*, 21: 413–430.
- Katz, M.B., 1976a. Broken Hill — a Precambrian hot spot? *Precambrian Res.*, 3: 91–106.
- Katz, M.B., 1976b. Lineament tectonics of the Willyama Block and its relationship to the Adelaide aulacogene. *J. Geol. Soc. Aust.*, 23: 275–285.
- King, H.F. and O'Driscoll, E.S., 1953. The Broken Hill lode. In: A.B. Edwards, (Editor), *Geology of Australian Ore Deposits*. Aust. Inst. Min. Metall., pp. 533–577.
- King, H.F. and Thomson, B.P., 1953. The geology of the Broken Hill District. In: A.B. Edwards, (Editor), *Geology of Australian Ore Deposits*. Aust. Inst. Min. Metall., pp. 578–600.
- Laing, W.P., 1969. The Geology of the Brewery Well Area, Northern Barrier Ranges, Western N.S.W. B. Sc. (Hons.) thesis, Univ. Sydney. (unpubl.)
- Laing, W.P., 1977. Structural Geology in a Critical Area Adjacent to the Broken Hill Orebody. Ph. D. thesis, Univ. Adelaide. (unpubl.)
- Laing, W.P., Marjoribanks R.W. and Rutland, R.W.R., 1978. Structure of the Broken Hill mine area and its significance for the genesis of the ore bodies. *Econ. Geol.*, 73: 1112–1136.
- Lewis, B.R., Forwood, P.S. and Roberts, J.B., 1965. Geology of the Broken Hill Lode, reinterpreted. 8th Commonw. Min. Metall. Congr., 1: 319–332.
- Maiden, K.J., 1972. Studies on the Effects of High-Grade Metamorphism on the Broken Hill Orebody. Ph. D. thesis, Univ. N.S.W. (unpubl.)
- Marjoribanks, R.W., 1976. Basement and cover relations on the northern margin of the Amadeus Basin, central Australia. *Tectonophysics*, 33: 15–32.
- Mawson, D., 1912. Geological investigations in the Broken Hill area. *Mem. R. Soc. S. Aust.*, 2: 211–319.
- O'Driscoll, E.S., 1964. Cross-fold deformation by simple shear. *Econ. Geol.*, 59: 1061–1093.
- O'Driscoll, E.S., 1968. Notes on the structure of the Broken Hill Lode and its tectonic setting. *Aust. Inst. Min. Metall. Monogr.*, 3: 87–102.
- Phillips, G.N., 1977. Broken Hill—a Precambrian hot spot?—A comment. *Precambrian Res.*, 4: 215–220.
- Pidgeon, R.T., 1967. Rb—Sr geochronological study of the Willyama Complex, Broken Hill, Australia. *J. Petrol.*, 8: 283–324.
- Ramsay, J.G. and Graham, R.H., 1970. Strain variation in shear belts. *Can. J. Earth Sci.*, 7: 786–813.
- Ransom, D.M., 1968. The relationship of orebody shape to country rock structure in the southern half of the Broken Hill lode. *J. Geol. Soc. Aust.*, 15: 57–64.
- Richards, J.R. and Pidgeon, R.T., 1963. Some age measurements on micas from Broken Hill, Australia. *J. Geol. Soc. Aust.*, 10: 243–259.
- Roberts, J.L., 1974. The structure of the Dalradian rocks in the SW Highlands of Scotland. *J. Geol. Soc.*, 130: 93–124.
- Rutland, R.W.R., 1973. A note in major structures in the Willyama Complex. *Trans. R. Soc. S. Aust.*, 97: 77–90.
- Rutland, R.W.R., 1976. Orogenic evolution of Australia. *Earth Sci. Rev.*, 12: 161–196.
- Rutland, R.W.R. and Etheridge, M.A., 1975. Two high-grade schistositic at Broken Hill and their relation to major and minor structures. *J. Geol. Soc. Aust.*, 22: 259–274.
- Rutten, M.G., 1969. *The Geology of Western Europe*. Elsevier, Amsterdam, 520 pp.
- Sanderson, D.J., 1973. The development of fold “axes” oblique to the regional trend. *Tectonophysics*, 16: 55–70.
- Scheibner, E., 1973. ERTS-1 geological investigations of New South Wales. *Rep. Geol. Surv. N.S.W.*, 73/382 (unpublished).

- Shackleton, R.M., 1958. Downward facing structures of the Highland Border. *Geol. Soc. London, Q. J.*, 113: 361—392.
- Shaw, S.E., 1968. Rb—Sr isotopic studies of the mine sequence rocks at Broken Hill. *Monogr. Australas. Inst. Min. Metall.*, 3: 185—198.
- Stanton, R.L., 1976. Petrochemical studies of the ore environment at Broken Hill, New South Wales, 4. Environmental synthesis. *Proc. Inst. Min. Metall.*, pp. B221—B233.
- Talbot, J.L., 1967a. The effects of the Palaeozoic orogeny on the Precambrian shield of South Australia. *Geol. Assoc. Can. Spec. Pap.*, pp. 59—66.
- Talbot, J.L., 1967b. Subdivision and structure of the Precambrian (Willyama Complex and Adelaide System), Weekaroo, South Australia. *Trans. R. Soc. S. Aust.*, 91: 45—57.
- Tobisch, O.T. and Glover, L., 1971. Nappe formation in part of the southern Appalachian Piedmont. *Bull. Geol. Soc. Am.*, 82: 2209—2230.
- Thomson, B.P., 1954. Tectonics and Archean Sedimentation of the Barrier Ranges, N.S.W. M.Sc. thesis, Univ. Adelaide. (unpub.)
- Thomson, B.P., 1969. The Precambrian crystalline basement. In: L.W. Parkin (Editor), *Handbook of South Australian Geology*. Geol. Surv. of South Australia.
- Vernon, R.H., 1969. Archean or Lower Proterozoic rocks, the Willyama Complex, Broken Hill area. *J. Geol. Soc. Aust.* 16: 20—55.
- Williams, P.F., 1967. Structural analysis of the Little Broken Hill area, New South Wales. *J. Geol. Soc. Aust.*, 14: 317—331.



PERGAMON

Journal of Structural Geology 26 (2004) 113–126

**JOURNAL OF  
STRUCTURAL  
GEOLOGY**

[www.elsevier.com/locate/jsg](http://www.elsevier.com/locate/jsg)

# Synchronous development of Type 2 and Type 3 fold interference patterns: evidence for recumbent sheath folds in the Allendale Area, Broken Hill, NSW, Australia

C.J. Forbes\*, P.G. Betts, G.S. Lister

*Australian Crustal Research Centre, School of Geosciences, Monash University, Melbourne, Australia*

Received 12 July 2002; received in revised form 14 March 2003; accepted 28 March 2003

## Abstract

Synchronous development of Type 2 and Type 3 fold interference patterns occur in the poly-deformed Broken Hill Inlier. The interference patterns have resulted from the superposition of recumbent F2 folds and  $\sim$ N–S-oriented upright F3 folds. The synchronous development of Type 2 and Type 3 fold interference patterns is attributed to variation in the hinge of F2 folds by as much as 90°, suggesting the development of a regional-scale sheath-like fold geometry during D2. Overprinting relationships along the eastern limb of the Pap Synform suggests that it formed part of a recumbent fold hinge that was flattened during horizontal crustal shortening. This has resulted in the development of a modified Type 3 fold interference pattern. The results of this study show that the Type 2 and Type 3 fold interference patterns can develop during the same deformation event in an evolving orogen.

© 2003 Elsevier Ltd. All rights reserved.

**Keywords:** Fold interference patterns; Sheath fold; Broken Hill; Australia; Proterozoic; Orogen

## 1. Introduction

The outcome of numerous studies of natural examples of fold interference patterns (e.g. Flin Flon, Manitoba, Canada; Stauffer and Mukherjee, 1971; Stauffer, 1988; Cantabrian Mountains, NW Spain; Julivert and Marcos, 1973), and numerical (e.g. Ghosh, 1970) and analogue (e.g. Watkinson, 1981; Ghosh et al., 1992, 1995; Grujic, 1993) models of fold superposition and the resultant geometries has been the recognition of four principle types of fold interference patterns. Ramsay (1962) and Ramsay and Huber (1987) classified the resultant geometries as Type 0 through to Type 3 interference patterns.

The identification of fold interference patterns in the field provides significant insight into the shortening history and kinematic controls of deformation within studied terranes. The geometry of superimposed fold generations to produce fold interference patterns is well understood (e.g. Ramsay, 1962; Thiessen and Means, 1980; Ramsay and Huber, 1987).

However, not all rocks deform in an ideal manner to produce ‘classic’ fold interference patterns, and map and outcrop patterns of fold interference patterns can easily become complex, as demonstrated by Thiessen (1986). Cross-sections through a fold interference pattern that result in the perfect representation of a Type 2 or Type 3 outcrop pattern are not always preserved. Thiessen (1986) showed that parallel cross-sections through refolded folds can produce a wide variety of patterns. Fold interference patterns that appear highly complex in outcrop can be described using simple refolding geometries, and vice versa; patterns that appear simple may be attributed to more complex refold histories. Therefore, it is important to attempt to observe the complete structure of an area and not make conclusions from observation of any one part of a structure.

The Palaeoproterozoic Broken Hill Block, central western New South Wales, Australia (Fig. 1) has undergone a complex deformation history during the Olarian Orogeny (1.60–1.58 Ga; Page et al., 2000) and Delamerian Orogeny (c. 520–490 Ma; Harrison and McDougall, 1981). This has resulted in the development of various tectonic models for the evolution of this area. There has been an emphasis on

\* Corresponding author. Tel.: +61-3-9905-1127; fax: +61-3-9905-5062.  
E-mail address: caroline@mail.eearth.monash.edu.au (C.J. Forbes).



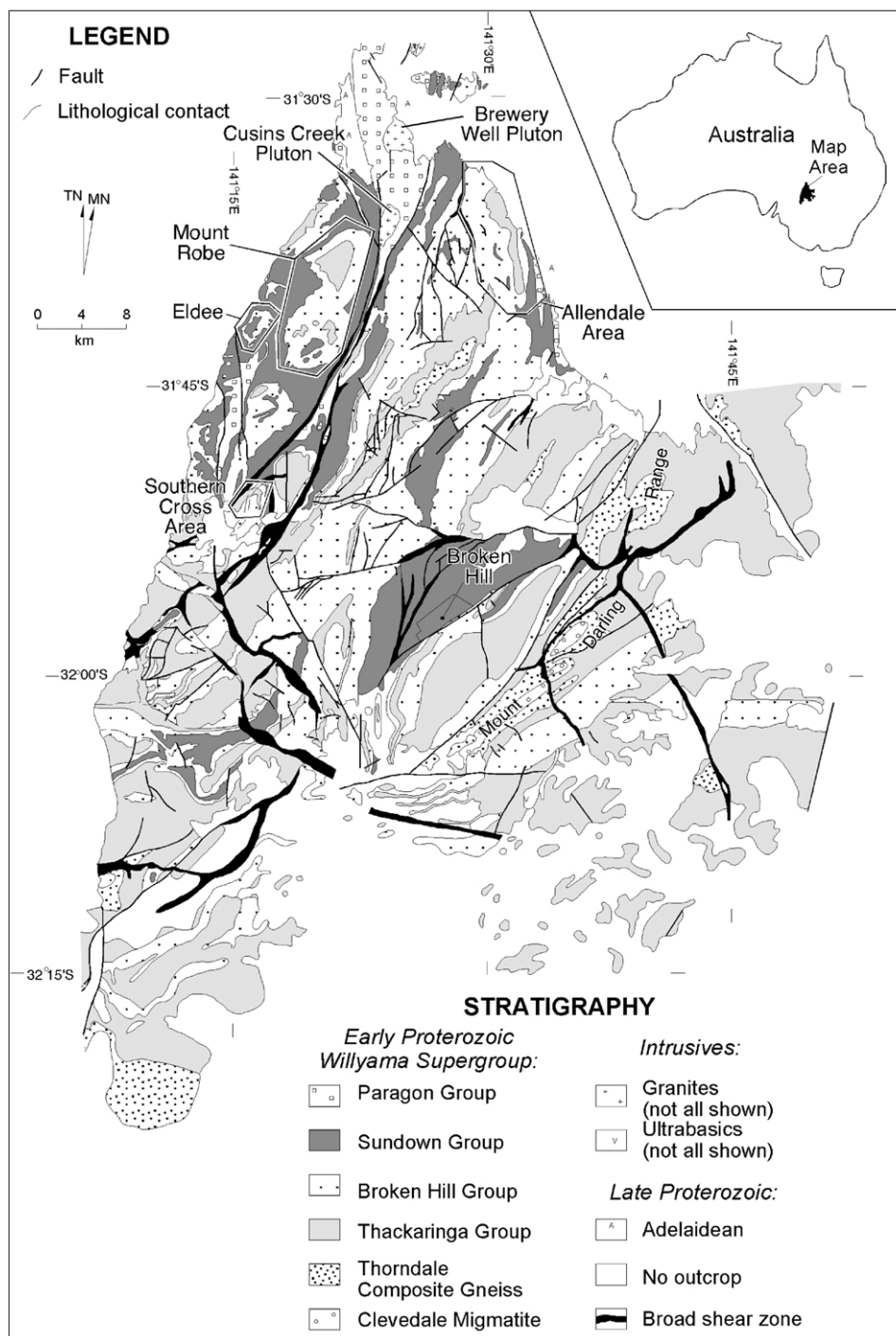


Fig. 1. Geological map of the Broken Hill Inlier showing the locality of the Allendale Area. The Eldee, Mount Robe and Southern Cross Areas are also shown (modified from Willis et al., 1983).

reconstructing stratigraphy and unfolding folds, but there have been few attempts to understand the relative timing of fabric forming events and their geometrical consequences.

Structural mapping conducted in the Allendale Area, located in the northern Broken Hill Block (Fig. 1), has revealed unusual fold interference patterns resultant from the superposition of upright, ~N–S-trending F3 folds over recumbent F2 folds. This deformation has

resulted in the synchronous development of Type 2 mushroom–crescent and modified Type 3 convergent–divergent fold interference patterns regionally throughout the area. Overprinting relationships suggest a hidden hinge zone within the eastern limb of the fourth generation Paps Synform (Fig. 2). The resultant geometry is a modified Type 3 fold interference pattern where the hinge of the earlier fold generation (D2) has

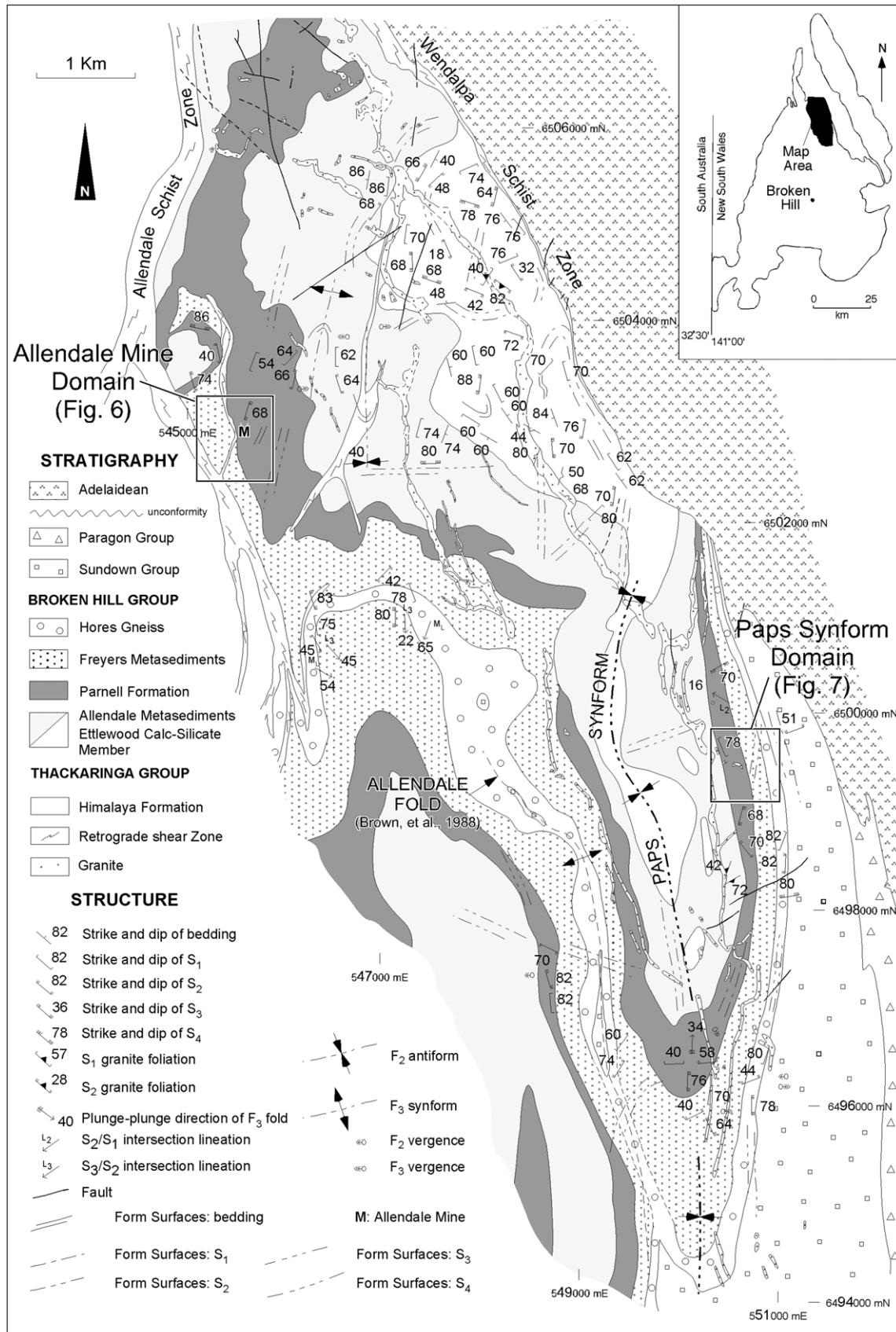


Fig. 2. Geological map of the Allendale Area showing the location of the Allendale Mine Domain and the Paps Synform Domain.

been flattened during D3 deformation, and now forms part of a straight limb of the F3 Paps Synform.

Synchronous development of Type 2 and Type 3 fold interference patterns and the discovery of an ‘opened’ recumbent fold raises the question of how these structural geometries could have developed. In this paper, we present structural analysis conducted in the Allendale Area. We focus on the development of fabrics and fold interference patterns associated with crustal shortening during the Olarian Orogeny.

## 2. Regional geology of the Broken Hill Block

The Broken Hill Inlier, western New South Wales (Fig. 1), comprises the polydeformed Early Proterozoic Willyama Supergroup (Fig. 3), which consists of metasedimentary rocks and metavolcanic rocks deposited within an intraplate rift basin (Stevens et al., 1988) between c. 1.73–1.64 Ga (Page and Laing, 1992; Donaghy et al., 1998; Nutman and Ehlers, 1998; Page et al., 2000). The Willyama Supergroup (Stevens et al., 1988) has been divided into several major stratigraphic groups (Fig. 3) based on detailed lithological mapping. The basal units of the Willyama Supergroup (Thackaringa Group and underlying packages; Fig. 3) comprise migmatitic gneiss and quartzofeldspathic rocks intercalated with psammopelites. These rocks have been dated, using U–Pb SHRIMP analysis of zircon within tuffaceous horizons, to have been deposited at c. 1.71 Ga (Love, 1992; Donaghy et al., 1998). Conformably overlying

these rocks is the Broken Hill Group (Fig. 3), which is a package of pelitic to psammopelitic metasediments and minor calc–silicate rocks, amphibolites and basic gneisses. These rocks have dominantly sedimentary protolith, although numerous quartz–feldspar–biotite gneisses have been interpreted partially as deformed volcanic rocks (e.g. Hores Gneiss; Stevens et al., 1988; Page and Laing, 1992) that were deposited by 1.69 Ga (Page et al., 2000). These are overlain by the Sundown and Paragon Groups (Fig. 3), which is a succession of psammite, pelite, calc–silicate rocks and graphitic phyllite and schist, interpreted to have been deposited during the post-extensional evolution of the basin (Willis et al., 1983; Walters, 1996). This sequence of rocks has a maximum depositional age of ~1.64 Ga (Page et al., 2000).

The basin was subsequently inverted during the Olarian Orogeny (c. 1.60–1.59 Ga; Page et al., 2000). Basin inversion involved complex polydeformation and high temperature–low pressure metamorphism, reaching upper amphibolite to granulite facies (e.g. Hobbs et al., 1984; Stevens et al., 1988). There have been several structural and tectonic interpretations for the evolution of the Broken Hill Inlier during the Olarian Orogeny (e.g. Marjoribanks et al., 1980; Hobbs et al., 1984; Stevens et al., 1988; Gibson, 2000; Page et al., 2000). Early structural analysis was based on regional-scale interpretations of stratigraphy and folds (e.g. Marjoribanks et al., 1980; Hobbs et al., 1984). Interpretations of the structural evolution include the development of an early generation of nappes of which the Broken Hill Inlier is part of an overturned limb of a regional-scale nappe (Marjoribanks et al., 1980). This nappe was interpreted to have been overprinted by several generations of upright folds during the Olarian Orogeny and during the Delamerian Orogeny (c. 520–490 Ma; Harrison and McDougall, 1981; Webster, 1996).

White et al. (1995) interpreted the regional geometry of the Broken Hill Inlier in the context of a high-temperature (mid-crustal level) fold and thrust belt that possibly originated under prograde metamorphic conditions. In this interpretation, the Broken Hill Inlier was divided into several discrete thrust slices that were interpreted to have undergone semi-independent structural evolutions. More recently, Gibson (2000) proposed that the earliest phases of deformation and associated high temperature–low pressure metamorphism resulted from significant extension in the middle crust. This extensional event has been interpreted to have occurred either during the early extensional phases of the basin c. 1.69 Ga (Gibson, 2000) or immediately prior to the Olarian Orogeny at c. 1.60 Ga (Venn, 2001). The extensional deformation may have been focussed in high-temperature shear zones, which developed in the middle groups of the Willyama Supergroup (Noble, 2000; Hills et al., 2001). Interpretations of an early extensional deformation phase in the Broken Hill Inlier are based on the development of a penetrative, lithology parallel foliation defined by high temperature–low pressure metamorphic

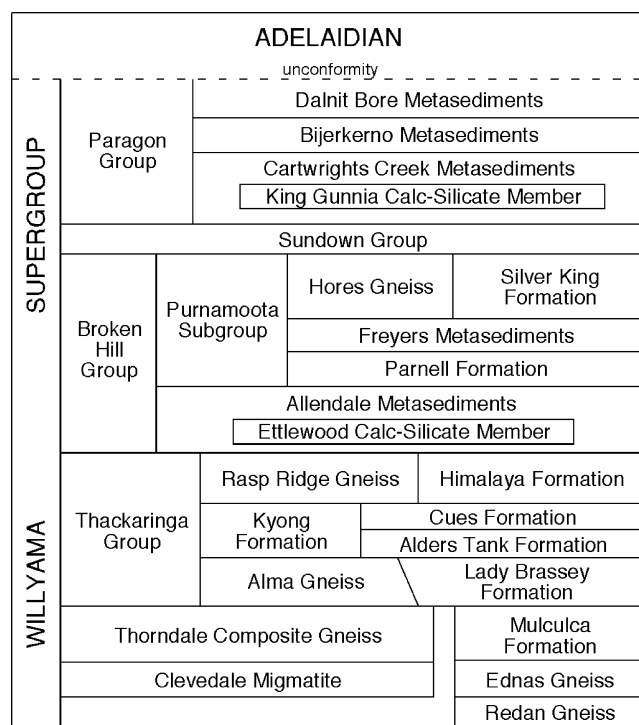


Fig. 3. Stratigraphic column of the Willyama Supergroup (Stevens et al., 1988).

assemblages and the absence of associated folding (Gibson, 2000). These shear zones have subsequently been folded during the Olarian Orogeny. Crustal shortening during the Olarian Orogeny was accompanied by high temperature–low pressure metamorphism, recumbent and upright folding and the emplacement of syn- to post-tectonic granites of the Mundi Mundi Suite (c. 1.59 Ga; Page et al., 2000) and pegmatites.

During the latest Neoproterozoic, the Broken Hill Inlier formed the basement to rift and passive margin successions of the Adelaidean cover sequences. These successions were deposited during continental break up of Australia and Laurentia (Powell et al., 1994). Basin inversion during the Delamerian Orogeny resulted in the development of a thin-skinned west-vergent fold and thrust belt (Paul et al., 2000). The influence of this orogenic event on Proterozoic basement is conjectural (e.g. Stevens, 1986; Webster, 1996).

### 3. Deformation history of the Allendale Region

Three fabric forming events have been identified within the Allendale Area. The first two fabrics are associated with upper amphibolite high-temperature–low pressure metamorphic conditions. The third fabric developed during lower-temperature metamorphism. The structural geometry of the area is dominated by fold interference of recumbent F2 folds superimposed by later ~N–S-trending upright F3

folds. Throughout the entire region, meso- and macroscopic scale outcropping Type 2 and Type 3 fold interference patterns suggest F2 folds were originally recumbent with variably oriented hinges.

#### 3.1. First generation structures

The first generation fabric within the Allendale Area is a lithology parallel, penetrative but differentiated gneissic foliation that is particularly well developed within pelitic horizons. Within these pelitic units the S1 fabric is defined by muscovite (after sillimanite?) + biotite + sericite + quartz + feldspar (Fig. 4a and b). In the psammitic layers S1 is defined by elongation of quartz and feldspar aggregates and the alignment of minor muscovite and biotite laths. The mineral assemblage defining S1 suggests that it developed during amphibolite facies, high-temperature/low-pressure metamorphic conditions (e.g. Hobbs et al., 1984). The orientation of S1 is highly variable due to later refolding. A mineral lineation defined by muscovite, biotite, sericite (after sillimanite?) and occasional andalusite occurs in the plane of S1 (and compositional layering). Retrogression of these minerals to white mica is common. Mineral lineations are shallowly to steeply north- or south-plunging (Fig. 5a). This trend most likely reflects the dominance of north–south upright folding during later deformation. No folds have been recognised on the macro- or meso-scale.

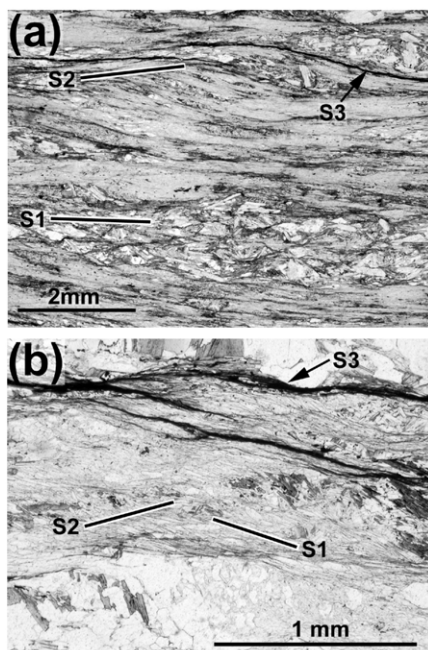


Fig. 4. Photomicrographs of rocks from the Allendale Area. (a) S1 within a pelitic unit showing quartz rich and mica rich domains. S2 is at a low angle to S1, is defined by biotite and crenulates the earlier fabric; (b) S1 is at a low angle to S3 and is difficult to distinguish. S2 is weakly preserved and is defined by biotite. S3 is defined by stylolites.

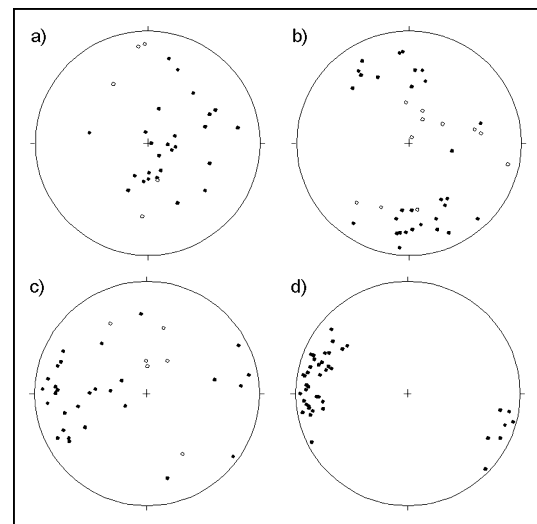


Fig. 5. Equal area stereographic projections presenting data from the Allendale Area. (a) Mineral lineations defined by muscovite, biotite, sericite (after sillimanite?) and occasional andalusite nodules. Filled circles: mineral lineations measured in the Allendale Mine Area; open circles: mineral lineations measured in the Paps Synform Domain; (b) filled circles: L2 intersections; open circles: F2 fold axes; (c) poles to S2 in the Allendale Mine Domain; filled circles: poles to S2 from F3 fold limbs; open circles: poles to S2 from F3 fold hinges; (d) poles to S3 in the Allendale Mine Domain.



### 3.2. Second generation structures

The second generation fabric is a weak to penetrative foliation that is characteristically spaced (on the millimetre scale) and is defined by muscovite and biotite in pelitic layers. In psammitic layers S2 is poorly defined, but when preserved is characterised by centimetre spaced elongation of biotite (Fig. 4a and b). This fabric is strongly differentiated and relatively weakly developed compared with S1. In hand specimen the S2 fabric is often defined by milky coloured wisps of retrogressed sillimanite.

Throughout the study area S2 is typically shallowly to moderately dipping (10–60°) and shows various relationships with compositional layering and S1. In the vicinity of the Allendale Mine (Fig. 2) S2 forms a composite foliation (Davis and Forde, 1994) with S1. On the eastern edges of the Inlier S2 is oriented at a high angle to S1 and compositional layering (Fig. 2). These relationships have been used to map larger scale F2 structures in the region. S2 is axial planar to F2 generation folds.

F2 folds are the oldest generation of folds recognised on a meso- to macroscopic scale in the study area. Their axial planes and fold axes are variably oriented due to later refolding (Fig. 2). They are characteristically tight to isoclinal and display similar fold styles. In the hinges of F3 upright folds, F2 folds are recumbent, and on the limbs of later fold generations they are typically shallowly to moderately inclined.

The intersection between S1 and S2, L2, is characterised by a millimetre spaced lineation defined by biotite and muscovite (after sillimanite?). The plunge of L2 is variable throughout the study area (Fig. 5b).

### 3.3. Third generation structures

The third generation foliation is approximately north–south to north–northeast-trending and is steeply dipping. S3 is a centimetre spaced fabric defined by dark stylolitic seams containing residual biotite and other insoluble opaque minerals (Fig. 4b). The microlithons between the stylolites contain crenulated S2 and S1 fabrics. On the limbs of many F3 folds, S3 is slightly oblique to compositional layering and S1 (Fig. 2) and can only be distinguished by its characteristic dark seams.

S3 is axial planar to open, upright folds that plunge variably approximately north or south (Fig. 2). Fold styles are typically similar with interlimb angles varying between 70 and 110°. This fold generation is responsible for the dominant north–south structural grain throughout the study area and the Broken Hill Inlier. The moderately north-plunging Paps Synform (Fig. 2) is a regional scale example of this generation of fold.

### 3.4. Fourth generation structures

A fourth deformation event was also identified locally. This event resulted in the development of approximately

east–west-trending crenulations with steeply north or south dipping axial planes. Minor refolding and warping of earlier fold generations occurred during this event, but its overall effect on the regional structural grain is relatively minor, except for the development of local changes in F3 plunges. The timing of D4 is poorly constrained, and may have formed during post-Olarian Orogeny deformation.

### 3.5. Shear zones

Throughout the Allendale Area there are locally developed shear bands preserved within the metasediments. The locally developed shear bands are often very weak and have not fully developed into distinctive S–C fabrics. In other areas, the S–C fabrics are very well developed and associated with weak to strong mineral lineations. Two distinctive types of shear zones were observed in the Allendale Area. The earlier shear zones are higher metamorphic grade and have steeply dipping muscovite, biotite, sericite (after sillimanite?) mineral lineations. The early shear zones were predominantly observed around the Allendale Mine Area. Later retrograde shear zones (Fig. 2) are defined by phyllitic metasediments and contain abundant sericite, muscovite and chlorite. Mineral lineations in retrograde shear zones are shallowly to moderately dipping and are defined by muscovite and chlorite. These shear zones are not focussed on in this study as they were active late in the evolution of the Allendale Area, and are associated with localised retrograde metamorphism.

## 4. Structural domains

Two structural domains have been delineated based on differences in orientations of the overprinting fabrics, which are inferred to reflect the position or location within larger-scale regional F2 folds. The two domains are the Allendale Mine Domain (Fig. 6) and the Paps Synform Domain (Fig. 7a). These structural domains have been distinguished based on variations in the relationship between major fold related fabrics S2 and S3, as well as variations in the types of fold interference patterns developed.

### 4.1. Allendale Mine Domain

The Allendale Mine Domain (Fig. 6) is located in the northwestern portion of the study area. It is bound to the west by the greenschist facies Allendale Shear Zone (Fig. 6). The map pattern is dominated by the overprinting of F2 recumbent folds by north–south oriented F3 upright folds. F3 folds and their associated cleavages cause the dominant north–south structural grain (Fig. 6). The intensity of F3 folds is variable throughout the domain. This is partly attributed to strain variations across the domain as well as rheological contrast between the pelite and psammitic dominated successions. For example, F3 folds in the pelitic

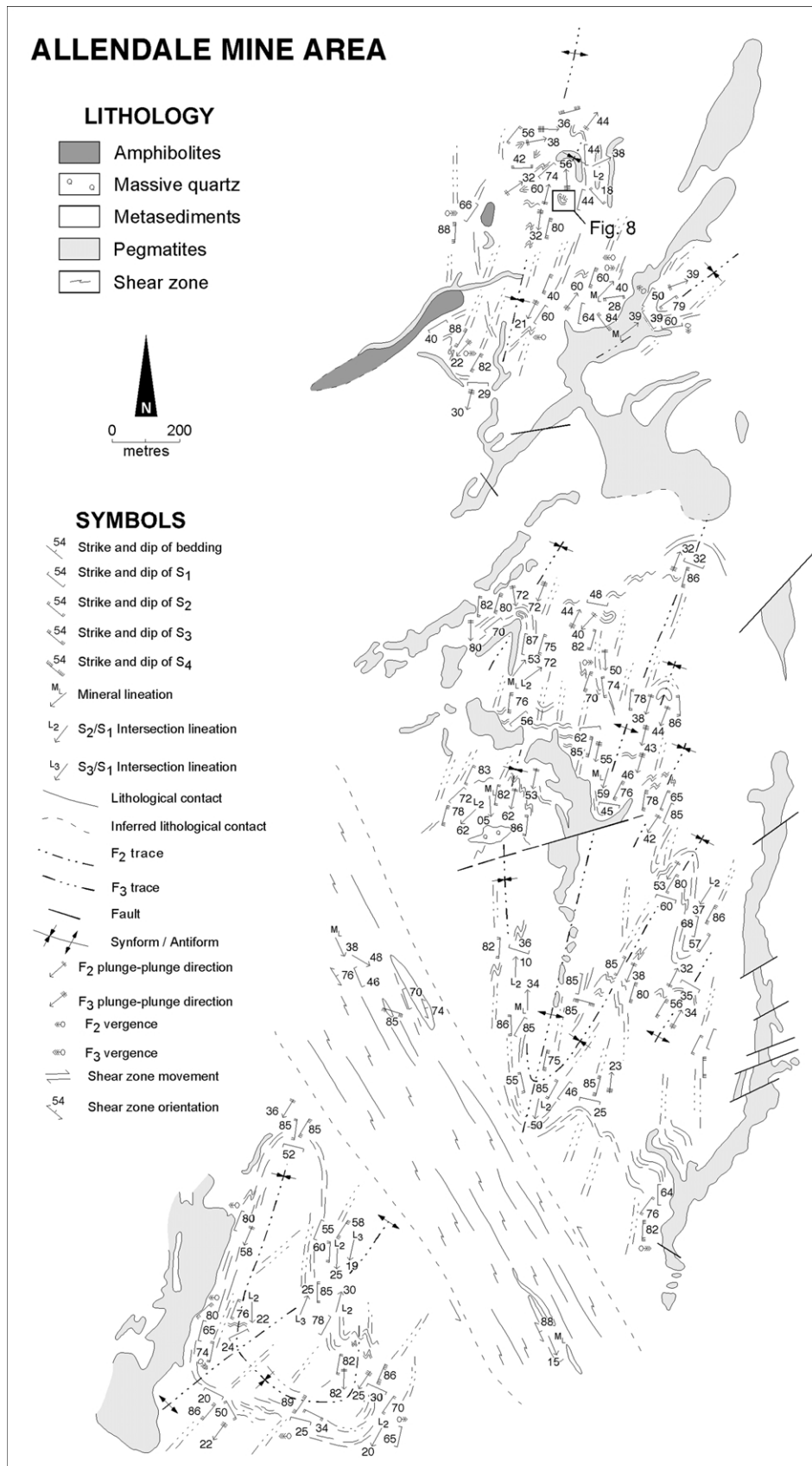


Fig. 6. Geological map of the Allendale Mine Domain. The outcrop location of the well-preserved Type 2 mushroom interference pattern (Fig. 8) observed in this area is shown.

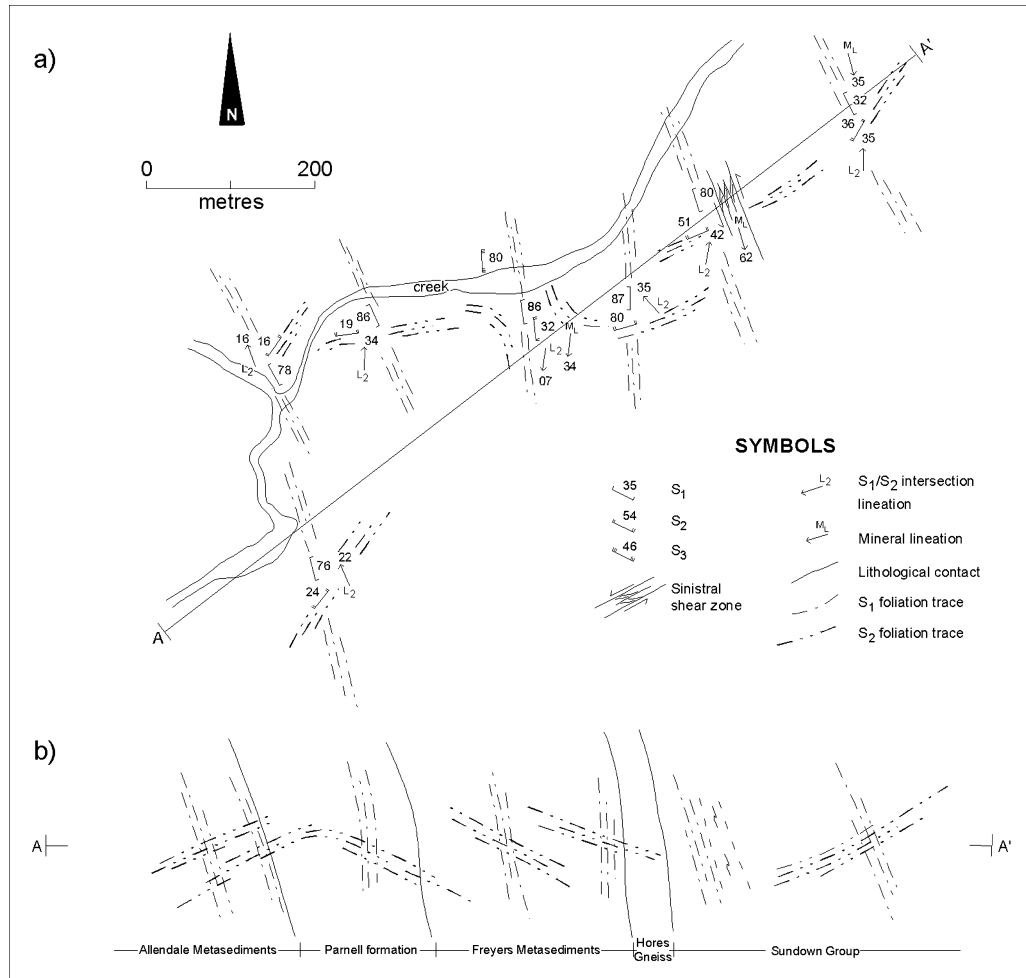


Fig. 7. (a) Geological map of the Paps Synform Domain; (b) creek section of the eastern Paps Synform limb showing S<sub>2</sub> consistently at a high angle to S<sub>0</sub>/S<sub>1</sub>. Locality of the creek section is shown in Fig. 2.

units are generally tight to isoclinal, compared with open to close folds within psammitic units. Numerous pegmatites have intruded sub-parallel to the F<sub>3</sub> axial plane throughout the domain.

Within the Allendale Mine Area, the S<sub>1</sub> fabric is parallel to lithological layering. Locally S<sub>1</sub> forms a composite fabric with S<sub>2</sub>, and is often slightly oblique to, or composite with, S<sub>3</sub> on F<sub>3</sub> fold limbs. The S<sub>2</sub> fabric varies from shallow (10–30°) to moderate (50–70°) dipping across F<sub>3</sub> fold hinges (Fig. 6). The S<sub>2</sub> fabric is at a low angle (10–30°) to S<sub>3</sub> (and S<sub>1</sub>) in F<sub>3</sub> fold limbs; however, the angle between S<sub>2</sub> and S<sub>3</sub> is high in the hinge zones of F<sub>3</sub> folds (up to 90°) (Fig. 5c and d). Meso-scale Type 2 fold interference patterns are locally developed within the hinge zones of F<sub>3</sub> folds and have also been mapped in macro-scale (Fig. 6), suggesting F<sub>2</sub> folds were originally recumbent within this domain, and that F<sub>2</sub> and F<sub>3</sub> generations were non-coaxial.

The meso-scale Type 2 mushroom interference pattern is best preserved in the northwest of the Allendale Mine Domain (Figs. 6 and 8). At this locality, S<sub>1</sub> is folded sub-parallel to a quartzofeldspathic leucosome layer,

highlighting the mushroom pattern (Fig. 8). F<sub>2</sub> folds are tight to isoclinal and are doubly plunging due to later refolding during D<sub>3</sub>. On the eastern side of the outcrop, the F<sub>2</sub> fold plunges moderately north–northeast, and on the western side, the F<sub>2</sub> fold plunges shallowly east (Fig. 8). The F<sub>3</sub> fold at this locality is approximately north–south-trending, steeply south plunging, open and upright. A well developed, steeply dipping crenulation cleavage (S<sub>3</sub>) has developed axial planar to the F<sub>3</sub> fold. S<sub>3</sub> crenulates S<sub>1</sub> and S<sub>2</sub>. The F<sub>3</sub> fold shows evidence of minor warping and is overprinted by weak F<sub>4</sub> folding (Fig. 8).

Across the Allendale Mine Domain the S<sub>2</sub> fabric is generally oriented at a low-angle (<15°) to S<sub>3</sub> (Fig. 6). High angular relationships between these fabrics occur locally within the hinge zones of mesoscale F<sub>2</sub> folds. We interpret this to indicate that the Allendale Mine Area is located on a limb of a regional scale F<sub>2</sub> recumbent fold. Unfortunately younging criteria and facing are unreliable (on a regional-scale) due to the high-strain and high-grade metamorphism in the region. Therefore, we are unsure if the Allendale Mine Domain

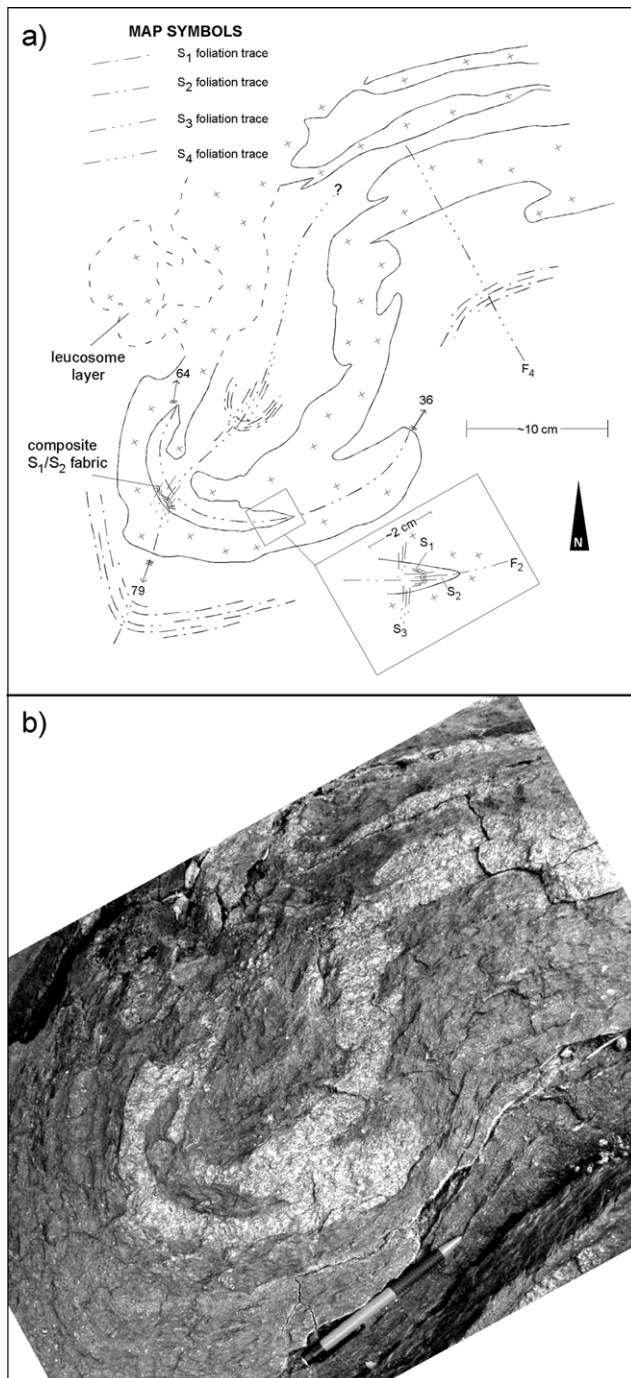


Fig. 8. (a) Sketch of the mushroom (Type 2) fold interference pattern observed in the Allendale Mine Domain. Axial traces of F2, F3 and F4 folds are shown. Locality of the outcrop is shown in Fig. 7; (b) Field photo of the same mushroom (Type 2) fold interference pattern sketched in (a). Pen is ~15 cm length.

is located on the upper or lower limb of a large-scale recumbent fold.

#### 4.2. Paps Synform Domain

The Paps Synform domain (Fig. 7a) comprises the map-scale third-generation, upright, shallowly north-plunging

Paps Synform, and numerous smaller scale F3 folds, which have north–northeast-trending axial surfaces and associated axial planar stylolitic cleavage. The F3 folds are truncated by numerous granitic dykes that are oriented subparallel to their axial plane.

In this domain the  $S_1$  foliation is parallel to lithological layering, and in part forms a fabric that has locally developed S–C shear planes. These shear zones are developed on the eastern limb of the Paps Synform where they extend for hundreds of metres along strike and are up to 30 m wide. This domain is distinguished from the Allendale Mine Domain because  $S_2$  is oriented at a high angle to  $S_1$  and lithological layering (Fig. 7). Typical angles between  $S_1$  and  $S_2$  vary between 45 and 90° (Fig. 7). The  $S_2$  fabric is generally shallowly (10–30°) to moderately (40–60°) dipping; however, in the hinge zones of meso- and map-scale F3 upright folds  $S_2$  is subhorizontal. This relationship between the fabrics is consistent over the entire domain, and suggests that the Paps Synform Domain is proximal to the hinge of a regional scale F2 recumbent fold. However, there is no obvious early recumbent hinge zones or folded lithology within the Paps Synform Domain (Fig. 7), suggesting the regional-scale F2 recumbent fold was ‘opened up’ during subsequent F3 folding (e.g. Fig. 9).

Refolding of  $S_2$  during subsequent deformation has resulted in the variations in orientation of the axial planes of F2 recumbent folds such that they are now shallowly to moderately inclined (Fig. 7). Assuming the high angular relationship (45–90°) between  $S_1$  and  $S_2$  is reflective of the original fabric relationships and has not been significantly modified during later deformation, this indicates a F2 fold hinge. The fold has been modified such that the north–south-trending limb of the Paps Synform now represents the remnant hinge zone of a F2 recumbent fold (Fig. 9). The geometry of this structure is inconsistent with that of a Type 2 or Type 3 fold interference pattern as proposed by Ramsay (1962). Instead, we propose that the geometry of the Paps Synform was formed in response to an episode of hinge ‘opening’ during the development of F3 upright folds (Fig. 9), producing a modified Type 3 fold interference pattern (Fig. 9).

#### 5. Discussion

Analysis of fold interference patterns at individual localities does not necessarily constrain the regional-scale three-dimensional geometry since folds are not always cylindrical, and the hinge orientation can be highly variable. In addition, analogue model experiments have shown that the initial shape of the earlier fold generation can have significant influence on the resultant geometry after a second episode of deformation (e.g. Watkinson, 1981; Ghosh et al., 1992; Grujic, 1993). The variation in fold interference patterns between second and third generation folds from Type 3 in the Paps Synform to Type 2 in the



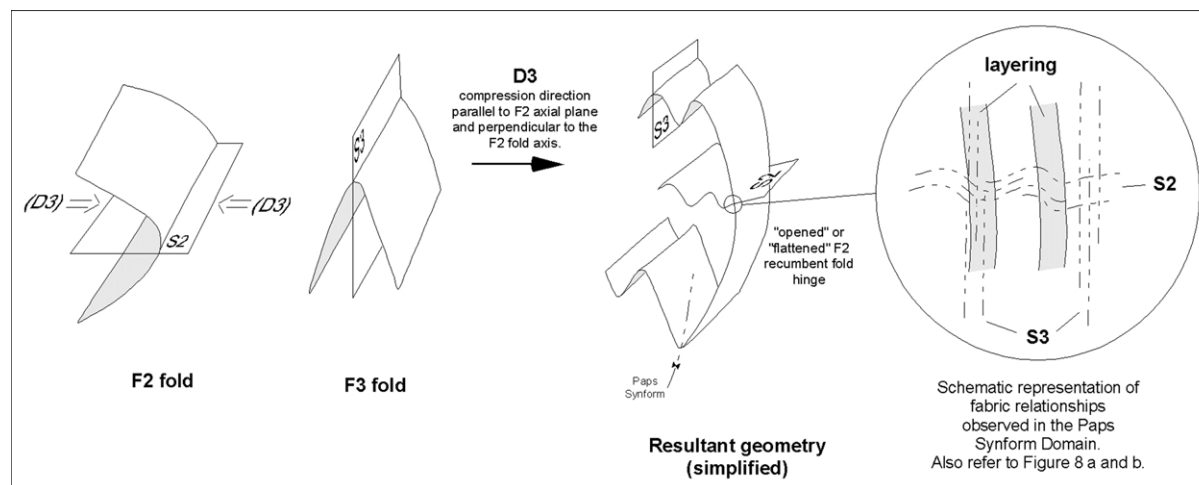


Fig. 9. Schematic diagram showing the mechanism of hinge flattening as the result of early open, recumbent folds being overprinted by later upright folds. A schematic representation of the fabric relationships in the Paps Synform Domain is shown in the enlargement.

vicinity of the Allendale Mine indicates that the fold hinge orientation of second generation folds change approximately  $90^\circ$  throughout the study area.

#### 5.1. Synchronous development of Type 2 and Type 3 fold interference patterns

Any structural analysis of the Broken Hill Inlier/Allendale Area requires an explanation of regional variations in the types of fold interference patterns. In this study we have recognised Type 2 and Type 3 interference patterns between second and third generation folds. We interpret that these fold interference patterns developed synchronously, as the S2 and S3 foliations are defined by the same mineral assemblage and style of cleavage. We suggest that this results from overprinting of a highly non-cylindrical recumbent fold generation by regional upright folds. These changes in fold interference styles throughout the area have not been recognised, resulting in the development of simplified deformational histories and geometrical models (e.g. Brown et al., 1983; Willis, 1999).

Type 2 and Type 3 fold interference patterns can both develop by the superposition of upright folds over recumbent folds. The production of Type 2 or Type 3 fold interference patterns is dependent on the orientation of structural elements of the two interfering fold generations. In both cases, the angle between the fold axial plane of two fold generations is high. Type 2 fold interference patterns develop when the angle of the fold hinges of the two fold generations is high (i.e. non-coaxial generations of folds). Conversely, Type 3 fold interference patterns develop when the angle of the fold hinges of the two fold generations is low (i.e. coaxial fold generations) (e.g. Odonne and Vialon, 1987; Ramsay and Huber, 1987). Therefore, whether Type 2 or Type 3 fold interference patterns develop is dependant on the orientation of the hinges of the two superimposing fold generations.

Structural analysis within the Allendale Area show that F2 folds characteristically have an open, recumbent geometry, and F3 folds are upright, doubly plunging and tight to open. The axial traces of F3 folds are consistently  $\sim$ N–S-trending across the Allendale Area, implying that the orientation of the axial trace of F2 fold generation must have initially varied as much as  $90^\circ$ .

We suggest that F2 meso-scale recumbent folds in the Allendale Area may have been part of a larger pre-existing structure with a sheath-like geometry (Fig. 10). If this macro-structure were overprinted by an upright folding event, Type 3 fold interference patterns would be produced on the flanks of the sheath-like fold where coaxial deformations occur. Within the nose of the sheath-like fold, non-coaxial deformation would occur so Type 2 fold interference patterns develop (Fig. 10).

The tectonic conditions under which a highly non-cylindrical recumbent (sheath) structure may have developed in the Broken Hill Block is conjectural. This geometry may develop as a sheath fold, *sensu stricto*, or may be a highly non-cylindrical nappe structure. Sheath folds develop under conditions of progressive simple shear and form as the result of high attenuation of deflections within layers in the shear zone (Minnigh, 1979; Cobbold and Quinquis, 1980; Alsop and Holdsworth, 1999). As a result, sheath folds tend to be considered as restricted to shear zones (e.g. Cobbold and Quinquis, 1980). Characteristic features of sheath folds include evidence of bulk simple shearing, strong stretching lineations, high strain zones and the development of strong mylonitic fabrics. Although all the indicators of sheath folding were not strongly developed or observed within the Allendale Area, evidence of sheath folding has been observed elsewhere in the Broken Hill Block. The Mount Robe (Venn, 2001) and Eldee (Hills et al., 2001) areas have been interpreted as large-scale sheath folds. Throughout the Broken Hill area, evidence of high strain zones has been observed. Wilson and Powell (2001)

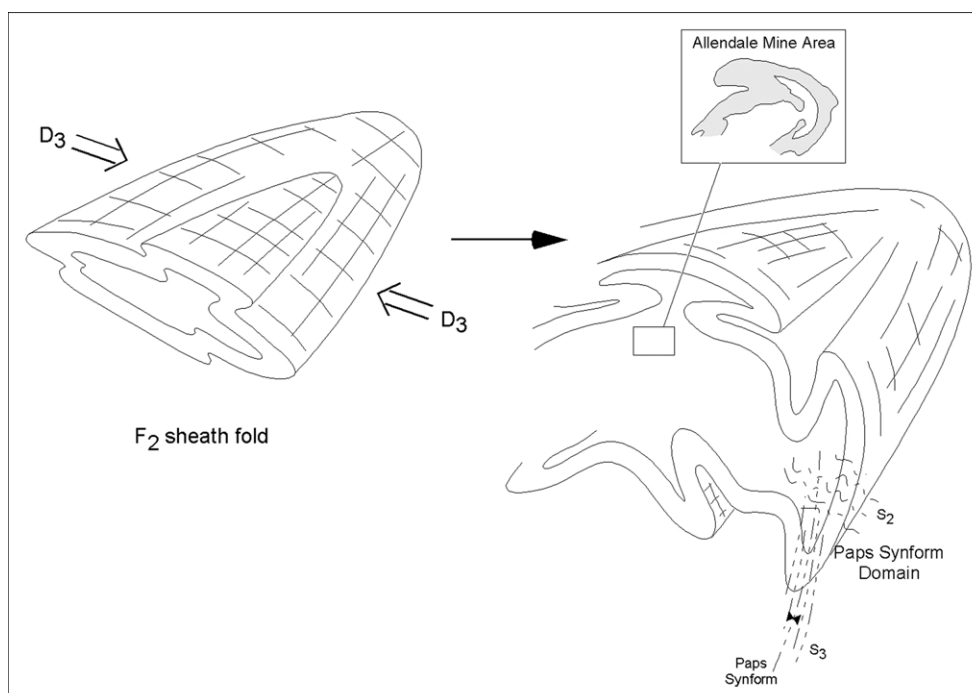


Fig. 10. Schematic representation of the 3D structural geometry of the Allendale Area. The early F2 sheath fold is shown to be overprinted by later upright folding during the D3 event to produce a complexly folded sheath structure. In the limbs of the sheath fold, Type 3 fold interference patterns are produced, whereas in the nose of the sheath fold, Type 2 fold interference patterns develop.

recognised early high-strain zones within the Southern Cross area (Fig. 1). These zones are characterised by a prominent foliation and sillimanite lineation, asymmetric extensional shear bands, tight to isoclinal intrafolial folds and pegmatites parallel to the foliation. To the north of the Broken Hill Block in the Euriowie area, a folded ductile high-temperature shear zone up to 200 m wide defined by a mylonitised granite was observed at the boundary of a granite gneiss (Alma Gneiss) and folded metasediments (Broken Hill Group) (Raetz et al., 2002). These high strain zones have not been placed in a regional-scale context. The presence of these shear zones throughout a large area of the Broken Hill Block suggests that the region was undergoing bulk shear strain during the Olarian Orogeny. If we have identified a sheath fold on the scale of 1–10 km in the Allendale Area, this implies that a large part of the crust underwent bulk simple shear during regional shortening.

Highly noncylindrical folds may also form during crustal-scale continental collision and overthrusting to develop fold and thrust belts and large-scale nappes. Large-scale sheath-like nappe structures have been described in the Western Gneiss Region of the Norwegian Caledonides as the result of the continental collision of Greenland and Scandinavia during the Silurian–Devonian (Vollmer, 1988). Nappe structures have been suggested as the dominant structural feature of Broken Hill geology for many years (e.g. Marjoribanks et al., 1980; Hobbs et al., 1984). However, the existence of these nappes has been highly debated due to the lack of small-scale nappe

structures (e.g. Gibson, 2000) and the absence of identifiable detachment structures within the Broken Hill Block.

At the time of the Olarian Orogeny, the Broken Hill Block has been placed in a collisional setting as a result of a west-dipping subduction zone that lead to continental-scale collision between North America and Australian Proterozoic Cratons (Betts and Giles, 2001; Giles and Betts, 2001). This collision lead to the development of a N–S oriented orogenic belt along the eastern margin of Proterozoic Australia (Betts and Giles, 2001; Giles and Betts, 2001; Betts et al., 2002), which also included Georgetown (e.g. Withnall et al., 1997; Blewett et al., 1998), Mount Isa (Isan Orogeny; c. 1.60–1.50 Ga; Bell, 1983; Page and Sun, 1998; Betts et al., 1999, 2000; Lister et al., 1999; Giles and Nutman, 2002), the Northern Gawler Craton (Betts et al., 2002) and the Broken Hill Block (Olarian Orogeny). It is during the earliest stages of this orogeny that sheath folds or large-scale noncylindrical folds in the Allendale Area may have developed.

## 5.2. Hinge flattening in the Paps Synform Domain

Although the processes and mechanisms of recumbent fold generation are well understood (e.g. Ez, 2000), how these folds behave during subsequent deformation and crustal shortening has only been considered in the context of fold interference patterns. There has been little discussion of how the orientation of the hinge zones of recumbent folds behave during horizontal shortening. The original hinge

orientation will have a marked effect on whether the hinge will be re-oriented (e.g. Cobbold and Watkinson, 1981; Watkinson and Cobbold, 1981; Odonne and Vialon, 1987) or will be flattened during later phases of folding/deformation.

The shape of earlier fold generations has significant influence on the fold interference pattern produced subsequent to later deformation (Watkinson, 1981; Ghosh et al., 1992; Grujic, 1993). Watkinson (1981) used analogue modelling to show that refolding of tight to isoclinal folds results in folding of the hinge zone so that Type 2 mushroom interference patterns are produced. In contrast, if open, rounded folds are refolded, the hinge is not refolded, and Type 1 dome and basin structures are produced. Natural examples of this style of refolding can be observed in the Cantabrian Mountains in northwestern Spain, where tight antiforms were refolded to produce Type 2 interference patterns, and open synforms were refolded to produce Type 1 basin structures (Julivert and Marcos, 1973).

The refolding of initially open early fold hinges into open dome structures may be analogous to the Allendale Area where refolding may have resulted in the opening of a pre-existing F2 recumbent fold hinge that is now located on the eastern limb of the Paps Synform. The macroscopic F2 fold in the Allendale Area would have had an open, recumbent fold profile shape, which is similar to parasitic F2 recumbent folds observed in the Allendale Mine Area.

However, contradictory to Watkinson (1981), refolding of the earlier open fold in the Allendale Area did not produce a Type 1 dome and basin structure but a modified Type 3-like geometry (Fig. 9). Studies of the influence of the tightness of the earlier fold generation on the resulting geometry after superposition of later fold generations (e.g. Watkinson, 1981; Ghosh et al., 1992; Grujic, 1993) have focussed on early upright, open folds, where the superimposing fold generation had a compression direction parallel to the axial plane and the fold axis of the early generation fold (e.g. the Cantabrian Mountains, NW Spain; Fig. 3b; Watkinson, 1981) (Fig. 9). In contrast, the early folds in the Allendale Area are recumbent. The geometry of overprinting F3 folds shows that the shortening direction during this event was parallel to the axial plane, and *perpendicular* to the fold axis of F2 folds (Fig. 9). However, the suggestion that initially open folds may deform into open dome structures during subsequent deformation is valid. Therefore, it is suggested that during the D3 event in the Allendale Area, a macroscale recumbent F2 fold hinge was unfolded. The F2 fold hinge was incorporated into the limb of a large-scale F3 fold—now the eastern limb of the Paps Synform (Fig. 9).

## 6. Conclusions

Fold interference patterns can become extremely complex, and not all rocks behave in an ideal manner to

produce ‘classic’ fold interference patterns. Fold interference patterns should be used in conjunction with detailed structural analysis and assessment of overprinting relationships to determine the true 3D geometry of an area.

The geometry of the Allendale Area is the result of fold interference of early D2 recumbent folds superimposed by later ~N–S-trending, upright D3 folds. Synchronous development of Type 2 and Type 3 fold interference patterns is interpreted to be the result of superposition of D3 upright folds over a large scale recumbent D2 sheath-like fold. A macroscale F2 hinge that has been opened by flattening and unfolding is preserved in the eastern limb of the Paps Synform. This F2 hinge zone can be recognised by the high angular relationship between the S2 and S3 fabrics in the area.

## Acknowledgements

CF would like to acknowledge the pmd\*CRC for support during part of the preparation of this manuscript. Catherine Spaggiari, Matt Noble and Quinton Hills are thanked for their assistance in the field, and Maurice Philips is thanked for his hospitality. David Giles, Laurent Aillieres, Barney Stevens, George Gibson and Maarten Krabbendam are thanked for helpful discussions. Constructive reviews and improvements to the manuscript from Barry Murphy, Djordje Grujic and Tom Blenkinsop were appreciated.

## References

- Alsop, G.I., Holdsworth, R.E., 1999. Vergence and facing patterns in large-scale sheath folds. *Journal of Structural Geology* 21, 1335–1349.
- Bell, T.H., 1983. Thrusting and duplex formation at Mount Isa, Queensland, Australia. *Nature* 304, 493–497.
- Betts, P.G., Giles, D., 2001. Proterozoic Australia and plate tectonics. *GSA Abstracts with Programs* 33, A-434.
- Betts, P.G., Lister, G.S., Pound, K.S., 1999. Architecture of a Palaeoproterozoic rift system; evidence from the Fiery Creek Dome region, Mt. Isa Terrane. *Australian Journal of Earth Sciences* 46, 533–554.
- Betts, P.G., Ailleres, L., Giles, D., Hough, M., 2000. Deformation history of the Hampden Synform in the Eastern fold belt of the Mt Isa Terrane. *Australian Journal of Earth Sciences* 47, 1113–1125.
- Betts, P.G., Giles, D., Lister, G.S., Frick, L.R., 2002. Evolution of the Australian lithosphere. *Australian Journal of Earth Sciences* 49, 661–695.
- Blewett, R.S., Black, L.P., Sun, S.S., Knutson, J., Hutton, L.J., Bain, J.H.C., 1998. U–Pb zircon and Sm–Nd geochronology of the Mesoproterozoic of North Queensland; implications for a Rodinian connection with the Belt Supergroup of North America. *Precambrian Research* 89, 101–127.
- Brown, R.E., Willis, I.L., Ströud, W.J., Stevens, B.P.J., 1983. The relationship between mapped rock units and the stratigraphic subdivision of the Willyama Supergroup in key areas of the Broken Hill Block. *The Aus.I.M.M. Conference, Broken Hill* pp. 51–70.
- Cobbold, P.R., Quinquis, H., 1980. Development of sheath folds in shear regimes. *Journal of Structural Geology* 2, 119–126.

- Cobbold, P.R., Watkinson, A.J., 1981. Bending anisotropy: a mechanical constraint on the orientation of fold axes in an anisotropic medium. *Tectonophysics* 72, T1–T10.
- Davis, B.K., Forde, A., 1994. Regional slaty cleavage formation and fold axis rotation by re-use and reactivation of pre-existing foliations; the Fiery Creek slate belt, North Queensland. *Tectonophysics* 230, 161–179.
- Donaghy, A.G., Hall, M., Gibson, G.M., 1998. The Palaeoproterozoic Thackaringa Group: deposition, deformation and stratigraphy: Broken Hill Exploration Initiative. Abstracts of Papers Presented at the Fourth Annual Meeting in Broken Hill, October 19–21, pp. 17–20.
- Ez, V., 2000. When shearing is a cause of folding. *Earth Science Reviews* 51, 155–172.
- Ghosh, S.K., 1970. A theoretical study of intersecting fold patterns. *Tectonophysics* 9, 559–569.
- Ghosh, S.K., Mandal, N., Khan, D., Deb, S.K., 1992. Modes of superposed buckling in single layers controlled by initial tightness of early folds. *Journal of Structural Geology* 14, 381–394.
- Ghosh, S.K., Khan, D., Sengupta, S., 1995. Interfering folds in constrictional deformation. *Journal of Structural Geology* 17, 1361–1373.
- Gibson, G.M., 2000. Tectonic evolution of the Paleoproterozoic Willyama Supergroup, Broken Hill: the early years: Broken Hill Exploration Initiative. Abstracts of Papers Presented at the May 2000 Conference in Broken Hill, pp. 45–47.
- Giles, D., Betts, P.G., 2001. Proterozoic interactions between Australia and North America. *GSA Abstracts with Programs* 33, A-434.
- Giles, D., Nutman, A.P., 2002. SHRIMP U–Pb monazite dating of 1600–1580 Ma amphibolite facies metamorphism in the southeastern Mt Isa Block, Australia. *Australian Journal of Earth Sciences* 49, 455–466.
- Grujic, D., 1993. The influence of initial fold geometry on Type 1 and Type 2 interference patterns: an experimental approach. *Journal of Structural Geology* 15, 293–307.
- Harrison, T.M., McDougall, I., 1981. Excess  $^{40}\text{Ar}$  in metamorphic rocks from Broken Hill, New South Wales: implications for  $^{40}\text{Ar}/^{39}\text{Ar}$  age spectra and the thermal history of the region. *Earth and Planetary Science Letters* 55, 123–149.
- Hills, G.G., Giles, D., Rosenbaum, G., Forbes, C., Lister, G.S., 2001. The Eldee Structure: a kilometre-scale sheath fold at the northwestern margin of the Broken Hill Block, N.S.W., Australia. *Geological Society of Australia Abstracts* 64, 81–82.
- Hobbs, B.E., Archibald, N.J., Etheridge, M.A., Wall, V.J., 1984. Tectonic history of the Broken Hill Block, Australia. In: Kröner, A., Greiling, R. (Eds.), *Precambrian Tectonics Illustrated*, pp. 353–368.
- Julivert, M., Marcos, A., 1973. Superimposed folding under flexural conditions in the Cantabrian zone, Hercynian Cordillera, N.W. Spain. *American Journal of Science* 273, 353–375.
- Lister, G.S., O'Dea, M.G., Somaia, I., 1999. A tale of two synclines: rifting, inversion and transpressional popouts at Lake Julius, northwestern Mt. Isa Terrane. *Australian Journal of Earth Sciences* 46, 233–250.
- Love, S., 1992. Possible ages and origins of some rocks of the Willyama Supergroup, New South Wales. Honours thesis, Australian National University.
- Marjoribanks, R.W., Rutland, R.W.R., Glen, R.A., Laing, W.P., 1980. The structure and tectonic evolution of the Broken Hill Region, Australia. *Precambrian Research* 13, 209–240.
- Minnigh, L.D., 1979. Structural analysis of sheath-folds in a meta-chert from the Western Italian Alps. *Journal of Structural Geology* 4, 275–282.
- Noble, M., 2000. Geology of the Broken Hill Synform, N.S.W. MSc. thesis, Monash University.
- Nutman, A.P., Ehlers, K., 1998. Evidence for multiple Palaeoproterozoic thermal events and magmatism adjacent to the Broken Hill Pb–Zn–Ag orebody, Australia. *Precambrian Research* 90, 203–238.
- Odonne, F., Vialon, P., 1987. Hinge migration as a mechanism of superimposed folding. *Journal of Structural Geology* 9, 835–844.
- Page, R.W., Laing, W.P., 1992. Felsic metavolcanic rocks related to the Broken Hill Pb–Zn–Ag orebody, Australia: geology, depositional age, and timing of high-grade metamorphism. *Economic Geology* 87, 2138–2168.
- Page, R.W., Sun, S.S., 1998. Aspects of geochronology and crustal evolution in the Eastern Fold Belt, Mt Isa Inlier. *Australian Journal of Earth Sciences* 45, 343–361.
- Page, R.W., Stevens, B.P.J., Gibson, G.M., Connor, C.H.H., 2000. Geochronology of Willyama Supergroup rocks between Olary and Broken Hill, and comparison to Northern Australia. Broken Hill Exploration Initiative: Abstracts of Papers Presented at the May 2000 Conference in Broken Hill, pp. 72–75.
- Paul, E., Sandiford, M., Flöttmann, T., 2000. Structural geometry of a thick-skinned fold-thrust belt termination: the Olary Block in the Adelaide Fold Belt, South Australia. *Australian Journal of Earth Sciences* 47, 281–289.
- Powell, C.M., Preiss, W.V., Gatehouse, C.G., Krapez, B., Li, Z.X., 1994. South Australian record of a Rodinian epicontinental basin and its mid-Neoproterozoic breakup (approximately 700 Ma) to form the palaeo-Pacific Ocean. *Tectonophysics* 237, 113–140.
- Raetz, M., Forbes, C., Lister, G.S., 2002. Stratigraphic omission explained by discovery of a regional folded ductile shear zone in the Eurioiwie Block, NSW. *Geological Society of Australia Abstracts* 67, 185.
- Ramsay, J.G., 1962. Interference patterns produced by the superposition of folds of “similar” type. *Journal of Geology* 60, 466–481.
- Ramsay, J.G., Huber, M.L., 1987. *The Techniques of Modern Structural Geology. Volume 2: Folds and Fractures*, Academic Press, London, pp. 491–502.
- Stauffer, M.R., 1988. Fold interference structures and coaptation folds. *Tectonophysics* 149, 339–343.
- Stauffer, M.R., Mukherjee, A., 1971. Superimposed deformations in the Missi meta-sedimentary rocks near Flin Flon, Manitoba. *Canadian Journal of Earth Sciences* 8, 217–242.
- Stevens, B.P.J., 1986. Post-depositional history of the Willyama Supergroup in the Broken Hill Block, NSW. *Australian Journal of Earth Sciences* 33, 73–98.
- Stevens, B.P.J., Barnes, R.G., Brown, R.E., Ströud, W.J., Willis, I.L., 1988. The Willyama Supergroup in the Broken Hill and Eurioiwie Blocks, New South Wales. *Precambrian Research* 40/41, 297–327.
- Thiessen, R., 1986. Two-dimensional re-fold interference patterns. *Journal of Structural Geology* 8, 563–573.
- Thiessen, R.L., Means, W.D., 1980. Classification of fold interference patterns: a re-examination. *Journal of Structural Geology* 2, 311–316.
- Venn, C.J., 2001. The geodynamic evolution of the Mount Robe and Mount Franks region, Broken Hill Australia: discovery of crustal-scale extensional shear zones and giant sheath folds. PhD thesis, Monash University.
- Vollmer, F.W., 1988. A computer model of sheath-nappes formed during crustal shear in the Western Gneiss Region, central Norwegian Caledonides. *Journal of Structural Geology* 10, 735–743.
- Walters, S.J., 1996. An overview of Broken Hill type deposits. In: Pongratz, J., Davidson, G.J. (Eds.), *CODES Special Publication No. 1, New Developments in Broken Hill Type Deposits*, University of Tasmania, pp. 1–10.
- Watkinson, A.J., 1981. Patterns of fold interference: influence of early fold shapes. *Journal of Structural Geology* 3, 19–23.
- Watkinson, A.J., Cobbold, P.R., 1981. Axial directions of folds in rocks with linear/planar fabrics. *Journal of Structural Geology* 3, 211–217.
- Webster, A.E., 1996. Delamerian refolding of the Palaeoproterozoic Broken Hill Block. *Australian Journal of Earth Sciences* 43, 85–89.
- White, S.H., Rothery, E., Lips, A.L.W., Barclay, T.J.R., 1995. Broken Hill area, Australia, as a Proterozoic fold and thrust belt: implications for the Broken Hill base-metal deposit. *Transactions of the Institution of Mining and Metallurgy (Section B: Applied Earth Sciences)* 104, B1–B17.
- Willis, I.L., 1999. The Stratigraphic and Structural Context of the Broken Hill, Sundown and Paragon Groups, Willyama Supergroup, Broken Hill. Observations and Interpretations from Key Sequences at Yanco Glen and Eurioiwie. Volume 1: Report, ExSolutions Geoscience.

- Willis, I.L., Brown, R.E., Ströud, W.J., Stevens, B.P.J., 1983. The Early Proterozoic Willyama Supergroup: stratigraphic subdivision and interpretation of high to low-grade metamorphic rocks in the Broken Hill Block, New South Wales. *Journal of the Geological Society of Australia* 30, 195–224.
- Wilson, C.J.L., Powell, R., 2001. Strain localisation and high-grade metamorphism at Broken Hill, Australia: a view from the Southern Cross area. *Tectonophysics* 335, 193–210.
- Withnall, I.W., Mackenzie, D.E., Denaro, T.J., Bain, J.H.C., Oversby, B.S., Knutson, J., Donchak, P.J.T., Champion, B.I., Wellman, P., Cruikshank, B.I., Sun, S.S., Pain, C.F., 1997. Georgetown Region. *AGSO Bulletin* 240, 19–116.

# Groundwater in the Broken Hill region, Australia: recognising interaction with bedrock and mineralisation using S, Sr and Pb isotopes

Patrice de Caritat <sup>a,\*</sup>, Dirk Kirste <sup>a,1</sup>, Graham Carr <sup>b</sup>, Malcolm McCulloch <sup>c</sup>

<sup>a</sup> Cooperative Research Centre for Landscape Environments and Mineral Exploration, c/- Geoscience Australia, GPO Box 378, Canberra, ACT 2601, Australia

<sup>b</sup> CSIRO Division of Exploration and Mining, PO Box 136, North Ryde, NSW 1670, Australia

<sup>c</sup> Research School of Earth Sciences, The Australian National University, Canberra, ACT 0200, Australia

---

## Abstract

The supergiant Pb–Zn–Ag Broken Hill orebody and numerous other minor mineral deposits occur within the limited outcrop of the Proterozoic Curnamona Province of Australia. The vast majority of this Province is concealed by up to 200 m of transported regolith, hampering conventional exploration strategies. Approximately 300 groundwater samples were collected over the southern Curnamona Province to test whether this medium could be helpful in the search for hidden mineral deposits. Sulphur, Sr and Pb isotope composition of the groundwaters were determined and S excess ( $S_{XS}$ ), i.e., the amount of S that can be ascribed neither to evaporation nor to mixing, was calculated. Many samples were recognised to have undergone an addition of  $^{34}\text{S}$ -depleted S, which can be attributed to oxidation of sulfides with a Broken Hill type  $\delta^{34}\text{S}$  signature (average  $\sim 0\text{‰}$  V-CDT). Furthermore, Sr isotopes identify the broad types of bedrock that the groundwater has been interacting with, from the less radiogenic Adelaidean rocks (and minerals) in the west (groundwater  $^{87}\text{Sr}/^{86}\text{Sr}$  ratio as low as 0.708) to the highly radiogenic Willyama Supergroup in the east ( $^{87}\text{Sr}/^{86}\text{Sr}$  ratio up to 0.737). The groundwaters have  $^{207}\text{Pb}/^{204}\text{Pb}$  and  $^{206}\text{Pb}/^{204}\text{Pb}$  ratios comparable to, or intermediate between, various mineralisation types recognised in the area (Broken Hill, Rupee, Thackaringa, etc., types). The few samples taken in the vicinity of known mineralisation yield positive indicators (positive  $S_{XS}$ , low  $\delta^{34}\text{S}$ ,  $^{87}\text{Sr}/^{86}\text{Sr}$  signature of bedrock type and Pb isotope fingerprinting of mineralisation type). This study also highlights several new locations under sedimentary cover where these indicators suggest interaction with mineralisation.

© 2004 Elsevier Ltd. All rights reserved.

---

## 1. Introduction

As a result of the increasing exploration maturity of many mineral provinces worldwide, the search for ore deposits is increasingly focusing onto areas where the potentially mineralized bedrock is not visible at the Earth's surface. Here, potentially thick in situ or transported regolith material obscures the geochemical and geophysical responses from underlying orebodies and

---

\* Corresponding author. Fax: +61 2 6249 9930.

E-mail address: [patrice.decaritat@ga.gov.au](mailto:patrice.decaritat@ga.gov.au) (P. de Caritat).

<sup>1</sup> Present address: Cooperative Research Centre for Landscape Environments and Mineral Exploration, c/- Department of Earth and Marine Sciences, The Australian National University, Canberra, ACT 0200, Australia.



alteration products. This is especially of concern where the regolith cover is greater than a few meters thick, and, especially, where it is allochthonous or transported. These situations are common in many countries around the world, including Australia, Canada, Chile, USA, etc., which attract a significant part of the world's exploration investments. In order to be successful in these terrains, exploration strategies different from those used in areas of bedrock outcrop or subcrop must be called upon, and special exploration tools are needed to deal with these virtually unexplored frontiers. Hydrogeochemistry is one such tool, and in this contribution the authors investigate the potential for using S, Sr and Pb isotopes coupled to standard water chemistry to recognize groundwater-basement interaction and to vector toward mineralisation under cover.

Groundwater geochemistry has been used in mineral exploration for a number of years. It was particularly popular in the 1970s (Taufen, 1997), when it was commonly applied to U exploration (Clarke and Kugler, 1973; Earle and Drever, 1982; Dean et al., 1982; Miller et al., 1984). Hydrogeochemical exploration has experienced renewed interest in the last few years (Giblin and Mazzucchelli, 1997; Leybourne et al., 1998; Pauwels et al., 1999, 2002; Caritat et al., 2001; Sader et al., 2003), and is likely to become more and more popular as technological developments and increasing affordability continue, and the drive to exploration under cover persists. The combined use of isotopes and trace elements in groundwaters in Australian conditions has previously been reported by Andrew et al. (1998), Whitford et al. (1998) and Caritat et al. (2001).

The advantages of hydrogeochemistry in exploration through thick regolith are that:

- (1) groundwater is a medium that has the potential to have been in direct contact with mineralisation;
- (2) groundwater is relatively easily and cheaply retrieved and analysed with high-performance equipment;
- (3) mineralisation may be located either in the basement rocks (e.g., fractures, alteration zones around VMS or vein-type deposits) or within the cover sequence (e.g., MVT deposits, U roll-front deposits);
- (4) exploration is not model-driven (sampling points are, in the most part, where pastoralists have drilled water bores, not where geophysics reveals 'blobs'); and
- (5) exploration is not commodity specific (multi-element analysis may reveal unexpected element accumulations).

If the groundwater has interacted with mineralisation at depth, it will have changed major, minor, trace element and/or isotope character. If such a geochemical signature is preserved and transported long enough to reach a bore from which groundwater can be sampled,

then there is potential for this medium to be very useful in mineral exploration. A hydrogeochemical exploration survey based on previously existing sampling points (bores, wells, springs, seepages) is likely to be of regional usefulness only at first, unless the density of such points is relatively high. Once a sub-area has been identified by hydrogeochemistry as having a high potential to host a blind ore deposit, more detailed (and expensive) exploration tools, such as drilling, can be focused on this much smaller area, thus enabling potentially huge cost savings.

The area for the present study is the Broken Hill region, which is host to a single known supergiant Pb–Zn–Ag orebody (~300 Mt; Stevens and Burton, 1998) and numerous smaller Pb–Zn–Ag, Cu–Au, Sn, W and U deposits. These occur mainly in the Paleo- to Neoproterozoic basement rock sequences, which crop out in the Barrier, Olary and Flinders Ranges. Those areas of exposed basement have undergone mineral exploration for more than 100 a, yet additional significant mineral discoveries have been limited.

The Barrier, Olary and Flinders Ranges form the arcuate eastern, southern and western margins, respectively, of the Callabonna Sub-basin (Fig. 1). The latter is a southern depocenter of the larger Lake Eyre Basin of central Australia. The Tertiary sediments and Quaternary soils in the southern Callabonna Sub-basin are up to 200 m thick and conceal ~90% of the highly prospective Proterozoic basement of the Curnamona Province. In the northern part of the Sub-basin, Mesozoic strata from the Great Australian Basin form a southerly thinning wedge of intervening transported material between the basement and the Cenozoic units.

## 2. Geological setting

The Curnamona Province consists of a sequence of Broken Hill equivalent rocks and Adelaidean rocks (Fig. 1). The former include complexly deformed high-grade metamorphic rocks of the Early Proterozoic Willyama Supergroup; the latter are more gently folded, mostly lower greenschist-grade Late Proterozoic sediments with minor volcanic rocks. This basement is covered by Mesozoic (only along the northern edge of the study area and beyond) and Cenozoic sediments. Detailed accounts of the geology of the Broken Hill Domain (see Fig. 1) have been reported in a number of studies (e.g., Stevens, 1980, 1986; Willis et al., 1983; Page and Laing, 1992; Stevens and Corbett, 1993).

The Willyama Supergroup comprises aluminous metasedimentary gneisses, plus locally abundant albite-rich rocks, basic gneisses (amphibolites), lesser quartzofeldspathic gneisses and substantial bodies of deformed pegmatite and leucocratic quartzofeldspathic rocks. The Willyama Supergroup can be found within the



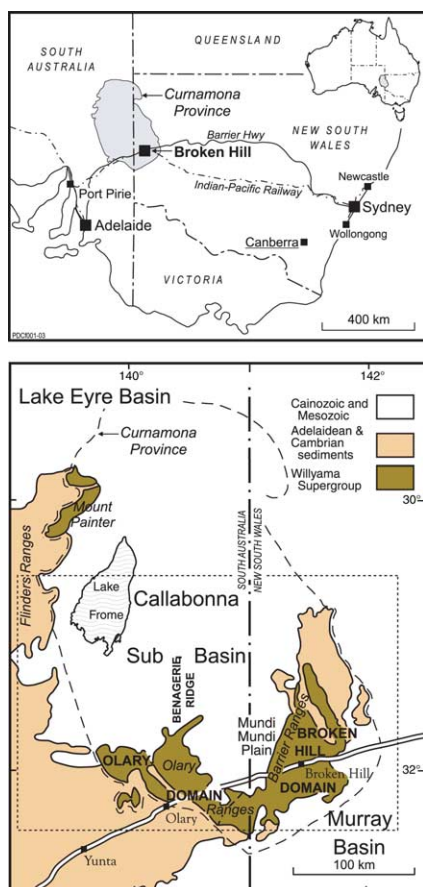


Fig. 1. Location of the study area (dashed rectangle) in the southern Curnamona province.

Broken Hill Domain, where it includes the Thackaringa and Broken Hill Groups, the Olary Domain, and the Redan Geophysical Zone, which both contain abundant albitite and calc-albitite (Stevens and Corbett, 1993). The Adelaidean sequence unconformably overlies the Willyama Supergroup and can be correlated with the more extensive occurrence of Adelaidean rocks in South Australia (Cooper et al., 1978; Preiss, 2000). It consists of a sequence of quartzite, quartzite conglomerate, limestone, siltstone, sandstone, shale, dolomite and diamictite forming various groups (Willis et al., 1983; Stevens et al., 1988; Stevens and Corbett, 1993). In the southern Curnamona Province, downthrown Proterozoic rocks west of the Broken Hill Domain are overlain by a thick fluvio-lacustrine sedimentary succession belonging to the Cenozoic Lake Eyre Basin, which extends across a vast area of central Australia. This basin is interpreted to have formed by tectonic subsidence in northeastern South Australia during the Late Paleocene (Callen et al., 1995). The Lake Eyre Basin comprises a number of sub-basins, including the Callabonna Sub-basin that

covers most of the study area. Quaternary sediments and soils commonly cover Tertiary units. Deposition in the Lake Eyre Basin occurred in 3 phases, described below (Callen et al., 1995).

- (1) In the first phase, sandstone, carbonaceous clastics and conglomerate of the Eyre Formation were deposited during the latest Paleocene to Middle Eocene.
- (2) The second phase includes deposition of grey, green and white clay, fine-grained sand and carbonate, with minor conglomerate of the Namba Formation during the Oligocene to Pliocene. It is informally divided into a lower member characterized by smectite and cyclic deposition, and an upper member with illite and kaolinite. The Namba Formation was deposited in low-energy lacustrine environments (Callen, 1990).
- (3) The third phase was characterized by the deposition of red and yellow-brown sand and sandy clay, and the development of gypsum and carbonate paleosols during the Pliocene to Quaternary.

The regional regolith and landscape features of the Broken Hill region are now being extensively studied. Recent works include those of Hill et al. (2000), Hill (2000), Gibson (2000) and Caritat et al. (2000a,b, 2001). Depth to fresh bedrock in the region varies from minimal in bedrock-dominated terrains up to approximately 200 m under basin cover (Caritat et al., 2000a). The dominant regolith materials in the region include saprolite, sediments, soils, ferricretes, silcretes, siliceous and/or ferruginous lags and carbonate accumulations (e.g., Hill, 2000; Hill et al., 2000). Areas of deepest weathering occur in areas of high preservation potential, including down-tilted fault block margins, under duricrust or lag-strewn surfaces, and in localised areas isolated from regional erosion or base-level lowering (Hill, 2000). Tonui et al. (2003) demonstrated that regolith geochemistry is a potentially useful tool for mineral exploration under cover in the Curnamona Province.

### 3. Methods

#### 3.1. Field

Approximately 280 groundwater samples (omitting duplicates) have been collected from the Broken Hill region (Fig. 2), both from areas of outcrop in the ranges and from the vast expanses of sedimentary cover in the surrounding basins (Caritat et al., 2001, 2002; Kirste and Caritat, 2002). These samples have been analysed for a comprehensive suite of major, minor and trace elements as well as for several stable and radiogenic

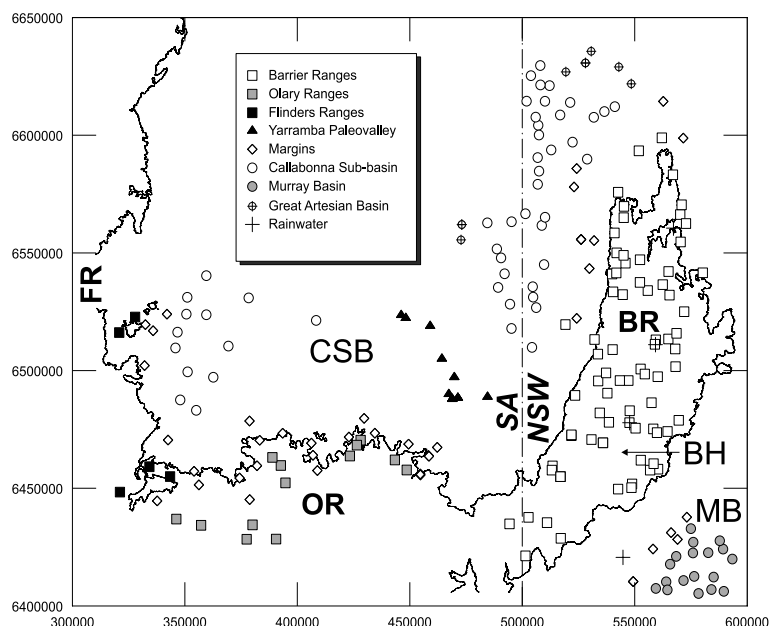


Fig. 2. Sample locations and symbols key. Locations are: BH, Broken Hill; FR, Flinders Ranges; OR, Olary Ranges; BR, Barrier Ranges; CSB, Callabonna Sub-basin; MB, Murray Basin; SA/NSW, South Australia-New South Wales state border. Coordinates: meters UTM Zone 54 WGS84; Outline: 200 m elevation contour.

isotopes. Here, this paper will focus on a subset of 164 samples for which S, Sr and/or Pb isotope data have been obtained.

The groundwater samples were collected mostly from existing stock water bores, the remainder being from exploration drillholes. Many water bores in the region were equipped with functioning pumps driven by windmills, submersible or helical pumps. Open holes were pumped with a Bennett® sampling pump. Every effort was made to obtain uncontaminated groundwater samples representative of aquifer conditions suitable for isotopic and trace element analysis.

### 3.2. Sulfur isotopes and sulfate concentrations

The S isotopic composition of  $\text{SO}_4^{2-}$  dissolved in groundwater was obtained from 159 samples. Depending on conductivity, a 250 or a 500 mL sample of freshly pumped and filtered groundwater was collected in a new high-density polyethylene (HDPE) sampling bottle. Filtration in the field was carried out using a 90 mm diameter Pall Gelman Supor® 0.45  $\mu\text{m}$  hydrophillic polyethersulfone membrane filter held in a cleaned custom-built plexiglass vacuum filtering unit. The collected sample was then acidified at a rate of  $\sim 1$  mL of ultra-pure  $\text{HNO}_3$  per 1000 mL of sample to prevent carbonate precipitation. Excess  $\text{BaCl}_2$  was added to form a stable  $\text{BaSO}_4$  precipitate, which was subsequently separated by filtration in the laboratory, rinsed and dried. The

$\text{BaSO}_4$  precipitate was sent to the Isotope Science Laboratory, Department of Physics and Astronomy, University of Calgary (Canada), for S isotope analysis on a Carlo Erba® NA 1500 elemental analyzer interfaced with a VG® Prism II mass spectrometer. High temperature reaction of the  $\text{BaSO}_4$  with  $\text{V}_2\text{O}_5$  and  $\text{SiO}_2$  generated  $\text{SO}_2$  for  $\delta^{34}\text{S}$  measurements (Yanagisawa and Sakai, 1983; Ueda and Krouse, 1986). Sulphur isotope compositions are reported using the conventional  $\delta^{34}\text{S}$  scale in parts per thousand, ‰:

$$\delta^{34}\text{S}_{\text{sample}}(\text{‰}) = \frac{R_{\text{sample}} - R_{\text{standard}}}{R_{\text{standard}}} \cdot 1000, \quad (1)$$

where  $R$  is the  $^{34}\text{S}/^{32}\text{S}$  abundance ratio of a sample or a standard, as indicated by the subscript. The standard for  $\delta^{34}\text{S}$  measurements is the V-CDT standard, as established by the International Atomic Energy Agency (IAEA), Vienna. Eight analyses of NBS127 ( $\text{BaSO}_4$ ) standard reference material ( $\delta^{34}\text{S} = +20.32 \pm 0.36\text{‰}$ ) gave a mean  $\delta^{34}\text{S}$  isotopic composition of  $+20.0715 \pm 0.5139\text{‰}$  ( $1\sigma$ ), resulting in an accuracy bias of  $\pm 1.22\text{‰}$ . The relative standard deviation (RSD) of 16 samples run at least in triplicate ranged from 0.47% to 6.45% and averaged 2.91% (precision). The RSD on 11 field duplicates ranged from 0.06% to 6.97% and averaged 2.29% (repeatability of sampling).

Dissolved  $\text{SO}_4^{2-}$  concentrations were measured by ion chromatography on a Dionex® 4000i IC at the Bureau of Rural Sciences, Canberra. Samples consisted of

unacidified, field-filtered aliquots diluted to allow bracketing by prepared standards. All samples were run in duplicate with accuracy and precision within 3%. (Measurements of  $\text{Cl}^-$  and  $\text{Br}^-$ , mentioned below, were performed the same way.)

### 3.3. Strontium isotopes and concentrations

The Sr isotopic composition of dissolved Sr was obtained from 38 groundwater samples representing a wide range of locations and groundwater compositions. A 125 mL sample of freshly pumped, filtered and acidified groundwater (as per above) was collected in a new HDPE Nalgene® sampling bottle rinsed 3 times with filtered sample water (this sample was used for major cation, trace cation and Sr isotope analysis; no contamination was detected). Upon return from the field, a 10 mL aliquot of each selected sample was separated for Sr isotope analysis, which was carried out on a Thermo-Finnigan-MAT® Neptune multi-collector inductively coupled mass spectrometer (MC-ICP-MS) at the Research School of Earth Sciences, The Australian National University, Canberra. Eleven aliquots were analysed there also on a more conventional Thermo-Finnigan-MAT® Triton thermal ionisation mass spectrometer (TIMS) as well as on the MC-ICP-MS. Results are reported as  $^{87}\text{Sr}/^{86}\text{Sr}$  ratios relative to a value of 0.710250 for standard reference material NBS987 ( $\text{SrCO}_3$ ). Strontium isotope analyses were performed with a precision of  $\pm 0.000010$  and an accuracy of  $\pm 0.000020$  (based on repeat analyses of NBS987). The MC-ICP-MS and TIMS results are in excellent agreement (Table 1).

Dissolved Sr concentrations were measured by ICP-MS at the Ecochemistry Laboratory, University of Canberra, on a different aliquot of the same acidified, field-filtered sample. (Measurement of Zn, mentioned below, was performed the same way.)

### 3.4. Lead isotopes and concentrations

The Pb isotopic composition of dissolved Pb was obtained from 29 samples selected mainly on the basis of their anomalous S concentration (see below) and low  $\delta^{34}\text{S}$  composition. A 1000 mL sample of freshly pumped, filtered and acidified groundwater (as per for Sr above) was collected in a new, rinsed HDPE sampling bottle. Contamination was deemed minimal based on the lack of correlation between Pb concentrations (by TIMS) and the  $^{206}\text{Pb}/^{204}\text{Pb}$  data, and the significantly different Pb isotope signatures of the PVC casing and the groundwater sample as tested at one location.

The Pb was initially concentrated on a Chelex® ion exchange resin (at pH 5) then separated by anion exchange chromatography. The Pb was loaded onto single Re filaments and isotope ratios were determined on a

VG® ISOMASS 54E solid source TIMS at the CSIRO Division of Exploration and Mining, Sydney, with a typical precision of  $\pm 0.05\%$  ( $2\sigma$ ) for the  $^{207}\text{Pb}/^{204}\text{Pb}$  ratio. Data have been normalised to the accepted values of international standard NBS981 by applying a correction factor of  $+0.08\%$  per atomic mass unit. Results are reported as  $^{206}\text{Pb}/^{204}\text{Pb}$ ,  $^{207}\text{Pb}/^{204}\text{Pb}$  and  $^{208}\text{Pb}/^{204}\text{Pb}$  ratios.

Dissolved Pb concentrations were measured by ICP-MS at the Ecochemistry Laboratory, University of Canberra, on acidified, field-filtered samples, as per the Sr discussed above. The dissolved Pb was determined again as part of the sample preparation for the isotope analysis after being concentrated by ion exchange, then measured by TIMS at the CSIRO Division of Exploration and Mining, Sydney.

### 3.5. Quality assurance and quality control (QA/QC)

All efforts were made throughout the project to ensure internal consistency and avoid contamination from sampling to analysis. This was achieved by using clean sampling equipment from the same source and following clear sampling protocols. Avoidance of contamination was best achieved by purging the bores before sampling, using new, quality sampling containers triply rinsed (with the water to be sampled), wearing powder-free latex gloves and not allowing smoking during sample manipulation. Preparation and analysis of all the samples were performed in the same laboratories. Additional QA procedures included: (1) analysis of rinse and travel blanks; (2) analysis of a number of control reference materials; (3) analysis in duplicate of 1 in every 10 samples; (4) analysis of field duplicate samples; and (5) verification of charge balances.

## 4. Results and discussion

The isotopic compositions of the groundwater samples, as well as a statistical summary, are given in Table 1. The  $\delta^{34}\text{S}$  values range from  $+2.29\text{‰}$  to  $+23.53\text{‰}$  (V-CDT), with a median value of  $+12.71\text{‰}$ . The  $^{87}\text{Sr}/^{86}\text{Sr}$  ratios range from 0.70797 to 0.73709, with a median value of 0.71949. The  $^{206}\text{Pb}/^{204}\text{Pb}$  ratios range from 16.213 to 18.576, with a median value of 17.212. The  $^{207}\text{Pb}/^{204}\text{Pb}$  ratios range from 15.406 to 15.840, with a median value of 15.538. The  $^{208}\text{Pb}/^{204}\text{Pb}$  ratios range from 35.898 to 38.397, with a median value of 36.927. Fig. 3 shows the regional distributions of the S, Sr and Pb isotopic results, based on boxplot-derived classes.

### 4.1. Sulfur system

Sulfate dissolved in groundwater from the Curnamona Province is weakly correlated to  $\text{Cl}^-$ , with

Table 1

Location details, concentrations of dissolved  $\text{Cl}^-$ ,  $\text{SO}_4^{2-}$ , Sr, Pb and Zn, and isotope compositions  $\delta^{34}\text{S}(\text{SO}_4^{2-})$ ,  $^{87}\text{Sr}/^{86}\text{Sr}$  (two methods),  $^{206}\text{Pb}/^{204}\text{Pb}$ ,  $^{207}\text{Pb}/^{204}\text{Pb}$  and  $^{208}\text{Pb}/^{204}\text{Pb}$  of the groundwater samples from the Curnamona Province region

ID	Site	Date	Eastings (m)	Northings (m)	$\text{Cl}^-$ (mg/L)	$\text{SO}_4^{2-}$ (mg/L)	Sr (mg/L)	Pb (mg/L)	Zn (mg/L)	$\delta^{34}\text{S}$ (‰ V-CDT)	$^{87}\text{Sr}/^{86}\text{Sr}^a$	$^{87}\text{Sr}/^{86}\text{Sr}^b$	$^{206}\text{Pb}/^{204}\text{Pb}$	$^{207}\text{Pb}/^{204}\text{Pb}$	$^{208}\text{Pb}/^{204}\text{Pb}$
BH001	Zacks Bore	9/9/99	464264	6505035	4500	1340	9.09	<0.001	0.4658	12.45	0.72114	0.72115			
BH002	Pasminco Jacks Dam	9/9/99	459041	6518933	12800	2350	17.64	<0.001	0.0027	12.28	0.71784				
BH004	Pasminco Benagerie Bore	9/9/99	446170	6523590	8760	2040	10.83	<0.001	<0.001	13.87					
BH005	Big Nancatee Bore	9/11/99	429700	6479700	1900	1790	8.19	<0.001	0.0775	13.01	0.71520	0.71518			
BH006	Pasminco Turkeys Nest	9/11/99	448211	6522347	5610	1520	8.02	<0.001	<0.001	13.38	0.72128	0.72129			
BH008	Torrominga bore	9/11/99	428150	6470432	3120	1650	6.91	<0.001	<0.001	9.73					
BH009	Jasons Bore	9/12/99	469789	6497195	4700	1510	8.48	0.0010	0.0317	12.44	0.72267	0.72267			
BH011	Brooks Dam Bore	9/12/99	467341	6490013	4640	1330	8.56	<0.001	<0.001	13.60					
BH012	Cultivation Bore (Pump Jack)	9/13/99	458292	6463925	898	1070	3.49	<0.001	0.5539	13.28					
BH014	Oonatra Dam Bore	9/14/99	448641	6457742	2750	2030	5.43	0.0010	<0.001	5.74			18.115	15.579	37.314
BH015	Bullocks Bush Bore	9/14/99	449445	6468753	2370	995	4.39	<0.001	0.0286	11.69					
BH016	Oonatra Bore 1	9/14/99	454653	6456088	2510	933	3.72	<0.001	<0.001	12.78	0.72223	0.72223			
BH017	Oonatra Bore 2	9/14/99	454707	6455667	2520	1410	5.04	<0.001	0.0022	11.04					
BH018	Black Oaks/Boundary Bore	9/15/99	426482	6468314	2550	870	6.18	<0.001	<0.001	10.62					
BH019	Pootheringla Well	9/15/99	434477	6473402	3460	2220	9.56	<0.001	0.0501	11.84					
BH021	Torrominga bore (south)	9/15/99	423399	6463697	2450	1500	6.01	<0.001	0.0028	11.75					
BH022	Cultivation Bore (Windmill)	9/15/99	458529	6463610	2140	1520	4.33	<0.001	<0.001	12.60					
BH023	Ironstone Bore	9/16/99	422949	6471761	2740	1650	6.64	<0.001	0.0832	10.45					
BH024	Wiparaminga Bore	9/16/99	443395	6462014	996	593	2.03	<0.001	<0.001	10.15	0.72509	0.72511			
BH025	Millierooka Bore	9/17/99	462203	6467384	1810	738	2.90	<0.001	0.0115	11.24					
BH026	Four Corners Bore	9/17/99	484560	6488854	4580	1290	7.60	<0.001	1.4769	13.23	0.72283	0.72282			
BH030	Wallaces Bore	9/18/99	495227	6517886	2280	893	3.71	0.0025	0.0834	13.07			18.576	15.566	38.282
BH031	Lockhart Bore	9/18/99	494555	6528214	2260	786	2.99	<0.001	0.4283	12.27					
BH032	New Chum extension	9/18/99	489274	6535305	2390	799	4.28	<0.001	0.0010	13.86	0.71971				
BH033	Corona Bore	9/19/99	495260	6563235	1450	495	2.67	<0.001	0.0090	15.36					
BH034	Glenroy Bore	9/19/99	484493	6562752	1750	696	2.41	<0.001	0.0244	12.79	0.72091	0.72095			
BH035	Birksgate Bore (Diesel)	9/19/99	473125	6562038	822	0.25	0.73	<0.001	0.0150	6.40					
BH036	Birksgate Bore (Windmill)	9/19/99	473126	6562031	793	0.25	0.72	<0.001	0.0092	11.19					
BH037	Lake Charles Bore	9/19/99	472796	6555549	2930	273	2.13	<0.001	0.0070	16.39	0.71792				
BH038	Furlough Bore	9/20/99	492160	6541129	1620	673	2.58	<0.001	0.1222	13.00					
BH039	Watsons Bore	9/20/99	490569	6547863	1760	728	3.25	<0.001	0.0069	13.52					
BH040	Glenapp Bore	9/20/99	488730	6551663	2240	975	3.87	<0.001	0.0172	13.46					
BH042	WMONB	9/22/99	468848	6487930	5050	1640	8.55	<0.001	<0.001	13.85					
BH043	WMONM	9/22/99	468848	6487914	4580	1410	7.54	<0.001	0.0101	12.17					
BH044	WMONU	9/22/99	468847	6487898	4540	1360	7.24	<0.001	<0.001	13.16					
BH046	EMONB	9/23/99	471384	6488383	5350	1770	8.96	<0.001	0.0066	13.27					
BH047	EMONM	9/23/99	471385	6488366	4710	1530	8.03	<0.001	0.0040	13.21					
BH048	EMONU	9/23/99	471385	6488349	4570	1300	7.51	<0.001	0.0027	13.37					
BH100	Zig Zag Bore	2/3/00	544679	6532250	1360	993	1.10	<0.001	0.0148	16.46					
BH101	Alberta Well	2/3/00	540392	6533442	1260	764	2.66	<0.001	0.0154	14.34					
BH102	Old Corona Well	2/3/00	539951	6541038	1800	829	3.01	0.0018	0.0115	13.22					

BH103	Near Neds Tank	2/3/00	529847	6543369	3510	1810	6.20	<0.001	<0.001	12.88				
BH104	South Bore	2/4/00	504325	6509845	1500	664	2.36	<0.001	<0.001	12.24	0.73167	0.73170		
BH105	Warners Bore	2/4/00	519210	6519534	515	253	0.98	<0.001	<0.001	14.30				
BH106	Stevens Bore	2/4/00	524201	6522198	1110	734	3.29	<0.001	<0.001	12.74				
BH107	Brewery Bore	2/5/00	540202	6508905	3520	2570	6.61	<0.001	0.0216	12.64	0.72225			
BH108	Poolamacca Well	2/5/00	533667	6506993	4520	2330	3.74	0.0019	0.0687	11.38			17.465	15.489 37.116
BH109	Homestead Bore	2/5/00	532144	6513201	1710	881	3.57	<0.001	0.0220	13.20				
BH113	House Bore	2/6/00	526186	6555740	3110	1000	2.78	<0.001	0.0020	13.27				
BH114	McDougalls Well	2/6/00	526124	6555711	786	341	0.86	<0.001	0.0045	13.74	0.72057	0.72055		
BH115	Three Corners	2/6/00	541963	6550007	936	740	2.29	0.0012	0.0082	6.25	0.72114		16.973	15.544 36.786
BH116	Copper Mine Bore	2/6/00	545925	6545652	1160	577	1.03	0.0022	0.0055	13.05				
BH117	Border Bore	2/7/00	501441	6566624	4860	1600	6.60	0.0131	0.0012	15.58			17.183	15.558 36.944
BH118	Glenmore Bore	2/7/00	508692	6561679	3260	1190	5.21	<0.001	<0.001	15.21				
BH119	Mount Bull Bore	2/7/00	510142	6565117	2460	766	3.04	<0.001	0.1557	12.72				
BH120	Nickatime Bore	2/8/00	541041	6558483	1870	2100	5.74	<0.001	0.0557	7.90				
BH121	Corner Bore	2/8/00	545122	6564978	1600	2100	2.96	<0.001	0.0087	8.80				
BH122	Gormans Bore	2/8/00	545250	6569751	1320	1610	4.84	<0.001	0.1404	10.09				
BH123	Texs Bore	2/9/00	509711	6545031	1370	886	3.03	<0.001	0.0609	12.91				
BH125	Kulka Bore	2/9/00	504676	6535630	984	850	2.01	<0.001	0.1584	13.70				
BH126	Danzie Bore	2/9/00	504859	6531184	1300	1410	3.29	<0.001	0.2192	13.05				
BH127	Mulga Valley Bore	2/9/00	506201	6526759	2200	1810	5.24	<0.001	0.1749	12.87				
BH128	Old Corona Well Bore	2/9/00	541834	6541485	394	201	0.70	<0.001	0.0048	11.83				
BH129	Four Corners Bore	2/10/00	531944	6555260	1870	635	1.84	<0.001	0.0020	13.70				
BH130	Eight Mile Bore	2/10/00	545045	6548955	2570	1680	5.64	<0.001	0.0215	11.06				
BH131	Black Tank Bore	2/10/00	552365	6547093	5880	2750	17.58	0.0032	0.0147	12.14				
BH132	Silverton Commons Borehole 1	2/11/00	521851	6472345	3590	2110	2.81	<0.001	0.0207	8.70				
BH151	Mundi Mundi Ck Well	6/1/00	523518	6489444	4210	2400	6.00	0.0011	<0.001	12.09				
BH152	Sundown Borehole	6/2/00	516997	6454920	1410	1270	1.70	0.0024	0.2581	5.49			18.562	15.626 37.753
BH153	Mt George Borehole	6/2/00	513488	6459454	332	654	1.08	<0.001	0.0545	2.29	0.72223	0.72224	18.539	15.615 37.255
BH154	Mt George Well	6/2/00	513144	6457685	3860	2680	5.73	<0.001	0.0045	9.89				
BH155	Penrose Park #1	6/3/00	521866	6472679	12000	4150	22.05	<0.001	0.0021	8.63				
BH158	Limestone Well	6/3/00	530785	6470670	2010	1320	3.52	0.0092	0.0993	7.72			18.432	15.840 38.397
BH159	House Bore	6/3/00	535909	6469290	884	472	1.34	0.0010	<0.001	8.70			17.751	15.754 37.743
BH201	Ninnerie Dam Bore	2/28/01	392686	6459671	368	210	0.85	<0.001	0.0990	12.19				
BH202	Mt Victoria Hut Bore	2/28/01	388924	6463088	1448	516	2.71	<0.001	0.2357	11.30				
BH203	Parkinsons Bore	2/28/01	393488	6473373	1737	724	2.68	<0.001	0.1169	11.50	0.71945			
BH204	North Koolka Bore	2/28/01	406258	6469170	2734	1982	7.37	<0.001	0.2074	9.74			17.626	15.598 36.966
BH205	Weeroopie Well	3/1/01	406967	6464014	1177	1936	2.60	<0.001	0.0447	12.75			17.927	15.781 37.538
BH206	Morts Bore	3/1/01	408910	6457527	3338	1566	6.93	<0.001	1.0199	10.04			16.803	15.478 36.499
BH209	Arkaroola Bore	3/2/01	374346	6454351	1943	914	5.41	<0.001	0.0875	12.70				
BH210	Marshes Bore	3/2/01	382071	6459561	1953	756	5.06	<0.001	0.8802	13.01				
BH212	Jagged Rocks Bore	3/2/01	383272	6470382	695	236	1.37	<0.001	2.8385	12.60			18.247	15.624 37.644
BH213	North Toweroo Bore	3/2/01	378754	6478579	1118	588	2.38	<0.001	0.4485	11.93				
BH214	Gums Well	3/3/01	378826	6445194	5306	1975	16.24	<0.001	0.1038	16.67	0.71520			
BH215	Diggings Bore	3/3/01	377491	6428307	4214	2337	9.07	<0.001	0.0229	22.20	0.71614			
BH216	Pipeline Bore	3/3/01	380100	6434422	749	588	1.32	<0.001	0.0281	14.37				
BH217	Goldmine Bore	3/3/01	390566	6428394	625	283	0.92	<0.001	0.0176	12.03				
BH218	Old Woolshed Bore	3/4/01	351222	6499456	5224	1723	11.40	<0.001	0.0500	14.15	0.71505			
BH220	Round Hill Bore	3/4/01	347948	6487504	2940	599	6.33	<0.001	0.2934	17.01				

(continued on next page)

Table 1 (continued)

ID	Site	Date	Eastings (m)	Northings (m)	Cl <sup>-</sup> (mg/L)	SO <sub>4</sub> <sup>2-</sup> (mg/L)	Sr (mg/L)	Pb (mg/L)	Zn (mg/L)	$\delta^{34}\text{S}$ (‰ V-CDT)	<sup>87</sup> Sr/ <sup>86</sup> Sr <sup>a</sup>	<sup>87</sup> Sr/ <sup>86</sup> Sr <sup>b</sup>	<sup>206</sup> Pb/ <sup>204</sup> Pb	<sup>207</sup> Pb/ <sup>204</sup> Pb	<sup>208</sup> Pb/ <sup>204</sup> Pb
BH221	Toolaby Bore	3/4/01	355077	6483098	4888	857	8.40	<0.001	0.1042	15.66					
BH223	Traceys Bore	3/5/01	342528	6470489	1114	277	5.23	<0.001	0.0162	19.44					
BH224	Hills Well Bore	3/6/01	343445	6454952	1119	1793	14.02	<0.001	0.0162	19.44	0.71509				
BH225	Parsons Bore	3/6/01	334244	6459134	1526	487	4.83	<0.001	0.2521	15.98					
BH227	Johnsons Bore	3/6/01	321150	6448350	1696	854	7.85	<0.001	0.2182	12.66	0.71502				
BH228	Oopina Bore	3/7/01	357225	6434243	4025	1615	6.22	<0.001	0.0189	9.95					
BH229	Comet Bore	3/7/01	346222	6436895	4749	2855	14.10	<0.001	0.4456	11.43					
BH230	Southern Cross Bore	3/7/01	337677	6444621	1605	2206	9.84	<0.001	0.0111	14.62					
BH231	Nillinghoo Bore	3/7/01	354088	6457212	247	1635	6.51	<0.001	0.0749	14.87					
BH232	Quarry Bore	3/7/01	356239	6451427	3406	1501	9.83	<0.001	0.0375	14.99					
BH233	Tyrells Well	3/8/01	345845	6509593	916	391	2.95	<0.001	0.0210	11.55			16.697	15.443	36.375
BH235	Big Six Mile Well Bore	3/8/01	350667	6523989	1797	771	4.17	<0.001	<0.001	13.73					
BH236	Middle Bore	3/8/01	351088	6531142	4056	1465	14.33	<0.001	0.0086	13.97					
BH237	Woolshed Bore	3/9/01	359566	6523732	2981	716	2.35	<0.001	<0.001	16.58					
BH238	Mulga Bore	3/9/01	359552	6540309	11830	3210	12.67	<0.001	<0.001	14.76	0.71598				
BH239	Sandyoota Well	3/9/01	378370	6530880	2690	3774	15.98	<0.001	0.0261	14.02	0.71476		16.728	15.456	36.439
BH240	House Bore	3/9/01	346752	6516302	2256	2106	8.86	<0.001	0.0038	12.71					
BH241	Lucky Hit	3/10/01	408382	6521323	4822	1840	7.32	<0.001	0.8173	11.68			16.589	15.469	36.130
BH242	Salt Well Dam Bore	3/10/01	369366	6510410	10325	2721	13.08	<0.001	0.0707	14.54					
BH244	House Bore	3/11/01	362653	6497169	5409	1307	5.63	<0.001	0.0177	14.40					
BH246	Kemps Bore	3/12/01	342053	6523983	1280	835	5.67	<0.001	0.0374	11.45	0.71381				
BH247	South Martins Bore	3/12/01	332455	6519533	323	102	2.14	0.0032	0.0667	10.95			16.880	15.471	36.821
BH248	Black Hill Wells Bore	3/12/01	327896	6522762	710	317	4.15	<0.001	0.0204	11.86					
BH249	Martins Well House Bore	3/12/01	320829	6516137	446	204	1.87	<0.001	<0.001	10.18	0.71275				
BH251	Castle Rock Bore	3/12/01	332084	6502125	1185	966	5.52	<0.001	0.1405	23.53					
BH302	One Tree Bore	10/23/01	569034	6428262	1505	497	2.19	<0.001	0.4041	12.32					
BH303	Colestead Bore	10/24/01	559411	6407430	2294	773	3.23	<0.001	0.0436	12.59	0.71953				
BH305	Angle Bore	10/24/01	564020	6410226	1517	585	2.18	<0.001	0.0654	12.76					
BH306	Old Kanbara Homestead Bore	10/24/01	558125	6424202	2939	964	4.44	<0.001	0.2161	13.17					
BH307	Elizabeth Bore	10/25/01	511025	6435376	87	159	0.17	<0.001	0.0054	7.28			16.881	15.492	36.660
BH309	Jetpump bore	10/26/01	548850	6451815	2309	1171	4.64	<0.001	0.0430	7.35	0.73403		17.262	15.495	36.498
BH310	LBH0005	10/26/01	548568	6450252	1051	573	1.54	<0.001	0.0679	7.43					
BH311	LA011	10/26/01	542638	6449621	5231	1677	6.95	<0.001	0.0109	14.11					
BH312	Oakdale Explo Bore	10/27/01	517130	6428707	851	614	0.76	<0.001	0.0137	10.60					
BH313	West Mountain Exploration Bore	10/28/01	501446	6421254	634	961	1.94	<0.001	0.0126	2.91	0.72542		16.824	15.494	36.639
BH314	Kadish Bore	10/29/01	494337	6434856	73	58.1	0.06	<0.001	0.0206	8.44					
BH315	Border Bore	10/29/01	549320	6410356	4397	1377	6.25	<0.001	0.0158	12.76					
BH319	Ascot Vale Bore	10/30/01	576448	6412516	1418	500	1.63	<0.001	0.0064	13.19					
BH320	Woolshed Bore	10/30/01	585095	6412239	1289	455	1.42	<0.001	0.0061	13.01					
BH321	Goodenough Bore	10/30/01	589621	6406200	2524	818	3.62	<0.001	0.0102	13.57	0.71471				
BH322	No. 2 Bore	10/30/01	566167	6431161	2525	860	2.78	<0.001	0.8743	12.97					
BH323	Bamboo Bore	10/31/01	568461	6421034	1734	647	2.23	<0.001	0.0438	12.75					
BH325	Eaglehawk House Bore	10/31/01	565766	6417718	1982	673	2.50	<0.001	0.0091	13.36					
BH326	Annies Bore	10/31/01	582676	6422601	1448	519	1.66	<0.001	0.0097	14.67			17.061	15.554	36.927
BH327	Swamp Bore	11/1/01	571716	6410782	1499	562	1.77	<0.001	0.0275	12.64					

BH328	Maynards Bore	11/1/01	584122	6406949	1714	479	2.00	<0.001	0.0076	13.13			
BH329	No. 2 Bore	11/1/01	564538	6406805	1472	536	2.00	<0.001	0.0160	12.42			
BH330	Block 2 Bore	11/1/01	575907	6422492	1250	481	1.73	<0.001	0.0299	13.88	16.874	15.525	36.780
BH331	Clevedale House Bore	11/2/01	552715	6461898	464	229	0.80	<0.001	0.0108	10.46			
BH332	Yallalee Bore	11/2/01	593402	6419902	1661	591	1.97	<0.001	0.2661	14.07			
BH333	Unnamed	11/2/01	589279	6424138	1390	484	1.80	<0.001	0.2107	13.72			
BH334	No. 4 Bore	11/2/01	578390	6405287	1537	525	1.96	<0.001	0.1281	13.75			
BH336	Agents Well	11/3/01	502792	6437622	334	559	1.13	<0.001	0.1601	8.46			
BH337	House Bore	11/3/01	535909	6469290	1472	806	2.57	<0.001	0.0350	10.02			
BH402	New Flow Bore/Lake Ellis Bore	2/8/02	528091	6630716	644	1.10	1.18	<0.001	0.0031	0.71033			
BH422	BHP Bore	2/12/02	528870	6589852	4381	1085	4.01	<0.001	0.0499	0.71958			
BH430	New Bore	2/13/02	505980	6607679	3014	<0.05	1.15	<0.001	0.0132	0.71541			
BH431	Mollies Bore	2/14/02	508018	6629613	2299	14.3	1.22	<0.001	0.0019	0.70797			
BH441	House Bore	2/16/02	567011	6583168	860	483	1.44	<0.001	0.0501	0.71353			
SCK01	No 1 Bore	3/15/01	573174	6437719	1942	660		<0.001	0.0180	12.40			
SCK02	No 3 Bore	3/15/01	574974	6432822	1525	546		<0.001	0.0200	12.90			
SCK03	Farmcote Well	3/15/01	560413	6458095	4369	1698		<0.001	0.0290	12.50			
SCK04	Rangers Bore	3/15/01	556855	6457698	2404	999		<0.001	0.0720	8.30			
SCK05	Old Railway Bore	3/16/01	547780	6482928	1410	868		<0.001	0.0810	8.40			
SCK07	Springs Shear	3/16/01	558246	6475206	472	202		<0.001	0.0270	10.30	0.73374	17.212	15.500 36.894
SCK10	Ironblow Bore	3/16/01	559894	6473624	1066	747		<0.001	0.1300	10.00			
SCK11	Mulga Springs	3/16/01	564596	6474097	2462	769		<0.001	0.0070	13.60		17.415	15.574 37.081
SCK12	Fords Well	3/17/01	547683	6477860	921	304		<0.001	0.0060	11.00		17.638	15.664 37.311
SCK13	Stephens Creek Bore	3/17/01	550385	6475517	277	100		<0.001	0.0180	12.40		17.408	15.538 37.023
SCK14	Hidden Bore	3/17/01	534487	6481988	4784	2389		<0.001	0.0200	6.40		16.621	15.453 36.159
SCK16	Parnell Bore	3/17/01	538545	6478007	4248	2647		<0.001	0.1200	7.20	0.73709	16.213	15.406 35.898
SCK17	Forking Bore	3/18/01	558407	6460426	2628	1829		<0.001	0.0330	8.00			
SCK18	Block 1 Bore	3/18/01	576053	6427041	1347	502		<0.001	0.2000	12.60	0.71942	16.620	15.408 36.347
SCK19	Lizzies Bore	3/18/01	587848	6427694	1369	481		<0.001	0.0100	13.90			
Minimum					73	<0.05	0.06	<0.001	<0.001	2.29	0.70797	0.71518	16.213 15.406 35.898
Median					1885	868	3.62	0.0021	0.0278	12.71	0.71949	0.72223	17.212 15.538 36.927
Maximum					12800	4150	22.05	0.0131	2.8385	23.53	0.73709	0.73170	18.576 15.840 38.397

<sup>a</sup> By MC-ICP-MS.

<sup>b</sup> By TIMS.



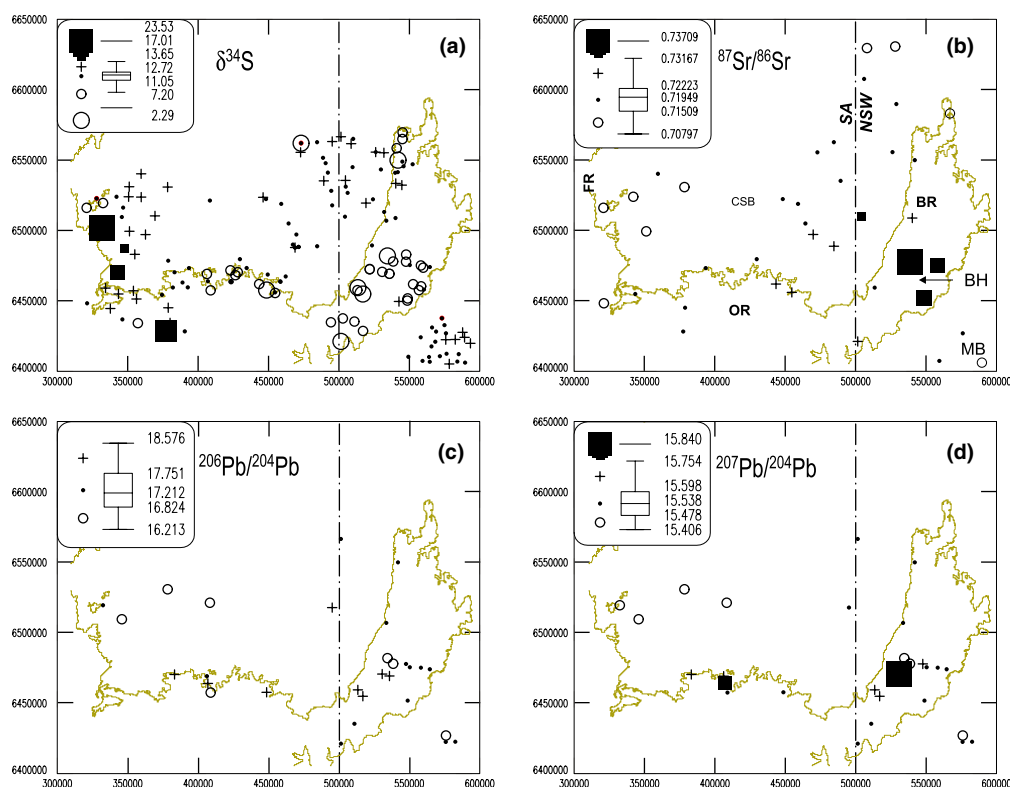


Fig. 3. Geochemical maps of (a)  $\delta^{34}\text{S}$  (‰ V-CDT), (b)  $^{87}\text{Sr}/^{86}\text{Sr}$ , (c)  $^{206}\text{Pb}/^{204}\text{Pb}$  and (d)  $^{207}\text{Pb}/^{204}\text{Pb}$  distributions in groundwaters from the Broken Hill region. The data values are classed according to the boxplot distributions using Exploratory Data Analysis conventions (large circles: lower outliers; small circles: <25th percentile; dot: 25–75th percentile; plus sign: >75th percentile; growing squares: upper outliers; e.g., Tukey, 1977; Velleman and Hoaglin, 1981). See Fig. 2 for abbreviations and map conventions.

$r^2 = 0.49$  (Fig. 4(a)). In general, recharge waters have slightly higher  $\text{SO}_4^{2-}/\text{Cl}^-$  (mass) ratios (0.2–2) than basin waters (0.001–1.4) (Fig. 4(b)), similar to, or higher than, the ratio in local rain water (0.27–2.7) (Blackburn and McLeod, 1983; Bill Ullman, pers. comm.; the authors' unpublished data). The average  $\text{SO}_4^{2-}/\text{Cl}^-$  ratio of the samples (0.51) is significantly higher than that of seawater (0.14). (All seawater data used herein are from Drever, 1997.) The fact that ratios in rainwater are greater than in seawater indicates that an addition of S occurred during atmospheric transport and/or precipitation. The similarity between the  $\text{SO}_4^{2-}/\text{Cl}^-$  ratios of the rainwater and the majority of groundwaters suggests that further increases in both  $\text{SO}_4^{2-}$  and  $\text{Cl}^-$  concentrations took place mainly by evaporation, an hypothesis borne out by stable isotope analysis (the authors' unpublished data). However, several samples, particularly – but not exclusively – from the recharge areas, have ratios significantly greater than average rainwater, indicating a further, post-precipitation addition of S (Fig. 4(b)).

There is no clear relationship between groundwater  $\delta^{34}\text{S}$  values and groundwater salinity or  $\text{Cl}^-$  concentration (Fig. 4(c)). The recharge waters generally have a lower S isotope composition than the basin waters,

suggesting that they contain a  $^{34}\text{S}$ -depleted S component.

Fig. 4(d) shows a distribution typical for the mixing of two isotopically different sources: one homogeneous (between +12.5‰ and +14.5‰) and constant, and the other inhomogeneous and variable (see Fig. 11–4 in Krouse, 1980; Kirste et al., 2003). Wakshal and Nielsen (1982) and Chivas et al. (1991) recognised two sources for S in rainfall and gypsum in playa lakes: (1) sea-salt and (2) oxidized volatile biogenic compounds, both of fixed isotopic composition (+20 to +21 and ~0‰, respectively). However, in both studies variations in  $\delta^{34}\text{S}$  values related more to geographic location than to mixing, suggesting that the variability observed in Fig. 4(d) may reflect mixing between input from atmospheric deposition and bedrock sources. Generally, the basin waters trend toward higher  $\delta^{34}\text{S}$  values with increasing  $\text{SO}_4^{2-}$  concentration and the recharge waters toward lower  $\delta^{34}\text{S}$  values. This isotopic and compositional distinction between the two types of water has been recognised before (Caritat et al., 2001, 2002) and results from a generally poor hydraulic connectivity between the upland regions and the surrounding basins. It has been noted by the same authors that evaporation is a

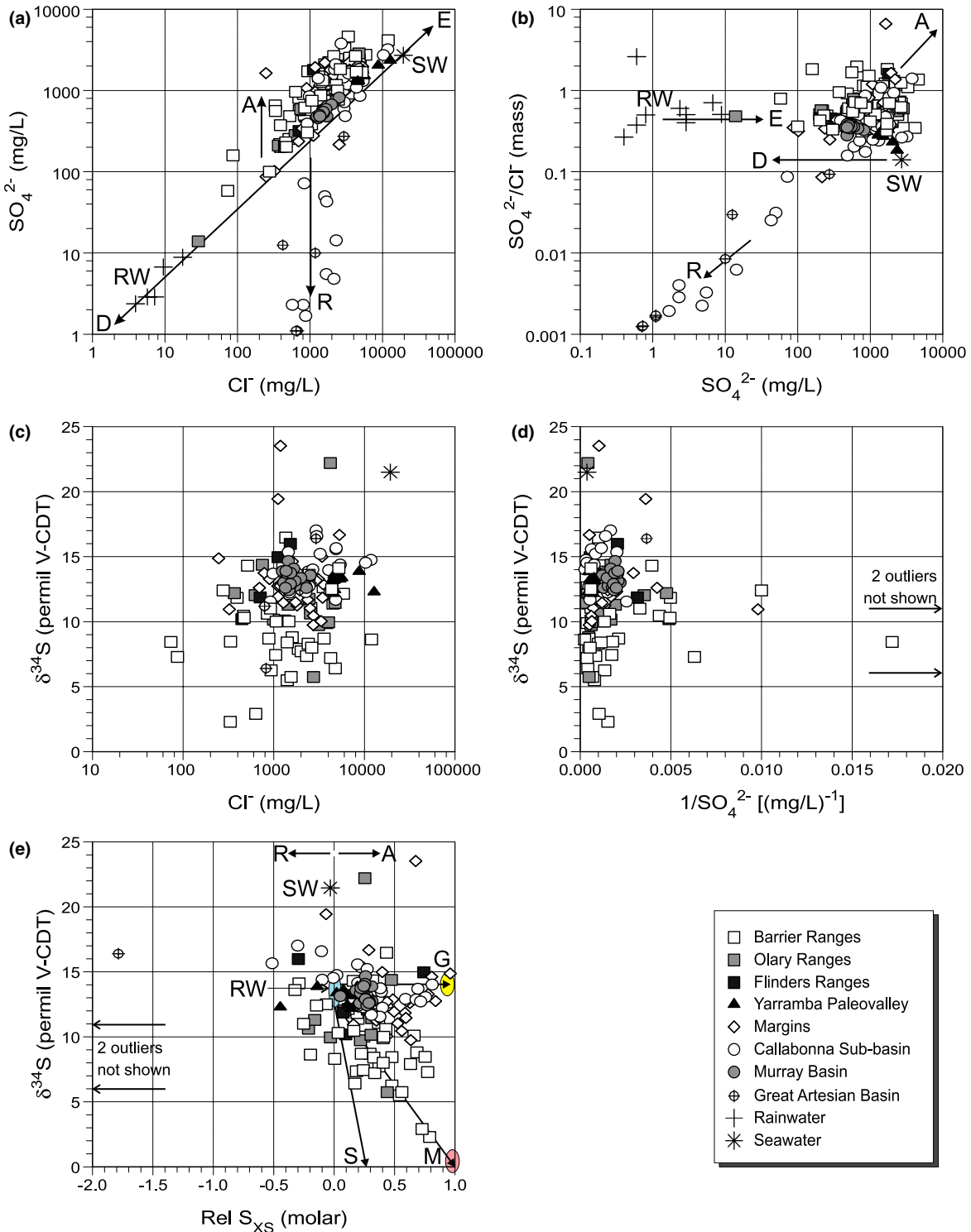


Fig. 4. Diagrams of (a)  $\text{SO}_4^{2-}$  vs  $\text{Cl}^-$ , (b)  $\text{SO}_4^{2-}/\text{Cl}^-$  vs  $\text{SO}_4^{2-}$ , (c)  $\delta^{34}\text{S}$  vs  $\text{Cl}^-$ , (d)  $\delta^{34}\text{S}$  vs  $1/\text{SO}_4^{2-}$  and (e)  $\delta^{34}\text{S}$  vs Rel  $\text{S}_{\text{XS}}$  (see text) for the groundwaters from the Broken Hill region. Minor ticks on log axes represent 2x, 4x, 6x and 8x the labelled values. Trends are D, dilution (of seawater); E, evaporation (of rainwater); A, addition (of  $\text{SO}_4^{2-}$ ); R, removal (of  $\text{SO}_4^{2-}$  (e.g.,  $\text{SO}_4^{2-}$  reduction). End-members are RW, rainwater (data from this study; Blackburn and McLeod, 1983; and Bill Ullman, pers. comm.); SW, seawater (Drever, 1997); G, gypsum; M, Broken Hill type mineralisation; S, sedimentary pyrite. See Fig. 2 for location of samples.

dominant process affecting the chemical composition of the recharge waters, whereas the basin waters appear to be largely connate, sourced by atmospheric precipitation then evaporated as the sediments were deposited in large inland lakes. The variations in salinity of the basin waters reflect differences in the extent of mixing of connate with meteoric water.

The S isotopic composition of groundwater  $\text{SO}_4^{2-}$  is influenced by the composition of rainfall and the potential contribution from oxidation of sulfide minerals along the flowpath. The  $\delta^{34}\text{S}$  of  $\text{SO}_4^{2-}$  in precipitation from the area could not be measured directly because of the low  $\text{SO}_4^{2-}$  concentrations in collected rain samples. Instead, this value is estimated indirectly from the average  $\delta^{34}\text{S}$  of surface gypsum in the area, which is +15.36‰ (data collated from Chivas et al., 1991; Shirliff, 1998; and the authors' unpublished data). Allowing a fractionation factor between gypsum and dissolved  $\text{SO}_4^{2-}$  of 1.65‰ (Thode and Monster, 1965) yields a groundwater  $\delta^{34}\text{S}$  value of +13.71‰. This corresponds well with the average  $\delta^{34}\text{S}$  of the basin groundwaters (+13.46‰) and is assumed to represent the average composition of atmospheric precipitation in the area, to which the authors assign a range of +12.5‰ to +14.5‰.

The  $\delta^{34}\text{S}$  of Broken Hill type Pb–Zn mineralisation clusters around 0‰ in the Barrier Ranges and around +4‰ to +7‰ in later vein mineralisation of the Olary Domain (Bierlein et al., 1996a). Sedimentary S or S sourced from early diagenetic pyrite typically displays more negative values than the mineralisation. Bierlein et al. (1996a) interpret  $^{34}\text{S}$ -depleted  $\delta^{34}\text{S}$  values in pyrites to be from mixing with sedimentary S and Chivas et al. (1991) report  $\delta^{34}\text{S}$  values for pyrites in the Cretaceous Bulldog Shale to be very low at approximately –40‰. Thus, there is the potential to detect groundwaters that contain S originating from atmospheric precipitation versus those that have a component of  $^{34}\text{S}$ -depleted, sulfide-derived S, as was suggested elsewhere by Gavriushin and Rabinovich (1971) and Waring et al. (1998). Further, combining the  $\delta^{34}\text{S}$  data with the  $\delta^{18}\text{O}$  composition of dissolved  $\text{SO}_4^{2-}$  yields additional information about where sulfide oxidation may have occurred along the groundwater flowpath and about the likely S isotopic composition of the sulfides (Kirste et al., 2003).

Fig. 4(e) shows a plot of  $\delta^{34}\text{S}$  vs 'Relative S excess' (Rel  $S_{\text{XS}}$ ), where  $S_{\text{XS}}$  is calculated as follows for the recharge waters, which are strongly influenced by evaporation:

$$[S_{\text{XS}}]_{\text{Recharge}} = ([\text{SO}_4^{2-}] + [\text{S}^{2-}])_{\text{GW}} - \left\{ ([\text{Cl}^-])_{\text{GW}} \cdot \left( \frac{[\text{SO}_4^{2-}]}{[\text{Cl}^-]} \right)_{\text{RW}} \right\} \quad (2)$$

and as follows for the basin and basin margin waters, which are strongly influenced by mixing with connate water

$$[S_{\text{XS}}]_{\text{Basin}} = ([\text{SO}_4^{2-}] + [\text{S}^{2-}])_{\text{GW}} - \left\{ ([\text{Cl}^-])_{\text{GW}} \cdot \left( \frac{[\text{SO}_4^{2-}]}{[\text{Cl}^-]} \right)_{\text{RBGW}} \right\}, \quad (3)$$

where square brackets denote concentrations in mmol/L and subscripts 'GW', 'RW' and 'RBGW' refer to 'groundwater sample', 'rainwater' and 'reference basin groundwater', respectively. The  $[\text{SO}_4^{2-}]/[\text{Cl}^-]$  ratio of local 'rainwater' was selected at 0.098 (0.27 as a mass ratio), the value from Fowlers Gap in Blackburn and McLeod (1983), a site inside the present study area. The 'reference basin groundwater sample' was selected from the Callabonna Sub-basin sample subset on the basis that it is: (1) unaffected by  $\text{SO}_4^{2-}$  reduction (i.e.,  $\text{SO}_4^{2-}/\text{Cl}^- > \text{seawater}$ ); and (2) most representative of the connate basin waters (i.e., highest  $\text{Cl}^-/\text{Br}^-$  ratio; see Caritat et al., 2002). The 'RBGW' sample thus selected is BH039 (Watsons Bore), which has a  $[\text{SO}_4^{2-}]/[\text{Cl}^-]$  ratio of 0.1527.

The dimensionless quantity 'Relative S excess' is then defined as:

$$\text{Rel } S_{\text{XS}} = \left( \frac{[S_{\text{XS}}]}{[\text{SO}_4^{2-}]} \right) \quad (4)$$

and is convenient to highlight small absolute S additions, which stand out more when considered in relation to total  $\text{SO}_4^{2-}$  concentrations. Several groundwater samples, particularly from the ranges, have both anomalous S concentrations (Rel  $S_{\text{XS}} > 0$ ) and low  $\delta^{34}\text{S}$  values (<+12.5‰) (Fig. 4(e)).

Fig. 4(e) reveals that 3 end-members largely account for the groundwater samples that have experienced an addition of S. These end-members are:

- (1) Rainwater: Rel  $S_{\text{XS}} \sim 0$  and  $\delta^{34}\text{S} \sim +12.5\%$  to +14.5‰ ('RW' on Fig. 4(e)).
- (2) Oxidation of Broken Hill type sulfidic mineralisation: Rel  $S_{\text{XS}} = 1$  and  $\delta^{34}\text{S} \sim 0\%$  ('M').
- (3) Gypsum dissolution: Rel  $S_{\text{XS}} = 1$  and  $\delta^{34}\text{S} \sim +12.5\%$  to +14.5‰ ('G').

The majority of the groundwater samples fall within the triangle defined by these 3 end-members. A potential fourth end-member represents the sedimentary/diagenetic pyrite from Mesozoic/Cenozoic sedimentary sequences (Rel  $S_{\text{XS}} = 1$  and  $\delta^{34}\text{S} \sim -40\%$ , 'S' on Fig. 4(e)). It must be noted that there is a great distance between the southern extent of the Bulldog Shale and the study area (~200 km, Chivas et al., 1991). Further, this end-member would only apply to groundwater samples collected from sedimentary basins, yet it does not appear to influence the basin waters very much. The recharge samples that fall between the 'M' and 'S' trends are at or above gypsum saturation and are thus likely to have precipitated this mineral, thus decreasing

their Rel  $S_{XS}$  values and moving to the left on the diagram.

Thus, interpretation of the S systematics suggests that: (1) S concentration has increased in many groundwaters by processes other than evaporation or mixing with connate basinal water; (2) this introduced S is in many cases depleted in  $^{34}\text{S}$  and may be derived from mineralisation in the basement. Thus, an isotopic signature of interaction with mineralised basement can be introduced to, and retained by, the groundwater.

#### 4.2. Strontium system

Strontium in groundwater originates from percolating rainwater, which often has a seaspray Sr component (marine accession) and a dust Sr component. This initial Sr concentration and isotopic signature can then be modified by interaction within the soil and aquifer systems, e.g., by precipitation of carbonates or dissolution of various Sr-containing minerals (weathering), cation exchange, etc. The age and initial  $^{87}\text{Rb}$  content of minerals undergoing dissolution are important parameters because, over time,  $^{87}\text{Rb}$  decays to  $^{87}\text{Sr}$  (with a half-life of  $4.88 \times 10^9$  a). There is no measurable fractionation of Sr isotopes during mineral precipitation and dissolution. Thus, the Sr isotope composition of groundwater enables one to distinguish better between the sources of Sr (and other weathering products), because seawater (and marine carbonates) and radiogenic and/or 'old' minerals have distinct isotopic signatures (e.g., Faure, 1972; McNutt, 2000).

Fig. 5(a) shows that there is a reasonable correlation between Sr and  $\text{Cl}^-$  concentrations ( $r^2 = 0.59$ ), but Fig. 5(b) shows also that the Sr/ $\text{Cl}^-$  (mass) ratio of local rainwater ( $\sim 0.002$ – $0.004$ ) overlaps with that of groundwater (average =  $0.002$ ), and that both are significantly higher than in seawater ( $0.000413$ ). This, the authors interpret, is because rainwater picks up Sr from dust during precipitation events (increasing the Sr/ $\text{Cl}^-$  ratio from a originally marine value). Then, Sr in the infiltrating rainwater may either be sequestered in any calcite that precipitates in the soil horizons (calcretes are common in the region; Chen et al., 2002) or taken up by ion exchange, consequently lowering the Sr/ $\text{Cl}^-$  ratio of soil water and shallow groundwater. Subsequently, the Sr/ $\text{Cl}^-$  ratio of the groundwater may increase again (and even exceed the rainwater value) through water–mineral interaction along the flowpath. The concomitant increases in Sr/Na and Sr/ $\text{Cl}^-$  ratios beyond the rainwater field (Fig. 5(b)) indicate addition of Sr for many samples (evaporation alone would not produce such a trend).

The Curnamona groundwaters span a wide range in  $^{87}\text{Sr}/^{86}\text{Sr}$  ratios (nearly  $0.030$ ) and show no clear correlation with salinity or  $\text{Cl}^-$  concentration (Fig. 5(c)). They have relatively radiogenic values (up to  $0.737$ ) (Figs. 5(c) and (d)), which is unusual for groundwater from sedi-

mentary basins (Harrington and Herczeg, 2003). Many of the groundwater Sr isotope values are significantly higher than the  $^{87}\text{Sr}/^{86}\text{Sr}$  composition of either seawater during or since the Proterozoic ( $0.702$ – $0.709$ ; Veizer, 1989) or local rainwater ( $0.713$ ; Ullman and Collerson, 1994; see Fig. 5(e)). This implies that the higher  $^{87}\text{Sr}/^{86}\text{Sr}$  ratios observed in these groundwaters can not be explained by inheritance from seawater, marine carbonates or rainwater, suggesting an input of radiogenic Sr through water–rock interaction with silicates.

In the Broken Hill region, rocks (granite, gneiss, pegmatite) and minerals (biotite, muscovite, K-feldspar, plagioclase, etc.) belonging to the Paleoproterozoic Willyama Supergroup are highly radiogenic, with  $^{87}\text{Sr}/^{86}\text{Sr}$  compositions commonly  $\gg 0.74$  (Pidgeon, 1967; Etheridge and Cooper, 1981). In contrast, Adelaidean rocks, which crop out abundantly in the Flinders Ranges to the west of the study area (Fig. 1), have significantly lower mean Sr-isotopic values than Paleoproterozoic craton rocks (Adelaidean shales  $^{87}\text{Sr}/^{86}\text{Sr}$  ratios range from  $0.68$  to  $0.72$ ; Foden et al., 2001). The Sr isotopic composition of the groundwater reflects quite closely this range of source materials (Fig. 3(b)), reflecting basement geology and sediments derived therefrom.

The Sr/Na ratio is useful for distinguishing between Sr released by the dissolution of carbonates or sulfates (enriched in Sr and depleted in Na, yielding higher Sr/Na) versus Sr released by the dissolution of silicates (enriched in Na, yielding lower Sr/Na) (Harrington and Herczeg, 2003). Fig. 5(e) suggests that both carbonates and silicates dissolve to contribute Sr to the groundwater, respectively resulting in high and low Sr/Na ratios. Silicate hydrolysis (low Sr/Na) is a significant process by which Sr of variable, but commonly radiogenic,  $^{87}\text{Sr}/^{86}\text{Sr}$  composition (mostly  $> 0.715$ ) is added to the groundwater. Carbonate weathering yields groundwaters with high Sr/Na, which all have low  $^{87}\text{Sr}/^{86}\text{Sr}$  values ( $0.712$  to  $0.715$ ). This carbonate may be hosted within the bedrock and be old, or alternatively may be much younger regolith carbonate (calcrete) in isotopic equilibrium with local rainwater.

The Sr system suggests that (1) the groundwaters have been interacting with minerals originating from the basement rocks (either in the fractured basement itself, or as part of the clastic basin-fill sequence), and that (2) the groundwaters are potentially relatively old since they have had time to weather relatively resistant minerals such as silicates (a suggestion supported by the authors  $\text{Cl}^-$ -isotope data, unpublished).

#### 4.3. Lead system

The Pb isotope composition of groundwater has the potential to directly reflect mineralisation because low-temperature organic or inorganic processes do not fractionate Pb isotopes (Gulson and Mizon, 1979; Gulson,

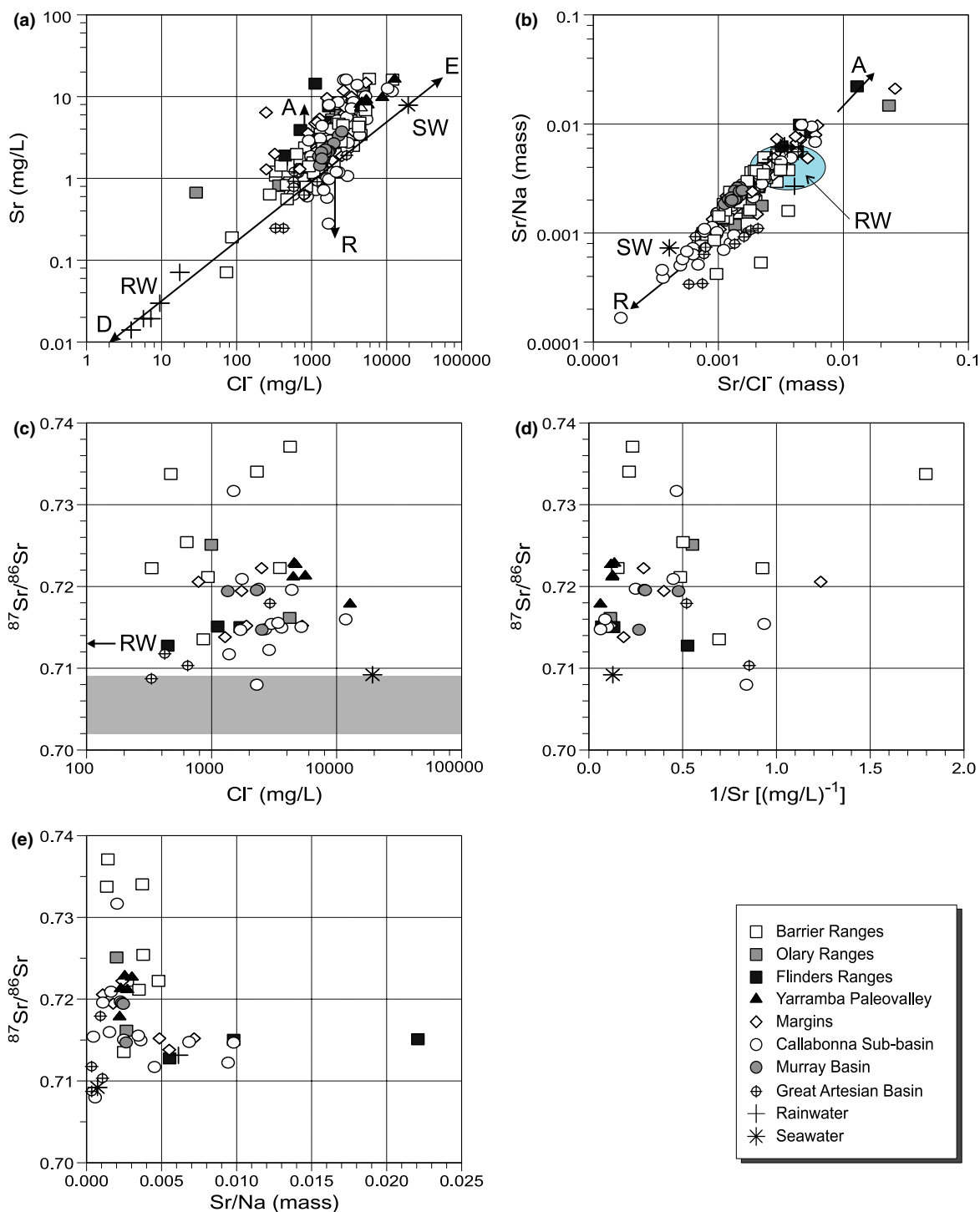


Fig. 5. Diagrams of (a) Sr vs Cl<sup>-</sup>, (b) Sr/Na vs Sr/Cl<sup>-</sup>, (c) <sup>87</sup>Sr/<sup>86</sup>Sr vs Cl<sup>-</sup>, (d) <sup>87</sup>Sr/<sup>86</sup>Sr vs 1/Sr and (e) <sup>87</sup>Sr/<sup>86</sup>Sr vs Sr/Na for the groundwaters from the Broken Hill region. Minor ticks on log axes represent 2x, 4x, 6x and 8x the labelled values. Trends are D: dilution (of seawater); E, evaporation (of rainwater); A, addition of Sr; R, removal of Sr (or addition of NaCl). End-members are RW, rainwater (data from this study; Blackburn and McLeod, 1983; and Bill Ullman, pers. comm.); SW, seawater (Drever, 1997); grey box in (c) represents the range of <sup>87</sup>Sr/<sup>86</sup>Sr values during and since the Proterozoic (Veizer, 1989). See Fig. 2 for location of samples.

1986). Various mineralisation types have distinct Pb isotope signatures (Gulson et al., 1985; Gulson, 1986), allowing discrimination between various mineralisation types, or even between barren and economic sulfide accumulations. However, dissolved Pb is prone to adsorb onto solid surfaces along the flowpath, commonly resulting in very low Pb concentrations (<1 µg/L) in groundwater, necessitating the use of ion exchange columns in the procedure.

The relationship between  $^{206}\text{Pb}/^{204}\text{Pb}$  ratios and  $\text{Cl}^-$  (Fig. 6(a)) suggests a broad tendency for lower Pb isotope ratios with higher  $\text{Cl}^-$  concentrations or salinity. The relationship between Pb isotope ratios and Zn, a metal common to many Pb-sulfides that is significantly more soluble and mobile in groundwater systems than Pb, is shown on Fig. 6(b) with Zn normalised to  $\text{Cl}^-$  to remove evaporative/salinity effects. The bulk of the data (see exceptions below) shows a broad tendency for lower  $^{206}\text{Pb}/^{204}\text{Pb}$  ratios to occur with higher Zn/ $\text{Cl}^-$  ratios (despite the fact that  $\text{Cl}^-$  itself is also higher, see above). This suggests that samples with a Pb isotope signature more similar to that of the Broken Hill main lode ( $^{206}\text{Pb}/^{204}\text{Pb}$  ratio ~16, Cooper et al., 1969; Gulson et al., 1985; Carr and Sun, 1996) also have more Zn in solution, even when normalised to  $\text{Cl}^-$ . This is consistent with Broken Hill being a Zn-rich deposit (commonly 10–20% Zn; Stevens and Burton, 1998), and suggests that the Zn/ $\text{Cl}^-$  ratio may be a useful exploration vector for Broken Hill type mineralisation in the region.

A group of 5 samples (circled in Fig. 6(b)) plot towards the top right hand side corner of the scatter diagram. Of these samples, one is from the Thackaringa Hills (BH152); mineralisation from this area, Thackaringa-style mineralisation, has been documented to have a relatively high  $^{206}\text{Pb}/^{204}\text{Pb}$  ratio (~17–18; Parr et al., 2003), almost coinciding with the value for the groundwater (18.6). Another two samples from that group (BH153 and BH158) are from the same geographic area, whereas the two others are from areas of basin cover further to the NW (BH030) and west (BH212).

It is also clear from the geochemical map (Fig. 3(c)) that all the occurrences bar one (BH030) with high, Thackaringa type,  $^{206}\text{Pb}/^{204}\text{Pb}$  ratios are located in an east-west strip along the southern edge of the Callabonna Sub-basin, i.e., extending directly west from the Thackaringa mineralisation. The geological controls on this pattern are not immediately obvious, as the main grain in the region is striking SW to NE.

Comparing the Pb isotope results with the Rel  $S_{\text{XS}}$  parameter (Fig. 6(c)) shows that both the group of samples with high  $^{206}\text{Pb}/^{204}\text{Pb}$  ratios mentioned before (Thackaringa type), and a large proportion of the samples with low  $^{206}\text{Pb}/^{204}\text{Pb}$  ratios (more Broken Hill type) have positive Rel  $S_{\text{XS}}$  values. This could indicate that oxidation of sulfide mineralisation of a certain Pb iso-

tope character was taking place at some point along the groundwater flowpath.

The  $^{208}\text{Pb}/^{204}\text{Pb}$  versus  $^{206}\text{Pb}/^{204}\text{Pb}$  diagram (Fig. 6(d)) has a steep slope (0.82) and the  $^{206}\text{Pb}/^{204}\text{Pb}$  ratios are not abnormally elevated. This indicates that the Pb isotope systematics are not adversely affected by any U mineralisation (Gulson, 1986), which is known to be present in the region, both in areas of outcrop (e.g., Olary Ranges, Mt Painter region) and within the sedimentary cover (e.g., Honeymoon deposit in the Yarramba paleovalley, Beverly deposit NW of Lake Frome).

In terms of  $^{207}\text{Pb}/^{204}\text{Pb}$  versus  $^{206}\text{Pb}/^{204}\text{Pb}$  (Fig. 6(e)), the Pb isotope results plot close to the growth curve that extends from the Broken Hill ore signature to the average background Pb isotope signature. Those samples with the lower  $^{206}\text{Pb}/^{204}\text{Pb}$  ratios (~16.5) may represent a Broken Hill type signature slightly 'diluted' by a minor amount of Pb with higher  $^{207}\text{Pb}/^{204}\text{Pb}$  and  $^{206}\text{Pb}/^{204}\text{Pb}$  ratios (background Pb or other mineralisation type). Six samples have  $^{206}\text{Pb}/^{204}\text{Pb}$  ratios <16.8, which is the upper limit for the 'Broken Hill type', 'late galena' and 'stratabound Pb–Zn deposits' groups of Parr et al. (2003). Of these, two are mineral exploration drillholes: one (SCK16) is from the vicinity of known mineralisation (Parnell Pb–Zn mine, a Broken Hill type deposit; Parr et al., 2003; Barney Stevens, pers. comm.) in the southern Barrier Ranges, the other (BH241) is in the middle of the Callabonna Sub-basin and is a BHP exploration drillhole. None of the 4 other samples (SCK14, SCK18, BH233, BH239) are from near known mineralisation or from exploration drillholes, and thus indicate areas for future exploration. All of the 6 samples may represent either unmixed (proximal) Pb–Zn mineralisation of one of the above types (see Fig. 6(e)), or a mixture of one of these types with another mineralisation Pb isotope signature with higher ratios (e.g., Thackaringa type) or with background Pb.

The samples with higher  $^{207}\text{Pb}/^{204}\text{Pb}$  and  $^{206}\text{Pb}/^{204}\text{Pb}$  ratios may represent various other local ore types recognised in the Broken Hill district (Thackaringa, Pyrite Hill, Ettlewood, etc.; Gulson et al., 1985; Bierlein et al., 1996b; Parr et al., 2003), as discussed above. Alternatively, they can be interpreted as mixtures between various Pb sources, including mixtures of Broken Hill type Pb signatures with background Pb signatures. At this stage, it is difficult to differentiate between these two alternative interpretations.

#### 4.4. Combined sulfur, strontium and lead systems

The relationship between  $\delta^{34}\text{S}$  and  $^{87}\text{Sr}/^{86}\text{Sr}$  values (Fig. 7(a)) shows that the samples with a sulfide mineralisation signature, i.e., with low  $\delta^{34}\text{S}$  (<+12.5‰), have a wide range of Sr isotope signatures (0.712–0.737). Of the recharge waters, it is clear that those from the



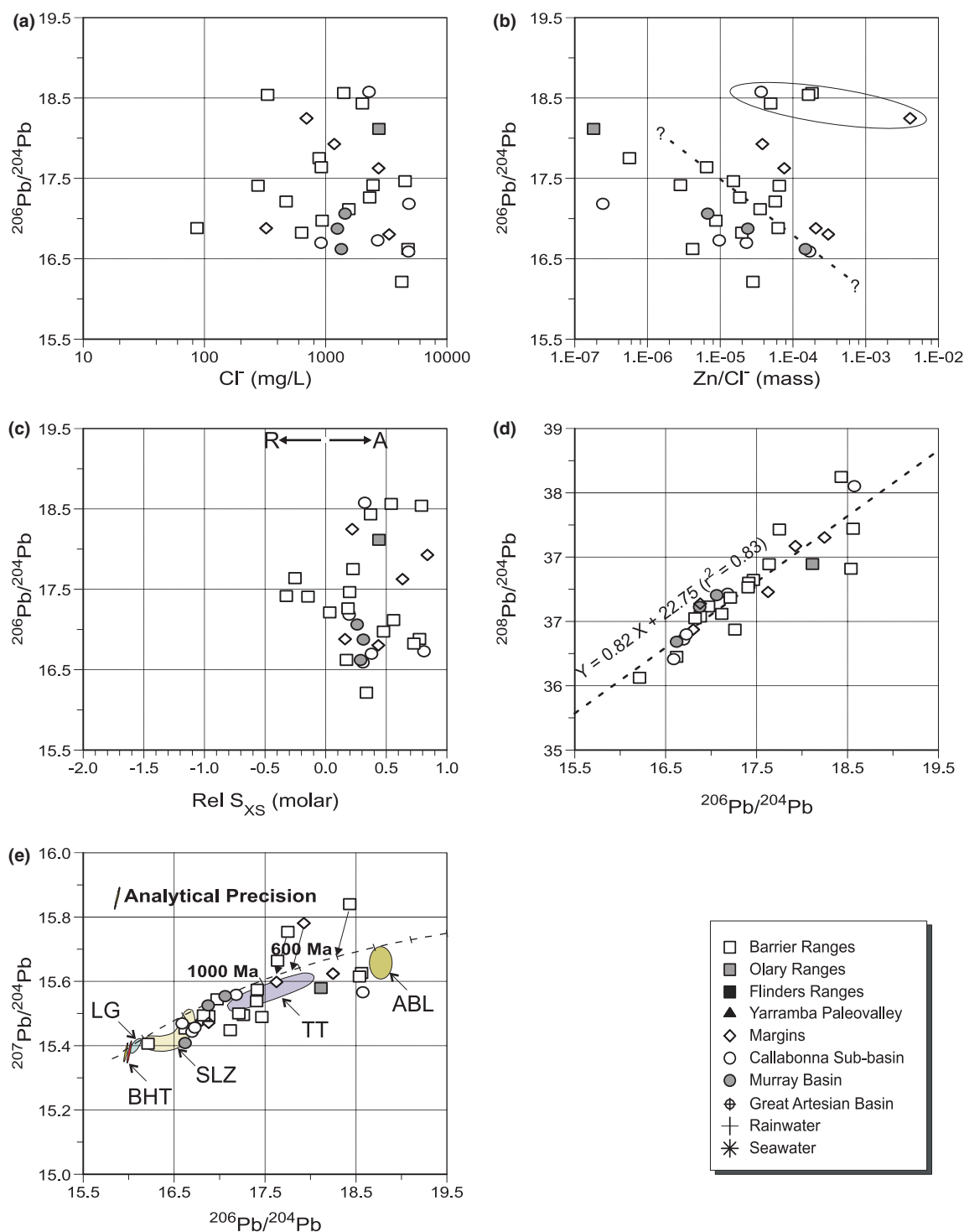


Fig. 6. Diagrams of (a)  $^{206}\text{Pb}/^{204}\text{Pb}$  vs  $\text{Cl}^-$ , (b)  $^{206}\text{Pb}/^{204}\text{Pb}$  vs  $\text{Zn}/\text{Cl}^-$ , (c)  $^{206}\text{Pb}/^{204}\text{Pb}$  vs Rel  $S_{\text{XS}}$  (see text), (d)  $^{208}\text{Pb}/^{204}\text{Pb}$  vs  $^{206}\text{Pb}/^{204}\text{Pb}$  and (e)  $^{207}\text{Pb}/^{204}\text{Pb}$  vs  $^{206}\text{Pb}/^{204}\text{Pb}$  for the groundwaters from the Broken Hill region. Minor ticks on log axes represent 2x, 4x, 6x and 8x the labelled values. Trends in (c) are A: addition of  $\text{SO}_4^{2-}$ ; R, removal of  $\text{SO}_4^{2-}$ . Fields in (e) are BHT, Broken Hill type deposits (two ellipses shown); LG, late galena; SLZ, stratabound lead zinc; TT, Thackaringa type deposits; ABL, average background Pb. These fields and the Mount Isa growth curve are from Parr et al. (2003). See Fig. 2 for location of samples.



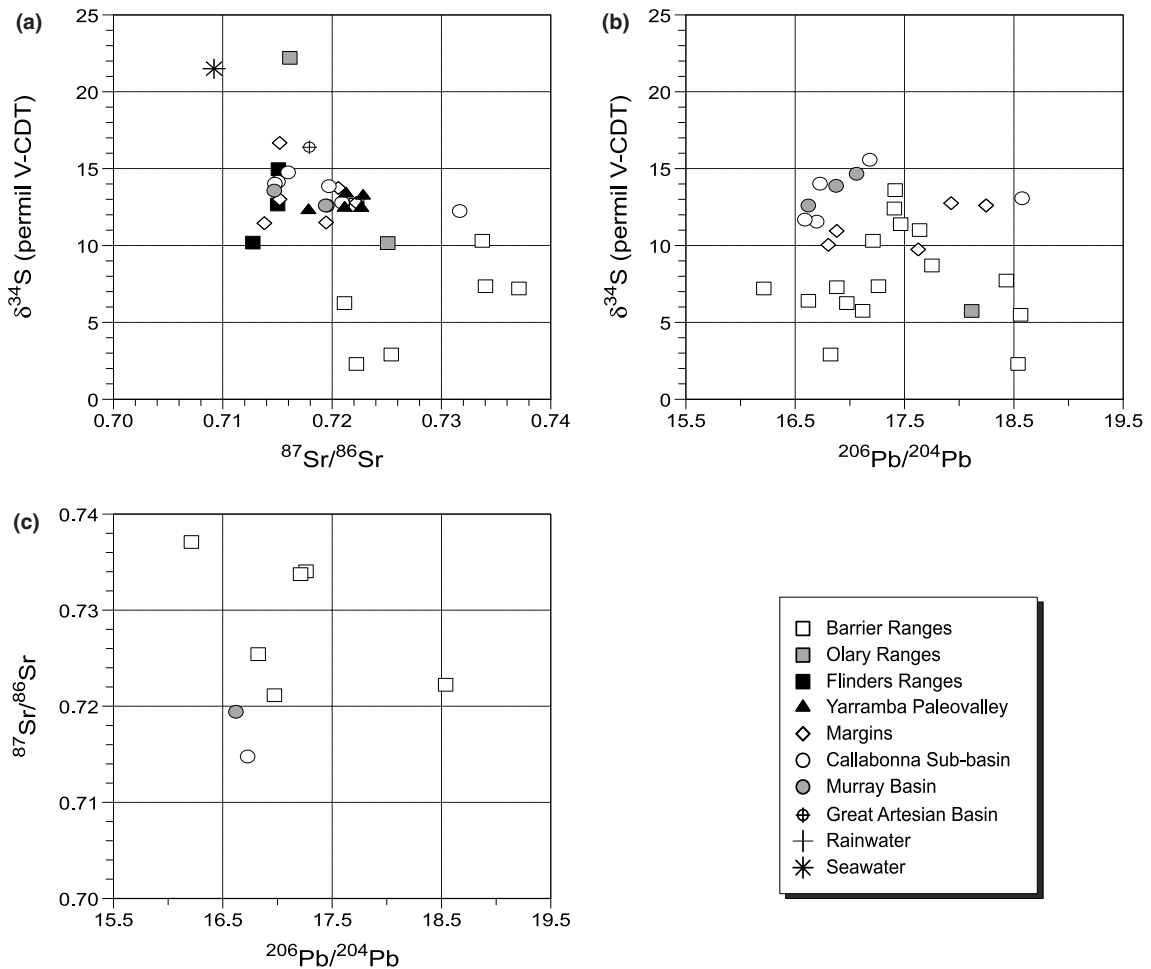


Fig. 7. Diagrams of (a)  $\delta^{34}\text{S}$  vs  $^{87}\text{Sr}/^{86}\text{Sr}$ , (b)  $\delta^{34}\text{S}$  vs  $^{206}\text{Pb}/^{204}\text{Pb}$  and (c)  $^{87}\text{Sr}/^{86}\text{Sr}$  vs  $^{206}\text{Pb}/^{204}\text{Pb}$  for the groundwaters from the Broken Hill region. See Fig. 2 for location of samples.

Barrier Ranges have both the lowest  $\delta^{34}\text{S}$  values (Broken Hill type sulfides) and the more radiogenic Sr isotope ratio (Willyama bedrock). The 3 recharge waters with  $\delta^{34}\text{S}$  of  $\sim +10\text{‰}$ , neatly reflect the bedrock type from which they originate: the one from the Flinders Ranges region has the lowest  $^{87}\text{Sr}/^{86}\text{Sr}$  value (0.714), the one from the Olary Ranges an intermediate value (0.725) and the one from the Barrier Ranges the most radiogenic Sr isotope composition (0.734). A few samples from basins, margins and the Yarramba paleovalley have S isotope signatures that indicate some component of  $^{34}\text{S}$  depleted sulfur ( $\delta^{34}\text{S} < +12.5\text{‰}$ ). Their  $^{87}\text{Sr}/^{86}\text{Sr}$  values mostly low to intermediate (0.713–0.724), except for one Callabonna Sub-basin sample (0.732). All, except one paleovalley sample, have a positive  $\text{Rel } S_{\text{XS}}$ , indicating that low  $\delta^{34}\text{S}$  sulfur was added, potentially from interaction with mineralisation. The samples with high  $\delta^{34}\text{S}$  values ( $> +12.5\text{‰}$ ) all have non-radiogenic Sr isotope ratios (0.714–0.718), indicating that they encountered neither

sulfide mineralisation nor typical Willyama type bedrock.

Fig. 7(b) shows that the samples with a low  $\delta^{34}\text{S}$  ( $< +12.5\text{‰}$ ) can have a wide range of  $^{206}\text{Pb}/^{204}\text{Pb}$  values ( $\sim 16.2$ – $18.6$ ). All the samples with  $\delta^{34}\text{S} < +10\text{‰}$  on Fig. 7(b) have  $\text{Rel } S_{\text{XS}} \geq 0$ , suggesting possible interaction with a range of different sulfide mineralisation styles as suggested by the Pb isotopic variability. Of all the samples with  $\delta^{34}\text{S} > +10\text{‰}$  on Fig. 7(b), all the basin and margin samples have  $\text{Rel } S_{\text{XS}} \geq 0$ , whilst the recharge samples have  $\text{Rel } S_{\text{XS}}$  either very close to zero or negative (see Fig. 6(c)). Thus, those basin and margin samples have experienced S addition, but the amount of S added was probably too small compared to the existing pool of S already present in the groundwater to markedly bring down the  $\delta^{34}\text{S}$  value. The Pb isotope ratios, though, are compatible with Broken Hill type mineralisation being encountered. Again, this indicates that samples BH241, SCK18, BH233, BH239, BH206, BH330,

BH326, BH117, BH247, BH204, BH205, BH212, BH030 (in order of increasing  $^{206}\text{Pb}/^{204}\text{Pb}$  ratios, *italics*:  $\delta^{34}\text{S} < +12.5\text{‰}$ ) are from areas worthy of further exploration activity. Of these, only BH241 is an exploration drillhole targeting mineralisation; it supports the interpretation that it is from this bore that the authors get the most ‘interesting’ basin sample in terms of S and Pb isotopes.

The two basin samples on Fig. 7(c) have Broken Hill type Pb isotope composition and also positive Rel  $S_{\text{XS}}$  values (not shown). The lack of strong relationships on Fig. 7(c) suggests that the full spectrum of Pb isotope signatures is found across the range of bedrock types encountered in the region, from less to more radiogenic. This implies that areas underlain by less radiogenic Adelaidean bedrock should not necessarily be discounted from the potential to host sulfides with low  $^{206}\text{Pb}/^{204}\text{Pb}$  ratios.

## 5. Conclusions

This study of S, Sr and Pb isotopes of groundwaters in the Broken Hill region has resulted in a number of significant findings for mineral exploration in the region.

1. The majority of the groundwater samples have undergone a net addition of S and this occurred predominantly, but not exclusively, early in their history (average  $\text{SO}_4^{2-}/\text{Cl}^-$  mass ratio = 0.51 compared to 0.140 for seawater) before significant evaporation or mixing occurred.
2. For a number of samples, that (relative) S excess coincides with low  $\delta^{34}\text{S}$  values ( $< +12.5\text{‰}$ ), suggesting sulfide mineralisation ( $\sim 0\text{‰}$  for Broken Hill type mineralisation) as a possible source for this S; the impact of Mesozoic or younger sedimentary pyrite is minimal.
3. Positive correlation between  $\text{Sr}/\text{Cl}^-$  and  $\text{Sr}/\text{Na}$  ratios, on the one hand, and the high  $^{87}\text{Sr}/^{86}\text{Sr}$  ratios (up to 0.737) of the groundwaters, on the other hand, indicate that Sr with a more radiogenic composition than rainwater (0.713) or Phanerozoic seawater (0.709) has been added to the waters.
4. Sr isotope signatures appear to faithfully reflect the radiogenic character of the basement rocks over (or through) which the drillholes are located. Over Adelaidean basement, the  $^{87}\text{Sr}/^{86}\text{Sr}$  composition of groundwater is clearly lower than over Willyama basement.
5. The groundwaters may have acquired their  $^{87}\text{Sr}/^{86}\text{Sr}$  composition by direct interaction with basement minerals (fractured aquifer systems) or by interaction with clastic material derived from the basement sequences within the basin fill (porous aquifer systems).

6.  $\text{Sr}/\text{Na}$  ratios suggest that silicate hydrolysis is a significant process by which Sr of variable, but commonly radiogenic,  $^{87}\text{Sr}/^{86}\text{Sr}$  composition is added to the groundwater.
7. Pb isotope ratios of the groundwaters suggest that either different mineralisation types are recognisable (e.g., Broken Hill, Thackaringa types), or that mixtures between Broken Hill type mineralisation and other types (or background Pb) are present.
8. Zn, an element commonly associated with Pb mineralisation, shows a moderate increase in concentration (even when normalised to  $\text{Cl}^-$ ) in samples with a more Broken Hill type Pb isotope signature. The groundwater  $\text{Zn}/\text{Cl}^-$  ratio could be a useful vector toward Broken Hill type mineralisation under cover.
9. Groundwater samples collected from the vicinity of Broken Hill type mineralisation (e.g., Parnell mine) or the Thackaringa mineralisation show Pb isotope compositions that indicate a direct genetic link with these types of mineralisation.
10. The Pb isotope systematics are not adversely affected by any U mineralisation in the area, as shown by the steep slope on the  $^{208}\text{Pb}/^{204}\text{Pb}$  versus  $^{206}\text{Pb}/^{204}\text{Pb}$  diagram.
11. Finally, the combination of S, Sr and Pb isotopes with conventional water composition analysis yields strong indicators that, in places, the groundwater has interacted with mineralisation in the subsurface. This powerful tool is shown to work in the vicinity of known mineralisation and thus holds tremendous promise for application to areas of thin to significant regolith cover. Several such new locations worthy of further exploratory efforts are identified herein.

## Acknowledgements

This work would not have been possible without the financial support of an Australian Government Cooperative Research Centre (CRC) grant and of the New South Wales Department of Mineral Resources. Neil Lavitt and Rod Dann made significant contributions to parts of this research, for which we are thankful. We gratefully acknowledge the invaluable assistance received from Eleanor Laing-Astolfi and Aleksandra Plasinzka (Bureau of Rural Sciences), Frank Krikowa (University of Canberra), Dave Garnett (Becquerel Laboratories) and Dale Longman, Mike Korsch and Barbara Gardner (CSIRO) in the laboratory, and from Mick Turner, Rod Dann, Leanne Hill, Angela Moonie, Rick Jones, Ian Anderson, Megan Lech, Colleen McMechan, Ian Hutcheon, Jaclyn Brachmanis, Andrew

Retter and Matt Lenahan in the field. We also thank all pastoral leaseholders for granting access to the land and, in the cases of Kalabity, Boolcomatta, Mulyangarie, Corona, Plumbago, Erudina, Pine Point, Fowlers Gap and Paringa stations, for also providing accommodation. Mineral exploration leaseholders are acknowledged for allowing us to carry out this project. The manuscript greatly benefited from the internal reviews by Colin Pain and Jonathan Clarke, and the journal reviews by Angela Giblin and an anonymous referee. *PdC* publishes with permission from the CEO of Geoscience Australia.

## References

- Andrew, A.S., Carr, G.R., Giblin, A.M., Whitford, D.J., 1998. Isotope hydrogeochemistry in exploration for buried and blind mineralisation. *The State of the Regolith*, vol. 20. Geological Society of Australia, Spec. Pub., pp. 222–225.
- Bierlein, F.P., Ashley, P.M., Seccombe, P.K., 1996a. Origin of hydrothermal Cu–Zn–Pb mineralisation in the Olary Block, South Australia: evidence from fluid inclusions and sulphur isotopes. *Precamb. Res.* 79, 281–305.
- Bierlein, F.P., Haack, U., Förster, B., Plimer, I.R., 1996b. Lead isotope study on hydrothermal sulphide mineralisation in the Willyama Supergroup, Olary Block, South Australia. *Australian Journal of Earth Sciences* 43, 177–187.
- Blackburn, G., McLeod, S., 1983. Salinity of atmospheric precipitation in the Murray-Darling drainage division, Australia. *Aust. J. Soil Res.* 21, 411–434.
- Callen, R.A., 1990. Curnamona, South Australia. 1:250,000 geological series. Explanatory notes. Sheet SH/54-14. *Geol. Surv. South Australia*.
- Callen, R.A., Sheard, M.J., Benbow, M.C., Belperio, A.P., 1995. Alluvial fans and piedmont slope deposits. In: Drexel, J.F., Preiss, W.V. (Eds.), *The Geology of South Australia*, vol. 2, *The Phanerozoic*. *Geol. Surv. South Australia Bull.*, vol. 54, pp. 244–251.
- Caritat, P. de, Killick, M.F., Lavitt, N., Tan, K.P., Tonui, E., 2000a. 3D conceptual modelling to aid mineral exploration in the southern Callabonna Sub-basin. *MESA J. (Quart. Earth Res. J. Primary Industries and Resources South Australia)* 19, 46–47.
- Caritat, P. de, Killick, M.F., Lavitt, N., Tonui, E., Dann, R., Turner, M.L., 2000b. Characterisation of the regolith, sediment and groundwater in the Mundi Mundi Curnamona region. In: *Broken Hill Exploration Initiative (BHEI): Abst. 2000 Annual Meeting, Broken Hill, May 2000. AGSO Record 2000/10*, pp. 16–19.
- Caritat, P. de, Kirste, D., Dann, R., Hutcheon, I., 2002. Groundwater composition in the Broken Hill area: salinity and mineral exploration applications. In: Phillips, G.N., Ely, K.S. (Eds.), *Proceedings and Field Guide, 'Victoria Undercover' (Benalla, VIC, 30 April–2 May 2002). CSIRO Publishing, Collingwood*, pp. 275–278.
- Caritat, P. de, Lavitt, N., Kirste, D., 2001. Groundwater geochemistry in the Broken Hill region, Australia. In: Cidu, R. (Ed.), *Proc. 10th Intern. Symp. Water–Rock Interaction WRI-10 (Villasimius, Italy, 10–15 June 2001)*, vol. 1. A.A. Balkema Publishers, Swets, Zeitlinger, Lisse, pp. 489–492.
- Carr, G.R., Sun, S.S., 1996. Lead isotope models applied to Broken Hill style terrains – syngenetic vs epigenetic metallogenesis. In: Pongratz, J., Davidson, G.J. (Eds.), *New Developments in Broken Hill Type Deposits*, 1. CODES Spec. Pub., pp. 77–87.
- Chen, X.Y., Lintern, M.J., Roach, I.C. (Eds.), 2002. *Calcrete: Characteristics, Distribution and Use in Mineral Exploration*. Cooperative Research Centre for Landscape Environments and Mineral Exploration.
- Chivas, A.R., Andrew, A.S., Lyons, W.B., Bird, M.I., Donnelly, T.H., 1991. Isotopic constraints on the origin of salts in Australian playas. 1. Sulphur. *Palaeogeo., Palaeoclim., Palaeoecol.* 84, 309–332.
- Clarke, W.B., Kugler, G., 1973. Dissolved helium in groundwater: a possible method for uranium and thorium prospecting. *Econ. Geol.* 68, 243–251.
- Cooper, J.A., Reynolds, P.H., Richards, J.R., 1969. Double-spike calibration of the Broken Hill standard lead. *Earth Planet. Sci. Lett.* 6, 467–478.
- Cooper, P.F., Tuckwell, K.D., Gilligan, L.B., Meares, R.M., 1978. *Geology of the Torrawingee and Fowlers Gap 1:100,000 sheets 7135, 7235*. New South Wales Geological Survey.
- Dean, J.R., Bland, C.J., Levinson, A.A., 1982. The measurement of  $^{226}\text{Ra}/^{223}\text{Ra}$  activity ratios in ground water as a uranium exploration technique. *J. Geochem. Explor.* 19, 187–193.
- Drever, J.I., 1997. *The Geochemistry of Natural Waters: Surface and Groundwater Environments*. Prentice-Hall, Englewood Cliffs, NJ.
- Earle, S.A.M., Drever, G.L., 1982. Hydrogeochemical exploration for uranium within the Athabasca Basin, northern Saskatchewan. *J. Geochem. Explor.* 19, 57–73.
- Etheridge, M.A., Cooper, J.A., 1981. Rb/Sr isotopic and geochemical evolution of a recrystallized shear (mylonite) zone at Broken Hill. *Contrib. Mineral. Petrol.* 78, 74–84.
- Faure, G., 1972. *Strontium Isotope Geology*. Springer-Verlag, Berlin.
- Foden, J., Barovich, K., Jane, M., O'Halloran, G., 2001. Sr-isotopic evidence for Late Neoproterozoic rifting in the Adelaide Geosyncline at 586 Ma: implications for a Cu ore forming fluid flux. *Precamb. Res.* 106, 291–308.
- Gavrilshin, A.I., Rabinovich, A.L., 1971. Sulfur isotopic composition of sulfate in natural waters from sulfide deposits in the Middle Urals. *Geochem. Internat.* 8, 550–552.
- Giblin, A., Mazzucchelli, R., 1997. Groundwater geochemistry in exploration; an investigation in the Black Flag District, Western Australia. *Aust. J. Earth Sci.* 44, 433–443.
- Gibson, D., 2000. Regolith, landform history and sampling strategies in the Wonnaminta area, Koonenberry Belt. In: *Broken Hill Exploration Initiative (BHEI): Abst. 2000 Annual Meeting, Broken Hill, May 2000. AGSO Record 2000/10*, pp. 41–44.
- Gulson, B.L., 1986. Lead isotopes in mineral exploration. *Developments in Economic Geology*, 23. Elsevier, Amsterdam.
- Gulson, B.L., Mizon, K.J., 1979. Lead isotopes as a tool for gossan assessment in base metal exploration. *J. Geochem. Explor.* 11, 299–320.

- Gulson, B.L., Porritt, P.M., Mizon, K.J., Barnes, R.G., 1985. Lead isotope signatures of stratiform and strata-bound mineralization in the Broken Hill Block, New South Wales, Australia. *Econ. Geol.* 80, 488–496.
- Harrington, G.A., Herczeg, A.L., 2003. The importance of silicate weathering of a sedimentary aquifer in arid Central Australia indicated by very high  $^{87}\text{Sr}/^{86}\text{Sr}$  ratios. *Chem. Geol.* 199, 281–292.
- Hill, S.M., 2000. The regolith and landscape evolution of the Broken Hill Block, Western New South Wales, Australia. Ph.D. Thesis, Cooperative Research Center for Landscape Evolution and Mineral Exploration (CRC LEME), Australian National Univ..
- Hill, S.M., Jones, G.L., Foster, K.A., Willis, S.M., Shirliff, G., West, D.S., Holzapfel, M., 2000. Mineralisation signatures in the regolith of the Broken Hill region. In: Broken Hill Exploration Initiative (BHEDI): Abst. 2000 Annual Meeting, Broken Hill, May 2000. AGSO Record 2000/10, pp. 53–56.
- Kirste, D., Caritat, P. de, 2002. Geochemical modelling of processes affecting the chemical composition of groundwaters in the Broken Hill region: effects of regolith properties on mineralised zone chemical signatures. In: 16th Australian Geological Convention, Adelaide, 1–5 July 2002. *Geol. Soc. Aust. abst.* 67, p. 421.
- Kirste, D., Caritat, P. de, Dann, R., 2003. The application of the stable isotopes of sulfur and oxygen in groundwater sulfate to mineral exploration in the Broken Hill region of Australia. *J. Geochem. Explor.* 78–79, 81–84.
- Krouse, H.R., 1980. Sulfur isotopes in our environment. In: Fritz, P., Fontes, J.Ch. (Eds.), *Handbook of Environmental Isotope Geochemistry, The Terrestrial Environment*, 1. Elsevier, Amsterdam, pp. 435–471.
- Leybourne, M.I., Goodfellow, W.D., Boyle, D.R., 1998. Hydrogeochemical, isotopic, and rare earth element evidence for contrasting water–rock interactions at two undisturbed Zn–Pb massive sulphide deposits, Bathurst Mining Camp, N.B., Canada. *J. Geochem. Explor.* 64, 237–261.
- McNutt, R.H., 2000. Strontium isotopes. In: Cook, P.G., Herczeg, A.L. (Eds.), *Environmental Tracers in Subsurface Hydrology*. Kluwer Academic Publishers, Boston (Chapter 8).
- Miller, W.R., Wanty, R.B., McHugh, J.B., 1984. Application of mineral-solution equilibria to geochemical exploration for sandstone-hosted uranium deposits in two basins in west central Utah. *Econ. Geol.* 79, 266–283.
- Page, R.W., Laing, W.P., 1992. Felsic metavolcanic rocks related to the Broken Hill Pb–Zn–Ag orebody, Australia: geology, depositional age, and timing of high-grade metamorphism. *Econ. Geol.* 87, 2138–2168.
- Parr, J.M., Stevens, B.P.J., Carr, G.R., 2003. Timing of multiple hydrothermal events in the Broken Hill terrane: Evidence from lead isotopes. In: Peljo, M. (compiler), Broken Hill Exploration Initiative: Abst. July 2003 Conf., Geoscience Australia Record 2003/13, pp. 126–129.
- Pauwels, H., Baubron, J.C., Freyssinet, P., Chesneau, M., 1999. Sorption of metallic compounds on activated carbon: application to exploration for concealed deposits in southern Spain. *J. Geochem. Explor.* 66, 115–133.
- Pauwels, H., Tercier-Waeber, M.-L., Arenas, M., Castroviejo, Y., Deschamps, Y., Lassin, A., Graziottin, F., Elorza, F.-J., 2002. Chemical characteristics of groundwater around two massive sulphide deposits in an area of previous mining contamination, Iberian Pyrite Belt, Spain. *J. Geochem. Explor.* 75, 17–41.
- Pidgeon, R.T., 1967. A rubidium–strontium geochronological study of the Willyama Complex, Broken Hill, Australia. *J. Petrol.* 8, 283–324.
- Preiss, W.V., 2000. The Adelaide Geosyncline of South Australia and its significance in Neoproterozoic continental reconstruction. *Precamb. Res.* 100, 21–63.
- Sader, J.A., Leybourne, M.I., McClenaghan, M.B., Hamilton, K., Robertson, K., 2003. Groundwater interaction with kimberlites – A geochemical investigation in northeastern Ontario. *Explore (Newslett. Assoc. Explor. Geochemists)* 118, 1–4.
- Shirliff, G., 1998. Massive gypsum, ferricretes and regolith landform mapping of western Balaclava, Broken Hill, NSW. Honours Thesis, Cooperative Research Centre for Landscape Evolution and Mineral Exploration (CRC LEME), Univ. Canberra.
- Stevens, B.P.J., 1980. A guide to the stratigraphy and mineralization of the Broken Hill Block. *New South Wales Geol. Surv. Records* 20.
- Stevens, B.P.J., 1986. Post depositional history of the Willyama Supergroup in the Broken Hill Block, NSW. *Aust. J. Earth Sci.* 33, 73–98.
- Stevens, B.P.J., Barnes, R.G., Brown, R.E., Stroud, W.J., Willis, I.L., 1988. The Willyama Supergroup in the Broken Hill and Euriovie Blocks, New South Wales. *Precamb. Res.* 40/41, 297–327.
- Stevens, B.P.J., Burton, G.R., 1998. The Early to Late Proterozoic Broken Hill Province, New South Wales. *AGSO J. Aust. Geol. Geophys.* 17, 75–86.
- Stevens, B.P.J., Corbett, G.J., 1993. The Redan Geophysical Zone, part of the Willyama Supergroup? Broken Hill, Australia. *Aust. J. Earth Sci.* 40, 319–338.
- Taufen, P.M., 1997. Ground waters and surface waters in exploration geochemical surveys. *Exploration Geochemistry*. In: Gubins, A.G. (Ed), *Proceedings of Exploration 97: 4th Decennial Internat. Conf. Mineral Exploration*, pp. 271–284.
- Thode, H.G., Monster, J., 1965. Sulphur-isotope geochemistry of petroleum, evaporites and ancient seas. *Am. Assoc. Petrol. Geol. Mem.* 4, 367–377.
- Tonui, E., Caritat, P. de, Leyh, W., 2003. Geochemical signatures of mineralization in weathered sediments and bedrock, Thunderdome prospect, Broken Hill, western New South Wales, Australia: Implications for mineral exploration under cover. *Geochem. Explor. Environ. Anal.* 3, 263–280.
- Tukey, J.W., 1977. *Exploratory Data Analysis*. Addison-Wesley, Reading, UK.
- Ueda, A., Krouse, H.R., 1986. Direct conversion of sulphide and sulphate minerals into  $\text{SO}_2$  for isotope analyses. *Geochem. J.* 20, 209–212.
- Ullman, W.J., Collerson, K.D., 1994. The Sr-isotope record of late Quaternary hydrologic changes around Lake Frome, South Australia. *Aust. J. Earth Sci.* 41, 37–45.
- Veizer, J., 1989. Strontium isotopes in seawater through time. *Ann. Rev. Earth Planet. Sci.* 17, 141–167.

- Velleman, P.F., Hoaglin, D.C., 1981. Applications, Basics and Computing of Exploratory Data Analysis. Duxbury Press, Boston, USA.
- Wakshal, E., Nielsen, H., 1982. Variations of  $\delta^{34}\text{S}(\text{SO}_4)$ ,  $\delta^{18}\text{O}(\text{H}_2\text{O})$  and  $\text{Cl}/\text{SO}_4$  ratio in rainwater over northern Israel, from the Mediterranean Coast to Jordan Rift Valley and Golan Heights. *Earth Planet. Sci. Lett.* 61, 272–282.
- Waring, C.L., Andrew, A.S., Ewers, G.R., 1998. Use of O, C, and S stable isotopes in regional mineral exploration. *AGSO J. Aust. Geol. Geophys.* 17, 301–313.
- Whitford, D.J., Andrew, A.S., Carr, G.R., Giblin, A.M., 1998. Application of isotope studies of Australian groundwaters to mineral exploration: the Abra Prospect, Western Australia. In: Arehart, G.B., Hulston, J.R. (Eds.), *Water–Rock Interaction Proceedings of the 9th International Symposium on Water–rock Interaction* (Taupo New Zealand, 30 March–3 April 1998). AA Balkema, Rotterdam, pp. 583–586.
- Willis, I.L., Brown, R.E., Stroud, W.J., Stevens, B.P.J., 1983. The Early Proterozoic Willyama Supergroup: stratigraphic subdivision and interpretation of high to low-grade metamorphic rocks in the Broken Hill Block, New South Wales. *J. Geol. Soc. Aust.* 30, 195–224.
- Yanagisawa, F., Sakai, H., 1983. Thermal decomposition of barium sulfate–vanadium pentoxide–silica glass mixtures for preparation of sulfur dioxide in sulfur isotope ratio measurements. *Anal. Chem.* 55, 985–987.

# Groundwater composition in the Broken Hill area: salinity and mineral exploration applications

Patrice de Caritat<sup>1</sup>, Dirk Kirste<sup>1</sup>, Rod Dann<sup>2</sup> and Ian Hutcheon<sup>3,\*</sup>

<sup>1</sup>Cooperative Research Centre for Landscape Environments & Mineral Exploration (CRC LEME)  
c/- Geoscience Australia, GPO Box 378, Canberra, ACT 2601, Australia

<sup>2</sup>CRC LEME, c/- University of Canberra, Canberra, ACT 2601, Australia

<sup>3</sup>Department of Geology & Geophysics, University of Calgary, Calgary, Alberta T2N 1N4, Canada

\*Current address until July 2002: CRC LEME, c/- Geoscience Australia

## INTRODUCTION

Groundwater samples were collected from bores and wells in an area straddling the NSW-SA border (Figure 1). This area encompasses hills from the Barrier Ranges (in the east) and from the Olary Ranges (south), the foothills of the Flinders Ranges (west) and extensive sediment-covered plains of the Callabonna Sub-basin (centre and north), and of the Murray Basin (southeast). The area is characterised by pastoral, localised agricultural and mining activities, all of which require an adequate supply of reasonably fresh water, which, in this semi-arid region, must often be found in the subsurface. This study aims to investigate the processes that control changes in groundwater chemistry as it flows from recharge zones in the hills to discharge zones in the low-lying lakes and salt pans. This information can be used for mineral exploration (dispersion of signatures from concealed mineral deposits) or for environmental and pastoral applications (sources of salt, stock water quality). The present report focuses on the Callabonna Sub-basin part of the study area.

## MATERIALS AND METHODS

A total of 117 groundwater samples were collected in a 130 by 210 km area extending approximately from 31° to 32° south and from 139° to 142° east. Virtually every pastoral and exploration bore or well that could be located, and that had not collapsed, was sampled. Sampling was performed with established windmills, electrical or mechanical pumps, or using a transportable compressed-air sampling pump. The pumped water was monitored for up to several hours of pumping (depending on pumping rate) until the pH, temperature (T), electrical conductivity (EC), redox potential (Eh) and dissolved oxygen (DO) showed stable values representing fresh groundwater conditions.

Immediately upon collection, a number of additional field analyses (alkalinity, Fe<sup>2+</sup>, S<sup>2-</sup>) and preservation procedures (filtration, acidification, etc.) were carried out. At each point, seven subsamples were taken routinely for analysis of:

- major and trace elements (by inductively coupled plasma-atomic emission spectrometry or inductively coupled plasma-mass spectrometry),
- anions (ion chromatography),
- Au (instrumental neutron activation analysis),
- F/I (ion specific electrodes),
- <sup>18</sup>O/<sup>2</sup>H of water (mass spectrometry),
- <sup>13</sup>C of dissolved inorganic carbon (mass spectrometry), and
- <sup>34</sup>S of dissolved sulfate (mass spectrometry).

Additional analyses (<sup>36</sup>Cl, <sup>87/86</sup>Sr, and Pb isotopes) have been performed on a limited number of samples.

## RESULTS

The groundwaters are dominantly brackish (total dissolved solids (TDS) from 325 to 25,413 mg/L); they have a circum-neutral pH (from 6.4 to 8.3) and a low temperature (from 19 to 31°C) (Caritat et al., 2001). Groundwater samples were divided into three groups: *recharge*, *margins* and *basin* waters. A fourth group, *palaeochannel*, includes samples from the Yarramba palaeochannel, which have distinct compositions. The recharge group can be further subdivided into the *Barrier*, *Olary* and *Flinders* groups to reflect the location around the basin (Figure 2). The Piper diagram on Figure 3 shows that the main water types are Na-Cl-SO<sub>4</sub>, Na-Cl and Na-Mg-Cl-SO<sub>4</sub>. Figure 4 shows the distribution of chlorine concentrations in groundwater.

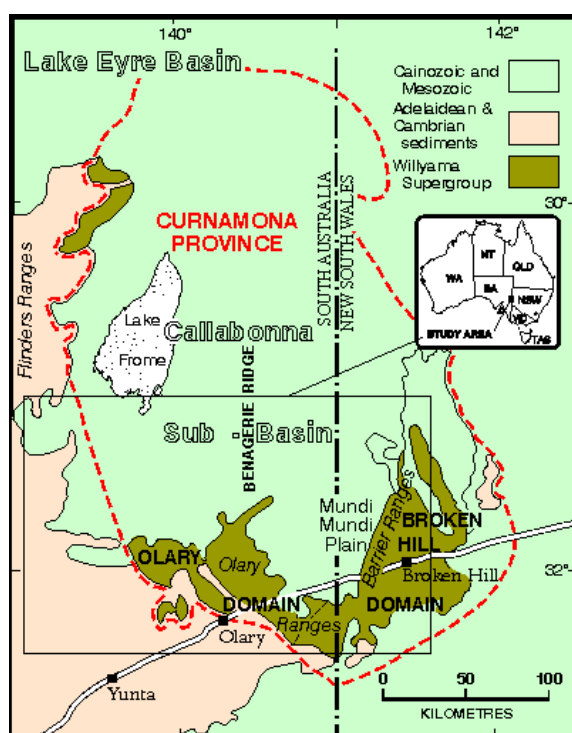


**FIGURE 1** Location map of the study area showing main geological subdivisions.



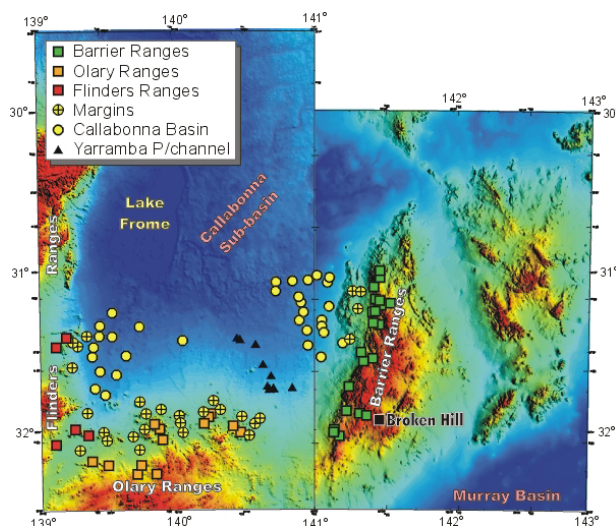


**FIGURE 2** Digital elevation model of the study area showing location of groundwater samples by groundwater group.

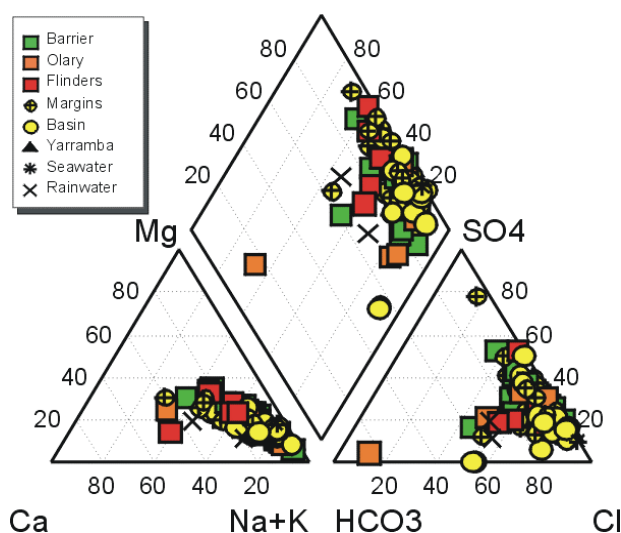


**FIGURE 3** Piper diagram showing the major ion composition of the main groundwater groups.

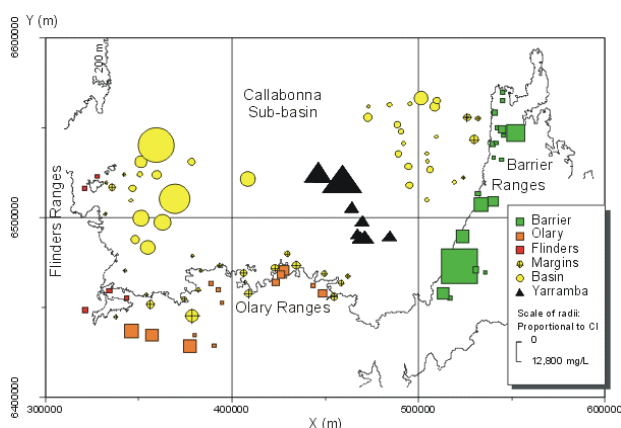


**FIGURE 4** Map of Cl concentration in groundwater (symbol sizes are proportional to Cl concentration), overlain on 200 m (asl) elevation contour.

Overall composition ranges of selected parameters for the different groups are given in Table 1. Examination of these results shows some interesting patterns. Firstly, the classical model of fresh water recharging the aquifer in the upland parts of the catchments and becoming increasingly saline with distance clearly is not operational here. Groundwater in the shallow aquifers in the hills (median EC values of 7150, 9510 and 5970 mS/cm for the three recharge areas) is nearly as saline as the basin water (median 10,430 mS/cm), but the palaeochannel has the greatest salinities (median 16,550 and maximum 38,600 mS/cm). The maximum EC values from the Barrier and Olary Ranges (34,900 and 35,300 mS/cm) are twice as high as those from the Callabonna Sub-basin (17,690 mS/cm).

Secondly, the recharge areas have quite variable salinities, with the Flinders Ranges waters being much fresher than the Barrier Ranges and especially the Olary Ranges waters (maximum EC value for Flinders is less than the median value of either the Barrier or Olary group). Median EC of the margins water (8010 mS/cm) is similar to the median Barrier and Olary Ranges water, but the maximum EC (18,360 mS/cm) is much less than for the Barrier or Olary Ranges water.

Group	EC μS/cm	Na mg/L	Mg mg/L	Cl mg/L	SO <sub>4</sub> mg/L
Western Barrier Ranges					
Min	2380	225	53.3	332	201
Med	7150	1290	246	1755	1465
Max	34900	6810	1250	12000	4150
Northern Olary Ranges					
Min	2490	45.6	19.5	28.9	13.9
Med	9510	1630	210	2450	870
Max	35300	3272	556	4749	2855
Eastern Flinders Ranges					
Min	2390	343	70	446	204
Med	5970	652	127	1119	487
Max	6930	790	295	1696	1793
Basin Margins					
Min	1871	206	47.6	247	102
Med	8010	1375	195	1900	1000
Max	18360	3046	488	5306	2220
Callabonna Sub-basin					
Min	575	333	29.7	515	0.25
Med	10430	1540	157	2260	850
Max	17690	7604	785	11830	3774
Yarramba Palaeochannel					
Min	14460	2690	258	4500	1290
Med	16550	2900	364	4700	1510
Max	38600	7400	961	12800	2350

**TABLE 1** Minimum, median and maximum values for electrical conductivity (μS/cm) and Na, Mg, Cl and SO<sub>4</sub> concentrations (mg/L) for the various groundwater groups.



Thirdly, the recharge waters show quite a range of composition in terms of major cations and anions. However, the Ca/Mg ratio of these waters is fairly constant, irrespective of sodium concentration, resulting in a linear trend on the Piper diagram (Figure 3). Anion relative concentrations vary in a less systematic fashion, but many do occur along a Cl-SO<sub>4</sub> trend, with some samples deviating from it due to higher HCO<sub>3</sub> concentrations. Median SO<sub>4</sub> concentration of the Barrier Ranges (1465 mg/L) is similar to the Yarramba palaeochannel (1510 mg/L), whilst for the other major cations and anions, the highest median value by far always is found in the palaeochannel.

Fourthly, the distribution of salinity or major cations or anions shows three distinct areas with generally high salinities in groundwater: the Barrier Ranges, the Yarramba palaeochannel and the westernmost part of the Callabonna Sub-basin. This will have consequences in terms of water usage for pastoralists, and water quality for other applications (e.g., mining).

## DISCUSSION

### Salinity and hydrogeology

Ion, ion ratio (Figure 5) and stable isotope (<sup>18</sup>O/<sup>2</sup>H) diagrams show that evaporation is a major process taking place in the recharge areas. Water-rock interaction (mineral dissolution, cation exchange) plays a secondary, but nonetheless important, role in governing water composition. The composition of groundwater from deeper in the basin is controlled to a large extent by evaporation (during recharge), mixing and water-rock interaction. Sodium and chlorine are the dominant ions responsible for the salinity of the groundwater, but magnesium and SO<sub>4</sub> are locally important contributors as well.

There appears to be a poor connectivity between the upland areas and the deep basin waters, suggesting the existence of a complex hydrologic system (Figure 6). This system is characterised by distinct aquifers in the elevated areas (unconfined, perched alluvial aquifers in valleys overlying fractured bedrock aquifers) and under

the low-relief plains (confined porous sedimentary aquifers) (Dann, 2001). The upland aquifers are more dynamic and responsive to climate inputs (floods/droughts); the basin aquifers are relatively isolated from the upland aquifers and from the surface, and are more sluggish.

### Mineral exploration

Groundwater, by flowing in the subsurface and interacting with the mineral assemblages of the rocks making up the aquifers, has the potential to acquire and retain a chemical and/or isotopic signature that characterises the minerals encountered. If this signature can be detected and traced back to its source, groundwater can be used as a geochemical sampling medium, or 'vector to mineralisation'. In this study, excess sulphur (Sxs) has been calculated by subtracting the effects of evaporation and gypsum dissolution from the total sulphur content in groundwater (SO<sub>4</sub> and S<sup>2-</sup>),

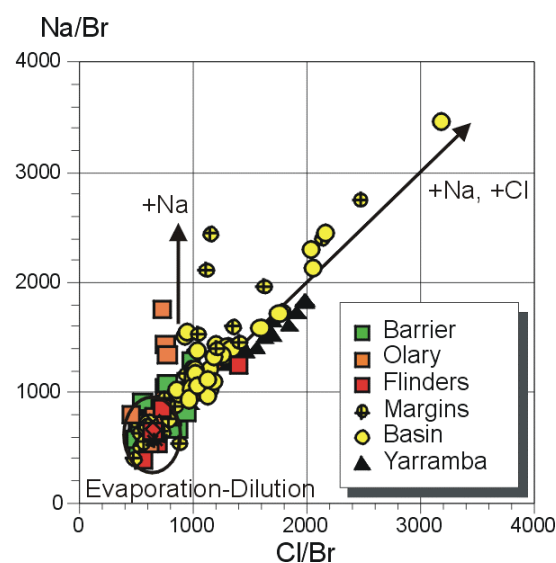


**FIGURE 5** Na/Br versus Cl/Br diagram (molar ratios) showing the evaporation-dilution field (low ratios) characteristic of most recharge waters, as well as trends of Na and Cl addition (mixing) and Na addition only (water-rock interaction).

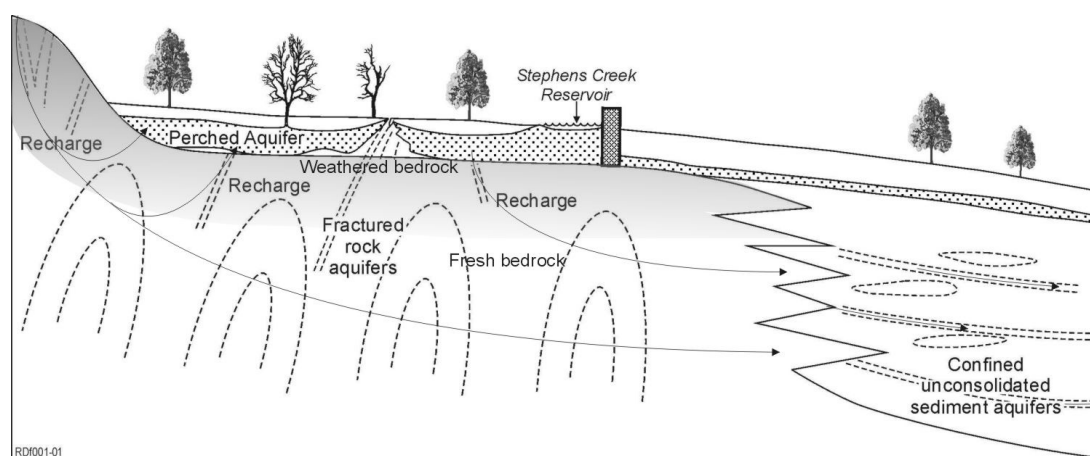


**FIGURE 6** Conceptual diagram of the aquifer systems where the outcropping Broken Hill Domain disappears under the sedimentary cover of adjacent basins, showing the three aquifer systems and possible groundwater flowpaths (after Dann, 2001).

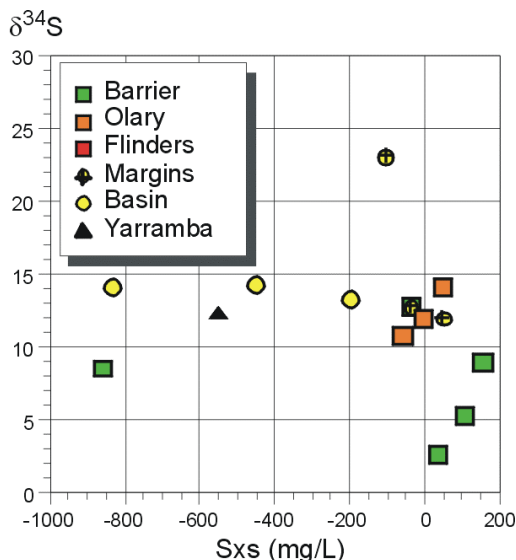


**FIGURE 7**  $\delta^{34}\text{S}$  of dissolved  $\text{SO}_4$  (‰ CDT) versus excess S ( $S_{xs}$ , mg/L, see text) diagram showing that those groundwaters with the lowest  $\delta^{34}\text{S}$  also have the highest excess S.

as a simple proxy for targeting groundwaters that may have oxidised/dissolved buried sulphide mineralisation. Sulphur isotopes, performed here on a selected number of samples only, is also a powerful method of detecting samples that may have interacted with sulphides in the subsurface (Figure 7), because Broken-Hill Type mineralisation has a distinctively low  $\delta^{34}\text{S}$  signature compared to other contributions (e.g., marine aerosols). Finally, lead isotopes also are very useful as they retain the signature of any orebody they may have originated from, thus providing a direct link to specific types of mineralisation. The combination of multiple chemical and isotopic tracers for detecting mineral deposits under cover appears to be the most promising approach.

## CONCLUSIONS

Detailed geochemical characterisation of groundwater in the semi-arid Broken Hill region has been carried out. Major element, trace element and isotope determinations allow recognition of the processes that control the composition of the groundwater. These include evaporation, mixing and water-rock interaction.

Of these, evaporation is the most important control on groundwater salinity in the recharge areas. The hydrology of the basin margins is a complex system of adjoining unconfined alluvial aquifers, fractured bedrock aquifers and large, probably stacked, confined basin aquifers. Aquifers in the upland areas (alluvial and bedrock) are more dynamic and responsive to climate events; aquifers in the basin areas are more sluggish and poorly connected to the upland systems. During its interaction with relatively fresh bedrock minerals, the groundwater acquires particular elemental and isotopic signatures. Results can be used in salinity management (major elements, O, H and Cl isotopes) and in mineral exploration (trace elements, excess S, S isotopes and Pb isotopes).

## ACKNOWLEDGMENTS

CRC LEME is funded under the Australian Government Cooperative Research Centres Program. Colleagues and students from LEME contributed to stimulating discussions. We are particularly thankful to land leaseholders and mineral exploration companies for access to the bores and permission to sample groundwater. We are grateful to Anita Andrew and Graham Carr (CSIRO), Ian Cartwright (Monash University), Richard Cresswell (BRS), Frank Krikowa (CRC LEME/University of Canberra), Eleanor Laing (BRS), Dale Longman (CSIRO) and Malcolm McCulloch (ANU) for analysing the samples and for discussions. Patrice de Caritat and Dirk Kirste publish with permission from the Chief Executive Officer, Geoscience Australia.

## REFERENCES

- CARITAT, P. de, LAVITT, N. & KIRSTE, D., 2001. Groundwater geochemistry in the Broken Hill region, Australia. In: CIDU, R. (Ed), Proceedings of the Tenth International Symposium on Water-Rock Interaction WRI-10 (Villasimius, Italy, 10-15 June 2001), A.A. Balkema Publishers, Swets & Zeitlinger, Lisse, 1, 489-492.
- DANN, R., 2001. Hydrogeochemistry and biogeochemistry in the Stephens Creek Catchment, Broken Hill, New South Wales. Honours Thesis, Unpublished, CRC LEME, University of Canberra.

# The Western Mineralisation – Rasp Mine

Pascal Blampain and Ian Plimer

*CBH Resources Ltd, Level 3, 2 Elizabeth Plaza, North Sydney, NSW 2060,  
Australia*

[pascalblampain@cbhresources.com.au](mailto:pascalblampain@cbhresources.com.au)

---

## Geology of CML7

CML7 contains up to 40 m of waste rock and tailings covering outcrops. Weathering is to a depth of 30-50 m, the Zinc Lodes are weathered to a depth of 30 m and the Lead Lodes are selectively weathered to a depth of 120 m. Exposure is restricted to a few remnant outcrops in the Kintore, BHP, Block 14 and Blackwood Open Pits and the CML7 geological map has been compiled from an 1887 topographic map, the map of Andrews (1922), mapping of outcrop before CML7 was covered with waste rock, remnant outcrops and open pits.

Measurement of lithological packages, graded bedding and bedding-schistosity relationships in oriented diamond drill holes and mapping in the Kintore and Block 14 Open Pits shows that the Zinc Lodes on CML7 are on the western limb on an inverted  $F_1$  nappe and that the Lead Lodes are on the limb of an inverted  $F_1$  nappe and in the hinge of a south- and north-plunging  $F_2$  Antiform (Broken Hill Antiform). Coplanar with the axis of the  $F_2$  antiform are  $S_2$  and  $S_3$  axial plane sulphide projections and the Main Lode Shear, a high metamorphic grade shear zone formed in  $D_{2/3}$  and within which the No 2 Lens and No 3 Lens have been transposed.  $F_3$  folds plunge both north and south and the Main Lode Shear have been deformed by easterly- and westerly-plunging open small  $F_4$  folds. The dominant structure on CML7 is  $F_2$ . The Main Lode Shear is transgressed by high-grade shear zones (e.g. Thompson Shear, van den Heyden and Edgecombe, 1990) and, in Block 14 Open Cut, is transgressed by retrograde shear zones of unknown age. In proximity to the Lead Lodes, the Main Lode Shear bifurcates into retrograde shear zones of unknown age and is pseudomorphed by retrograde assemblages of unknown age along strike in Kintore Open Pit.

The gross structure of CML7 is in accord with that published by Laing *et al.* (1978). However, the structure within 20 m of the Lead Lodes is unrelated to the regional structure and probably reflects the extreme competency differences between galena-rich and the enclosing silicate rocks. Until 2005, the geology of the area immediately to the east of the Broken Hill orebody was known from the Andrews (1922) map, a few diamond drill holes and remnant outcrop. Eastward diamond drilling in 2005 has shown an upward-facing repetition of the stratigraphy from the top of the Broken Hill Group to the top of the Thackaringa Group thereby confirming the Laing *et al.* (1978) position of the Broken Hill Antiform.

On CML7, Unit 3.10 was rarely intersected in drilling and comprised foliated felsic gneiss equivalent to the Rasp Ridge Gneiss. Unit 3.10 crops out west and east of CML7. In places, the foliated felsic gneiss contains swathes and schlieren of sillimanite. The contact between Unit 3.10 and Unit 4.1/4.3 is sheared and the structural style and metamorphic grade are unchanged across the lithological boundary. Units 4.1 and 4.3 comprise well-bedded psammopelitic and psammitic metasediment sequences and Unit 4.4 is a distinctive sequence comprising psammopelitic metasediments and amphibolite veined by garnet which grades into garnet amphibolite which in turn grades into a foliated feldspar-quartz-garnet-biotite rock, locally known as "Potosi Gneiss" (Main *et al.*, 1983). The amphibolite is of tholeiitic basaltic composition and



commonly has a sharp garnetised upper and lower contact and associated with the amphibolite are grains, stringers, veins and pods of pyrrhotite, pyrrhotite-chalcopryrite, sphalerite and galena. Minor layer-parallel horizons of coarse grained garnet-biotite are associated with amphibolite and are probably altered mafic tuffs. Unit 4.5 is dominantly a psammitic unit with minor psammopelite and pelite layers, common bedding and graded bedding and, towards the top of the Unit, minor lode horizons comprising blue quartz  $\pm$  ferroan gahnite  $\pm$  manganoan almandine  $\pm$  pyrrhotite  $\pm$  chalcopryrite  $\pm$  sphalerite  $\pm$  galena. In places, the lode horizon is concordant with  $S_0/S_1$ , whereas in other places it is discordant and replaces metasediments.

A massive pelite (Unit 4.6) with rare bedding and interbedded psammopelite and psammite is used as a stratigraphic marker horizon in drilling on CML7. However, Unit 4.6 is not present in the southern segment of CML7 (although possibly occurs at depth) and is replaced by a thinner facies equivalent comprising a faintly bedded sillimanite-feldspar-biotite pelite. In places, on the south of CML7, Unit 4.6 is replaced by a spotted garnet psammopelite. The thinnest segments of Unit 4.6 are associated with the thickest development of sulphide rocks. Unit 4.6 is black (rarely dominantly white) and comprises crenulated elongate bundles of  $S_1$  sillimanite, crenulated  $S_1$  biotite, K feldspar and rotated disarticulated almandine porphyroblasts up to 4 cm in size about which  $S_2$  sillimanite and biotite are wrapped. In places, Unit 4.6 is cut by Potosi Gneiss (foliated garnet-plagioclase gneiss) and usually drill intersections of Unit 4.6 intersected one to three 5-20 cm thick garnet horizons towards its stratigraphic base. The domination of psammite and common occurrence of graded bedding in Units 4.5 and 4.7, which envelops Unit 4.6, suggests that Unit 4.6 was originally shale formed during a low energy sedimentation phase between periods of high rates of clastic sedimentation.

Unit 4.7 dominantly comprises poorly bedded psammopelitic and psammitic metasediments with rare  $S_1$  foliated garnet-plagioclase gneiss at the base of Unit 4.7, a spotted psammopelite and quartz-gahnite and quartz-garnet rocks. In places,  $S_1$  is crenulated by  $S_2$ . The metasediment sequence in Unit 4.7 is thickening upwards with the Broken Hill orebodies present in the highest energy part of the metasediment sequence. Within Unit 4.7 is a pelite of similar appearance to Unit 4.6 although it contains more K feldspar and less sillimanite than the Unit 4.6 pelite. The stratigraphic relationships of this pelite with the dominant psammites and psammopelites of Unit 4.7 are unclear. Although amphibolite is present in Unit 4.7 elsewhere at Broken Hill (Haydon and McConachy, 1987), it has not been observed in Unit 4.7 on CML7 and Unit 4.4 amphibolite deep on the western part of CML7 is correlated with magnetic amphibolite on the eastern part of CML7. However, cm thick horizons of garnet-biotite in Unit 4.7 may have been altered mafic tuff. The lode horizon rocks comprise blue quartz  $\pm$  gahnite  $\pm$  spessartine  $\pm$  pyrrhotite  $\pm$  galena (blue quartz lode and quartz-gahnite rock), plumbian orthoclase pegmatite – quartz  $\pm$  galena  $\pm$  pyrrhotite (green feldspar pegmatite), quartz-spessartine rocks  $\pm$  pyrrhotite  $\pm$  galena  $\pm$  chalcopryrite (quartz-bearing garnetite), garnet  $\pm$  quartz  $\pm$  chalcopryrite  $\pm$  galena  $\pm$  löllingite  $\pm$  tetrahedrite (garnetite) and sulphide rocks. Lode horizon rocks occur in proximity to massive sulphide rocks.

The foliated garnet-plagioclase gneiss contains minor pegmatites and pygmatic veins of pegmatite composition suggesting formation of axial plane  $F_1$  pegmatites. Both the  $F_1$  pegmatites and  $S_1$  have been folded by  $F_2$  and a weak  $S_2$  is defined by biotite crenulation and axial plane  $S_2$  pegmatites. Equidimensional garnets, 2-4 mm in size in both the foliated garnet-plagioclase gneiss and the pegmatites are rimmed by biotite. The Potosi Gneiss occurs in both Units 4.4 and 4.7 and, in Unit 4.7, is a local name for a foliated garnet-plagioclase-K feldspar-biotite-quartz gneiss with abundant small garnet porphyroblasts both in the matrix and pegmatitic segregations. At the stratigraphic upper contact of the Potosi Gneiss is foliated augen feldspar gneiss which may represent early ( $D_1$ ?) shearing along the competency boundary between Potosi Gneiss and metasediments. The K-feldspar: plagioclase ratio of the Potosi Gneiss is variable, as is the garnet content. On CML7, the foliated garnet-plagioclase gneiss is a minor part of Unit 4.7 and occupies at least three distinct stratigraphic positions stratigraphically above the Lead Lodes. It crops out on CML7 as lensoidal masses and has been intersected to the east of the Broken Hill orebodies in the latest program of diamond core drilling. At the termination of lensoidal masses of the foliated garnet-plagioclase gneiss are



quartz-rich rocks and spotted garnet-bearing psammopelites. In the immediate area of the Broken Hill mines, the thinnest horizons of foliated garnet-plagioclase gneiss occur associated with the maximum sulphide rock development and the geochemistry of the foliated garnet-plagioclase gneiss is used as an indicator of proximity to sulphide rocks.

Stevens and Barron (2002) showed that the foliated garnet-plagioclase gneiss of the Hores Gneiss to the north and west of the Broken Hill orebody contains inclusions which they interpret as imperfectly-consolidated sediment rip-up clasts, mass flow cobbles, amygdulites or lithophysae, eutaxitic textures, euhedral feldspar phenocrysts, bipyramidal embayed quartz phenocrysts after  $\beta$ -quartz and calc-silicate ellipsoids. They suggest that the garnet-plagioclase rocks of the Hores Gneiss were submarine lavas, shallow intrusions and/or volcanoclastic deposits. The SHRIMP zircon date of  $1686 \pm 3$  Ma (Page et al., 2000) dates the supracrustal rocks at the top of the Broken Hill Group which is the stratigraphic position of the Broken Hill orebody, thereby constraining the age of the Broken Hill orebody. The thin foliated garnet-plagioclase gneiss of Stevens and Barron (2002) occurs between Units 4.6 and 4.8, is interpreted as Unit 4.7 and this volcanoclastic mass to the north and west of Broken Hill is the strike equivalent of the thick metasediment-dominated Unit 4.7 in the Broken Hill mines area.

In many places on CML7, the foliated garnet-plagioclase gneiss grades transverse to  $S_1/S_0$  into feldspathic psammite and psammopelitic metasediments. In Unit 4.7, there was no gradation into amphibolite as is present in Unit 4.4. Feldspathic psammite and psammopelite also contain equidimensional garnet porphyroblasts, 2-4 mm in size, and rimmed by biotite. There is nomenclature confusion in the literature as to what constitutes Potosi Gneiss and most commonly it has been used to describe a spotted foliated to weakly foliated felsic rock with spots defined by 2-4 mm sized equidimensional garnets rimmed by biotite. However on CML7, such spotted rocks are transgressive to stratigraphy and hence the occurrence of garnet-bearing feldspathic psammite and psammopelite and garnet-plagioclase gneiss may represent a pre-metamorphic overprint on reactive feldspathic rocks. On CML7, the Potosi Gneiss is mapped as a quartz-plagioclase-K feldspar-garnet-biotite gneiss with biotite-rimmed garnet porphyroblasts. Hence elsewhere in the Broken Hill field, what is termed in the literature as Potosi Gneiss proximal to the Broken Hill mines may be an alteration type rather than a lithological horizon coplanar with other strata in Unit 4.7 (i.e. Hores Gneiss). There is a gradation from the garnet-bearing feldspathic psammite and the garnet-plagioclase gneiss into a blue quartz-garnet  $\pm$  biotite  $\pm$  pyrrhotite  $\pm$  chalcopyrite rock suggesting replacement of high metamorphic grade garnet-bearing rocks by blue quartz.

On CML7, the complete section of the Zinc Lodes (C Lode, B Lode, A Lode and 1 Lens) and the Lead Lodes (2 Lens and 3 Lens) sulphide rocks has been intersected in recent diamond core drilling. Each sulphide rock mass at Broken Hill is spatially separated by metasediments and has a characteristic chemistry and hence a characteristic mineralogy. Most of the sulphide rocks on CML7 display a cataclastic texture and contain angular to rounded clasts of wall rocks including bleached pelite and psammite, quartz, plumbian orthoclase, garnetite, garnet quartzite, quartz-gahnite rocks and other sulphide rocks.

The stratigraphically lowest sulphide mass (C Lode) comprises quartz-gahnite-sphalerite-galena-pyrrhotite-garnet. C Lode comprises transgressive masses, layer parallel masses,  $S_2$  axial plane masses and cataclastic ore along  $S_0/S_1$ ,  $S_2$  and  $S_3$ . Minor quartz-bearing garnetites are associated with C Lode and there is a halo of spotted garnet-bearing psammopelite associated with C Lode. B Lode comprises quartz-sphalerite-galena-garnet-gahnite-pyrrhotite-chalcopyrite associated with quartz-bearing garnetite. Most of B Lode is on the westerly-dipping limb of an  $F_2$  antiform and, in the hinge of the antiform, B Lode is a cataclastic high metal content ore with bleached clasts of angular wall rocks. The edge of B Lode is characterised by sheared retrogressed pelites partially replaced by cataclastic pyrrhotite-chalcopyrite. The up-dip extensions of A Lode have been intersected in diamond core drilling on CML7 and these comprise quartz-bearing garnetite with minor pyrrhotite, galena and gahnite and blue quartz-gahnite-garnet-pyrrhotite rocks. Garnet rocks equivalent to A Lode are replaced by blue quartz-gahnite rocks. The down dip extensions of A Lode occur within the Western Mineralisation as



quartz-sphalerite-galena-hedenbergite-garnet  $\pm$  rhodonite rocks. The Eastern Mineralisation comprises quartz-orange garnet-hedenbergite with associated cataclastic massive sulphide ore and quartz-galena  $\pm$  chalcopyrite-sphalerite veins. The No 1 Lens has not been intersected on CML7 and stratigraphic equivalents of No 1 Lens are characterised by blue quartz-gahnite-garnet rocks.

On CML7 there has been extensive mining of No 2 Lens. Exposures in the Kintore and Block 14 Open Pits remain and drill intersections comprise galena-sphalerite-calcite-fluorite-fluorapatite  $\pm$  garnet. The stratigraphically highest sulphide rock, No 3 Lens, is exposed in Block 14 Open Pit and comprises a quartz-galena-sphalerite-rhodonite  $\pm$  garnet rock. In Block 14 Open Pit, the Lead Lodes occur in a downward-facing  $F_1$  limb that has been folded into a S-plunging  $F_2$  antiform and N- and S-plunging  $F_3$  antiforms. The Main Lode Shear is coplanar with  $S_{2/3}$  and No 3 Lens on the eastern limb of the Broken Hill Antiform has been dragged up into the Main Lode Shear. Axial plane to  $F_{2/3}$  are fans of droppers of cataclastic galena-rich ore derived from No 3 Lens. The  $F_2$  and  $F_3$  folds and the Main Lode Shear have been folded by  $D_4$  to produce E- and W-plunging folds and a cataclastic mass of No 3 Lens has been injected along  $S_4$  and transgresses the No 2 Lens in Block 14 Open Pit.

On CML7, stratigraphically above the sulphide rocks are psammite and psammopelitic metasediments, foliated garnet-plagioclase gneiss and a massive pelite horizon (Unit 4.8). It appears that Unit 4.8 is discontinuous; it has not been intersected by CBH in drilling on CML7 but appears in the drill core from CRA drilling in the 1980s. It is similar in appearance to Unit 4.6 although it contains less sillimanite and more K feldspar than Unit 4.6. Unit 4.8 comprises abundant crenulated biotite, disarticulated rotated almandine garnet porphyroblasts, crenulated sillimanite and K-feldspar and contains minor magnetite and laminated garnet-quartz  $\pm$  magnetite horizons.

Drilling of the Western Mineralisation has shown that Unit 4.7 (including the sulphide rocks) has been transgressed by N- and NW-trending epidotised tholeiitic dolerite dykes. The dykes show marginal alteration to biotite schist and contain pelitic enclaves altered to biotite.

### The Western Mineralisation

The Western Mineralisation has been correlated with A Lode (Haydon and McConachy, 1987), B Lode (Gentle, 1968) and A, B & C lodes (Leyh, 2000). Drilling by CBH suggests that whilst a stratigraphic relationship exists between the Western Mineralisation and the ore lenses associated with the main lode system, the Western Mineralisation is spatially, and probably, chemically separated from the Zinc and Lead Lodes of the main line of lode system. The system is terminated at depth by the Globe Vauxhall Shear Zone where it is repeated as the Centenary Mineralisation. The Centenary Mineralisation however, is located both within the Hores Gneiss (Unit 4.7) and the Freyers Metasediments (Unit 4.5).

Earliest drill records indicate that the Western Mineralisation was identified prior to World War I but, despite a number of drilling campaigns, the zinc-dominant Western Mineralisation was not economically attractive until recent times. Data from previous operators who have drilled and sampled the Western Mineralisation has enabled CBH to calculate a robust global resource of 10mt @ 4.9% Zn, 3.5% Pb and 43g/t Ag over a strike length of some 1.7km. The system remains open along strike and down dip for much of CML7. In particular the main target for extensions to the resource is the northern reverse plunge which mirrors the geometry of the main line of lode.

The dominant host mineral assemblage is blue quartz – gahnite with an increasing garnet content where sulphide content increases. Where the Western Mineralisation is characterised by garnet quartzite, sulphide content is commonly low and dominated by pyrrhotite. Pyrite content is very low with rare chalcopyrite occurring as late stage fracture infill.



Mineralisation style is not dissimilar to that of the main line of lode, where sulphide mineralisation is controlled by stratigraphy with grade controlled by structure. Grade is enhanced at the intersections of fold hinges and associated with transgressive shear zones.

The depletion in chondrite-normalised REE in the Western Mineralisation compared to the main line of lode sulphide rocks suggests a more distal setting for sulphide formation. The system is relatively poor in iron and silver compared with the main line of lode. The lower silver content could reflect depletion during retrograde metamorphism or the general low lead tenor of the Western Mineralisation, the lower iron content more likely reflects the change in composition of an evolving ore fluid.

There is limited mapping of the ore system through four main development drives put in by Broken Hill South during the 1950s and 1960s. This mapping shows marked variability in the orientation of high grade zones, both along strike and between levels. This variable geometry is expected to reflect complex structures that will require close spaced drilling and underground mapping that can then be used to predict the location of similar structures and locate these high grade zones. Safe underground access is currently unavailable and CBH is planning an exploration decline to the existing main underground levels for further geological studies.

### **The Eastern Mineralisation**

Minor historical drilling and limited surface mapping has indicated the presence of mineralisation and lode horizons east of the main lode. The paucity of data and exploration has resulted in difficulty in deriving a realistic geological model that can place this mineralisation into perspective.

More recent drilling by CBH and Normandy and subsequent geological interpretation indicates that mineralisation falls into three separate settings. These include distinct stratigraphic positions, an updip extension of the 3 Lens synform and shear structures associated with transposition of sulphides from the main orebody.

There is sufficient drilling to enable compilation of complete cross sections through the Broken Hill Group rocks on CML7 in few places and unequivocal correlation between the stratigraphic successions either side of the main lode shear remains elusive. Some of the major differences between these sequences that make correlation difficult are the presence of magnetic amphibolite, Potosi Gneiss and metasediments and the absence of the stratigraphic marker Unit 4.6 and its associated banded iron formation that is readily observable in drill core in the west of the lease area. This Eastern Mineralisation and associated package of magnetic rocks has been traced for the entire 3.8km strike extent of CML7 west of the Western Mineralisation.

The cultural aspects of Broken Hill mean that the geology of the Eastern Mineralisation will only be resolved through deep drilling programs as much of the geology has since been obscured by mining waste, dwellings, concrete and tar.

### **Acknowledgements**

Wolfgang Leyh added to knowledge of the Western and Eastern Mineralisation while with Normandy and later with work for CBH. Honours theses by Kate Kitchen and Annette Patchett (both University of Melbourne) added to the geochemical understanding of the Western Mineralisation. John Collier (now Bendigo Mines) was involved in the CBH drilling program and Geoff Scott added sagacious restraint, knowledge and perspective throughout the CML7 investigations.

### **References**

Andrews, E.C., 1922. The geology of the Broken Hill district. *New South Wales Geological Survey, Memoir*, **8**, 432 pp.





- Gentle, L.V., 1968. Geology of the Western Limb and Western Mineralization at Broken Hill South Limited. In: Radmanovich, M., editor, Broken Hill Mines -1968. *Australasian Institute of Mining and Metallurgy, 75<sup>th</sup> Anniversary Edition*, 179-183.
- Haydon, R.C. & McConachy, G.W., 1987. The stratigraphic setting of Pb-Zn-Ag mineralization at Broken Hill. *Economic Geology*, **82**, 826-856.
- Laing W.P., Marjoribanks, R.W. & Rutland, R.W.R., 1978. Structure of the Broken Hill mine area and its significance for the genesis of the orebodies. *Economic Geology*, **73**, 1112-1136.
- Leyh, W.R., 2000. Detailed lithostructural mapping of the Broken Hill type mineralization in the Broken Hill Block, NSW. In: Peljo, M., compiler, Broken Hill Exploration Initiative: abstracts of papers presented at the May 2000 conference in Broken Hill. *Australian Geological Survey Organisation, Record*, **2000/10**, 4-7.
- Main, J.V., Mason, D.O. & Tuckwell, K.D., 1983. The characteristics and interpretation of whole rock geochemical data, Willyama Supergroup, New South Wales – trends towards ore. *Australasian Institute of Mining and Metallurgy, Conference Series*, **12**, 115-131.
- Page, R.W., Stevens, B.P.J., Gibson, G.M. & Conor, C.H.H., 2000. Geochronology of the Willyama Supergroup rocks between Olary and Broken Hill, and comparison to Northern Australia. In: Peljo, M., compiler, Broken Hill Exploration Initiative: abstracts of papers presented at the May 2000 conference in Broken Hill. *Australian Geological Survey Organisation, Record*, **2000/10**, 72-75.
- Stevens, B.P.J. & Barron, L.M., 2002. Volcanic textures in the Palaeoproterozoic Hores Gneiss, Broken Hill, Australia. *Quarterly Notes of the Geological Survey of New South Wales*, **113**, 1-22.
- Van de Heyden, A. & Edgecombe, D.R., 1990. Silver-lead-zinc deposit at South Mine, Broken Hill. In: Hughes, F.E., editor, Geology of the Mineral deposits of Australia and Papua New Guinea. *Australasian Institute of Mining and Metallurgy*, 1073-1077.



# Origin of a vertical lineation in conjugate transcurrent shear-zones at Broken Hill, Australia

P.F. Williams<sup>a,\*</sup>, R.H. Vernon<sup>b</sup>

<sup>a</sup>*Department of Geology, University of New Brunswick, Fredericton, NB Canada, E3B5A3*

<sup>b</sup>*School of Earth Sciences, Macquarie University, Macquarie, NSW 2109, Australia*

## Abstract

Shear-zones at Little Broken Hill are interpreted as conjugate transcurrent structures. They developed before dolerite dyke emplacement in response to N–S horizontal shortening. They were reactivated as conjugate transcurrent structures after dyke emplacement in response to horizontal E–W shortening. Shear-zone deformation was accompanied by retrograde metamorphic conditions for at least the later part of the history. Displacement on the shear-zones was accommodated by coeval deformation within the shear-zone-bound blocks. This deformation involved shear on the pre shear-zone  $S_1$  foliation and resulted in incomplete retrogression of earlier peak metamorphic mineral assemblages. It also resulted in a vertical extension and a component of dip slip on the shear-zones.

A near-vertical stretching-lineation occurs parallel to the intersection of the shear-zones and is interpreted as a localised response to an overall vertical extension. Localisation of the lineation is explained in terms of grain-scale partitioning of deformation mechanisms. In the country rock, vertical extension was achieved by shear on  $S_1$  with very little intragranular deformation. Consequently this deformation failed to produce a lineation. In the shear-zones, where all fabric elements were tending to vertical, the only deformation mechanism available for vertical extension was intragranular deformation, which resulted in a shape fabric, viz the stretching-lineation. Shear within the zones had both horizontal and vertical components parallel to the shear-zone foliation. Because the shear was achievable by slip on the foliation and did not involve intragranular mechanisms, it did not modify the lineation. Late shear-zone movement resulted in local crenulation of the shear-zone foliation about the early-formed stretching-lineation. The result was vertical plunging folds and a more pronounced “stretching” lineation.

It is concluded that stretching-lineations in shear-zones should not be considered indicators of movement direction or of instantaneous or finite strain axes. © 2001 Elsevier Science B.V. All rights reserved.

**Keywords:** shear zones; conjugate; tranpression; deformation mechanisms; lineation

## 1. Introduction

Transcurrent ductile-faults or shear-zones are a major feature of many orogens, and though in tectonic terms their geometry and history may appear quite simple, generally problems exist in relating the structures

observed at various scales to a simple transcurrent movement. We commonly think of faulting in terms of rigid blocks moving relative to one another on brittle failure surfaces or ductile zones. Obviously if the blocks were truly rigid, many faults and shear-zones would be impossible geometrically, but we nevertheless simplify the problem by assuming rigidity and that conclusions are still correct to a first approximation. This is probably true in many situations, but the assumption may obscure

\* Corresponding author. Fax: +1-506-453-5055.

E-mail address: pfw@unb.ca (P.F. Williams).

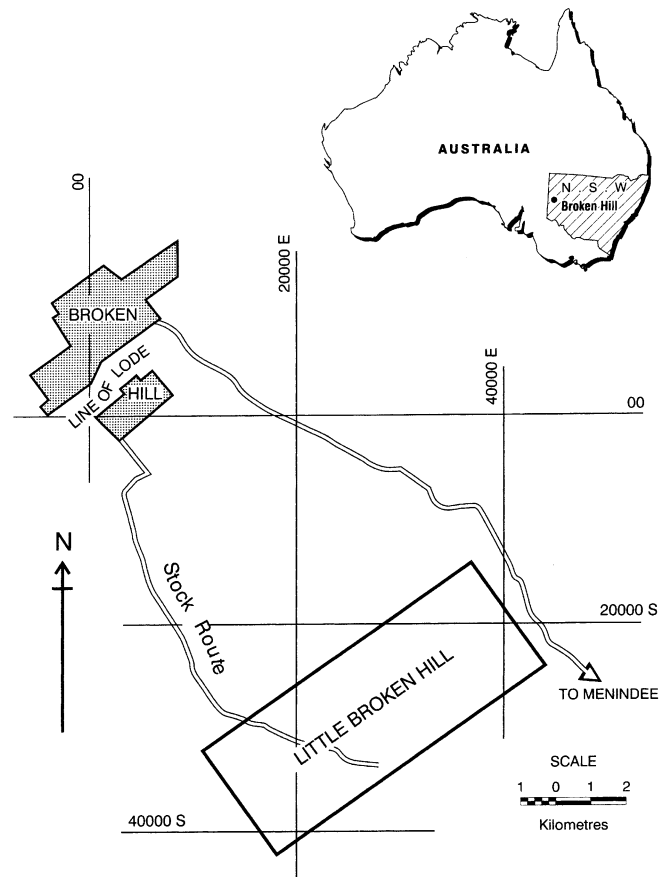


Fig. 1. Map showing location of Little Broken Hill. The Mine Grid on the detailed map is in feet to be consistent with source maps.

some fundamental truths in other situations. In this paper, we look at a shear-zone problem in terms of displacement across the zones and possible strains in the zone-bound blocks.

Many shear-zones that appear to be transcurrent on the basis of sound geological evidence are characterised by a vertical lineation (e.g. Lister and Price, 1978; Hudleston et al., 1988; Robert, 1989; Robin and Cruden, 1994). This may lead to them being interpreted as thrusts that have subsequently been rotated to a steep attitude or simply as steep dip-slip faults. Other examples are characterised by both a vertical and a more spatially restricted horizontal lineation (e.g. Garnett and Brown, 1973; Caron, 1994; Goodwin and Williams, 1996; Lin et al., 1998). In this situation the horizontal lineation is generally confined to a narrow zone or zones within a broader zone

defined by the vertical lineation. All these shear-zones may have had a history of dip-slip, as well as transcurrent movement. However, although in many zones the separation of markers indicates a major transcurrent motion — far larger than could possibly be matched by the dip-slip — the vertical lineation is commonly best developed and most extensive. This fact and the general consistency of the relationships suggest a general explanation, rather than an ad hoc multiple-movement history. Consequently, various writers have attempted to model transcurrent shear-zones in ways compatible with the coeval development of a vertical lineation and these models generally consider the shear-zones to be transpressive. We also propose a transpressive model, but propose shortening in the shear-zone-bound blocks, as well as in the shear-zones. In addition we consider deformation

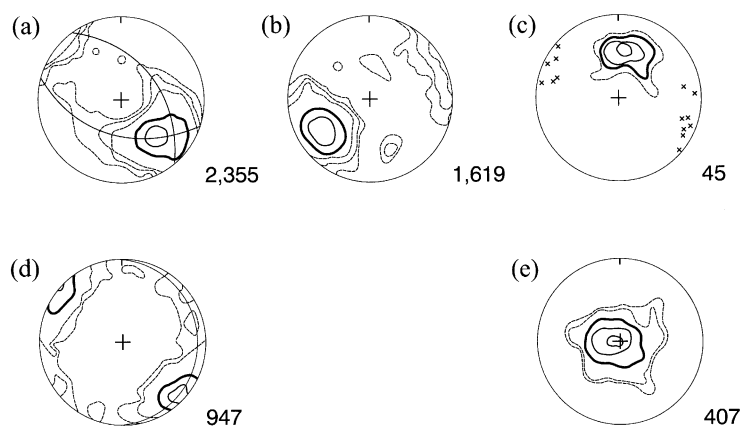


Fig. 2. Orientation diagrams for Little Broken Hill. (a) Poles to  $S_1$ . (b) Sillimanite lineation. (c)  $F_2$  fold hingelines (contoured) and axial surfaces (crosses). (d) Poles to  $S_3$  &  $S_4$  combined. (e) Stretching-lineation. The thick contour in each diagram is 5%/1% area. Dashed contours, in decreasing order from the 5% contour are 2.5, 1.0 and 0.5%/1% area. Solid contours, in increasing order from the 5% contour are 10 and 20%/1% area. Number of contoured data points is shown at bottom right of each diagram. All data plotted on lower hemisphere equal-area nets.

mechanisms and grain-scale strain-path partitioning in order to explain our observations.

We describe a series of ductile shear-zones from the Broken Hill district of Australia, which are dominantly transcurrent, but are characterised by a steeply plunging lineation. “Drag” (Hobbs et al., 1976, p. 306) at the margins of these zones commonly indicates the opposite sense of movement to that indicated by displaced markers and we offer an explanation for this and for the vertical lineation that is consistent with transcurrent motions. Fundamental to our interpretation is the belief that strain-path distribution is heterogeneous and strongly influenced by anisotropy present prior to a given deformation. The basic idea is not new, but we show how it can be applied to this specific example and potentially to other similar situations.

The area described is SE of Broken Hill (Fig. 1) and because of similarity in lithology and mineralisation to Broken Hill, is known locally as Little Broken Hill. Initial structural mapping of the area at 1:1200, concentrating on the mineralised rocks was carried out by one of us (Williams, 1967) and W.A. Brook for Zinc Corporation Ltd. More recently the present authors have carried out detailed structural, micro-structural and petrological work on some of the shear-zones at the northeastern end of the area, particularly around the Rockwell Crush. In this paper we concentrate on the structure and deformational history

associated with the shear-zones which are generally retrogressed relative to the country rock. For a detailed description of the structure and earlier history of the high-grade country rocks the reader is referred to Williams (1967). However, some background knowledge of the high-grade rocks is necessary here and is summarised below.

## 2. Brief summary of the high-grade rocks

The high-grade rocks include sillimanite-bearing schists, “Potosi gneiss” (a feldspar-quartz-biotite-garnet gneiss) and amphibolites. Thin “banded iron formation” (BIF) consisting of magnetite, quartz, garnet, and apatite forms excellent marker horizons. All units are lenticular and elongate parallel to the regional foliation ( $S_1$ ). The latter is defined by transposed layering, differentiated layering axial-planar to intrafolial folds, and a general preferred orientation of all metamorphic minerals. This foliation is probably a product of a progressive deformation involving more than one generation of isoclinal folds. Sillimanite defines a lineation in  $S_1$  and the hinges of folds with  $S_1$  parallel to their axial-surfaces are aligned parallel to the lineation. Throughout the area,  $S_1$  dips moderately and generally northwesterly (Fig. 2a) and the  $F_1$  sillimanite lineation plunges shallowly southwesterly (Fig. 2b).

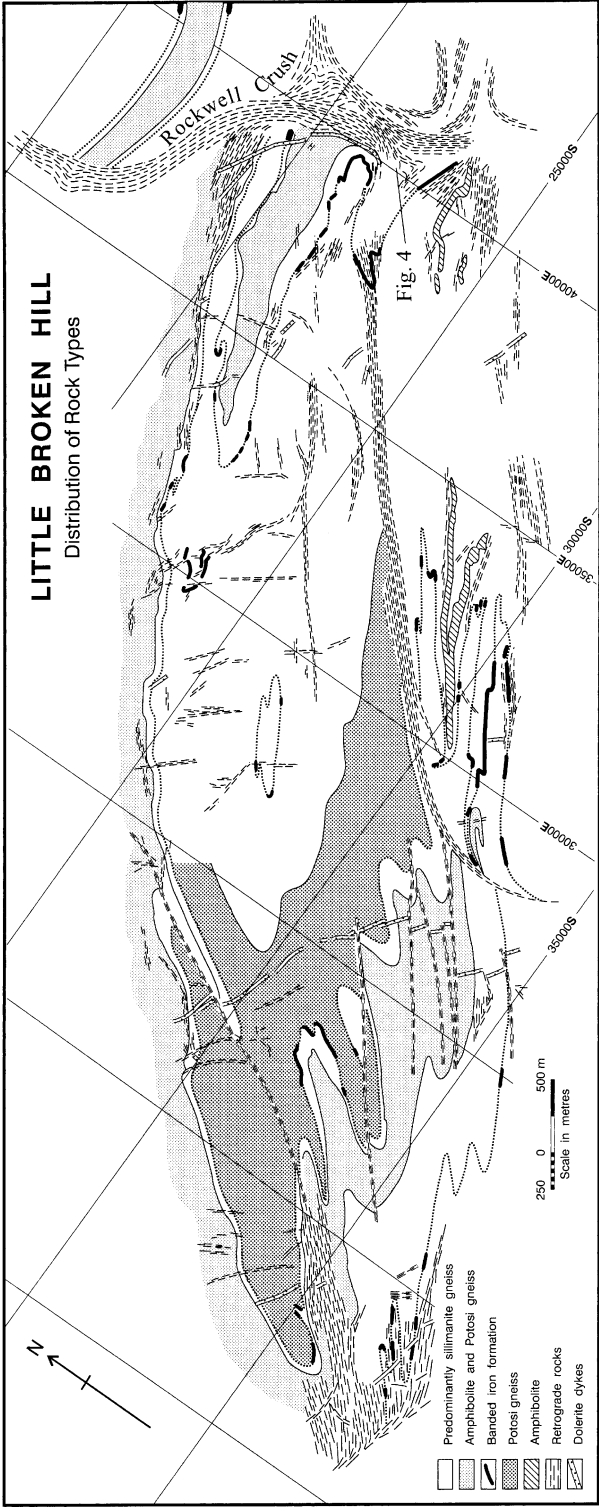


Fig. 3. Map of Little Broken Hill showing distribution of rock types and shear-zones. The large shear-zone at the northeastern edge of the map is the Rockwell Crush. The grid is in feet to be consistent with the surveyed grid and original maps.

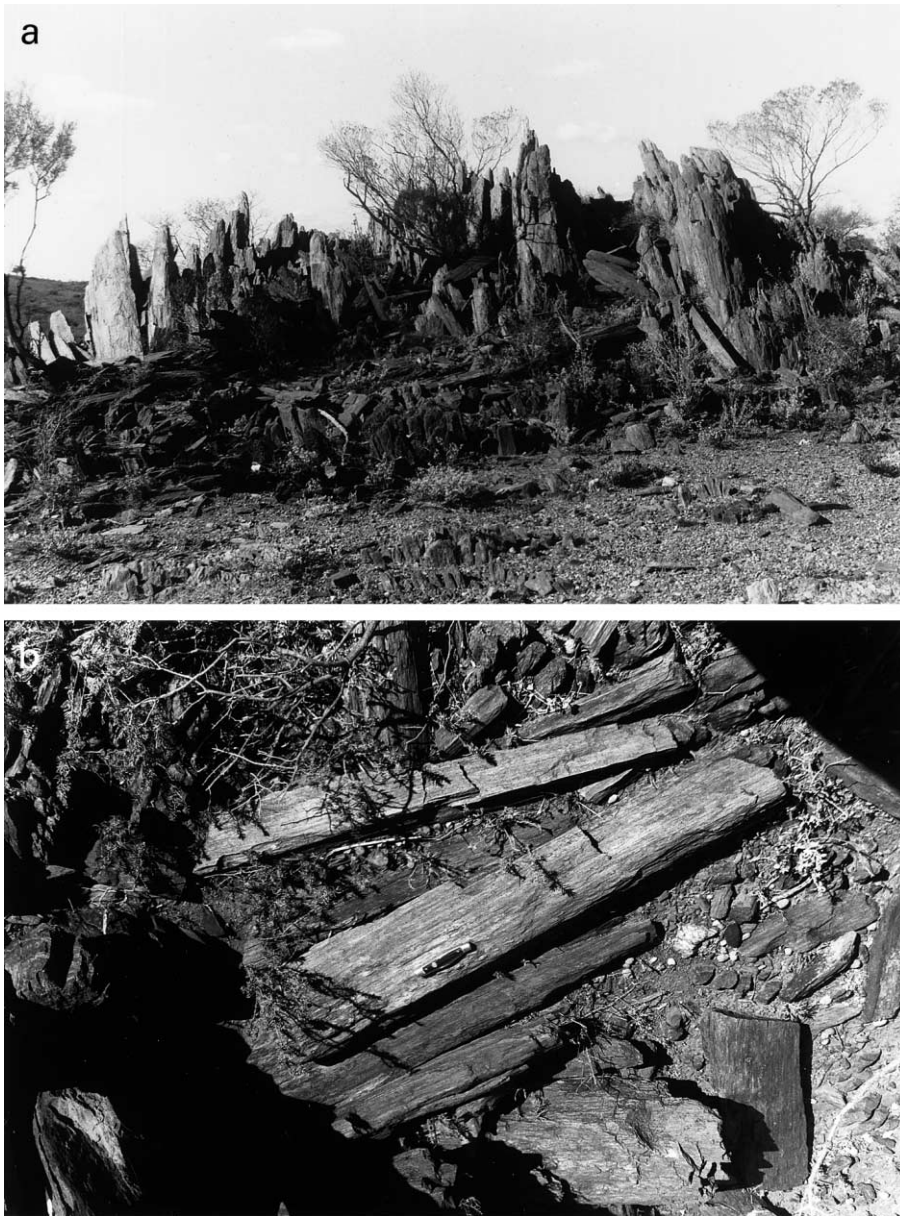


Fig. 4. Shear-zone lineation at intersection of Rockwell Crush and NE shear-zone (location indicated in Fig. 3). Outcrop in (a) is approximately 2 m high. Pocket knife in (b) is 10 cm long.

Locally open folds ( $F_2$ ) with upright axial-planes and northerly plunges overprint  $S_1$  (Fig 2c). The general weak arcuate trend of  $S_1$  (Figs. 2a and 3) is due to this deformation. No overprinting relationships between these folds and other post- $F_1$  folds have been observed, but their relative timing is indicated by their

relationship to metamorphism. They fold the  $F_1$  sillimanite lineation, but the sillimanite is stable and locally a new lineation defined by coarser sillimanite parallel to  $F_2$  hinges overgrows the more fibrous  $F_1$  lineation.  $F_3$  folds associated with the retrograde zones also fold the  $F_1$  sillimanite lineation but the

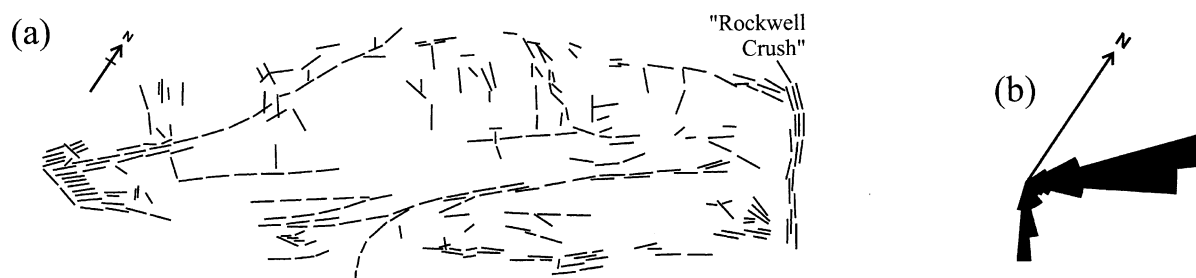


Fig. 5. Map (a) and rose diagram (b) for shear-zones showing frequency of equal length segments/orientation for area covered by Fig. 3.

sillimanite is pseudomorphed by “sericite”. Under the microscope, sillimanite and more particularly feldspar are commonly seen to be retrogressed to sericite and the alteration tends to be concentrated in films parallel to  $S_1$ .

### 3. Shear-zones

The shear-zones are labelled  $F_3/F_4$  and are characterised by steeply dipping retrograde foliations and a steeply plunging lineation (Figs. 2d and e). Locally the lineation dominates the appearance of the outcrop (Fig. 4). The shear-zones are sinuous, commonly bifurcate and occur in two principal orientations, one striking northwesterly and the other northeasterly (Figs. 3 and 5). They commonly terminate within the area, curving into the local  $S_1$  orientation. Where members of the two orientation groups intersect, displacement of one by the other may be small. They are labelled  $F_3/F_4$  because they formed as  $F_3$

structures and were reactivated later with local overprinting by another generation of structures ( $F_4$ ) as discussed below. Not all zones are reactivated and where reactivation has occurred, distinguishing  $F_3$  and  $F_4$  structures is not always possible. Where they cannot be distinguished we refer to them as  $F_3/F_4$  structures. Where there is overprinting evidence we separate them if it is useful to do so. The centres of the zones are dominated by new fabrics not found outside the zones, and earlier fabrics may be totally obliterated. The zone margins however, are transitional with both new and old fabrics recognisable to a lesser or greater extent.  $S_1$  typically curves from its regional orientation to the local shear-zone orientation in the marginal zone.

The zones are dominated by muscovite and chlorite schists, with the schistosity generally parallel or subparallel to the zone-margin. Amphibolites and “Potosi Gneiss”, traceable into the zones, occur as irregular, commonly folded boudins in various states of retrogression. Retrogression is generally stronger in the centre of

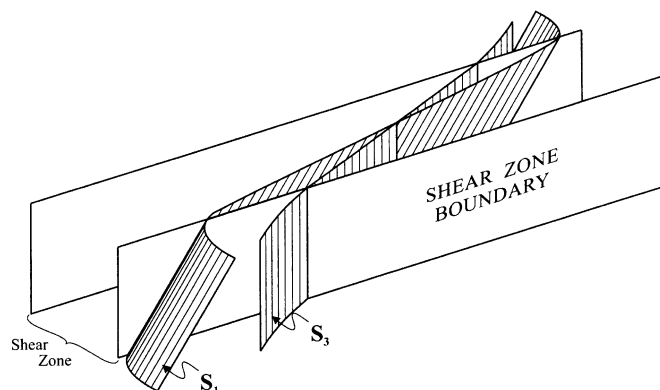


Fig. 6. Diagrammatic representation of simple NW shear-zone, showing relationship of various fabric elements.



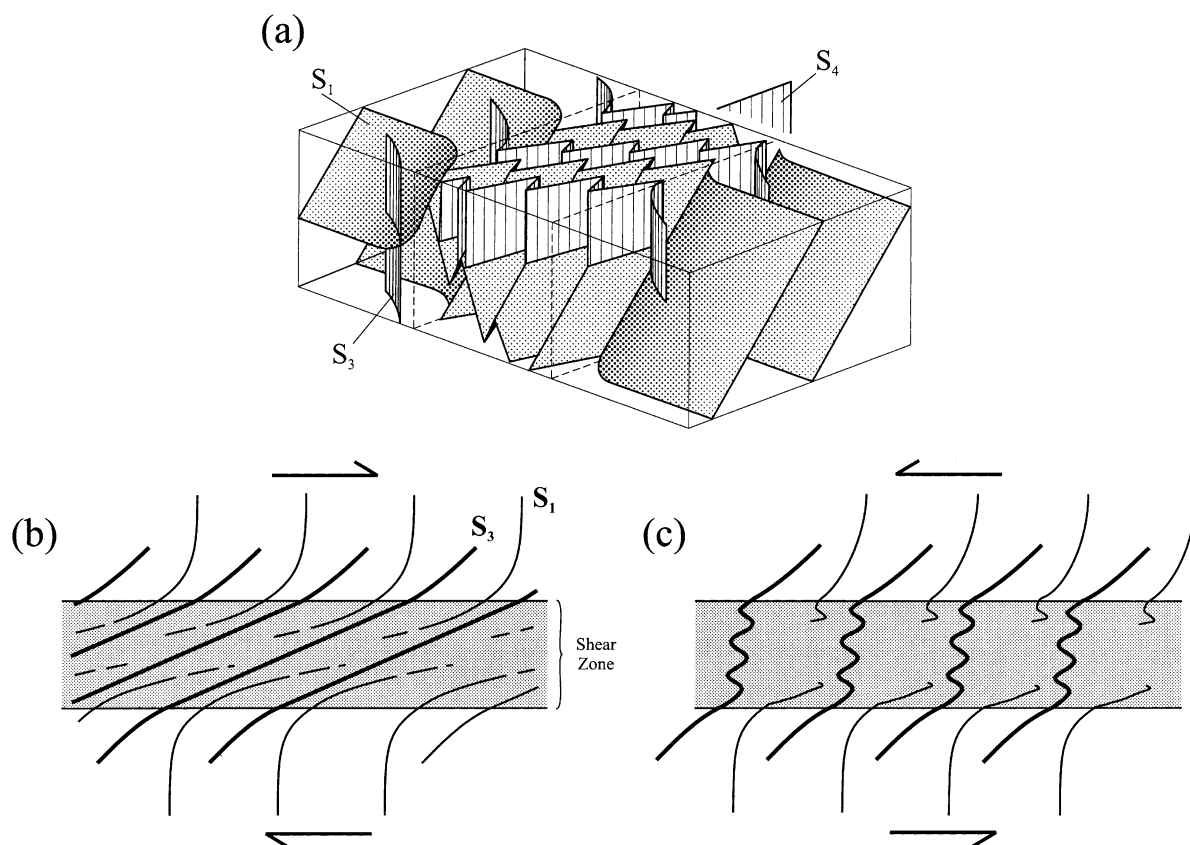


Fig. 7. (a) Diagrammatic representation of complex NW shear-zone showing relationship of various fabric elements. (b) and (c) Plan view of shear-zone showing development of  $F_4$  folds as a result of reversal in shear-zone-parallel displacement.

the zones than in the margins (see below for discussion). In some zones more than one generation of schistosity ( $S_3$  and  $S_4$ ) is present and one or both schistosities are commonly overprinted by crenulation cleavage ( $S_5$ ). Typically  $S_5$  occurs as a pair of conjugate surfaces intersecting in a horizontal lineation parallel to the edge of the zone in which they occur. The sense of shear on the two surfaces indicates that they are a product of vertical shortening parallel to  $S_3/S_4$  and they are therefore not shear-bands.

Zones belonging to the two shear-zone orientation groups are described separately in more detail below.

### 3.1. Northwesternly striking shear-zones

The NW-striking shear-zones are generally approximately vertical and vary in complexity. Simple zones

which are not very numerous are no more than a few metres wide. Complex zones are more numerous and are up to approximately 250 m wide. The zones are generally sinuous and bifurcate locally. They displace the high-grade foliation, producing a horizontal separation that may be dextral or sinistral.

The simple zones (Fig. 6) all have a dextral separation and are characterised by a new foliation ( $S_3$ ) which occurs within the zones and in their margins. The new foliation is sigmoidal, steeply dipping, and varies in strike by 30–40° being approximately parallel to a given zone near its centre and inclined to the zone by 30–40° in its margins. The curvature is in sympathy with the dextral separation of the zone, like the foliations described by Ramsay and Graham (1970), and a similar curvature is observed in the high-grade foliation ( $S_1$ ), in the margin of the zone.  $S_3$  is best developed where it is parallel to the zone and

disappears gradually into the country rock in the margins of the zone. Where  $S_3$  is well developed, the high-grade foliation is obliterated.

The complex zones have a sinistral separation and their structure is represented diagrammatically in Fig. 7. Typically, their margins are identical to the simple zones, with a weakly developed  $S_3$  and dextral curvature of both  $S_1$  and  $S_3$ . Within the zone, both foliations are tightly folded. Folds in  $S_3$  have approximately vertical plunges, whereas folds in  $S_1$  have plunges that vary between the plunge of the intersection of the shear-zone with the wall-rock-orientation of  $S_1$  and the plunge of the folds in  $S_3$ . A new foliation ( $S_4$ ) is locally parallel to the zone margins and to the axial planes of the folds in  $S_3$ . Both foliations are best described as schistosity in the field, but where weakly developed,  $S_4$  can be seen locally in hand specimen to be a crenulation cleavage. Where it appears as a schistosity, it is still seen in thin section to be domainal. In thin sections cut perpendicular to the steep lineation, the layer silicates occur in alternating domains: one with a very strong preferred orientation parallel to the foliation and the other with very little preferred orientation or a preferred orientation at a high angle to the domain boundary. In thin sections cut parallel to the lineation and perpendicular to the foliation, a strong preferred orientation of all layer silicates is parallel to the trace of the foliation. We interpret this foliation as a transposed crenulation cleavage that has undergone extensive recrystallisation. The two dominant orientations of the mica grains (their orientation in the microlithons and in the cleavage septa) and the domainal pattern of these orientations is preserved, but the curved surfaces of the crenulations are lost.

A strong lineation is also parallel to the folds, which is partly defined by the intersection of  $S_3$  and  $S_4$  in the complex zones. It is also defined in all zones by elongate minerals and mineral aggregates, commonly with a pull-apart or boudinaged appearance, indicating that it is a stretching-lineation. This interpretation is confirmed at one locality, where garnet grains in a thin schistose layer on the edge of a zone have biotite replacement haloes. There is a gradual transition within the zone margin from thin haloes near the outer edge to complete replacement towards the inner edge. This progressive change is accompanied by a change in aspect ratio from the typical equant

form of the garnet, to elongate aggregates of biotite with a smaller equant garnet core, to thin films of biotite with an aspect ratio of the order of 100:10:1. The long dimension of the films is parallel to the lineation and the intermediate dimension is parallel to the foliation.

Strongly deformed quartz veins in the complex zones are folded about moderately to steeply plunging axes and have axial planes that trend approximately parallel to the margins of the zones. One such vein from the major NW trending shear-zone known as the Rockwell Crush (Fig. 3) has a lineation that plunges steeply, parallel to the stretching-lineation and wraps around the closure of less steeply plunging folds. It has been used as a starting material for deformation experiments and its  $c$ -axis fabric has been measured carefully (Ralser et al., 1991) from several thin sections from one unoriented specimen. The  $c$ -axis fabric is an asymmetrical type 1 girdle, indicating non coaxial shearing (c.f. Lister and Hobbs, 1980) parallel to the margins of the zone and parallel to the lineation. We have measured a field of view from one oriented thin section from the same vein. The plot does not define a complete asymmetrical girdle but has the same maxima and the same asymmetry with respect to foliation and lineation as found in Ralser et al.'s fabric diagram, allowing us to identify the sense of shear, from the combined information, as NE-side-down.

### 3.2. Northeasterly striking shear-zones

The NE-striking shear-zones are generally similar in strike to  $S_1$  and are locally parallel to it. They are approximately vertical and therefore generally steeper dipping than  $S_1$ . They vary considerably in width and in the sharpness of their boundaries. Many have very diffuse boundaries. This is particularly true in the SW of the area where there is a broad zone of retrogression and widespread development of a retrograde foliation, without complete obliteration or transposition of  $S_1$ . This zone is responsible for the NE striking  $S_3/S_4$  maximum being so much stronger than the NW striking  $S_3/S_4$  maximum in Figs. 2d and 5b. In such areas the steepness of  $S_1$  roughly correlates with the degree of development of  $S_3/S_4$  such that  $S_1$  is steepest where  $S_3/S_4$  is best developed. Millimetre-scale folds of  $S_1$  with  $S_3/S_4$  as axial-plane foliation, but no

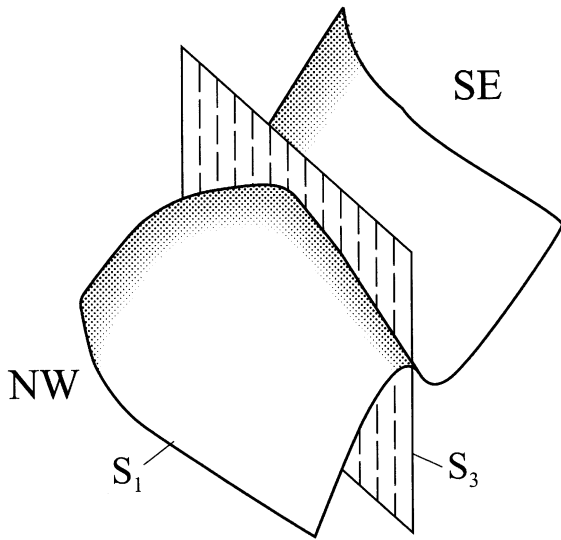


Fig. 8. Diagrammatic representation of  $F_3$  folds in margin of NE shear-zone.

larger  $F_3/F_4$  folds, occur in these areas of diffuse  $S_3/S_4$  development.

The well-defined zones are sinuous, bifurcate locally, and vary considerably in thickness from a few decimetres to approximately 250 m. In the margins of the zones, “drag” in  $S_1$  is common and takes the form of shallowly plunging periclinal folds, which generally suggest a N-side-up vertical component of movement (Fig. 8). No complex margins with a curved  $S_3$  plane, as described for the NW shear-zones, have been observed. The zones themselves are generally characterised by a single, steeply dipping foliation and steeply plunging lineation defined by mineral aggregates. Locally tight to isoclinal folds of  $S_3$  within the zones plunge parallel to the lineation and have an axial-plane crenulation cleavage ( $S_4$ ), which is parallel to the zone boundary. Also, folds of  $S_1$  in one broad zone plunge moderately NE (locality X in Fig. 9), approximately parallel to the intersection of the zone and the orientation of  $S_1$  outside the zone.

Since the zones strike approximately parallel to the general strike of layering, recognisable displaced markers, other than the dykes discussed below, are rare and those that do occur show both dextral and sinistral (e.g. Fig. 10) separations.

#### 4. Intersection of shear-zones

Two relationships have been observed at the intersection of well exposed  $S_3/S_4$  zones. (1) Both zones change direction towards their mutual intersection, so that they meet at a more acute angle than they would do otherwise. In this situation, the  $S_3/S_4$  foliations in each zone appear to simply merge without evidence of overprinting. (2) Zone A clearly overprints zone B and passes through it without deflection and without change in the morphology and geometry of  $S_3/S_4$ . In this situation zone B curves, on either side of zone A, towards the zone A orientation. In the curved areas the zone B  $S_3/S_4$  is overprinted by a crenulation cleavage that is parallel to the zone A  $S_3/S_4$  and this crenulation cleavage transposes the former into the orientation of the latter.

Where the Rockwell Crush (Figs. 3, 9 and 11) intersects a NE shear-zone, the situation is more complex. There are areas where, on a small scale, the A and B situation described above is applicable, but the overprinting relationships are not consistent. In the area SW of the Rockwell Crush around X in Fig. 11, the relationship is appropriate to the Rockwell Crush having been overprinted by the NE shear-zone, whereas around Y (Fig. 11) the Rockwell Crush overprints the NE shear-zone.

#### 5. Dolerite dykes

Vertical dolerite dykes, typically up to several metres thick, traverse the area in a northwesterly direction (Figs. 3, 9 and 11). They bifurcate locally and appear to be weakly boudinaged throughout the area. Where the dykes intersect the NE shear-zones, they are cut and offset by the zones. Locally the sense of offset is obscured by bifurcation of the dykes, but wherever the offset can be determined, it is dextral, with only one exception (this in an area of poor outcrop where it is possible that two dykes are involved). Horizontal displacements are typically 50–100 m.

There are few intersections of the dykes and the NW shear-zones because the two are almost parallel. The one recorded occurrence involves a simple zone. The dyke, which cuts straight across the zone, has two short branches that intrude along the zone, clearly

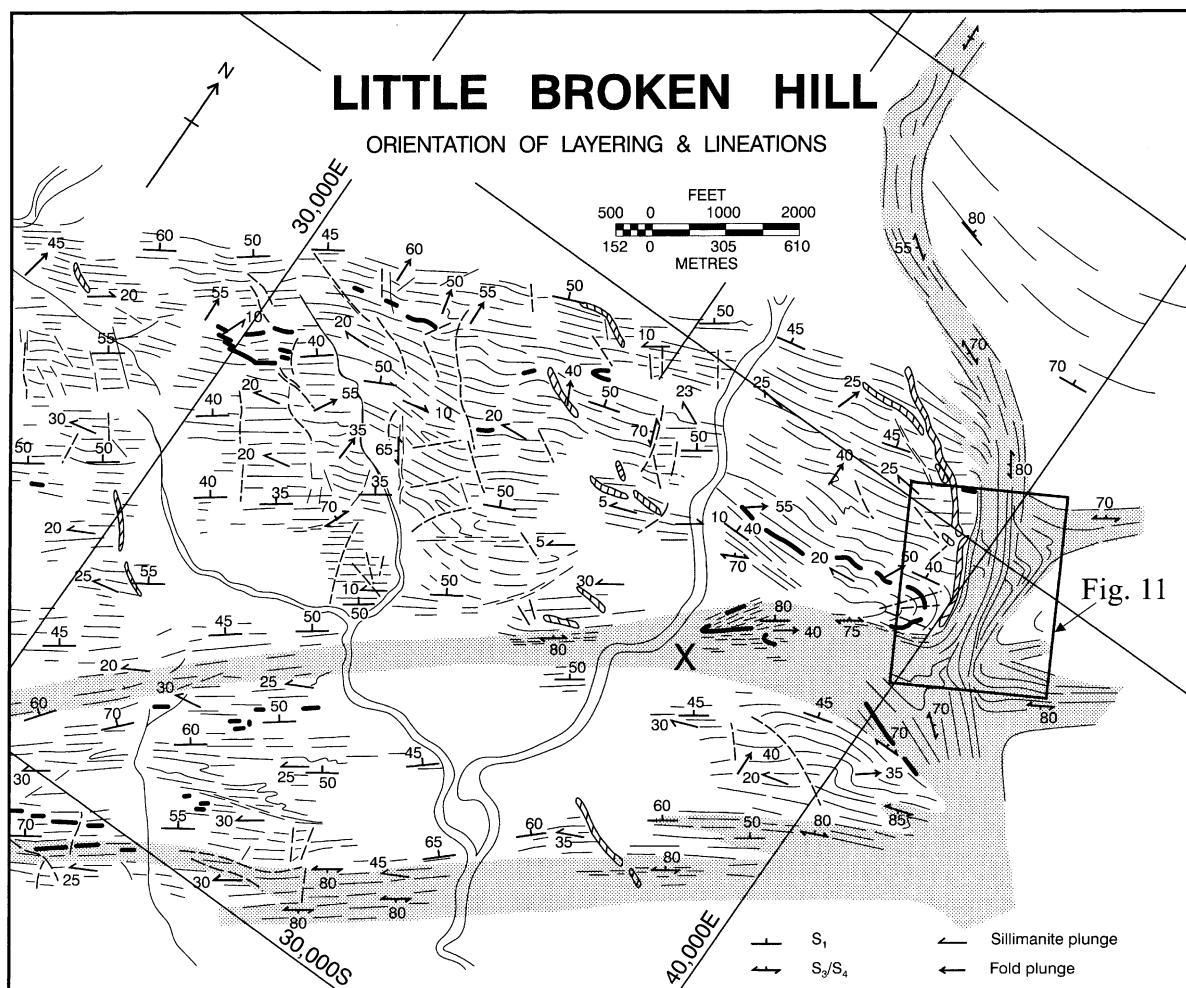


Fig. 9. Form surface map of NE half of Little Broken Hill.

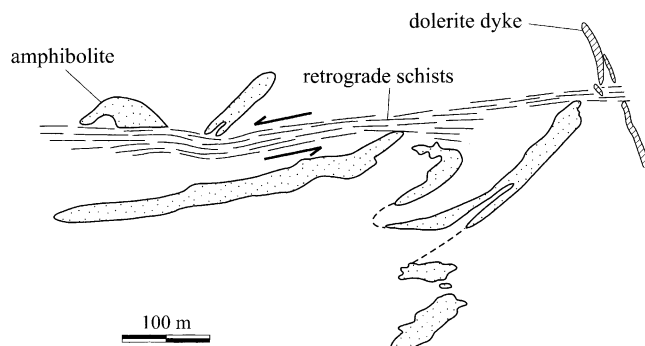


Fig. 10. Detailed sketch map showing shear-zone parallel displacement of a folded amphibolite.

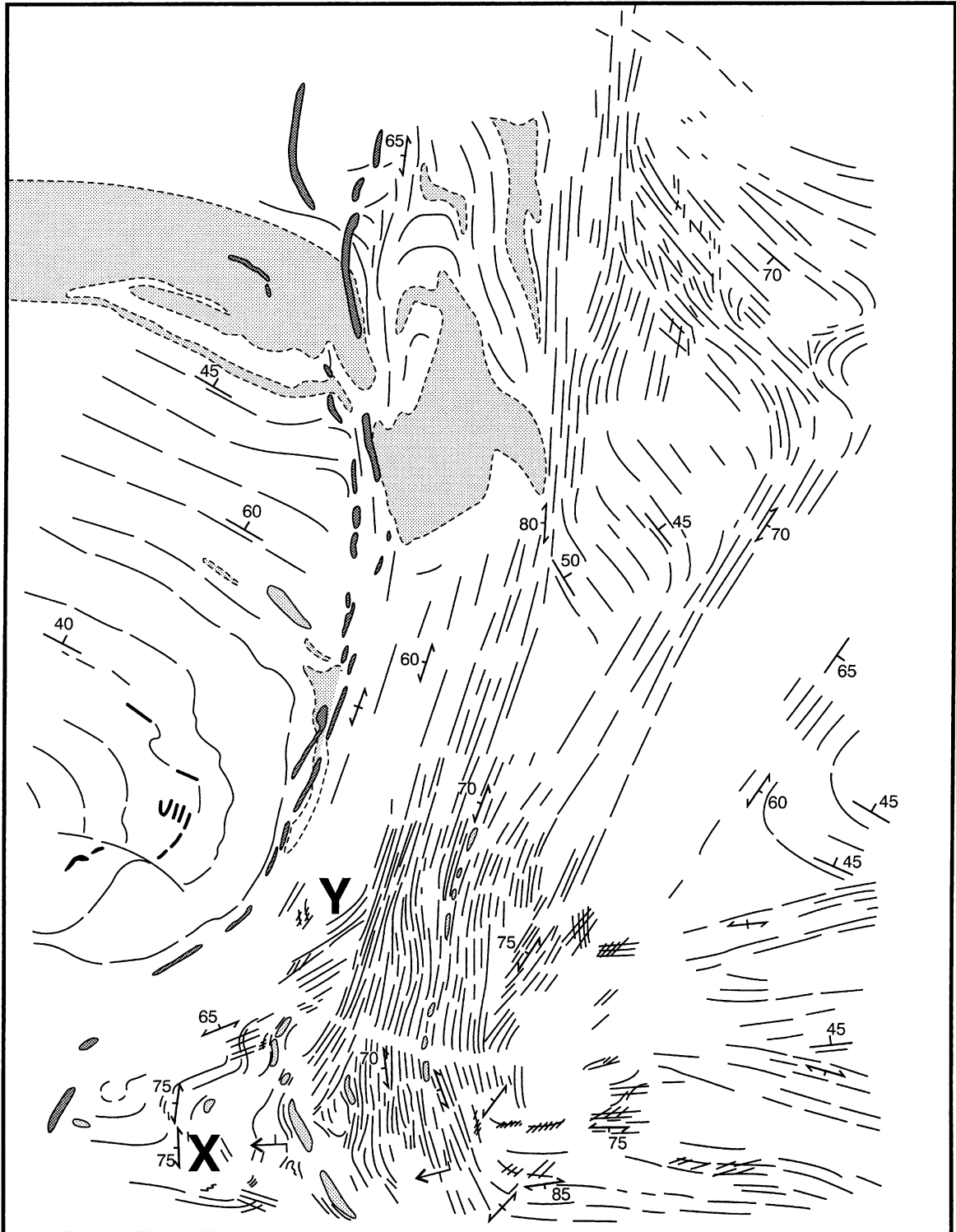


Fig. 11. Detailed form surface map of a portion of the Rockwell Crush. Symbols as in Fig. 9.

indicating overprinting of the zone by the dyke. Another dyke converges on the Rockwell Crush then follows its margin along a sinuous path into the NE shear-zone, where it overprints the  $S_3/S_4$  foliation (Fig. 11). The dyke is boudinaged, but not more than other dykes outside the retrograde zones, and there is no evidence to suggest that the dyke is older than the Rockwell Crush. On the contrary, on this margin, the Rockwell Crush, as described above, is overprinted by the NE shear-zone that in its margin is overprinted by the dyke. Thus, the evidence indicates that the dyke was intruded after initiation of the Rockwell Crush. However, a boudin of retrogressed dolerite in the centre of the zone is strongly overprinted by  $S_3/S_4$ , the degree of retrogression here suggesting that the foliation is  $S_4$ . It may not be the same dyke, but nevertheless indicates dyke emplacement before cessation of movement on the shear-zone.

## 6. Interpretation of primary movement on shear-zones

The orientation of the two sets of shear-zones suggests a conjugate pair of transcurrent zones, and this interpretation is supported by a number of lines of evidence. The symmetry of all  $S_3/S_4$  fabric elements,

excepting the quartz fabrics (discussed below), is monoclinic for individual shear-zones with a symmetry plane approximately horizontal (perpendicular to the stretching-lineation) for each zone. Grouped together, the zones have orthorhombic symmetry, if we ignore the unequal development of the two orientation groups which we consider to be a sampling problem, as stated above. Where marginal “drag” reorientates the  $F_1$  sillimanite lineation, it distributes it in small circles about an approximately vertical axis (Fig. 12). This is consistent with the folds having formed by a deformation approximating flexural slip, in response to horizontal shear. The dolerite dykes are approximately vertical and perpendicular to the symmetry plane, but are markedly offset by the shear-zones, indicating that the movement had a large sub-horizontal component.

The displacement history parallel to the shear-zones is also consistent with the conjugate transcurrent fault interpretation, in that the senses of movement, which reverse after dyke emplacement in both zones, are complementary before and after dyke emplacement. The simple NW shear-zones are typical of dextral transcurrent shear-zones. The simplest explanation of the complex NW shear-zones is that they developed as simple dextral zones, but were reactivated sinistrally, so that the early-formed  $S_3$  was

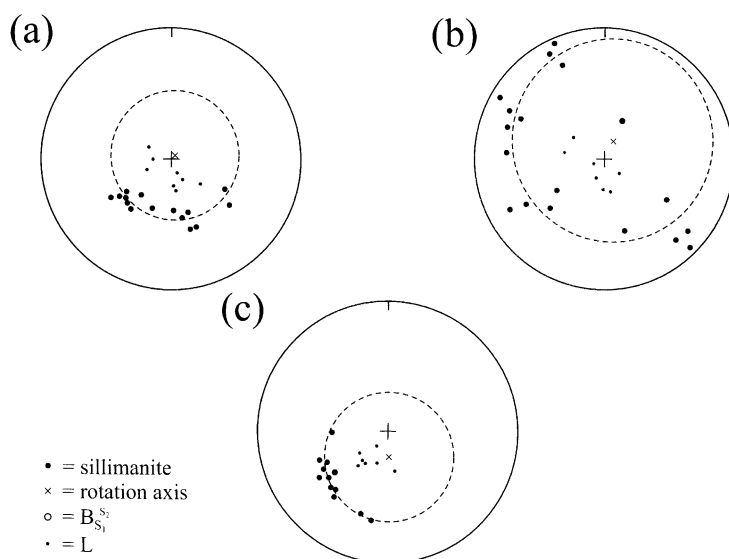


Fig. 12. Orientation diagrams showing redistribution of sillimanite lineation by  $F_3/F_4$  folds in the margins of shear-zones. Lower hemisphere stereographic projection.

folded and transposed into  $S_4$  (as in Fig. 7b and c). The deformation appears to have been progressively focussed into the centre of the zones, since the younger structures are concentrated there and the degree of retrogression is highest there. Consequently,  $F_3$  structures were preserved in the margins of the zones. Relationships between the NW shear-zones and the dolerite dykes are consistent with dextral shear being pre-dyke and sinistral reactivation being post-dyke.

In the NE shear-zones, the dykes are displaced dextrally, with one possible exception.  $S_1$  markers are displaced dextrally and sinistrally, and a given zone may displace an  $S_1$  marker one way and a dolerite dyke the other way. An interpretation consistent with this evidence is one in which early formed zones moved sinistrally, after which the dykes were emplaced, and finally the zones were reactivated dextrally. Consequently, displacement of the dykes is consistently dextral, but the net displacement of  $S_1$  markers depends on the relative magnitude of the sinistral and dextral movements that affected them.

Thus, combining the evidence from both sets of zones, the pre-dolerite dyke movement pattern is consistent with a conjugate set of transcurrent shear-zones with an approximately N–S shortening direction. On the other hand, the post-dolerite dyke movement is consistent with transcurrent movement and an approximately E–W shortening direction.

Individual lines of evidence for the transcurrent interpretation can be questioned, but the strength of the interpretation lies in the overall consistency. Another consistency is that all the observed structures from  $F_2$  onwards can be explained in terms of approximate principal shortening directions that rotate progressively in an anticlockwise direction.  $F_2$  is consistent with an E–W shortening direction,  $F_3$  with a N–S shortening, the dolerite dykes with a NW–SE shortening,  $F_4$  with an E–W shortening, and boudinage of the dolerite dykes with a SW–NE shortening.

Our interpretation is also consistent with regional evidence (Stevens, 1986) that indicates the existence of shear zones as early as 1600–1570 Ma ago, an intrusive age for the dolerite dykes of 560–500 Ma and renewed shear-zone deformation at around 520 Ma ago. We have no direct evidence of the absolute timing of the deformation described here, but

these dates are possible. There may or may not have been a long quiescent period between  $F_3$  and  $F_4$  and further, both  $F_3$  and  $F_4$  may have been continuous or episodic; we have no way of knowing. However, only the relative timing is important to the story presented here.

## 7. Interpretation of the stretching-lineation

As pointed out above, the overall symmetry of the shear-zones is orthorhombic, and this remains the same if the stretching-lineation is included. A bulk deformation consistent with this symmetry would be a near-vertical extension parallel to the lineation, combined with near-horizontal shortening and orthogonal extension in the plane perpendicular to the lineation with the axes bisecting the angles between the shear-zones. The vertical orientation of the stretching-lineation might be taken as an indication that the bulk maximum extension was vertical, but on the other hand the microfabric may be more closely related to the strain partitioning than to the bulk finite strain. Alternatively, the kinematic picture may be triclinic and only apparently monoclinic (see Lin et al., 1998; Jiang and Williams, 1998). Either way the lineation would then simply indicate *an* extension direction, rather than the bulk maximum extension direction. Even if we assume that it represents the maximum extension direction, such a model poses problems for the following reasons. (1) If the lineation is approximately parallel to the principal extension direction within the shear-zone, the shear-zone would need to have a large dip-slip component (see Lin et al., 1998; Jiang and Williams, 1998). (2) If there is extension parallel to the lineation in the shear-zone but no lineation in the country rock does this mean that the extension occurred only in the shear-zone and if so how and why? We attempt to resolve these problems below.

In experiments performed by Price and Torok (Price and Torok, 1989; Price personal communication, 1989), slate, phyllites and schists deform at room temperature, confining pressures <20 MPa and strain-rates no greater than  $10^{-6} \text{ sec}^{-1}$  without loss of continuity, as long as the imposed strain path is a simple shear and the foliation is parallel to the imposed shear plane. In other orientations, the rock fractures, since under the experimental conditions, intragranular



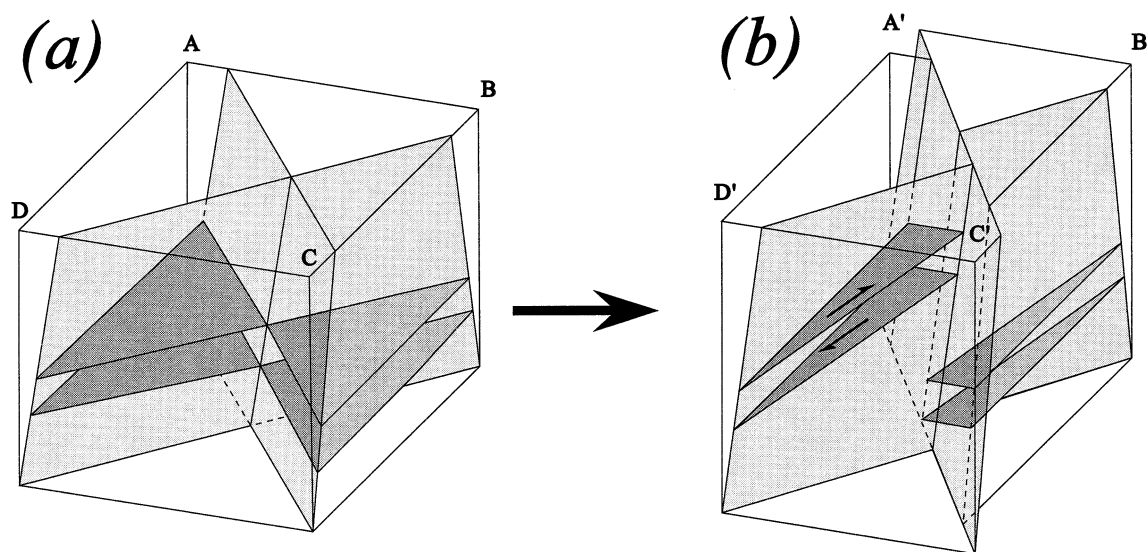


Fig. 13. Model for deformation at intersection of two shear-zones. Shear-zones are represented by light stipple and  $S_1$  by dark stipple. Shortening parallel to AB is accommodated by (1) extension parallel to BC achieved by transcurrent shear on the shear-zones, (2) vertical extension achieved by simple shear parallel to  $S_1$  and vertical displacement on the shear-zones.

ductile mechanisms are inadequate to accommodate the strain. This indicates that the foliation in the slate comprises a weak deformation mechanism. A similar conclusion has been drawn by Williams and Price (1990) on the basis of a series of experiments performed on an artificial salt-mica schist (see also Weijermars, 1992). They concluded that if a body of foliated rock is constrained to deform it will: (a) tend to use the foliation as a slip surface if the foliation is suitably oriented to accommodate the strain, (b) tend to develop new slip surfaces if the existing one is incapable of accommodating the strain, and (c) only deform primarily by intragranular mechanisms if there are no suitable intergranular slip systems present. As in crystal slip by dislocation glide, the shear strength of the foliation and the resolved shear stress parallel to it decide whether the foliation is an active deformation mechanism or whether some other mechanism operates (c.f. Lister and Paterson, 1979). We believe that, in general, slip on foliations is a favoured deformation mechanism because of the weakness of the foliation in micaceous rocks. The following interpretation is predicated on this premise.

If a prescribed shape-change can be achieved by slip on a foliation without any other mechanism operating (e.g. simple shear where the pre-existing folia-

tion is parallel to the shear-plane), deformation occurs by slip on the foliation and intragranular deformation is minimised. The more it is minimised, the less tendency there is for a lineation defined by grain-shape to develop, even at large strains. Further, if shear occurs under high-temperature conditions, an existing shape-fabric is likely to be obliterated by grain-growth and recrystallisation. Conversely, where deformation is achieved by intragranular mechanisms, we expect that shape fabrics (S and/or L) tend to develop. How well they develop is a function of the relative rates of strain and recrystallisation. Thus we argue that slip on an existing foliation is an inefficient process for developing stretching-lineations, whereas extension parallel to an existing foliation involves intragranular mechanisms and is an efficient mechanism for developing stretching-lineations. However, a complex interplay of mechanisms, initial fabric and microstructure is likely. For example, shear on a pre-existing foliation might be an efficient process for developing a lineation in a situation where large (relative to the scale of individual shear planes) porphyroblasts are undergoing retrogression to fine grained aggregates and are weak during the process.

We now concentrate on the area around the Rock-

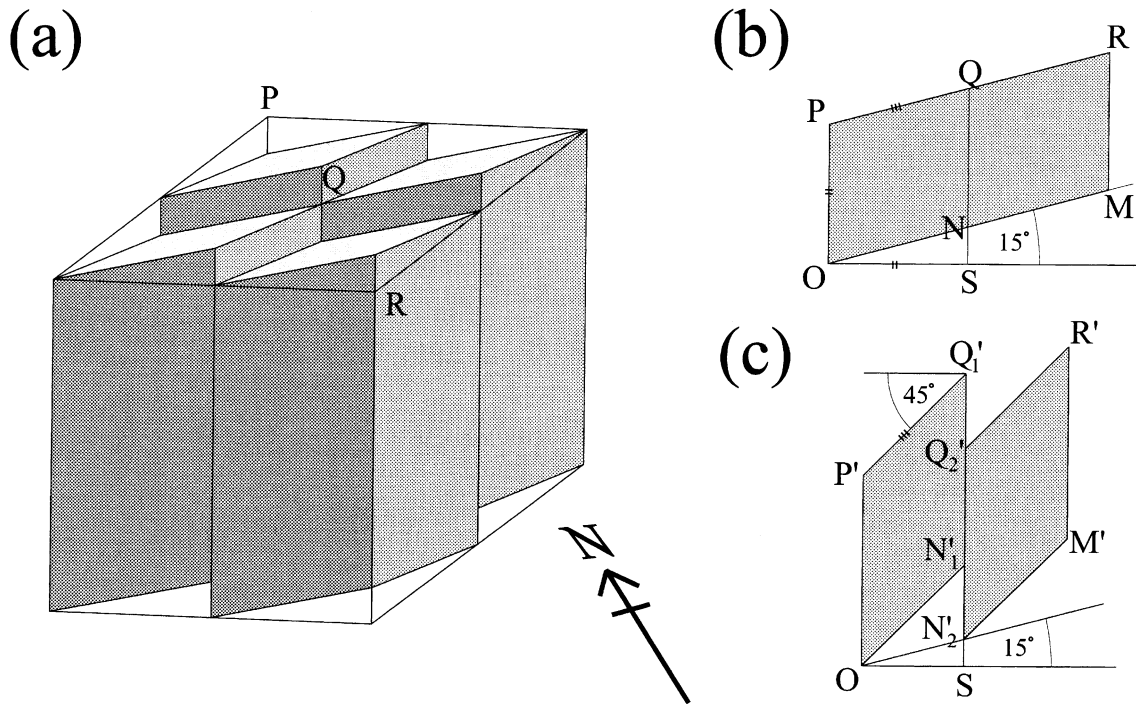


Fig. 14. (a) Effect of  $S_1$ -parallel simple-shear on an initially horizontal surface cut by a pair of intersecting shear-zones parallel to the sides of the block. (b) section through block parallel to PR such that OM is parallel to  $S_1$  which has an initial dip of  $15^\circ$ . (c) section represented in (b) after steepening of  $S_1$  by simple shear parallel to  $S_1$  and rotation of individual blocks. Note that the local dip of an  $S_1$  marker is now  $45^\circ$  but its regional inclination at a scale much larger than the blocks will be unchanged at  $15^\circ$ .

well Crush, where the detailed relationships are best known, but draw on general evidence (e.g. the sense of displacement of the dykes) from elsewhere in the area. If, as proposed above, a general horizontal shortening has occurred, first N–S and then E–W,  $S_1$  must be steeper now than it was originally. So we assume that at the start of the shear-zone development  $S_1$  was shallowly dipping and not a very useful slip-surface for achieving a bulk-strain that involved a significant horizontal component of extension. This is why the shear-zones developed. Once the shear-zones were initiated they, plus the shallowly dipping  $S_1$ , constituted a mechanism for vertical extension, as shown in Fig. 13. The transcurrent faults at this stage acted as accommodation features, enabling the rock-body to shorten by a combination of slip on  $S_1$  and spin of individual blocks, without there having to be a regional tilting of the body as a whole (Fig. 14b and c). The vertical extension and dip-slip displacement are important from the point of view of explaining

the vertical lineation, as discussed below. The extension could have been achieved by folding, but horizontal shortening would not produce folds if the surface was already dipping significantly. Nor would folds produce the horizontal extension. Thus we envisage a deformation where horizontal shortening was accommodated by (1) horizontal extension achieved by transcurrent movement on the shear-zones and (2) vertical extension achieved by slip on  $S_1$  and dip-slip on the shear-zones. The relative magnitude of the two components is unknown, but the horizontal component may have been the more significant, at least in the early stages of deformation because (1) we expect that the shear-zones would have formed with thrust geometry if the vertical component had been the larger, and (2) as shown in Fig. 14, the dip-slip component of movement is N-side-up on the NW shear-zones and would have produced the opposite sense of “drag” to that produced by the transcurrent component. What is observed is

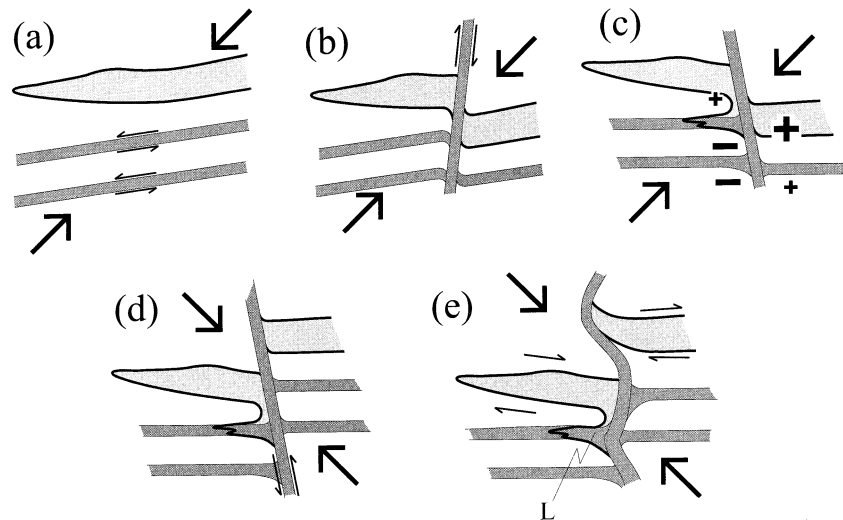


Fig. 15. Diagrammatic representation of the development of the structure around the intersection of the Rockwell Crush with two major NE shear-zones (see Figs. 9 and 11). The thick lines represent the BIF and the lightly shaded areas represent the Amphibolite and Potosi gneiss unit of Fig. 4. Dark shading represents the shear-zones. (a) and (b)  $F_3$  transcurrent movement began first in the NE shear-zones and then in the Rockwell Crush with the appropriate “drag” developing in markers intersecting the Rockwell Crush. (c) As N–S shortening continued vertical extension resulted in dip-slip displacements (relative movements indicated by + and – signs, large + is on highest upthrown block, large – is on lowest block and small +s are on intermediate blocks, see Fig. 14) which produced marginal structures in the markers along the edge of the NE shear-zone. At the same time horizontal shortening increased the angle between the shear-zones. (d) With the onset of  $F_4$  the shortening direction changed to E–W and the Rockwell Crush was transcurrently reactivated with the deformation concentrated in the centre of the zone. There may or may not have been vertical extension during this episode. (e) Finally with E–W shortening continuing there was a diffuse transcurrent shear deformation involving slip on  $S_1$  and NE shear-zones which bent the Rockwell Crush into its present observed configuration (compare with Fig. 9).

consistently the “drag” expected from the transcurrent component, indicating that it was dominant, at least in the early stages of the deformation.

Given the above scenario, an adequate slip-mechanism existed to accommodate vertical extension within the shear-zone bounded blocks, so that we do not expect a new shape fabric to have been strongly developed there. However, in the shear-zones, there was no suitably oriented foliation to accommodate the shear. Thus, intragranular deformation was necessary and so a new shape fabric developed as seen in  $S_3$ . The lack of a horizontal lineation on  $S_3$  could be due to the following: (1) Where  $S_3$  is best preserved  $F_3$  strain magnitudes are small. (2) Where it was best developed it is strongly overprinted by  $S_4$ . (3) Original shape fabrics have been modified by later recrystallisation. As  $S_3$  developed, it rotated towards parallelism with the shear-zone boundaries and therefore became an increasingly good slip-mechanism to accommodate the transcurrent and dip-slip components of shear. Consequently, shear

tended less to produce or modify the shape fabric. However, vertical extension of the shear-zone-bound blocks required vertical extension within the shear-zones, and potential mechanisms other than intragranular ones were progressively eliminated as  $S_1$  and  $S_3$  approached parallelism with the zone boundaries. Thus this component of the strain gave rise to a vertical linear shape fabric.

When the sense of shear on the shear-zones reversed,  $S_3$ , where not parallel to the shear-zone boundary, was rotated, crenulated and finally transposed back into the shear-zone orientation as  $S_4$ . Where  $S_3$  was precisely parallel to the zone boundary at the start of the  $F_4$  deformation it was presumably simply reactivated. Crenulation of  $S_3$  about a vertical axis accentuated the vertical lineation, and shear parallel to the shear-zones was accommodated by slip on  $S_3$  and  $S_4$ . Any continued vertical extension was accommodated by  $S_1$  slip in the blocks and by intragranular mechanisms in the shear-zones, further strengthening the vertical lineation.

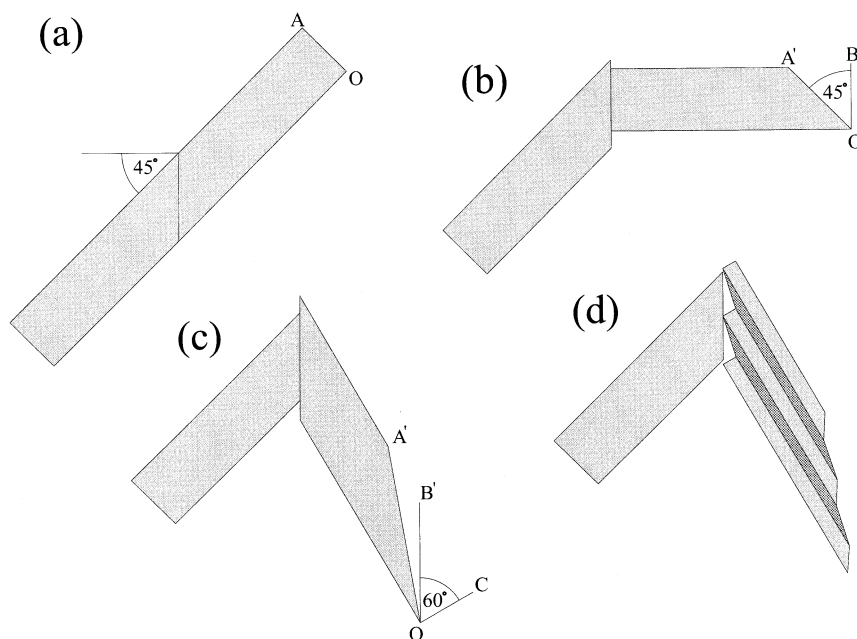


Fig. 16. Diagrammatic representation of folding and strain-path partitioning of structure adjacent to a NE striking shear-zone — see text for discussion.

Fig. 15 shows how the complex structure around the intersection of the Rockwell Crush and major NE shear-zone (Fig. 11) can be explained by the deformation history outlined above. The fold in BIF, which has an isoclinal trace on the map (immediately NW of the NE shear zone in Figs. 3 and 9), is actually conical in the hinge, with limbs that have the same strike but different dips. It is different in style to any other folds of any scale seen in the area. It folds  $S_1$  and most closely resembles the  $F_3$  marginal “drag”, except that it is much tighter than the normal  $F_3$  “drag” structures. However, it can be interpreted in terms of “drag” if related to both shear-zones. A possible sequence of events, consistent with the general interpretation, is presented in Fig. 15. All the features of this structure and of the rest of the area can be explained by means of the general interpretation presented here, except for the quartz fabric reported above.

## 8. Magnitudes of strain and displacement

As a check of our explanation, we consider whether our interpretation is capable of producing strain and

displacement magnitudes consistent with the observations. In general, no quantitative limits can be placed on the significance of the stretching-lineation. Microstructural observations indicate that linear aggregates that most commonly define the lineation owe their shape not only to the stretching, but to segmentation by development of  $S_4$ . So, for example, at the end of  $F_3$  transcurrent movement a given mineral aggregate may have been elongate in the foliation with its longest dimension horizontal. During  $F_4$  crenulation, such an aggregate, if large enough, would have been chopped up into segments. If the initial intermediate dimension of the aggregate was longer than the spacing of the crenulations, it would be elongate parallel to the crenulations after deformation. However, not all of the elongation is due to segmentation; real extension also occurred. If we assume that initial dips were approximately  $15^\circ$  (Fig. 14b) and that they were steepened by slip on  $S_1$  to the present value of approximately  $45^\circ$  (Fig. 14c), then the vertical stretch of the fault-bounded-blocks is approximately 1.4 (OP' in Fig. 14c). To maintain strain continuity, the shear-zone-rocks must have undergone the same extension. This is not a large strain but combined with

the segmentation mechanism, would be sufficient to account for the observation of a strong lineation, as well as the lineation-parallel microboudinage. However, the elongation of the retrograding garnet grains cannot be explained by such a strain.

The lineation defined by the biotite aggregates resulting from retrogression of garnet grains occurs in the area indicated by the “L” in Fig. 15e. It is in the marginal “drag” structure associated with the NE shear-zone, and occurs in a rock that is not generally lineated, except for the biotite aggregates. It occurs in a unit on the S side of the fold that now dips approximately 60° at that site, whereas on the other side of the fold it dips 45–50° in approximately the opposite direction. The strain-path for the development of the fold cannot be determined rigorously. However, we can do an order calculation by making the simplistic assumption that the fold developed in the late stages of  $F_3$  (Fig. 15c) by flexural slip of a layer of constant volume that was dipping at about 45° (Fig. 16a). In this situation (assuming that the fold is a “drag” structure), the two angular shears of 45° and 60° have to be summed (Fig. 16b and c) and the result ( $\angle COA'$  in Fig. 16c) gives a shear and stretch of approximately 2.7 and 3.1, respectively. A stretch of approximately 10 is needed to achieve the observed aspect ratio and this would be achieved if the strain was concentrated in incompetent layers (e.g. Fig. 16d) that only represented approximately 20% of the total thickness. We have no way of knowing what thickness was involved or what layers were competent at the time of deformation, but rock types vary considerably at this locality and the stretched garnet grains are restricted to a thin layer. Thus the observed strain is not incompatible with our interpretation.

The strain-paths discussed above do not explain the vertical shear-fabric observed in quartz. The fabric, as well as the folds associated with the NE shear-zones, require significant vertical displacement on the shear-zones (Figs. 13 and 14). To determine a feasible value, we make the same assumptions as above concerning the initial dip and the method of increasing it. The down-dip displacement along a section, such as P–R in Fig. 14b, is given by  $SN'_1-SN'_2$  in Fig. 14c and is approximately 0.5 of the horizontal dimension of the block at the intersection of two shear-zones (Q in Fig. 14a). The value across any single shear-zone is only half as much (Fig. 14a), but this is a considerable

displacement, adequate to explain the folds and, depending on the active width of a zone, also adequate to explain the quartz fabrics.

## 9. Discussion

We have presented an example of a set of shear-zones that have a vertical stretching-lineation, but nevertheless appear to be transcurrent. Our model is capable of explaining all the observations. It differs from most other models for similar shear-zones in that it includes significant deformation of the country rock and also takes account of likely specific deformation mechanisms. We believe that both of these aspects of the model may be more generally applicable and discuss them in turn.

The fact that shear-zones commonly die out along their length is strong evidence that the country rock has undergone coeval deformation. Other models that do not allow for this deformation, require complex histories involving a period of vertical displacement or require some form of extrusion (e.g. Sanderson and Marchini, 1984; Robin and Cruden, 1994). The Sanderson and Marchini model is a type of extrusion model (see also Fossen and Tikoff, 1993). It explains the vertical lineation by allowing extension within the shear-zone, but requires bounding faults, which are not generally present, to separate the shear-zone from the undeformed wall rock. The Robin and Cruden model is a more sophisticated extrusion model, which maintains strain compatibility with the wall rocks, but predicts lineation patterns that in our experience are not generally observed. Further, an intrinsic problem with this model is that extrusion is a geometrically work-hardening situation. The narrower the zone becomes through extrusion, the greater the resistance to further extrusion (see Lin et al., 1998). In addition, the alignment of layer silicates in shear-zones parallel to the extrusion direction results in fabric hardening, since the layer silicates will act as strong fibres.

Our model has no need for extrusion, because the wall rocks undergo the same vertical extension as the shear-zone rocks. Because different deformation mechanisms exist in the wall-rock, the resultant fabric is different. If such a mechanism did not exist (e.g. if  $S_1$  was vertical throughout the area), extrusion might

occur. We would expect however, that in contrast to the Robin and Cruden (1994) model, the extrusion would be spread over an increasingly broader zone than the zone in which shear occurs (see Lin et al., 1998).

The model presented here relies heavily on the premise that grain-shape lineations tend not to develop in rocks that are deforming by slip on a pre-existing foliation. Evidence in support of this premise is found in experimentally deformed materials. For example, Williams and Price (1990) deformed artificial salt-mica schist in ductile simple shear experiments in which the schistosity was parallel to the plane of shear. At angular shear strains of 30° no deformation-related shape fabric developed (unpublished observation by P.F. Williams). Similarly, no shape fabric developed in a slate deformed in a similar experiment by Price and Torok (1989). However, in other experiments by Williams et al. (1977), on salt and salt-mica schist and involving similar magnitudes of strain, excellent shape fabrics developed (e.g. Williams et al., 1977; Fig. 2e). In these experiments the bulk shortening was coaxial and was initially parallel to the foliation. The salt layers underwent intragranular deformation and salt-mica schist layers underwent microscale transposition probably involving initial slip on the foliation followed by intragranular deformation.

Since the lineation is parallel to the intersection of the zones at Little Broken Hill it is presumably parallel to a bulk finite strain axis. Initially the horizontal component of shear-zone displacement was probably large compared to the vertical extension, so that the lineation would have been parallel to the intermediate axis of finite strain. After reversal of the displacements and further vertical extension, it is possible that the lineation is now parallel to the bulk strain maximum extension axis. However, we have no way of determining the relative magnitudes of the components of the deformation, so that the relationship is unknown. Further, it is possible that it may vary from place to place.

The relationship of the lineation to strain within a given shear-zone is more complicated. The orientation of the finite strain axes within the zone is the resultant of the dip and strike slip components of shear and the pure shear extensional component. Similarly, the instantaneous axes are related to the

instantaneous values of the three components. Given this situation, the lineation is inclined to both instantaneous and finite axes at potentially large angles, except in the special cases where one or two of the components approach zero. In view of this possibility, we argue that shear-zone parallel stretching-lineations should not be assumed to be parallel to movement vectors or to finite or instantaneous principal strain axes. Such a relationship should be demonstrated.

## Acknowledgements

Figures were prepared by Angel Gomez and photographs by Bob McCulloch. P.F. Williams gratefully acknowledges a Research Grant from NSERC. The manuscript benefited from critical reading by Dazhi Jiang and Jim Ryan.

## References

- Caron, A., 1994. Structural and microstructural study of the Dover Fault and its country rocks: An example of a reactivated transpressional zone in northeastern Newfoundland. Unpublished Ph.D. thesis, University of New Brunswick, Canada.
- Fossen, H., Tikoff, B., 1993. The deformation matrix for simultaneous simple shearing, pure shearing and volume change, and its implication to transpression-transension tectonics. *J. Struct. Geol.* 15, 413–422.
- Garnett, J.A., Brown, R.L., 1973. Fabric variation in the Lubec-Belleisle Zone of southern New Brunswick. *Can. J. Earth Sci.* 10, 1591–1599.
- Goodwin, L.B., Williams, P.F., 1996. Deformation path partitioning within a transpressive shear zone, Marble Cove, Newfoundland. *J. Struct. Geol.* 18, 975–990.
- Hobbs, B.E., Means, W.D., Williams, P.F., 1976. *An Outline of Structural Geology*. John Wiley and Sons, New York.
- Hudleston, P.J., Schultz-Ela, D., Southwick, D.L., 1988. Transpression in an Archean greenstone belt, northern Minnesota. *Can. J. Earth Sci.* 25, 1060–1068.
- Jiang, D., Williams, P.F., 1998. High-strain zones: a unified model. *J. Struct. Geol.* 20, 1105–1120.
- Lin, S., Jiang, D., Williams, P.F., 1998. Transpression (or transtension) zones of triclinic symmetry: natural example and theoretical modelling. In Holdsworth, R.E., Strachan, R.A., Dewey, J.F., (Eds.), *Continental Transpressional and Transtensional Tectonics*. Geological Society, London, Special Publications, 135, 41–57.
- Lister, G.S., Hobbs, B.E., 1980. The simulation of fabric development during plastic deformation and its application to quartzite: the influence of deformation history. *J. Struct. Geol.* 2, 355–370.
- Lister, G.S., Paterson, M.S., 1979. The simulation of fabric devel-

- opment during plastic deformation and its application to quartzite: fabric transitions. *J. Struct. Geol.* 1, 99–115.
- Lister, G.S., Price, G.P., 1978. Fabric development in a quartz-feldspar mylonite. *Tectonophysics* 49, 37–78.
- Price, G.P., Torok, P.A., 1989. A new simple shear deformation apparatus for rocks and soils. *Tectonophysics* 158, 291–309.
- Ralser, S., Hobbs, B.E., Ord, A., 1991. Experimental deformation of a quartz mylonite. *J. Struct. Geol.* 13, 837–850.
- Ramsay, J.G., Graham, R.H., 1970. Strain variation in shear belts. *Can. J. Earth Sci.* 7, 786–813.
- Robert, F., 1989. Internal structure of the Cadillac tectonic zone southeast of Val d'Or, Abitibi greenstone belt, Quebec. *Can. J. Earth Sci.* 26, 2661–2675.
- Robin, P.-Y. F., Cruden, A.R., 1994. Strain and vorticity patterns in ideally ductile transpression zones. *J. Struct. Geol.* 16, 447–466.
- Sanderson, D.J., Marchini, W.R.D., 1984. Transpression. *J. Struct. Geol.* 6, 449–458.
- Stevens, B.P.J., 1986. Post-depositional history of the Willyama Supergroup in the Broken Hill Block, NSW. *Australian Journal of Earth Sciences* 33, 73–98.
- Weijermars, R., 1992. Progressive deformation in anisotropic rocks. *J. Struct. Geol.* 14, 723–742.
- Williams, P.F., 1967. Structural analysis of the Little Broken Hill area of New South Wales. *J. Geol. Soc. Australia* 14, 317–332.
- Williams, P.F., Price, G.P., 1990. Origin of kinkbands and shear-band cleavage in shear zones: an experimental study. *J. Struct. Geol.* 12, 145–164.
- Williams, P.F., Means, W.D., Hobbs, B.E., 1977. Development of axial-plane slaty cleavage and schistosity in experimental and natural materials. *Tectonophysics* 42, 139–158.



**Appendix C**  
**Important Information about your Environmental Site**  
**Assessment**

## Important Information About Your

# Environmental Site Assessment

*These notes have been prepared by Golder Associates Pty Ltd using guidelines prepared by ASFE; The Association of Engineering Firms Practising in the Geosciences, of which Golder Associates Pty Ltd is a member. They are offered to help you in the interpretation of your Environmental Site Assessment (ESA) report.*

### Reasons For Conducting An ESA

ESA's are typically, though not exclusively carried out in the following circumstances :

- as pre-acquisition assessments, on behalf of either purchaser or vendor, when a property is to be sold;
- as pre-development assessments, when a property or area of land is to be redeveloped or have its use changed, for example, from a factory to a residential subdivision;
- as pre-development assessments of greenfield sites, to establish "baseline" conditions and assess environmental, geological and hydrogeological constraints to the development of, for example, a landfill; and
- as audits of the environmental effects of an ongoing operation.

Each of these circumstances requires a specific approach to the assessment of soil and groundwater contamination. In all cases, however, the objective is to identify and if possible quantify the risks which unrecognised contamination poses to the proposed activity. Such risks may be both financial, for example, clean-up costs or limitations on site use, and physical, for example, health risks to site users or the public.

### The Limitations of An ESA

Although the information provided by an ESA can reduce exposure to such risks, no ESA, however diligently carried out, can eliminate them. Even a rigorous professional assessment may fail to detect all contamination on a site. Contaminants may be present in areas that were not surveyed or sampled, or may migrate to areas which showed no signs of contamination when sampled.

### An ESA Report Is Based On A Unique Set of Project Specific Factors

Your environmental report should not be used :

- When the nature of the proposed development is changed, for example, if a residential development is proposed instead of a commercial one;

- When the size or configuration of the proposed development is altered;
- when the location or orientation of the proposed structure is modified;
- When there is a change of ownership; or
- For the application to an adjacent site.

To help avoid costly problems, refer to your consultant to determine how any factors which have changed subsequent to the date of the report may affect its recommendations.

### ESA "Findings" Are Professional Estimates

Site assessment identifies actual subsurface conditions only at those points where samples are taken, when they are taken. Data derived through sampling and subsequent laboratory testing are interpreted by geologists, engineers or scientists who then render an opinion about overall subsurface conditions, the nature and extent of contamination, its likely impact on the proposed development and appropriate remediation measures. Actual conditions may differ from those inferred to exist, because no professional, no matter how qualified, and no subsurface exploration program, no matter how comprehensive, can reveal what is hidden by earth, rock and time. The actual interface between materials may be far more gradual or abrupt than a report indicates. Actual conditions in areas not sampled may differ from predictions. Nothing can be done to prevent the unanticipated, but steps can be taken to help minimise its impact. For this reason, owners should retain the services of their consultants through the development stage, to identify variations, conduct additional tests which may be needed, and to recommend solutions to problems encountered on site.

### Subsurface Conditions Can Change

Subsurface conditions are changed by natural processes and the activity of man. Because an ESA report is based on conditions which existed at the time of subsurface exploration, decisions should not be based on an ESA report whose adequacy may have been affected by time. Speak with the consultant to learn if additional tests are advisable.

### ESA Services Are Performed For Specific Purposes And Persons

Every study and ESA report is prepared in response to a specific Brief to meet the specific needs of specific individuals. A report prepared for a consulting civil engineer may not be adequate for a construction contractor, or even some other consulting civil engineer. A report should not be used by other persons for any purpose, or by the client for a different purpose. No individual other than the client should apply a report even apparently for its intended purpose without first conferring with the consultant. No person should apply a report for any purpose other than that originally contemplated without first conferring with the consultant.

### **An ESA Report Is Subject To Misinterpretation**

Costly problems can occur when design professionals develop their plans based on misinterpretations of an ESA. To help avoid these problems, the environmental consultant should be retained to work with appropriate design professionals to explain relevant findings and to review the adequacy of their plans and specifications relative to contamination issues.

### **Logs Should Not Be Separated From The Engineering Report**

Final borehole or test pit logs are developed by environmental scientists, engineers or geologists based upon their interpretation of field logs (assembled by site personnel) and laboratory evaluation of field samples.

Only final logs are customarily included in our reports. These logs should not under any circumstances be redrawn for inclusion in site remediation or other design drawings, because drafters may commit errors or omissions in the transfer process. Although photographic reproduction eliminates this problem, it does nothing to minimise the possibility of contractors misinterpreting the logs during bid preparation. When this occurs, delays, disputes and unanticipated costs are the all-too-frequent result.

To reduce the likelihood of boring log misinterpretation, the complete report must be available to persons or organisations involved in the project, such as contractors, for their use. Those who do not provide such access may proceed under the mistaken impression that simply disclaiming responsibility for the accuracy of subsurface information always insulates them from attendant liability. Providing all the available information to persons and organisations such as contractors helps prevent costly construction problems and the adversarial attitudes which may aggravate them to disproportionate scale.

### **Read Responsibility Clauses Closely**

Because an ESA is based extensively on judgement and opinion, it is necessarily less exact than other disciplines. This situation has resulted in wholly unwarranted claims being lodged against consultants. To help prevent this problem, model clauses have been developed for use in written transmittals. These are not exculpatory clauses designed to foist liabilities onto some other party. Rather, they are definitive clauses which identify where your consultant's responsibilities begin and end. Their use helps all parties involved recognise their individual responsibilities and take appropriate action. Some of these definitive clauses are likely to appear in your ESA report, and you are encouraged to read them closely. Your consultant will be pleased to give full and frank answers to your questions.